The nature of autogenic processes and the propagation of environmental signals in sediment transport systems

Thesis submitted in accordance with the requirements of the University of Liverpool for the degree of Doctor of Philosophy by

Chloe Griffin

December 2023

The history of the Earth is written in rocks, if we are patient enough to read it. It is through this patient enquiry that we can unreal the mysteries of the Earth and foster a deeper appreciation for the dynamic forces that have shaped our planet

Charles Lyell

Contents

List of tables

List of figures

Acknowledgements

Firstly, I owe endless thanks to my supervisory team, Rob Duller and Kyle Straub. Thank you all for the guidance, encouragement and wisdom you have provided me with over the last few years. Doing a PhD during a global pandemic was difficult, but without the support you both provided me with it would have not been possible. You both deserve the upmost credit and I greatly appreciate everything you both have done for me. Rob, thank you for all your support over the last 5 years, from starting my MESci dissertation to completing my PhD. I have fond memories of our blackboard sessions where we'd talk science, go off on endless tangents and return full circle to the beginning. I've learnt that every idea you throw at me completes part of a puzzle somewhere, and to trust the process and wait for the light-bulb moment a few months later. I've definitely learnt to take a more chilled out approach to life thanks to your no stress nature. Kyle, an endless thank you for setting up the rice pile and for your guidance and knowledge whilst running experiments. It's safe to say your experimental expertise saved my PhD. I had a great few weeks working with you and your lab group at Tulane and I only wish I could have visited earlier and for longer (no thanks to covid). Thank you for always including me in the TSDS research group and letting me Zoom into your meetings across the pond; it definitely made me feel part of a scientific community. Thanks also to Jonny Higham, for your advice, technical guidance and for spending countless hours fixing and running models for me over the last few years. I also thank both Leo Uieda and Silvio De Angelis for their help in various aspects of data analysis and thought-provoking discussions.

I am grateful to the University of Liverpool, who paid my tuition fees, research expenses and my stipend. I am also grateful to the IAS and SEPM who funded my trip to Tulane and provided financial support for which allowed me to attend many great conferences over the last 4 years.

During my PhD I was supported by friends and colleagues throughout the department, over all the research groups, which made my final years at Liverpool a great experience. Thanks also extend to everybody in the department at Tulane for being so welcoming during my brief time visiting, and to Jose for letting me gatecrash your office. Thank you to Chris, Charlotte, Graham and Stephen for trusting me to demonstrate in your undergrad labs for many years; I never thought I'd enjoy the experience as much as I did. Also, thank you to the rest of the PhD team demonstrating on Thursday geography labs, the constant laughs and chaos were something to look forward to each week and definitely kept me going for the last 4 years. Thank you to Kate, India, Alfie and Pete, in whom I found great friends, for the constant rice jokes and the short

courses in volcanology, magnetics and coding but also for the many laughs we shared. I thank both Kate and Alfie for taking me out of the office and into the field during my PhD. The few weeks of fieldwork were a welcome break from model runs and coding and reminded me what rocks look like and that deep down, I'm still a geologist. I don't thank you for the many cows we encountered on these trips.

Thank you to my family for supporting my venture into university, especially as we learnt about higher education for the first time together. Thank you to my friends for always checking in as to how I am, how things are going and what I'm up to. To Luke, thank you for your ongoing support and encouragement, listening to my rice pile rants and making life outside of work fun and enjoyable.

Thesis abstract

The internal (autogenic) dynamics operating ubiquitously within sediment transport systems mediate the transport of sediment through a system, which controls the morphology of landscapes and dictates the architecture of the stratigraphic record. Autogenic processes are characterised by localized episodes of sediment storage and release that occur throughout a sediment transport system, which generate fluctuations in sediment transport and add noise to a time series of sediment flux and the resulting strata. This noise can obscure or shred evidence of sediment flux signal generated by external (allogenic) environmental perturbations. This complex interaction of allogenic and autogenic processes makes records of environmental change difficult to interpret. The duration and magnitude of autogenic processes within sediment transport systems denote thresholds for the propagation of environmental signals through landscapes and preservation in strata. If the sediment flux signal is of the same duration and/or magnitude as the autogenic processes within the system, then the signal will be shredded (e.g. degraded in amplitude), and hence be rendered undetectable in the output flux. Conversely, when the sediment flux signal is of longer duration and/or magnitude than the autogenic processes, then it will overwhelm the magnitude of the variability present within the system and hence produce a detectable, measurable response at the system outlet. However, the concept of signal preservation has become complex, where a signal is only defined as preserved when a detectable response is present, meaning that signals which cannot be differentiated by autogenic noise, or those rendered undetectable by stratigraphic incompleteness can be misinterpreted. Therefore, the aim of this thesis is to develop a quantitative understanding of the nature and timescales of autogenic processes, which can be used to quantify thresholds for signal shredding and detection in both landscapes and strata. This is achieved using both a physical avalanching rice pile and a numerical granular pile, which can elucidate the nature of autogenic processes within sediment transport systems and offer a rich suite of autogenic statistics along a simple 1D transport path, comparable to sediment transport within field scale systems. The results of this thesis: (1) provide a quantitative understanding of the nature and timescales of autogenic processes operating within sediment transport systems, and use this understanding to develop a framework that can predict the severity of signal shredding and establish robust confidence limits of signal detectability in landscapes and strata; (2) quantify the effect of stratigraphic incompleteness and the assumption of linear sedimentation rate on the preserved structure of autogenic processes and consequently the detectability of environmental signals; and (3) provides insight into how the magnitude of the stochastic processes operating within sediment transport systems governs the amount of degradation environmental signals experiences and the thresholds for signal detectability within different geomorphic environments. The results in this thesis contribute to a quantitative understanding of the nature of autogenic processes, which is crucial for (1) the accurate reconstruction and confident justification of past environmental signals (2) quantifying the reliability of landscapes and strata as archives of future paleoenvironmental variability and (3) understanding the geomorphic environments and sedimentary records which best preserve evidence of paleo-surface processes and environmental signals.

1. Introduction

1.1. Motivation

In the last decade, interest in Earth surface dynamics has accelerated as we address questions regarding the response of landscapes to environmental change (Hessler and Fildani, 2019; Straub *et al.*, 2020). The physical record of these processes lies in the resultant stratigraphy, but to fully employ this indispensable record, we must understand the processes that give rise to clastic strata (Hessler and Fildani, 2019; Straub *et al.*, 2020). The sediment grains that constitute clastic strata originate from the upland erosional segments of a sediment transport system (STS) (Schumm, 1971). This sediment can be mobilised by a variety of erosional agents (e.g. gravity, wind, water, ice, and/or anthropogenic activity) and transported down-system via a complex channelized region until permanent deposition within a sedimentary basin (Romans *et al.*, 2016). Here, it undergoes gradual burial, compaction, and lithification over geological timescales (Lai *et al.*, 2018), preserving a record of Earth surface processes.

Landscapes evolve in response to environmental perturbations over a range of spatio-temporal scales (Daniels, 2008; Rohais *et al.*, 2012; Romans *et al.*, 2016; Allen, 2017; Blum *et al.*, 2018; Straub *et al.*, 2020); commonly these are considered a simple function of climatic shifts, tectonic uplift or eustatic change (Forzoni *et al.*, 2014). However in modern times anthropogenic modification is becoming an increasingly dominant mechanism of environmental forcing worldwide (Jones *et al.*, 2013; Lane *et al.*, 2019). These forcing conditions (Figure 1.1) operate over a range of timescales, from minutes (e.g. storms, earthquakes, floods or dam removal) to millions of years (e.g. climatic cycles, mountain building, land use alterations) (Romans *et al.*, 2016). Environmental forcings generate variations in sediment flux and the grain size distribution exported from upland catchments (e.g. tectonics, climate and anthropogenic change) and also control the availability of down-system accommodation for deposition (e.g. eustatic change) (Armitage *et al.*, 2011; Whittaker, 2012; Li *et al.*, 2018; Sharman *et al.*, 2019). The variations produced as a result of environmental forcing shape the architecture of the stratigraphic record and provide a unique record of Earth surface processes and environmental change which exceeds the spatiotemporal scales of other environmental archives (e.g. ice cores or lake varves) (Wilkinson *et al.*, 2009; Castelltort *et al.*, 2015; Romans *et al.*, 2016; Sharman *et al.*, 2019). Therefore, the geomorphic expression of landscapes and their resultant stratigraphic products allow scientists the ability to answer epistemic questions in our understanding of landscape sensitivity to major environmental events and decode the temporally variable controls on sediment production (Whittaker *et al.*, 2010; Mahon *et al.*, 2015; Brooke *et al.*, 2018).

However, direct communication of sediment supply signals from source to sink is improbable. Even under steady forcing conditions, sediment movement through transport systems is non-linear, which can cause environmental sediment flux signals to undergo varying degrees of modification during transport from source to sink (Paola, 2016; Romans *et al.*, 2016; Hajek & Straub, 2017; Scheingross *et al.*, 2020). The dynamics operating within landscapes temporally reconfigure STSs (e.g. autogenic processes), which shape the architecture of the stratigraphic record (Hajek & Straub, 2017; Burgess *et al.*, 2019; Scheingross *et al.*, 2020). A quintessential example of autogenic processes is the avulsion of channels within a channel-floodplain system (Figure 1.1.) (Stouthamer & Berendsen, 2007; De Haas *et al.*, 2016; Hajek & Straub, 2017; Straub *et al.*, 2020). Episodes of sediment storage and release as a result of autogenic processes have the effect of obscuring, buffering, or completely destroying ('shredding') sediment flux signals as they propagate across the Earth's surface (Jerolmack & Paola, 2010; Van De Wiel & Coulthard, 2010; Hajek & Straub, 2017; Toby *et al.*, 2019; Straub *et al.*, 2020). Alongside this, spatial variations in sedimentation rate and phases of no deposition or erosion can limit the recording of environmental signals within stratigraphy (Foreman & Straub, 2017; Trampush & Hajek, 2017; Straub *et al.*, 2020). These processes can render signals undetectable (Table 1) within a time series of sediment flux at the system outlet, and hence undetectable within the stratigraphic record, complicating the latter reconstruction of past environmental signals from the sedimentary record (Allen, 2008; East *et al.*, 2015; Paola, 2016; Hajek & Straub, 2017; Harries *et al.*, 2019). The emphasis of many studies has been to quantify thresholds for the preservation of environmental signals in both landscapes and strata (e.g. Burgess *et al.*, 2019; Foreman & Straub, 2017; Jerolmack & Paola, 2010; Li *et al.*, 2016; Straub & Esposito, 2013; Straub & Foreman, 2018; Toby *et al.*, 2019, 2022; Wang *et al.*, 2011), however, to further understand these thresholds, the thresholds for signal modification (e.g. signal shredding) and signal detectability must be quantified and differentiated to further enhance understanding of signal propagation and preservation.

Table 1.1: Key terms with associated definitions

Term	Definition
Autogenic	Natural variability or dynamics which arise solely from the interaction of internal system components within a sediment transport system. For example, bed and bar form formation (Hooke, 2007), dune migration (Ewing *et al.*, 2006), hillslope landslides (Roering *et al*,. 2021), channel avulsion (Jerolmack & Mohrig, 2007), deltaic growth (Kim & Jerolmack, 2008).
Environmental (allogenic) forcing	Large scale external factors which control the volume of sediment and the accommodation available on the Earth's surface. Allogenic forcing mechanisms include: climatic change, tectonic uplift, eustatic change or anthropogenic activity.
Environmental signal	Attributes of landscape structure, sediment transport capacity and the characteristics of the resultant stratigraphy that can be linked directly to environmental forcing.
Self-organized	Ordered or patterned autogenic behavior.
Signal degradation	The smearing of externally-driven signals by sediment transport processes across a range of spatiotemporal scales, resulting in the amplitude of the environmental signal at the system output being severely degraded when compared to the amplitude of the original signal (Griffin *et al.*, 2023).
Signal detection	Signals which produce a measurable response in a power spectrum which exceeds the respective confidence band.
Signal shredding	The smearing of externally-driven signals by sediment transport processes across a range of spatiotemporal scales (Jerolmack & Paola, 2010).
Stochastic	Processes which are defined by a random probability distribution.
Stratigraphic incompleteness	The concept that sedimentary records contain temporal gaps of varying duration and hence the sediment present imperfectly samples the time between the start and end of the stratigraphic section. Either not all time steps are represented by preserved sediment (incomplete) or all time steps are represented by preserved sediment (complete).

The work in this thesis quantifies thresholds for the shredding and detectability of sediment flux signals and develops an understanding of the controls on the detectability of signals within a landscape using a physical avalanching rice pile. The rest of this chapter provides an overview of allogenic and autogenic dynamics controlling landscape evolution, our current understanding of thresholds for signal shredding and signal preservation within landscapes and strata, and finally the use of granular piles as an analogy for landscapes. Chapter 2 presents the methods used in this thesis: the suite of physical rice pile experiments and the numerical granular avalanching system. The physical experiments support the theoretical framework presented in Chapter 3, where two autogenic timescales, defined by the temporal structure, are utilised to differentiate timescales of signal shredding from signal detectability. Chapter 4 builds on the theory presented in Chapter 3, and presents a framework for the detectability of environmental signals within a record that is temporally incomplete (akin to stratigraphic incompleteness). Chapter 5 utilises a numerical granular pile to explore signal shredding and detectability thresholds within landscapes where the magnitude of autogenic noise is low. Chapter 6 discusses the overarching themes of each chapter in relation to the importance of this work and the implications for signal reconstruction from landscapes and strata.

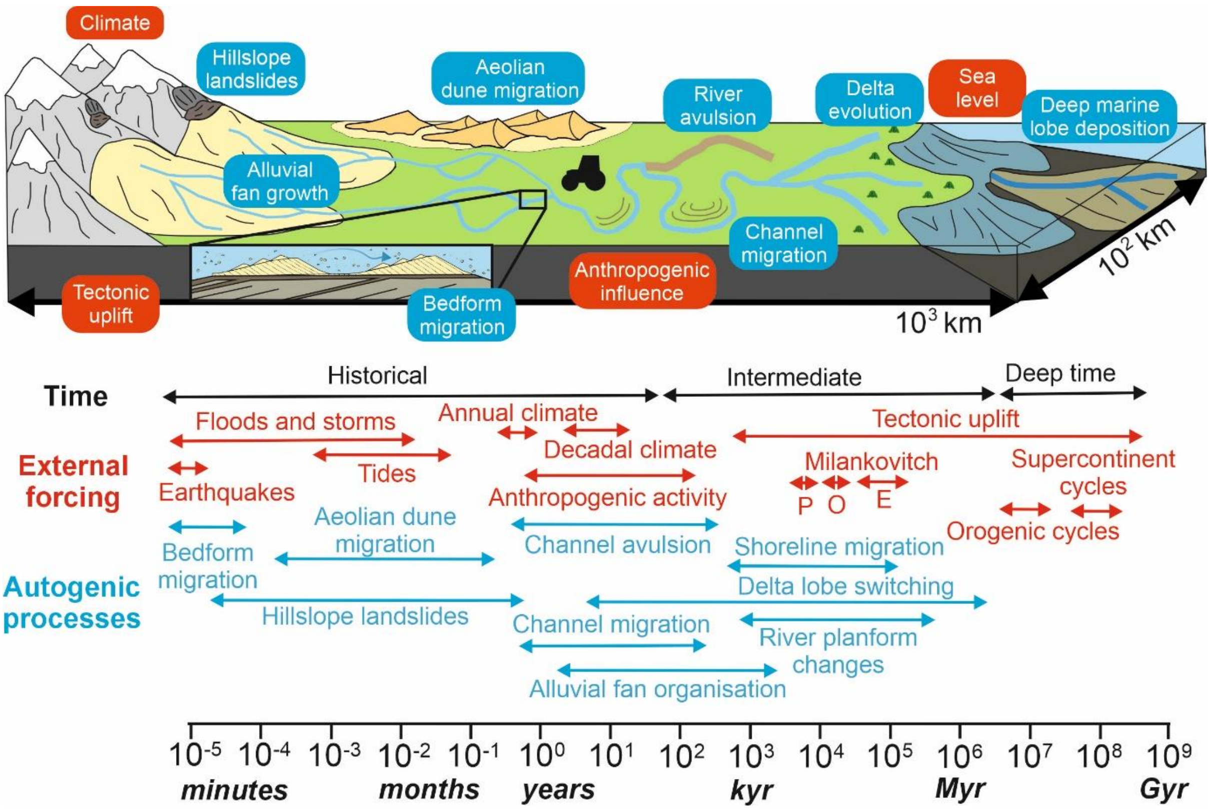

Figure 1.1: Conceptual overview of the Earth's surface (10^3 km in length and 10^2 km wide) showing the interaction of allogenic and autogenic processes over a range of timescales.

Allogenic processes (red; e.g., climate, tectonics, sea level and anthropogenic change) operating over a range of spatiotemporal scales control sediment availability and accommodation. Autogenic processes (blue), operating over similar spatiotemporal scales, arise spontaneously in sediment transport systems. These processes generate periods of sediment storage and release which creates heterogeneity in the distribution of sediment across a landscape and influences the propagation of sediment flux signals. Allogenic and autogenic processes operate over similar timescales and hence simultaneously control the evolution of landscapes and the production of strata. Timescales of autogenic processes from Glade et al., (2019), Clarke et al., (2010), Straub & Wang, (2013) and Voller et al., (2019). Figure adapted from Hajek & Straub, (2017) and Romans et al., (2016).

1.2. Allogenic forcing and the generation of sediment supply signals

STSs are sensitive to external (allogenic) variations in environmental conditions over a range of spatiotemporal scales, from minutes to millions of years (Romans *et al.*, 2016; Allen, 2017; Straub *et al.*, 2020) (Figure 1.1). Allogenic forcing (namely climatic, tectonic eustatic or anthropogenic change) can trigger temporary or sustained changes in any physiological, biological or chemical attribute of the Earth's surface, which are known as environmental signals (Straub *et al.*, 2020; Tofelde *et al.*, 2021). Environmental signals can be recorded within many time-series generated from environmental measurables, including but not limited to, speleothems (Fairchild *et al.*, 2006), ice cores (Masson-Delmotte *et al.*, 2006), tree rings (Gagen *et al.*, 2022), ecological populations (Cazelles, 2004), isotope and chemical data (Leng & Marshall, 2004) and sedimentary parameters (sediment flux, size distribution and composition; Tofelde *et al.*, 2021). Whilst this thesis focuses on signals in the form of temporal variations in sediment flux that propagate down-system, upstream propagation of signals (e.g. oscillations in relative sea level) driven by base level change can also be a major control on stratigraphic architecture (Romans *et al.*, 2016). However, the study of sediment flux signals integrates geomorphology, sedimentology and stratigraphy to study the propagation of environmental signals across different timescales (Jerolmack & Paola, 2010; Simpson & Castelltort, 2012; Armitage *et al.*, 2013; Ganti *et al.*, 2014; Romans *et al.*, 2016; Blum *et al.*, 2018; Li *et al.*, 2018; Duller *et al.*, 2019; Caracciolo, 2020; Straub *et al.*, 2020; Tofelde *et al.*, 2021; Toby *et al.*, 2022).

Throughout geological history, a combination of climate and tectonics has regulated erosion and delivery of sediment to a STS (Forzoni *et al.*, 2014; Caracciolo, 2020). However, these processes operate over a variety of temporal scales. Over mesotimescale (10^4 to10^6 years; Romans *et al.*, 2016), tectonically active areas can experience denudation rates three orders of magnitude higher than their inactive counterparts (Hovius, 1996; Hecht & Oguchi, 2017), hence generating low frequency, long period sediment flux signals (Allen & Densmore, 2000). Over short timescales (10^2 – 10^4 years; Romans *et al.,* 2016), increased precipitation as a result of climatic shifts can generate sharp peaks and troughs in sediment flux which generally leads to the supply of high frequency (e.g. Milankovitch scale) sediment flux signals to basins (Allen & Densmore, 2000; Castelltort & Van Den Driessche, 2003). However, direct human denudation has increased by a factor of 30 since the mid 20th Century (Zalasiewicz et al. 2015; Cendrero et al. 2022), hence anthropogenically induced sediment flux signals have intensified (Waters *et al.*, 2016; East *et al.*, 2022) as a result of deforestation (Syvitski & Kettner, 2011), road constructions (Waters *et al.*, 2016), dam removal (Ritchie *et al.*, 2018), land use change (Giri *et al.*, 2019) and mining (Wilkinson *et al.*, 2009) to name a few (see review by Syvitski *et al.*, (2022). Although the movement of sediment during construction activities accounts for approximately 30% of all humanly transported sediment (Hooke, 2000), agricultural practices are the most dominant process of global anthropogenic sediment evacuation (Sherriff *et al.*, 2019). The intensity of modern anthropogenic activities has been found to trigger more drastic geomorphic change than natural forcing mechanisms (East *et al.*, 2022), due to the onset of high amplitude, short durations perturbations, hence these have great potential to impact landscapes and therefore be preserved in the future rock record (Corcoran *et al.*, 2015).

Sediment flux signals of environmental change are suggested to propagate from source to sink, allowing for the reconstruction of past environmental perturbations and providing insight into the response of landscapes to future environmental change (Forzoni *et al.*, 2014; D'Arcy *et al.*, 2017; Harries *et al.*, 2019; Sharman *et al.*, 2019; Straub *et al.*, 2020; Tofelde *et al.*, 2021). However, the response of a STS to external environmental perturbations is complex (Schumm, 1973), meaning not all sediment flux signals input to the system are faithfully transmitted down the system. Sediment transport dynamics operating within the Earth's surface control sediment transport and generate impediments for signal storage (e.g. buffering, shredding or stratigraphic incompleteness; (Jerolmack & Paola, 2010; Simpson & Castelltort, 2012; East *et al.*, 2015; Romans *et al.*, 2016; Toby *et al.*, 2019; Straub *et al.*, 2020; Tofelde *et al.*, 2021), complicating the reliable reconstruction of environmental signals from the geological record (Figure 1.2). Therefore, understanding how and when landscape dynamics impede the stratigraphic storage of environmental signals is of critical importance for: predicting the spatiotemporal scales of mass transfer, understanding landscape sensitivity and resilience (Thoms *et al.*, 2018), predicting the export and burial of terrestrial organic carbon (Kao *et al.*, 2014), interpreting the stratigraphic record for natural resource exploration and production (Bhattacharya *et al.*, 2016), and finally understanding the Earth's response to ongoing and future natural and anthropogenic change (Densmore *et al.*, 2007; Forzoni *et al.*, 2014; Mahon *et al.*, 2015; D'Arcy *et al.*, 2017; Sharman *et al.*, 2019).

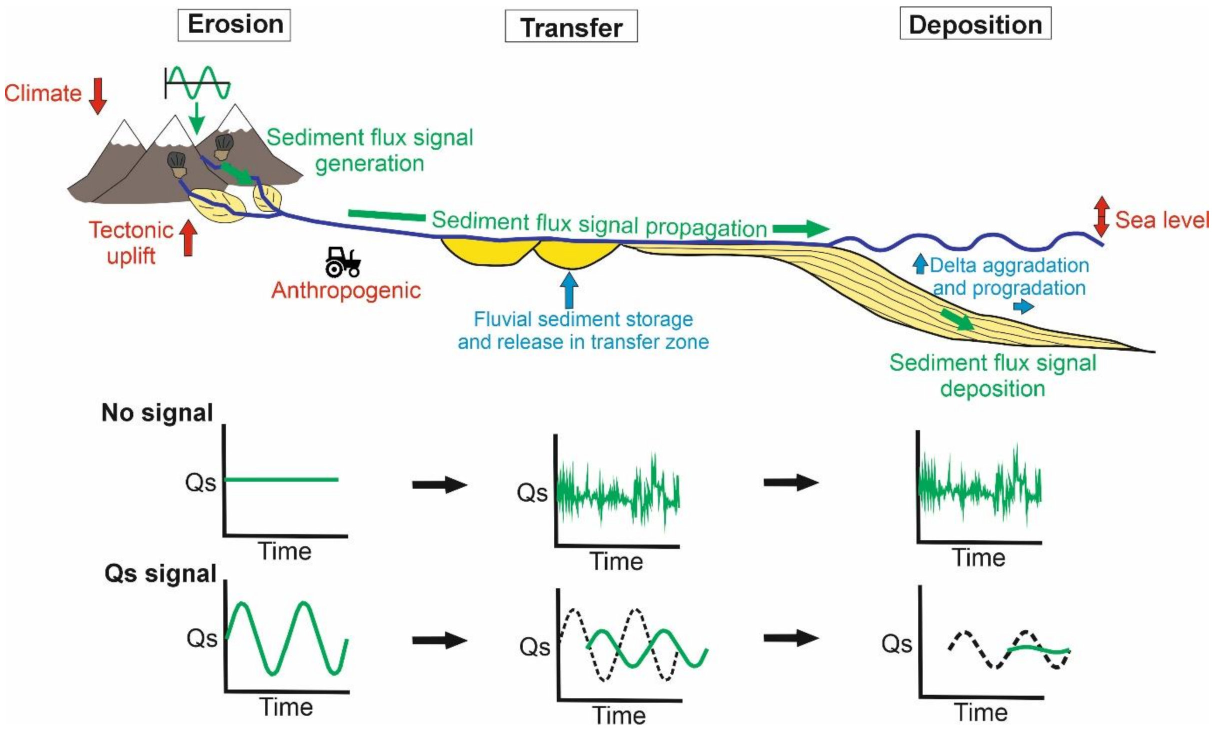

Figure 1.2: Source to sink signal propagation.

Simplified source to sink sedimentary system, where a sediment flux (Qs) signal (green) is generated in an eroding catchment in response to an environmental perturbation (red). The signal is transported through a landscape in a channelized zone via a series of storage and release events (autogenic processes; blue) to depositional sink. In the absence of signals coming from the erosion zone, autogenic processes in the transfer zone add variability, or 'noise', in measures of sediment flux. When a sediment flux signal is transported through a system, autogenic processes modify and attenuate the signal. This means that the signal measured in the zone of deposition may not resemble the true input signal. Adapted from Romans et al., (2016).

1.3. Autogenic processes within sediment transport systems

The transportation and distribution of sediment across the Earth's surface is environment dependent due to the combined effects of: variations in sediment properties (e.g. grain size, shape, density and cohesion), sediment transport processes and the thresholds for sediment transport (Jerolmack, 2011; Benavides *et al.*, 2022). This means that the power to transport sediment is unevenly distributed within sedimentary environments, which generates landscape instability and eventually triggers landscape re-organization (Hajek & Straub, 2017). A quintessential example of this process is channel avulsion: in fluvial systems, water and sediment are transported in geographically confined channels, causing in-channel sedimentation rates to greatly exceed that of the surrounding floodplains. This preferential aggradation eventually leads to perched channels, which triggers channel avulsion to reinstate a degree of landscape stability (Ganti *et al.*, 2016; Li *et al.*, 2022; Mohrig *et al.*, 2000). These morphodynamic processes occur entirely as a consequence of crossing sediment transport thresholds and trigger internal system re-configuration are referred to as autogenic processes (Beerbower, 1964; Hajek & Straub, 2017; Swanson *et al.*, 2019; Scheingross *et al.*, 2020). Examples of autogenic processes abound: on small scales, these processes drive bed and barform formation and over larger scales control the generation and evolution of channel networks, delta lobes, shoreline features and alluvial fans (Phillips, 1999; Muto & Steel, 2004; Chin & Phillips, 2007; Hooke, 2007; Jerolmack, 2009, 2011; Ganti *et al.*, 2013; Murray *et al.*, 2014; Pelletier *et al.*, 2015; Paola, 2016; Straub *et al.*, 2020; Brooke *et al.*, 2022). The vast range of scales over which autogenic processes operate generates a vast spectrum of autogenic frequencies in landscape morphology (Jerolmack & Paola, 2010).

Autogenic processes naturally occur in the absence of any external environmental perturbations and are ubiquitous across landscapes, hence are imperative in shaping the geometry of landscapes and the architecture of the resulting stratigraphic record (Paola, 2016; Hajek & Straub, 2017; Burgess *et al.*, 2019; Scheingross *et al.*, 2020). However, landscape dynamics in all environments inevitably result from both autogenic and allogenic processes (Hajek & Straub, 2017; Mouchené *et al.*, 2017). This is because allogenic processes influence water discharge, sediment composition and topographic gradients which control STS morphology and dynamics (Edmonds & Slingerland, 2010). The complex interaction of these processes complicates the preservation of stratigraphic sequences. Whilst autogenic processes operate independently of allogenic forcing, variations in boundary conditions as a result of allogenic forcing influence the morphology of STSs and the rate at which morphodynamic processes occur (e.g. channel migration rate and avulsion frequency) (Chadwick & Lamb, 2021; Edmonds & Slingerland, 2010; Li *et al.*, 2017; Reitz & Jerolmack, 2012; Straub *et al.*, 2015; Wickert *et al.*, 2013). For example, increasing the rate of accommodation generation (Wickert *et al.*, 2013), the sediment supply rate (Bryant *et al.*, 1995) and/or water discharge (Van Dijk *et al.*, 2009) increases the rate of autogenic processes within a STS, and hence the rate of sediment transport. Therefore, understanding the relationship between autogenic and allogenic processes within STSs is important as the rates and scales of autogenic processes, controlled by allogenic forcing, determine surface and stratigraphic architecture but also the propagation and preservation of environmental signals (Straub *et al.*, 2020).

Autogenic processes are commonly associated with the self-organised behaviour of STSs over sufficiently long timescales (Swanson *et al.*, 2019), where the products of autogenic dynamics are distributed in statistically spatially ordered patterns (Hajek *et al.*, 2010; Budd *et al.*, 2016) and create organised depositional architecture (Hoyal and Sheets, 2009). Hence, the self-organization of a physical system can be viewed as both a statistical and a measurable property (Phillips, 1999). Self-organization of STS occurs over a sufficiently long timescale (Swanson *et al.*, 2019), that is scaled to the size of the system and the nature of the interactions between the individual system components (Hajek & Straub, 2017). Examples of these processes include the regular spacing of bedforms and point bars in meandering rivers (Hajek & Straub, 2017), the size distribution of sediment storage and release events within a sediment flux time series, or the organization of surface topography and the resultant stratigraphic products (Paola, 2016). The interaction between flow and sediment as result of autogenic processes generates episodes of sediment storage (deposition and aggradation) and release (erosion and bypass) within landscapes over a range of spatiotemporal scales resulting in stochastic sediment transport through a STS (Jerolmack & Paola, 2010; Jerolmack, 2011; Van De Wiel *et al.*, 2011). Whilst sediment storage and release is ubiquitous in all sedimentary environments (Hajek & Straub, 2017), the timescales of sediment storage can vary between systems. For example, suspended sediment in rivers experiences minimal storage in comparison to bedload sediment which can experience sediment retention times between minutes to years (Lambert & Walling, 1988). Furthermore, portions of sediment liberated by landslides on hillslopes can be rapidly transported downslope and be deposited directly into the fluvial network, whereas the majority of sediment will remain trapped in the catchment for thousands of years (Cislaghi & Bischetti, 2019). Stochasticity over a variety of scales generates significant noise in measures of sediment flux over the full range of autogenic frequencies (Kim & Jerolmack, 2008; Jerolmack & Paola, 2010; Van De Wiel & Coulthard, 2010; Romans *et al.*, 2016). This noise has the ability to obscure evidence of allogenic forcing within landscapes and strata, when the signal is of the same magnitude as autogenic processes (Jerolmack & Paola, 2010; Van De

Wiel & Coulthard, 2010; Morris *et al.*, 2015). Furthermore, unlike allogenic processes which can generate distinctive periodicity, autogenic noise is commonly found to encompass random sediment transport fluctuations (Jerolmack & Paola, 2010; Paola, 2016). These fluctuations are assumed to be of small magnitude and uncorrelated (Ventra & Nichols, 2014), but several studies using both experimental and field data have shown that sediment flux variations as a result of purely autogenic processes can also record evidence of cyclicity (Burgess *et al.*, 2019; Foreman & Straub, 2017; Hajek *et al.*, 2012; Kim & Jerolmack, 2008; Meyers, 2012; Miall, 2015; Stouthamer & Berendsen, 2007; Van De Wiel & Coulthard, 2010). For example, channel avulsion within experimental delta systems has been found to produce cyclic sedimentation packages (e.g. Kim & Jerolmack, 2008), and automatically induced variations in channel and sheet flow can produce cyclic sedimentation in fault-bounded basins (e.g. Kim & Paola, 2007), within fluvial deltas (e.g. Van Dijk *et al.*, 2009) and on alluvial fans (e.g. Clarke *et al.*, 2010; Nicholas & Quine, 2007). This makes isolating the individual impacts of allogenic and autogenic processes a major challenge without prior knowledge of the styled allogenic forcing conditions imposed on a STS (Clarke, 2015). To differentiate these processes, it is important to understand and characterise the nature and timescales of autogenic processes, to correctly decipher palaeo-environmental variations and palaeo Earth surface processes (Powell *et al.*, 2012).

A key aim of geomorphologists and stratigraphers is to accurately reconstruct landscape response to past environmental change. However, inference of environmental signals from a time series of sediment flux or from the stratigraphic record is complicated without a thorough understanding of the nature of autogenic processes. To accurately interpret the environmental record, quantitative frameworks set by autogenic processes must be utilised which can establish robust confidence limits of environmental signal transfer and detectability within landscapes and strata. The next section reviews three impediments to signal storage within STSs, and the current temporal thresholds used to quantify signal propagation and preservation potential in both landscapes and strata.

1.4. The propagation and preservation of sediment flux signals through channelized landscapes and to strata

Sections 1.2 and 1.3 discussed how external environmental perturbations generate sediment flux signals that can propagate through a STS and have the potential to be preserved in depositional basins. However, complex sediment transport dynamics within the central, channelized transport zone of a STS can have fundamental implications for the propagation and storage of environmental signals. The transfer zone of STSs (Allen, 2017) conveys sediment from source to sink, and hence plays a key role in the propagation and preservation of external sediment flux signals. This region is composed of self-formed fluvial systems, which funnel water and sediment down-system through a network of narrow, channelized corridors (Figure 1.1, 1.2). The evolution and reconfiguration of fluvial networks within the transfer zone (as a result of autogenic processes) generates temporally variable patterns of deposition, stasis and erosion on a variety of scales. This variability can modify or destroy evidence of external sediment flux signals (Jerolmack & Paola, 2010). Hence, understanding fluvial processes over a range of spatiotemporal scales is important for predicting the modification and propagation of sediment flux signals.

Within fluvial systems, sediment storage and release processes operate on a range of spatiotemporal scales (Paola *et al.,* 2016; Van de Wiel & Coulthard, 2010) (Figure 1.1.). On bed scale, the migration of in-channel bedforms (i.e., ripples, dunes and bars) can be thought of as small-scale autogenic morphology (Goldstein *et al.,* 2011; Paola *et al.,* 2016). These millimetre to meter scale features evolve and migrate rapidly (seconds to minutes), temporarily storing and releasing sediment along their trajectory (Jerolmack & Mohrig, 2005). The dimensions and regular spacing of these bedforms within fluvial systems has also been found to be autogenically controlled (McElroy & Mohrig 2009; Ganti *et al.,* 2011; Faulkner *et al.,* 2016). On a channel scale, fluvial systems migrate gradually through time via simultaneous bank erosion and bar deposition (Lauer & Parker, 2008). This causes local influxes of floodplain stored sediment into the trunk channel (Darby *et al.,* 2002), reactivating and eroding regions of the floodplain previously in stasis (Tipper, 2015). The rate of river migration can range from less than 0.5 metres to more than 50 metres per year (Greenberg & Ganti, 2024), and hence can cause dramatic evolution of the fluvial system over decades. On a landscape scale, rivers can be relocated to an entirely different position on the floodplain by channel avulsion, triggered by landscape instability (Hajek & Straub, 2017). As sediment is confined to channelized corridors, in channel sedimentation rates exceed those of the surrounding floodplain. Hence, aggradation in channels allows them to become topographically perched, leading to avulsion to restabilise the system (Mohrig *et al.,* 2000). The avulsion timescale, T_a, can be estimated as the time for the river to aggrade to one channel depth (Jerolmack & Mohrig, 2007). Estimated avulsion timescales for modern rivers can be in the range of 10^1 (Kosi River, India) to 10^3 (Mississippi River) (Slingerland & Smith; 2004). Alongside variations in space and time, sediment storage potential within fluvial systems will vary depending on the efficiency of sediment transport. For example, sediment transported as bedload will experience much longer storage times than its suspended sediment counterpart, which may experience near linear sediment transport (Kleinhans & van Rijn, 2002). Furthermore, the competence and capacity of the river will influence sediment transport thresholds and hence sediment storage potential (Church, 2002; Curtis *et al.*, 2010). A river with high competence and/or capacity will convey sediment over a large range of grain sizes more efficiently down system, decreasing sediment storage potential (Grant, 2012).

As channelized clastic systems are characterised by measurable and predictable morphodynamic relationships (Colombera *et al.,* 2017; Paola *et al.,* 2006; Rodriguez-Iturbe *et al.,* 1992), fluvial systems have offer quantitative understanding as to the link between sediment flux signals, Earth surface processes and stratigraphic products. Three primary impediments to signal storage arise from sediment transport dynamics within channelized systems and limit the storage and recovery of environmental signals from landscapes and strata. In this section, each impediment is reviewed and highlight the respective quantitative thresholds that can predict under what conditions sediment supply signals are transferred to the stratigraphic record.

1.4.1. Landscape diffusion

Firstly, deterministic models of Earth surface dynamics within STSs predict the diffusion of environmental signals through space and time (Paola *et al.*, 1992). The diffusion framework has been applied to a range of STSs, for example, alluvial fans, deltas, coastlines, hillslopes and fluvial systems (Flemings & Jordan, 1989; Paola, 2000; Straub *et al.*, 2020). This framework is used to describe the response and evolution of surface topography to a change in boundary conditions that influence the flux of sediment provided to a basin (Paola *et al.*, 1992), where landscape equilibrium is achieved when elevation is stable as a function of time. For a system of defined length, the time required for a landscape to reach a new equilibrium state is known as the basin response time, or equilibrium timescale, (Paola *et al.*, 1992; Paola, 2000) which scales as:

$$T_{eq} = \frac{L^2}{v}$$

Where *L* is system length and *v* is diffusivity. For natural fluvial systems, estimates of T_{eq} tend to span 10^5-10^6 years (Paola *et al.*, 1992; Dade & Friend, 1998; Castelltort & Van Den

Driessche, 2003). The diffusion coefficient, v, captures the specific properties of a STS and hence requires a unique set of parameters per landscape which carries considerable amounts of uncertainty (Paola 2000). To reduce the uncertainty and make the equilibrium timescale measurable from landscape quantities, Métivier & Gaudeme (1999) reformulated this equation as follows:

$$T_{eq} = \frac{LWH_{max}}{Q_s}$$

Where W is the width of the floodplain, H_{max} is the elevation difference from the start to the end of the system and Q_s is volumetric sediment discharge.

The equilibrium timescale can be utilised as a temporal threshold for the propagation and preservation of sediment flux signals within STSs. When the periodicity of an input signal is less than T_{eq}, the input signal is substantially buffered by a landscape (Métivier, 1999; McNab *et al.*, 2023), as a complete new topographic equilibrium is unlikely to be attained. Conversely, when the signal periodicity is greater than T_{eq}, the system will reach equilibrium with forcing conditions allowing signals to propagate down-system (Duller *et al.*, 2019; McNab *et al.*, 2023).

Landscape buffering processes reduce the amplitude of the recorded signal relative to the known input signal and increase the timescale over which system response is observed relative to the timescale of the actual perturbation. This results in the smoothing out high frequency signals during propagation (Allen, 2008; Armitage *et al*., 2013; Covault *et al*., 2013; East *et al*., 2015; Forzoni *et al*., 2014; McNab *et al*., 2023; Pizzuto *et al*., 2017; Romans *et al*., 2016; Spohn *et al*., 2021; Straub *et al*., 2020). Consequently, this results in either no identifiable signal at the system outlet or a transformed signal with both a modified period (time lagged) and amplitude (decreased) (Métivier & Gaudemer, 1999; Hoffmann, 2015). The buffering of sediment flux signals occurs due to the redistribution of sediment mass over the Earths surface over a range of spatiotemporal scales which includes the simultaneous, cumulative effects of intermittent sediment transport and sediment storage within a landscape (Fryirs *et al.*, 2007). The distribution of sediment storage sites can provide key information regarding the buffering capacity of a system (Castelltort & Van Den Driessche, 2003; Armitage *et al.*, 2013; Forzoni *et al.*, 2014). For example intermontane valley fills (e.g. floodplains, alluvial fans and terraces) have been described as important landforms which decouple hillslopes from fluvial processes and hence buffer externally derived sediment flux signals within mountain catchments (Blöthe

& Korup, 2013; Clarke, 2015; Fryirs *et al.*, 2007; Knight & Harrison, 2013; Pizzuto *et al.*, 2017). The potential for signal buffering increases with system length; the longer the STS, the longer the time and the more sediment required for equilibrium to be achieved, hence increasing sediment delivery times. This was quantified by Castelltort & Van Den Driessche (2003); the attenuation of the amplitude of Milankovitch scale sediment supply signals over all periodicities (20 kyr, 40 kyr and 100 kyr) means signal transfer is more probable within short STSs or the proximal region of larger systems.

However, the representation of STSs as diffusive does not allow for the incorporation of stochastic sediment transport as a result of autogenic processes, as the lateral stochastic system dynamics present are averaged over space and time (Hajek & Straub, 2017; Métivier, 1999; Paola, 2016; Phillips & Jerolmack, 2016; Simpson & Castelltort, 2012; Toby *et al*., 2022). As autogenic processes have no role in signal propagation and storage within a diffusional framework, this can lead to a loss of predictive capability when evaluating the limits of environmental signal propagation across the Earth's surface, as only long timescale signals can be assessed in relation to T_{eq} (Toby *et al.*, 2022). However, autogenic processes are inherent to 3D STSs (Toby *et al.*, 2022) and therefore any theoretical framework must incorporate stochastic dynamics. For example, Van De Wiel & Coulthard (2010) found that the non-linearity of bedload fluctuations is indicative of self-organised criticality (SOC), meaning that sediment flux from these systems is unpredictable. Therefore, attributing individual sediment flux peaks to environmental perturbations is impossible, as these peaks may represent autogenic signals generated by internal system dynamics.

1.4.2. Signal shredding

Alongside the attenuation of signals with distance from the source, environmental signals can be smeared through both space and time due to sediment storage and release as a result of autogenic processes (Jerolmack & Paola, 2010; Van De Wiel & Coulthard, 2010; Romans *et al.*, 2016; Toby *et al.*, 2019; Straub *et al.*, 2020; Tofelde *et al.*, 2021). Motivated by fluid velocity fluctuations in turbulent flows, Jerolmack & Paola (2010) advanced on this work to quantify how stochastic sediment transport as a result of autogenic processes can influence the propagation and preservation of environmental signals across landscapes. Jerolmack & Paola (2010) outlined a concept called 'signal shredding', defined as: 'the smearing of an input signal over a range of space and timescales by stochastic processes such that an input signal is not detectable at the outlet of a system'. Shredding was hypothesised to occur where the input period of the signal is small in comparison to the magnitude of morphodynamic turbulence within the system.

Jerolmack & Paola (2010) utilised a numerical model of an avalanching rice pile to demonstrate this theory. Using a suite of numerical models, it was demonstrated that the degree of signal alteration during propagation is dependent on the maximum spatiotemporal scales of autogenic processes within a system. Using this theory, they defined a timescale, T_x, which scaled with the largest autogenic sediment transport fluctuations:

$$T_x \sim \frac{L^2}{q_0}$$

Where L is the length of the system and q_0 is the rate of sediment input. The conceptual utility of this timescale is that environmental signals with periodicity greater than T_x pass through a transport system unmodified and are recorded in the output flux, whereas those with periods less than T_x are shredded prior to recording. However, a second scenario exists in which sediment flux signals can survive shredding; when the amplitude of the input signal is greater than the maximum autogenic sediment release event. This threshold is defined as:

$$M \sim L^2 S_c$$

Where S_c is the critical threshold slope, which at field scales approximates the volume of sediment required to be eroded for channel generation post avulsion ($M = LH_{max}$).

The theory of Jerolmack & Paola (2010) provided insight into the ability of autogenic processes to shred external environmental signals and quantified two thresholds for the preservation of environmental signals within landscapes defined by the spatiotemporal limits of autogenic processes (i.e. the duration and magnitude of noise within a STS). Since the development of this framework, other models and field observations have demonstrated that autogenic processes can shred environmental signals within landscapes (Lazarus *et al.*, 2019). However, the framework of Jerolmack & Paola does not extend into signal propagation and preservation in stratigraphy, as signal loss due to vertical cut and fill processes is not included. The storage of environmental signals in stratigraphy requires sediment to be buried below the autogenic reworking depth. This means that an environmental signal may be preserved in reference to the surface process signal shredder, but may be shredded by reworking of previously deposited sediments and hence not be recorded in stratigraphy.

To extend the work of Jerolmack & Paola, (2010), Toby *et al*., (2019) developed a quantitative framework that can successfully predict the conditions necessary for the stratigraphic storage of sediment supply signals. Within landscapes, this was found to be an individual temporal threshold (T_x). However, Toby *et al*., (2019) proposed this threshold for stratigraphy was a time-dependent magnitude threshold. This threshold is set by the maximum scale of autogenic processes (sediment storage, bypass and release) over the timescale of interest, defined in this study by a change in the volume of terrestrial delta deposits as a function of measurement duration. Using this framework, periodicities of signals that produce stratigraphic signatures can be differentiated from those that do not induce a stratigraphic response. However, it is also recognised that short-period input signals can induce a surface response, but are not of sufficient duration or magnitude to induce a preservable stratigraphic response. Whilst previous work demonstrates that only the the longest or largest signals should be preserved within landscapes and strata (Jerolmack & Paola, 2010; Foreman & Straub, 2017; Burgess *et al.*, 2019), Toby *et al.*, (2019) show the potential for high-frequency input signals to be faithfully recorded. This framework suggests that commonly discussed sediment supply signals resulting from Milankovitch scale orbital forcing or punctuated tectonic uplift fall very close to the proposed threshold. Therefore, it is suggested that extraction of these environmental signals from a time series of stratigraphic measurables generated from common field exposure and methods is challenging (Toby *et al*., 2019).

Whilst the deterministic and stochastic signal propagation frameworks are generally considered separately, it has been highlighted that parallels exist between the two. Given that both timescales emerge due to the long-term spatial distribution of sediment deposition, it is hypothesised that T_{eq} and the compensation timescale (T_c) are equal within a factor of 2 (Straub *et al.*, 2020; Toby *et al.*, 2022). Therefore, when both these timescales are exceeded, basin-wide topography and strata are set by allogenic forcing (Straub *et al.*, 2020; Toby *et al.*, 2022). In terms of signal propagation and preservation, the exchange of sediment over timescales smaller than T_{eq} must occur through stochastic processes such as channel migration and avulsion. High-frequency sediment flux signals will be shredded by autogenic processes, however, signals with periodicity that exceed the thresholds for shredding will be buffered in a deterministic sense unless the period of the input signal exceeds T_{eq} (Straub *et al.*, 2020; Toby *et al.*, 2022).

1.4.3. Stratigraphic incompleteness

Signals with periodicity that exceed the thresholds for signal shredding (e.g. Jerolmack & Paola, 2010; Toby *et al.,* 2019) are not definitively preserved within stratigraphy due to the effects of stratigraphic incompleteness. Stratigraphers have long known that all stratigraphic sections are incomplete (Hutton, 1788; Ager, 1973; Sadler, 1981), as hiatuses permeate sedimentary records often with unknown duration. These hiatuses occur over a variety of spatiotemporal scales from laminae to basin scale unconformities, which reduce the preservation of time within stratigraphic sections (Sadler, 1981; Schumer & Jerolmack, 2009; Foreman & Straub, 2017; Davies *et al.*, 2019). Stratigraphic incompleteness is not just the result of erosion, but rather the combined effect of unsteady geomorphic processes causing variations in the frequency and magnitude of deposition, stasis and erosion due to internal system dynamics (i.e. autogenic processes) (Hajek & Straub, 2017; Kim & Jerolmack, 2008; Straub *et al.,* 2020; Straub & Foreman, 2018; Tipper, 2015). Autogenic reorganization of STSs causes wide areas of landscapes to be in stasis at one time (Ganti *et al.*, 2011; Tipper, 2015; Hajek & Straub, 2017), which coupled with periods of erosion leaves subtle hiatal surfaces within strata that in many cases can be difficult to identify (Sadler, 1981; Strauss & Sadler, 1989; Trampush & Hajek, 2017; Boulesteix *et al.*, 2019; Straub *et al.*, 2020). Therefore, the more intermittent the STS, the greater the opportunity for long-term hiatuses to form (Jerolmack & Sadler, 2007; Ganti *et al.*, 2020).

Stratigraphic incompleteness has further consequences for the detection of environmental signals from a time series of stratigraphic measurables (Romans & Graham, 2013), and raises fundamental questions regarding the reliability of strata as an archive of palaeo-Earth surface processes (Kemp, 2012; Hilgen *et al.*, 2015; Foreman & Straub, 2017; Trampush & Hajek, 2017; Duller *et al.*, 2019; Straub *et al.*, 2020; Tofelde *et al.*, 2021). The reconstruction of environmental signals from strata remains challenging even from a temporally complete stratigraphic record (Jerolmack & Paola, 2010; Toby *et al.*, 2019; Straub *et al.*, 2020), hence stratigraphic incompleteness can only hinder the reconstruction of environmental signals further. Stratigraphic dating limits means that sediment age is often assigned by linear interpolation between dated horizons (Abels *et al.*, 2010; Ramos-Vázquez *et al.*, 2017), providing additional challenges to the incompleteness problem by distorting the apparent representation of time in strata, relative to true time (Barefoot *et al.*, 2023). The uneven representation of time in strata can distort even relatively simple input signals within a time series rendering them undetectable in the output flux. Trampush & Hajek, (2017) demonstrated the significant alteration of a simple geochemical signal associated with the Paleocene-Eocene Thermal Maximum (PETM) as a result of stratigraphic incompleteness. The apparent period and amplitude of the PETM event preserved within synthetic sections differed substantially from the input signal where in the most extreme cases, the record failed to record any evidence of this extreme climate event.

As the uneven preservation of time can warp the representation of sediment flux signals in stratigraphy, the scientific community has focused efforts on constraining the timescale of discretization required to obtain a complete stratigraphic record and the signal duration necessary for confident signal extraction from proxy records. A first-order control on the incompleteness of the stratigraphic record relates to the timescales over which the record is discretized (Sadler, 1981; Sadler & Strauss, 1990). The durations of stratigraphic hiatuses within both numerical and physical experiments have been found to be heavy-tailed, where the chance of an exceptionally long hiatus increases with the duration of observation (Schumer & Jerolmack, 2009; Ganti *et al.*, 2011). This is because, over increasingly long-time windows, lateral migration of channels allows for sedimentation patterns everywhere in the basin to be equal. The truncation timescale of this distribution is set by the compensation timescale, T_c; at this timescale, stratigraphy follows a predictable pattern of compensational stacking. T_c represents the maximum timescale of autogenic organization in stratigraphy and denotes the maximum time window over which channels can rework previously deposited sediments (Sheets *et al.,* 2002; Ganti *et al.*, 2011; Wang *et al.*, 2011):

$$T_c = \frac{l}{r}$$

Where l is the maximum vertical roughness, often equated to the maximum channel depth, H_{max}, and r is the long-term aggradation rate. Up to T_c, a power law decay in deposition rate with measurement duration is observed. However, as measurement duration exceeds T_c, deposition rates become stable as the maximum autogenic timescale of the respective basin has been exceeded (Straub & Foreman, 2018). Therefore, T_c denotes the minimum discretization timescale necessary to obtain a complete stratigraphic record (Straub & Foreman, 2018).

Motivated by the finding that stratigraphic incompleteness can warp periodic input signals e.g. Trampush & Hajek (2017), Foreman & Straub (2017) quantified the minimum periodicity of an input signal required for confident signal extraction from a proxy record, where they found that T_c also provides a threshold for faithful signal transfer. External environmental perturbations with periodicity less than T_c cannot be recovered from individual sections without error and the potential for spurious signals. Once the periodicity of the perturbation exceeds T_c, sedimentary layers and associated proxies are available for sampling, however only when the periodicity is greater than $2T_c$ can the true signal be faithfully and consistently recovered from strata. This has significant implications for the preservation of high-frequency sediment flux signals within stratigraphy and demonstrates that only sufficiently long-duration signals should be preserved within a time series of stratigraphic measurables.

Whilst incompleteness has known consequences for the reconstruction of environmental signals, the impact of incompleteness on the spectral record of autogenic processes is currently unknown. This will allow robust confidence limits for signal detectability within environmental measurables to be established.

1.5. Structure and timescales of morphodynamic stochasticity in sediment transport systems

The thresholds and frameworks for signal propagation and preservation presented in section 1.3 (e.g. Foreman & Straub, 2017; Jerolmack & Paola, 2010; McNab *et al.*, 2023; Toby *et al.*, 2019) are defined by the spatiotemporal scales of autogenic processes within the STS in question. Therefore, the accurate detection of statistically significant cycles from a time series hinges on our ability to resolve the structure of the natural variance generated by autogenic processes (Weedon, 2003; Vaughan *et al.*, 2011; Meyers, 2012, 2019; Weedon *et al.*, 2019). The most commonly used statistical approach for quantifying autogenic variability and detecting imposed periodicity is the method of power spectral analysis (Butt & Russell, 1999; Roering *et al.*, 2001; Weedon, 2003; Aziz *et al.*, 2008; Vaughan *et al.*, 2011; Meyers, 2012, 2019; Abels *et al.*, 2013; Foreman & Straub, 2017; Hajek & Straub, 2017; Dunkley Jones *et al.*, 2018; Toby *et al.*, 2019; Burgess *et al.*, 2019; Lazarus *et al.*, 2019; Smith, 2020). This technique allows us to quantify the magnitude of autogenic variance as a function of frequency ('spectral power') (Weedon, 2003; Vaughan *et al.*, 2011; Meyers, 2019), where the background structure of the power spectra provides insight into the style, strength and timescales of autogenic dynamics in STSs (Jerolmack & Paola, 2007; Hajek & Straub, 2017).

The background structure of power spectra generated from a time series of environmental measurables is commonly found to be composed of red and white noise (Figure 1X). Red noise represents a simple stochastic process that is physically motivated by climatic and depositional system dynamics (Hasselmann, 1976; Sadler & Strauss, 1990; Weedon, 2003; Meyers, 2012).

In this thesis, red noise refers to the observation that spectral power increases as the frequency decreases; events are temporally correlated (Grumbacher *et al.*, 1993) and larger-scale fluctuations have larger characteristic timescales. In terms of sediment flux events, this highlights the occurrence of individual sediment flux events which gradually increase in mass and hence duration. White noise represents Earth system components with a slower response time (Meyers, 2012), and refers to the observation that spectral power is constant with increasing frequency (Figure 1X); events show no correlation and the time series is stationary (Grumbacher *et al.*, 1993). In terms of sediment flux events, this spectral regime highlights the occurrence of sediment flux events of all sizes and duration occurring randomly. Somewhat less regularly, blue noise is also found within some power spectra generated from environmental measurables (Fisher *et al.,* 1985; Petchey, 2000; Scheuring & Zeöld, 2001; Hajek & Straub, 2017). Blue noise occurs beyond the largest spatiotemporal scales of stochasticity and refers to the observation that spectral power decreases as frequency decreases (Figure 1X); events are temporally anti-correlated. In terms of sediment flux events, this means that after the largest event size has occurred, an event of the same duration and magnitude is improbable. Whilst the background structure of autogenic processes in different sediment transport routing segments may show similarity, the sediment transport processes that define the cause and extent of temporal correlation may vary.

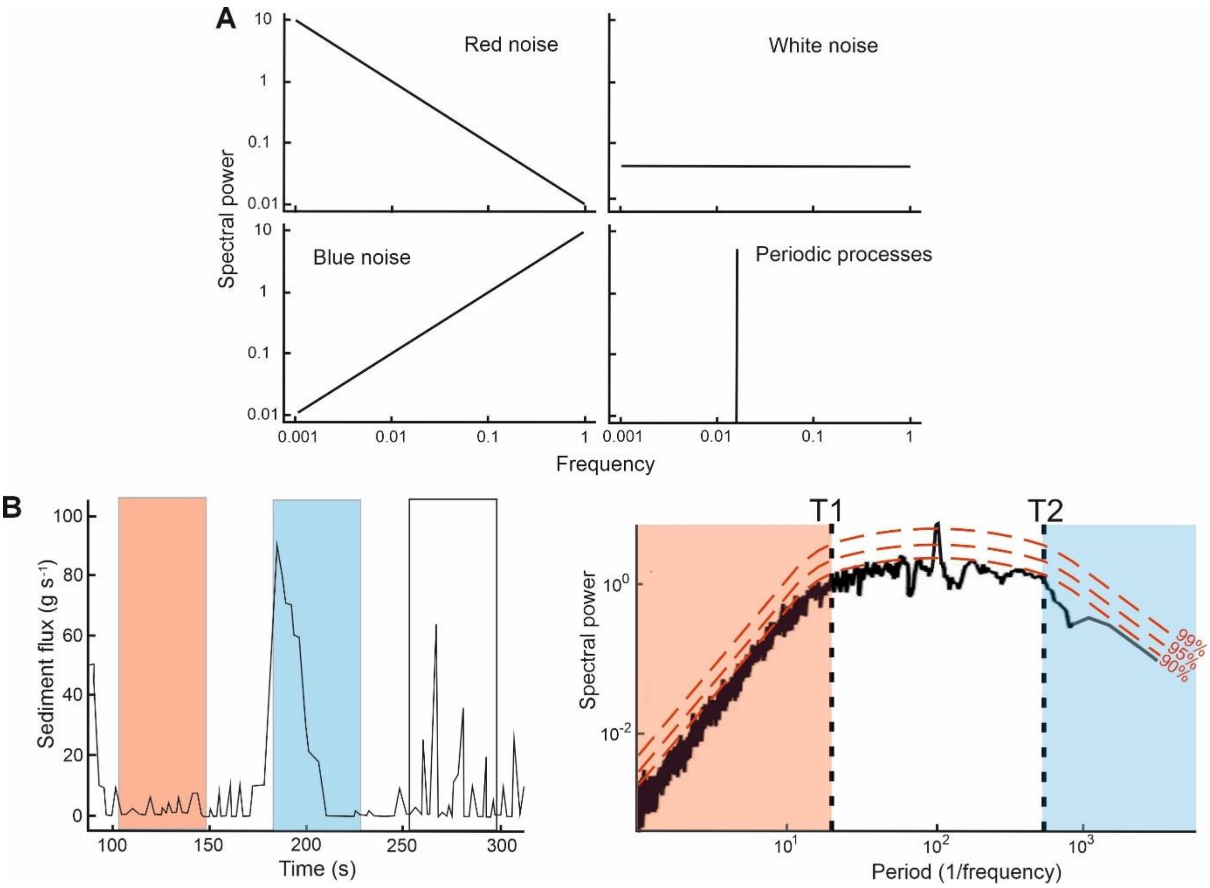

Figure 1.3: Illustration of the structure of noise within power spectra.

(A) Simplified diagrams highlighting the structure of noise found in natural systems. Red noise describes when spectral power decreases as frequency increases. White noise describes when power plateaus with frequency. Blue noise describes when power increases as frequency increases. The 'periodic' spectrum corresponds to a single peak at a given frequency. Adapted from Vaughan et al., (2011). (B) Example sediment flux time series highlighting the portions of the time series which contributes to generating the noise regimes seen within power spectra. Red noise is generated when sediment flux variations are consistently low, generating high frequency noise. White noise is generated when sediment flux events merge together; the onset of one event can trigger another event, increasing the duration and flux out of the system and causing randomness in event size. Blue noise is generated when a large sediment flux event occurs and is succeeded by much smaller flux events as the system regrades. This generates power spectra with a structure composed of red noise over short timescales, white noise over intermediate timescales and blue noise over long timescales. The breaks in spectral gradient (T1 and T2; vertical dashed lines) denote autogenic timescales within power spectra. Peaks in the power spectra linked to periodic signals can be differentiated from background noise by employing confidence levels. The spectrum shows a peak at 100s. The 90%, 95% and 99% confidence levels are shown (red dashed lines), and the spectral peak breeches the 99% confidence level.

The spectral gradient breaks between the various spectral regimes have been found to denote characteristic autogenic timescales (Figure 1.3) which provide the thresholds for signal propagation and preservation. Jerolmack & Paola (2007) found the spectral transition from red noise to white noise occurs at the maximum avulsion timescale (the longest timescale between avulsion events) within a numerical delta system. Similarly, Jerolmack & Paola (2010) defined T_x as the spectral transition between red noise and white noise within a numerical rice pile. Also, Hajek & Straub (2017) found the spectral transition from red noise to blue noise within an experimental delta to occur at the compensation timescale, T_c. This means that signals with periodicity that coincide with the timescales over which temporal correlation (red noise) occurs in a STS are likely to not be preserved in the output flux (e.g. the signals are shredded; Jerolmack & Paola 2010). Defining the spatiotemporal scales of morphodynamic stochasticity is critical to applying signal transfer thresholds to field-scale systems. However, at present, the theory to fully predict what a characteristic distribution shape should be for a given landscape under different boundary conditions is insufficient. Hence, it is critical to characterise the timescales and magnitude of autogenic fluctuations in landscapes with differing levels of stochasticity and understand how this distribution is preserved in strata.

Strictly periodic processes (e.g. those that repeat perfectly over a defined periodicity, e.g. environmental signals) produce a single narrow peak in a power spectrum (Figure 1X), where all the power is concentrated at one frequency (Vaughan *et al.*, 2011). Typically, in climate analysis, these are strongest within the Milankovitch bands. However, power spectra can be poor estimators of periodic processes when generated from a time series containing a strong random component, as power spectra generated from purely stochastic processes can contain narrow peaks that are difficult to distinguish from periodic processes. Therefore, to detect periodic signals, a frequency-dependent threshold is generated above which a random fluctuation in the power spectra is unlikely, namely confidence levels (Figure 1X). The autoregressive lag-1 (AR1) stochastic noise model (Gilman *et al.*, 1963) is the most commonly applied spectral estimation method applied for evaluating the presence of periodic processes in power spectra due to its simplicity (Weedon, 2003; Meyers, 2019). However, if the power spectra produced from real data do not share the same structure as an AR1 process, then recovery of environmental signals is fraught with error and spurious signals (peaks that breech the confidence level but arise due to stochastic variability rather than periodic processes). If confidence levels are to be meaningful, they must accurately reflect the background structure of the power spectra and should not artificially favour any region of the spectrum (Vaughan *et* *al.*, 2011; Meyers, 2012). As numerous studies aim to resolve allogenic signals that may have similar temporal and/or spatial scales to autogenic processes (e.g. Milankovitch scale orbital forcing; Aziz *et al.*, 2008; Abels *et al.*, 2013; Hilgen *et al.*, 2015), this highlights the requirement to define the temporal structure of autogenic processes and develop a model with a strong statistical fit to the spectral geometry, which will allow the accurate detection of environmental signals over all autogenic timescales.

1.6. Utilising physical and numerical experiments to study autogenic dynamics and signal propagation.

Theory and thresholds for the propagation and preservation of environmental signals have been developed using various numerical and physical scale models of STSs. This thesis utilises a suite of physical rice pile experiments and numerical sandpile experiments to test hypotheses on the propagation and preservation of periodic sediment supply signals across landscapes. As the timescales required for the largest components of STSs (e.g. rivers or delta systems) to self-organise are beyond the timescales of human observation and modern instrumental records, field scale systems are generally unsuitable targets to fully characterise the spectral structure of autogenic processes and the interaction between autogenic and allogenic processes (Paola *et al.*, 2009). To overcome this, physical and numerical experiments are utilised where boundary conditions and data collection resolution can be precisely defined.

One such genre of experiment, pertinent to this thesis, is granular avalanching experiments, encompassing both sand and rice piles. More than three decades ago, Bak *et al.*, (1987) proposed the theory of SOC as an explanation for the origin of spatiotemporal variance in natural systems using a numerical granular pile. They further observed how the addition of a singular grain could cause a multitude of collapse events on the pile whose size could vary from one cell in the model to the full length of the pile. The magnitude-frequency distribution of the collapse events on the pile was found to follow an inverse power law. After the largest collapse event, the system would self-organise to return to this critical threshold. SOC has been used to define the dynamics in many environmental systems, including but not limited to, earthquakes (Godano *et al.*, 1993), forest fires (Clar *et al.*, 1996), river meandering (Stølum, 1996), bank failures (Fonstad & Marcus, 2003; Croke *et al.*, 2015), riffle-pool sequences and other fluvial bedforms (Clifford, 1993), aeolian bedforms (Anderson, 1990) and sediment yield (De Boer, 2001).

Motivated by this study, numerical granular avalanching systems have since been utilised to further understand the fundamental behaviour of sandpiles (Hwa & Kardar, 1992; Christensen *et al.*, 1996; Frette *et al.*, 1996; Malthe-Sørenssen *et al.*, 1999; Manna, 1999). Hwa & Kardar (1992) advanced on the work of Bak *et al.*, (1987) to quantify the underlying sediment transport mechanisms responsible for producing SOC in sandpiles. Power spectra generated from a time series of sediment flux from a numerical sandpile exhibit three spectral regimes, where each regime denotes different sediment transport mechanics. Firstly, the correlated region over short timescales denotes isolated avalanche events with an upper cut-off time equal to the maximum duration of one avalanche. Secondly, over intermediate timescales, an uncorrelated regime persists, which occurs due to the interaction (merging) of avalanches. Thirdly, over the longest timescales an anti-correlated regime persists where the sandpile encounters avalanches on the order of system size. The existence of these system scale events is a unique feature of systems with threshold instabilities (Hwa & Kardar 1992). Jerolmack & Paola (2010) advanced on the theory presented by Hwa & Kardar (1992) with an application to understanding signal propagation through STSs, from which they devised their signal shredding framework (mentioned in section 1.3.2).

Rice piles are able to elucidate the nature of autogenic processes and offer a rich suite of autogenic statistics that arise from sediment storage and release along a 1D transport path, analogous to sediment transport along a 2D transport path in field scale systems. Hence these systems provide a basis from which STSs and strata can be understood. However, previous theory has been developed solely from numerical granular systems, which evolve in relation to user-defined thresholds which control the propagation of particles through the system rather than natural physical thresholds. Furthermore, numerical granular systems have strict sediment transport thresholds, where grains cannot leave the system without experiencing at least temporary storage. In physical systems, grains have the capacity to propagate down-system with minimal storage, allowing the full range of sediment transport mechanics to occur (Benda & Dunne, 1997; Ganti *et al.*, 2013). These theories are yet to be tested on a physical rice pile, which does not suffer from these limitations.

1.7. Research questions

The aim of this thesis is to understand the nature of autogenic processes within STSs and quantify how these processes influence the ability of landscapes and stratigraphy to record evidence of external sediment flux signals. Physical and numerical granular avalanching experiments were used to address this aim by using time series analysis techniques to investigate the following research questions:

Research Question 1: *What is the spectral structure of autogenic processes in a STS and how do autogenic timescales control signal propagation and preservation?*

Autogenic processes operating within all STS control the transport of sediment from source to sink, hence to understand signal preservation potential, the nature of autogenic processes must first be quantified. The duration and magnitude of stochastic Earth surface processes, relative to environmental signals, impacts our ability to separate signal from noise in landscapes and strata. Therefore, quantifying the spatiotemporal limits of autogenic processes can provide insight into the thresholds for signals in geomorphic environments and strata. Research question 1 is addressed by the following objectives:

> Objective 1.1: To characterise the full temporal structure and the timescales of autogenic processes within a physical rice pile.
>
> Objective 1.2: To delimit the scaling controls on the temporal structure and autogenic timescales.
>
> Objective 1.3: To define thresholds for the degradation and detectability of external environmental signals over the full range of autogenic timescales.

Research Question 2: *How does stratigraphic incompleteness influence the preserved structure of autogenic processes and influence signal detectability?*

Records of stratigraphic measurables measured in the field from which power spectra are generated are temporally incomplete over a range of scales, due to both stasis and erosion as a result of autogenic processes removing time from stratigraphic sections. Quantifying the impact of incompleteness on the preservation of paleo Earth surface processes, and hence the recovery of environmental signals, provides understanding as to which records best preserve evidence of paleoenvironmental variability. Research question 2 is addressed by the following objectives:

Objective 2.1: To investigate how incompleteness over varying scales influences the preservation of the full temporal structure and timescales of autogenic processes in stratigraphy.

Objective 2.2: To investigate how sampling resolution and interpolation of an incomplete time series influences the record of surface processes and autogenic timescales preserved.

Objective 2.3: To quantify the effect of incompleteness and interpolation on the detectability of periodic sediment flux signals over the full range of autogenic timescales.

Research Question 3: *How does the magnitude of autogenic noise within a STS influence the degradation and detectability of environmental signals?*

The duration and magnitude of sediment storage and release varies between geomorphic environments, hence the magnitude of autogenic noise, and the potential for signal detection, varies spatially within landscapes. Understanding the sensitivity of STSs which promote more continuous, faster sediment transport to environmental signals can provide insight into which STS segments may best preserve evidence of high frequency environmental change. Research question 3 is addressed by the following objectives:

Objective 3.1: To compare the full temporal structure and the timescales of autogenic processes within a numerical granular pile to that of the physical rice pile.

Objective 3.2: To explore how signal degradation and detectability is influenced by the magnitude of autogenic noise.

Objective 3.3: To investigate the occurrence of resonance within STS.

Objective 3.4: To evaluate the use of DEM’s to simulate physical experiments.

1.8. Thesis structure

This thesis is presented as a series of academic papers. Therefore Chapter 3-5 present methods, results, contextual literature and discussion which refer to one or more of the research questions outlined in section 1.7, so there is inevitable repetition of key concepts throughout this thesis. This thesis includes three manuscripts, but Chapter 3 and Chapter 4 have been published; hence these chapters have been modified to keep with the formatting of the rest of the thesis. The status of each manuscript and author contributions are stated in section 1.9. All references have been grouped into an ensemble reference list at the end of this thesis. Experimental metadata are given in Appendix 1; these are available from the Harvard Dataverse online repository (Griffin & Straub 2023). A list of symbols and acronyms is given in Appendix 2.

Chapter 1 provides an introduction, overview and rationale for this thesis, illustrating the wider context and a broad overview of the autogenic and allogenic controls on STSs. Most importantly, this chapter introduced the impediments to environmental signal propagation and preservation in both landscapes and strata caused by stochastic autogenic processes. The overall aim of this thesis, and individual research questions are outlined.

Chapter 2 outlines the theoretical background to the experiments and the methodology utilised in this thesis. The physical rice pile apparatus is outlined, and the calibration experiments and results are explained. The set-up of the discrete element model (DEM) utilised for the numerical granular experiments is also outlined. Finally, an overview of the time series analysis techniques used throughout this thesis are given.

Chapter 3 addresses research question 1. This paper utilises a physical avalanching rice pile to characterise the temporal structure of autogenic processes within STS and introduces a new theoretical framework that utilises key autogenic timescales to set temporal limits on the degradation and detection of sediment flux signals.

Chapter 4 addresses research question 2. This paper utilises the suite of physical rice pile experiments presented in Chapter 3, from which time is systematically removed to quantify the implications of incompleteness and imperfect sampling. From this, a theoretical framework is developed that enables scientists to both predict the detectability of a particular environmental signal and reconstruct signal properties using an estimate of completeness.

Chapter 5 addresses research question 3. This paper utilises a suite of numerical granular pile experiments, where the sandpile is generated as a discrete element model and utilises spherical grains to model systems with a high concentration of suspended sediment. The results of the numerical system are compared to the physical rice pile to show how the magnitude of storage and release processes operating within STSs controls the degradation and detectability of environmental signals.

Together, Chapter 3 to 5 provide a thorough understanding of the nature of autogenic processes operating within the Earth's surface and their controls on the propagation, degradation and detection of environmental signals thesis.

Chapter 6 concludes the thesis by summarising the results of the individual papers (Chapters 3 to 5), synthesising these in reference to the original aim of this thesis and provides an extended discussion on the wider implications of the research and avenues for future work.

1.8.1. Publication status of the chapters

Chapter 3: Griffin, C., Duller, R.A., & Straub, K.M (2023). The degradation and detection of environmental signals in sediment transport systems. *Science Advances*, v. 9 (44), p. 1-11, doi/10/1126/sciadv.adi8046

Status: Published in *Science Advances*

Submitted: 21.08.2023

Published: 04.11.2023

The author contributions to this chapter are as follows:

R.A.D and K.M.S conceived the initial idea of the study
C.G. lead the development of the experimental matrix with input from R.A.D and K.M.S
C.G. and K.M.S. ran the suite of rice pile experiments.
All authors contributed to the data analysis and interpretations
C.G. wrote the manuscript with edits provided by R.A.D and K.M.S
C.G. revised the manuscript after review with edits provided by R.A.S and K.M.S

Chapter 4: Griffin., C., Duller, R.A., & Straub, K.M (2024). The incomplete record of autogenic processes sets limits on signal detectability. *Journal of Geophysical Research: Earth Surface*, v 129 (4), e2023JF007538

Status: Published in *JGR: Earth Surface*
Submitted: 14.11.2023

Published: 01.04.2024

The author contributions to this chapter are as follows:

C.G. conceived the initial idea of the study
C.G. lead the development of the experimental matrix with input from R.A.D and K.M.S
C.G. and K.M.S. ran the suite of rice pile experiments.
All authors contributed to the data analysis and interpretations
C.G. wrote the manuscript with edits provided by R.A.D and K.M.S

Chapter 5: Turning the volume down: How does the magnitude of autogenic noise in a sediment transport system influence the preservation of environmental signals?

Status: In preparation for submission to *JGR: Earth Surface*

The author contributions to this chapter are as follows:

C.G. conceived the initial idea of the study
C.G. lead the development of the experimental matrix with input from J.E.H, R.A.D and K.M.S
C.G. and J.E.H ran the suite of MFiX-DEM experiments.
C.G. and K.MS. ran the suite of rice pile experiment
All authors contributed to the data analysis and interpretations
C.G. wrote the manuscript with edits provided by R.A.D and K.M.S

1.8.2. Published datasets

Griffin, C., Straub, K. M., 2023. Physical rice pile experiments, Harvard Dataverse

All data can be accessed at https://dataverse.harvard.edu/dataset.xhtml?persistentId=doi:10.7910/DVN/SO5XJP under the dataset Rice Pile Experiments conducted at Tulane University in 2022.

Author contributions to the experiments are as follows:

Chloe Griffin and Kyle Straub – conducted experiments

2. Methods

2.1. Experimental background

To quantify the structure and timescales of autogenic processes and their control on the propagation of external environmental signals under controlled input conditions, this project primarily utilises a suite of physical rice pile experiments alongside a numerical granular avalanching system. Both granular piles offer the opportunity to quantify a rich suite of autogenic statistics due to sediment storage and release along a 1D path, analogous to sediment storage and release along a 2D path in field scale routing systems. Using a system with simple operation procedures, the interaction between autogenic processes and external environmental signals over measurable timescales can be studied.

The work of Jerolmack & Paola, (2010) forms a basis for the experimental set up and matrix utilised in chapters 3 to 5. The structure and timescales of autogenic processes within the numerical avalanching rice pile were quantified using a time series of efflux, and used to propose a framework for the propagation and storage of environmental signals. From an experiment run under constant input rate, the structure of autogenic noise exhibits two regimes: temporal correlation (red noise) over short timescales transitioning to no correlation (white noise) over all succeeding timescales. The transition between the noise regimes denotes the saturation timescale T_x, which is noted to scale as L^2/q_0, where L is system length and q_0 is input rate (Jerolmack & Paola, 2010). T_x was defined as an upper temporal limit on the ability of autogenic processes to "shred" environmental signals, where the conceptual utility of this is that signals with periods greater than T_x are recorded in the output flux, whereas signals with periods less than T_x are shredded. However, shredded signals can be detectable in the output if the signal has sufficient magnitude to overwhelm autogenic processes. This magnitude was proposed to scale as as $M \sim L^2S_c$, where S_c is the critical threshold slope, which at field scales approximates the volume of sediment required to be eroded for channel generation post-avulsion (Jerolmack & Paola, 2010).

Current work on the nature of stochastic processes relies heavily on numerical models of avalanching systems (Hwa & Kardar, 1992; Frette *et al.*, 1996; Jerolmack & Paola, 2010), however these systems rely on user-defined thresholds to control 'grain' propagation through the model domain and do not account for grain bypass. To overcome these limitations, this thesis utilises a physical rice pile which allows the natural dynamics of the system to be captured without user defined thresholds, and hence is more comparable to natural environmental systems. Using the rice pile, the temporal structure of autogenic processes and the dynamics operating at different temporal scales control the propagation of environmental signals can be explored and evaluated. In a similar manner to Jerolmack & Paola (2010), signal periodicity was scaled relative to the autogenic timescales within the rice pile, and signal magnitude was scaled as percentages of the mean feed rate.

Chapter 5 utilises a different methodology; a granular pile built as a discrete element model (DEM). The DEM system is built to the same geometry as the physical rice pile apparatus, and evolves by natural thresholds defined in the governing equations.

2.2. Physical rice pile experiments

The suite of rice pile experiments used in this thesis was conducted in the Sediment Dynamics Laboratory at Tulane University. The experimental apparatus is constructed of two vertical, parallel glass sheets 0.37m long, positioned 0.026m (Figure 2.1). Rice was fed to the pile from a dry particle feeder (Schenk Accurate) positioned 0.008m from the top surface, allowing a rice pile to form at a critical angle so that a dynamic topographic equilibrium was achieved. Rice input to the system was controlled at 1 second intervals via a computer connected to the sediment feeder which directly feeds the pile. Over the suite of experiments, influx was defined between the minimum and maximum range available on the sediment feeder (0 g s^{-1} and 0.78 g s^{-1}). Efflux was measured using an Ohaus EX12002 balance (accuracy and precision of 0.1 grams) and recorded at approximately 1 s intervals. The balance has a maximum mass of 12 kg, and all experiments were run until the balance was saturated. The dimensions of rice grains used in the experiments have a diameter of 0.0025±0.5 m, length of 0.008±0.5 m and a mass of 0.02 g (Table 2.1). The experimental set-up used here is similar to that of the physical rice pile of Frette *et al.,* (1996).

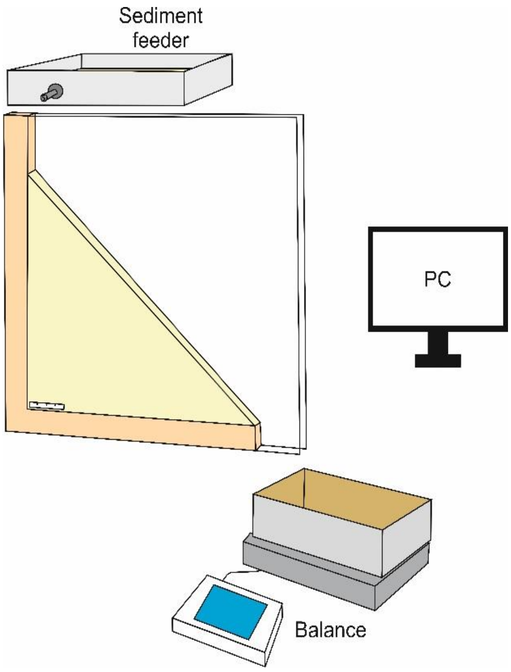

***Figure 2.1**: Schematic diagram of the physical rice pile experiment.*

Rice is fed directly from the sediment feeder between two glass sheets, separated to create a channel in which a rice pile can build. Input rate can be controlled through a computer interface. Efflux from the pile is measured cumulatively every second. Diagram not to scale.

Table 2.1: Characteristics of the rice used in the experiments

Name	Par Excellence ® Premium Brown Rice
Description	Long grain, parboiled
Length	0.008 ± 0.5 mm
Width	2.5 ± 0.5 mm
Aspect ratio	3.2
Average mass	0.195 g
No. density	0.78 ± 0.1 g/cm^3
Angle of repose	45-47°

To ensure the efflux data are driven only by the internal autogenic dynamics of the rice pile and not triggered by external noise, accelerations were analysed within the room when the sediment feeder was on and off, when sediment feeder was on but with no rice delivery, and when rice was delivered. Accelerations were measured using the Phyphox application on iPad, which records x, y and z accelerations at an increment of ~0.05 seconds to two significant digits of acceleration with SI units. The raw acceleration data, alongside power spectra of the time series, were analysed to confirm external vibrations were not triggering avalanches, or that external vibrations did not occur at repeating frequencies (Figure 2.2)

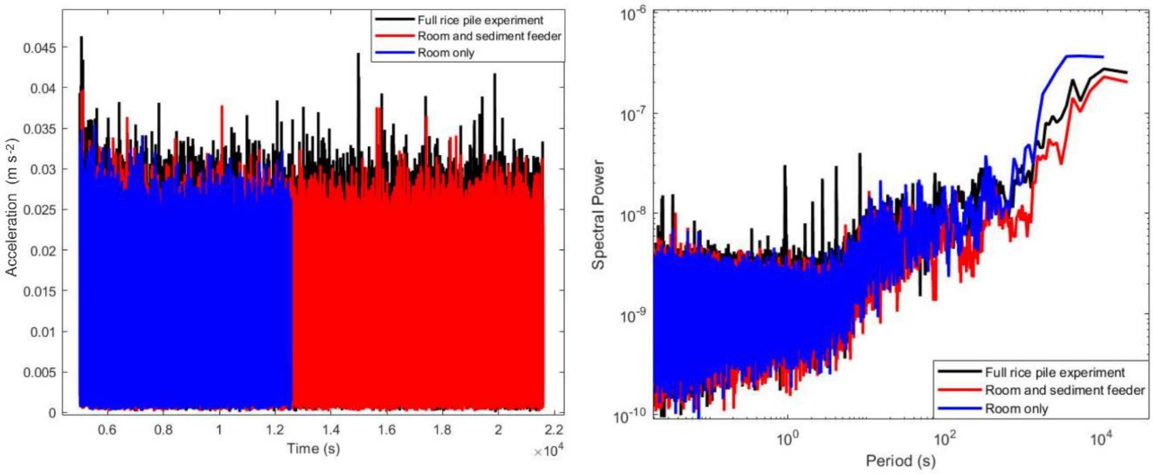

Figure 2.2: Acceleration analysis to ensure the dynamics evident are inherent to the rice pile

Left: Raw acceleration time series for the room only, the room and the sediment feeder with no rice pile and then over the duration of a full experiment. Right: Power spectra (generated using the Multi-taper (MTM) method with 2 tapers) of the acceleration time series for all three scenarios. Neither the raw time series nor power spectra show evidence of external noise occurring at repeating frequencies.

A series of experiments were conducted where rice was fed directly from the sediment feeder to the scale, to confirm high temporal control over the driving rates and cycles imposed. Power spectra were generated from the time series, which confirms white noise was present across all frequencies, except a spike in power if periodicity was imposed (Figure 2.3)

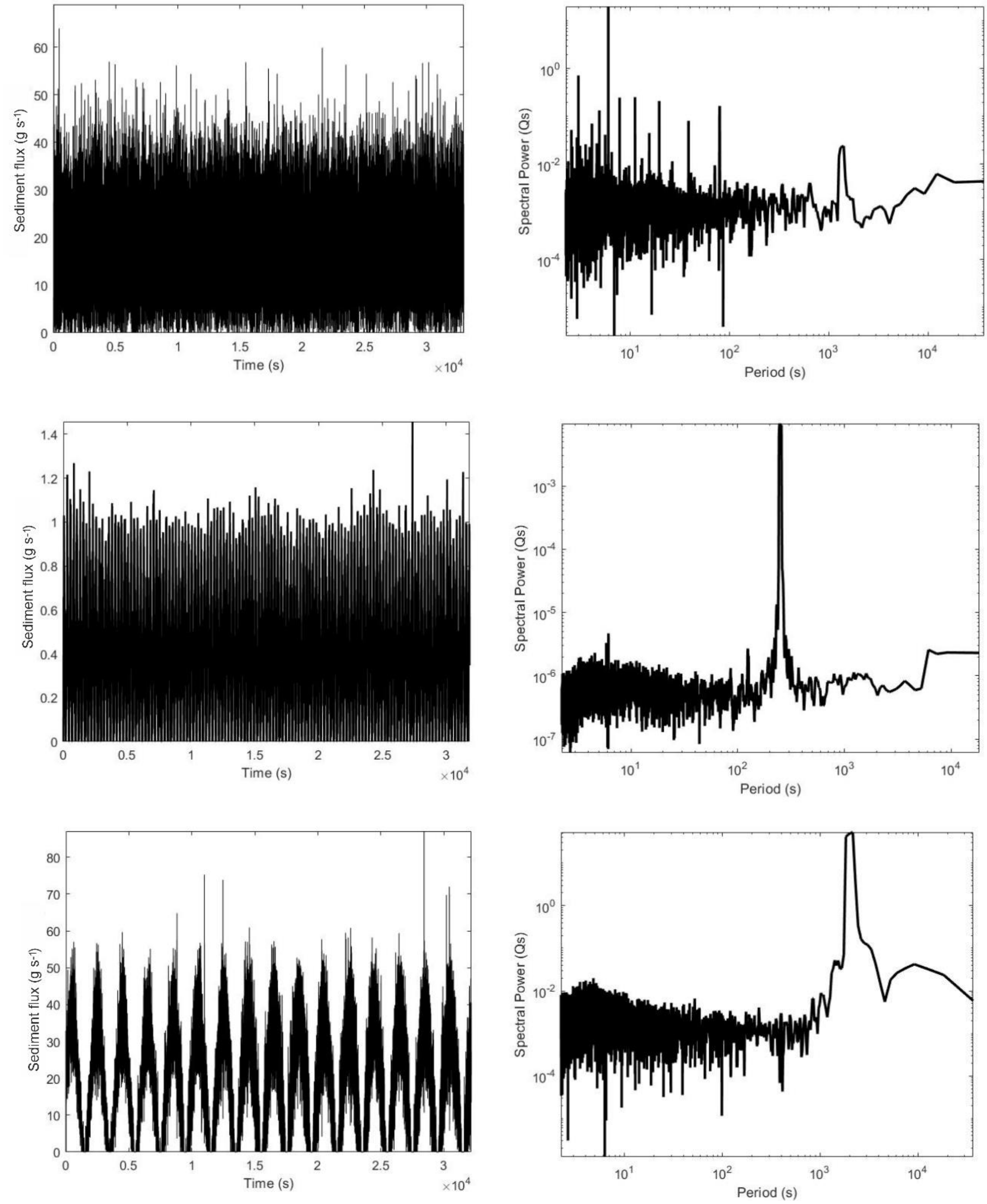

Figure 2.3: Time series and power spectra from three calibration experiments where rice was fed directly from the sediment feeder to the scale.

Top: Cyclic experiment (periodicity 6s, amplitude 0.37 g s^{-1}*), with a signal evident at 6s. Middle: Cyclic experiment (periodicity 250s, amplitude 0.37 g* s^{-1}*), with a signal evident at 250s. Cyclic experiment (periodicity 2000s, amplitude 0.37 g* s^{-1}*), with a signal evident at 2000 s.*

2.3. Discrete element modelling

The numerical sandpile experiments were performed using MFiX: Multiphase Flow with Interphase eXchanges, created by the National Energy Technology Laboratory (NETL). MFiX (https://mfix.netl.doe.gov) is a general purpose open-source computer code, written in Fortran, used for modelling the hydrodynamics, heat transfer and chemical reactions in fluid-solids systems (Xu *et al.*, 2017). MFiX can be used to model both fluids and solids using two-fluid models (TFM) continuum discrete methods (CDM) or discrete element models (DEM) from a single source code. The geometry and boundary conditions of the model can be controlled using the graphic user interface (GUI), allowing precise conditions to be established. The discrete element method (MFiX-DEM) was employed to generate the quasi-2D granular pile. The DEM can describe solid flows at a particular level, using a Eulerian reference frame for the continuum fluid and a Lagrangian discrete framework for the particle phase (Garg, 2013). DEM simulations can provide noteworthy insights that are unattainable through physical experimental methods (Marchelli & Di Felice, 2021).

The DEM is a popular numerical technique, originally applied by Cundall, (1971), for computing the behavior of discrete particles. Individual, or clusters of, computational particles compose the solid phase of the DEM, where each individual particle trajectory can be tracked. The DEM resolves particle-particle collisions with small time steps, allowing a high level of accuracy at a cost of being computationally expensive (Garg *et al.*, 2012; Li *et al.*, 2012; Lu *et al.*, 2022). The trajectory, linear and angular velocities of each particle are predicted through its Newtonian linear and rotational motion equations (Gopalakrishnan & Tafti, 2013; Marchelli & Di Felice, 2021). For simplicity, each particle is assumed to have the same density (ρ) and diameter (d). The motion of a particle (a) with mass (m), moment of inertia (I) and coordinate (r) are described by Newton's equation for rigid body motion:

$$m\,\frac{d^2r}{dt^2} = F_{g,a} + F_{c,a} \tag{1}$$

$$I\,\frac{d\omega_a}{dt} = T_{cp} \tag{2}$$

Where ω_a is the angular velocity of the particle and T_{cp} is the torque acting on the centre of mass of the particle. The terms on the right-hand side of equation 1 account for the gravitational force and the sum of individual contact forces exerted by every other particle in contact with particle a (Xu *et al.*, 2017).

Collisions between individual particles or between the particle and the domain boundary are calculated using the soft-sphere approach of Cundall & Strack (1979). In the soft-sphere model, particle slightly overlap during contact (Marchelli & Di Felice 2021). In the MFiX-DEM, a linear spring dashpot soft sphere model is used to calculate the collisional force $F_{c,a}$. Here, the total contact force on an individual particle is the sum of the normal and tangential forces with its directly neighbouring particles (Xu *et al.*, 2017).

$$F_{c,a} = \sum\nolimits_{b \in B} (F_{n,ab} + F_{t,ab}$$

Where b is another particle in the model and B is the set of particles in contact with particle a (Xu *et al.,* 2017). The full details of the governing equations and a detailed verification study of the MFiX-DEM was pursued by (Li *et al.,* 2012).

The granular pile was built using a 3D computational domain replicating the physical experiment, with dimensions of 0.3 x 0.3 x 0.02 m (Figure 2.4). The domain geometry is discretised by a non-uniform grid of 20, 10 and 5 cells in the X, Y and Z directions respectively. The walls of the domain utilise the non-slip boundary condition. Particles enter and leave the domain via a defined inlet and outlet region. The point-source inlet is generated as a 0.008 x 0.006 m region, allowing only individual particles to enter the domain, increasing accuracy in the input rate. The inlet has a mass flow boundary condition and the outlet has a pressure outflow boundary condition which spans the open down-system end of the domain. Spherical grains with a diameter and density of 0.003 m and 1500 kg m^{-3} respectively are used as the granular medium. The particle input parameters utilised in the DEM can be found in Table 2.2 Grains are fed into the system from the inlet at the mass flow rate defined in the GUI. Input conditions to the system can be precisely controlled by defining an input rate in kg s^{-1}.

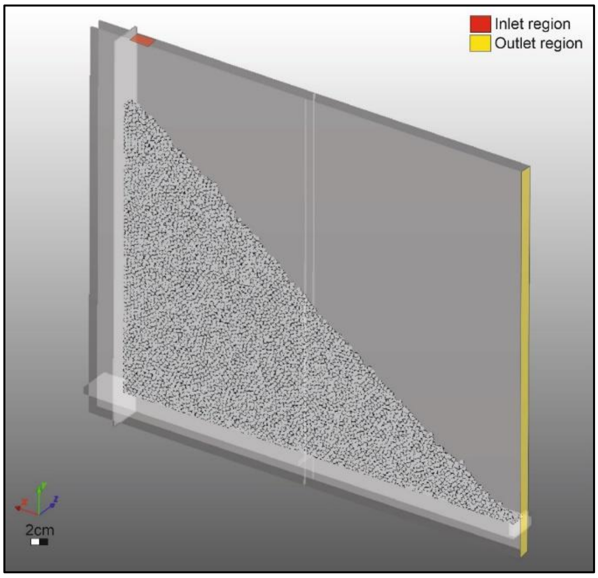

Figure 2.4: MFiX-DEM numerical granular pile domain

MFiX-DEM domain built to the same geometry as the physical rice pile. Grains enter the pile through the inlet region at the up-system end, and can exit through the outlet region. Each of the 11,311 particles in the model can be tracked via a coordinate axis system.

Table 2.2: Particle properties utilised in the MFiX-DEM

Particle Properties	
Diameter (m)	0.003
Density (kg m^{-3})	1250
Friction coefficient	0.7
Normal spring constant (N/m)	100
Spring norm/tan ratio	2/7
Damping norm/tan ratio	0.5
Coefficient of restitution	0.45

To reduce the computational time and to ensure each model run started with a granular pile in dynamic equilibrium, an initial run was completed to pre-assign the particles. This run was 150 seconds long, with a solid volume fraction of 0.1 and a mass flow rate of 0.01 kg s^{-1}, inputting 11,311 grains. At the end of the run, the particle coordinates were saved and velocities reset to 0, generating an input file used in all the experiments in chapter 5. Although the particles are pre-assigned to the model domain, at the start of each run the model takes approximately 2000s to stabilise. The total model run time was set to 30,000 s, with the first 2000 s discounted.

The DEM evolves under natural thresholds defined in the governing equations, which redistribute mass down the granular pile in the same manner as the physical rice pile system during the experiment. Efflux is not measured directly in the DEM; instead the number of particles in the model is differenced between each time step, generating an efflux time series over 28,000s. Throughout the model run, the evolution of the pile was monitored by saving data files at 0.001 second intervals. The data saved in the output files includes: particle ID, X, Y and Z velocity and X, Y and Z coordinates for each particle present.

The main limitation of the MFiX-DEM in regards to this thesis is that it is currently only capable of utilising spherical particles. Previous work utilising granular systems to understand self-organised criticality have utilised rice due to the high aspect ratio allowing interlocking behaviours and high intergranular friction which enables the system to become self-organised (Amaral & Lauritzen 1996). This interlocking behaviour is not possible with spherical grains, and previous experiments using rice with lower aspect ratios found the system did not evolve to a critical state (Frette *et al.,* 1996). Although grain shape cannot be modified currently, physical parameters in the model can be adjusted to increase the similarity of the behaviours: the friction coefficient (FC) and the coefficient of restitution (CoR). Each parameter has a range between 0 and 1, allowing intergranular friction and the nature of the granular interactions to be controlled. The ideal combination of parameters for this system was found using a sensitivity analysis: a detailed analysis is presented in Chapter 5.

2.4. Time series analysis

The conventional procedure for detecting evidence of periodic cycles within a time series generates a power spectrum with confidence levels. This technique allows the magnitude of autogenic variance to be quantified as a function of frequency ('spectral power') (Weedon, 2003; Meyers, 2019; Smith, 2023). The most common spectral estimation technique used to analyse climatic or depositional time series is the multi-taper method (MTM) of Thomson, (1982). The MTM generates an average power spectrum for an evenly sampled time series, where the spectrum does not prescribe an apriori model for the processes generating the time series. To achieve this, the time series is divided into a series of special data windows (tapers). These tapers individually suppress different parts of the time series to reduce the smearing of power across a range of frequencies that occurs when the signal being measured is not periodic in the sample interval. After each taper is applied, a power spectrum is generated from which an average spectrum is generated; this smooths out spurious irregularities and reduces the variance of the spectral estimation (Yiou *et al.*, 1996). The greater the number of tapers applied the greater the reduction in variance, however, a high number of tapers can make spectral peaks appear as flat-topped (quasi-periodic) rather than clear spikes (periodic) (Weedon, 2003). The MTM method represents a good method for producing spectral estimates with high-frequency resolution and low bias, which is essential in cases with low signal-to-noise ratios (Mann & Lees, 1996). As the MTM can only be applied to evenly sampled time series, Chapter 4 applies the Lomb-Scargle Periodogram (LSP) as the time series utilised is non-linear. The LSP is the best-known algorithm for detecting and characterising periodicity in unevenly sampled time series (VanderPlas, 2018).

In the mixed power spectra encountered in stratigraphic analysis (where the spectrum is generated from both random and periodic components), spectral peaks related to the spectral background must be differentiated from statistically significant periodicity. Originally, statistically significant peaks within a power spectrum were picked out by eye however more recently an estimate of the spectral background structure has been generated from which associated confidence levels are estimated (Weedon, 2003). A confidence level of 95% implies that 5% of the data above this level is random variance (Vaughan *et al.*, 2011). Below the confidence level data is assumed to be stochastic variance, whereas spectral peaks emerging above the confidence level are considered to be statistically significant periodicity (Weedon, 2003). To make a statistical statement about the presence of imposed periodicity within the power spectra generated from the physical rice pile experimental confidence bands were generated from 25 realizations of a rice pile experiment run under a constant input rate. Numerical confidence bands were generated by constructing a spectral model and suite of associated confidence bands through adaptation of the bending power law (BPL) model (McHardy *et al.*, 2004) to account for two spectral gradient breaks.

3. The degradation and detection of environmental signals in sediment transport systems

This chapter has been published as: Griffin, C., Duller, R.A., & Straub, K.M (2023). The degradation and detection of environmental signals in sediment transport systems. *Science Advances*, v. 9(44), p.1-11, doi/10/1126/sciadv.adi8046.

Abstract

Autogenic processes contribute noise to sediment transport systems that can degrade or mask externally-derived environmental signals and hinder our ability to reconstruct past environmental signals from landscapes and strata. To explore this further efflux is measured from a physical rice pile to ascertain the temporal structure of autogenic noise, and how this influences the degradation and detection of environmental signals. Our results reveal a tripartite temporal spectral structure segmented at two key autogenic timescales. The shorter autogenic timescale set limits on environmental signal degradation, while the longer autogenic timescale sets limits on environmental signal detection. This work establishes a framework that can be used to explore how autogenic processes interact with external environmental signals in field-scale systems to influence their detectability. We anticipate that the temporal structure and associated timescales identified will arise from autogenic processes in numerous sediment transport systems.

3.1. Introduction

Sediment transport systems (STSs) are sensitive to external environmental perturbations; these can be natural (e.g. related to climatic or tectonic processes) or anthropogenic in origin (Gomez *et al.*, 2007; Romans *et al.*, 2016; East *et al.*, 2018; Ibáñez *et al.*, 2019; Straub *et al.*, 2020). STSs respond and adjust to these perturbations in a number of ways and over a range of temporal and physical scales (Romans *et al.*, 2016; Toby *et al.*, 2019). A fundamental response of a STS to these perturbations is a variation in the generation of sediment supplied to the STS and transmitted down-system as an environmental signal (Straub *et al.*, 2020; Tofelde *et al.*, 2021). These environmental sediment flux signals can generate geomorphic and stratigraphic signatures that allow for the reconstruction of past environmental perturbations (Castelltort *et al.*, 2015; Mahon *et al.*, 2015; Harries *et al.*, 2019; Sharman *et al.*, 2019; Straub *et al.*, 2020; Tofelde *et al.*, 2021) and provide insight into the response of landscapes to future environmental change (Knight & Harrison, 2013; Duller *et al.*, 2019).

However environmental sediment flux signals can undergo varying degrees of modification during their propagation through STSs and to strata (Jerolmack & Paola, 2010). This is primarily due to episodes of sediment storage and release that occur along the length of STSs in a stochastic manner and are referred to as autogenic processes (Jerolmack & Paola, 2010; Romans *et al.*, 2016; Hajek & Straub, 2017; Straub *et al.*, 2020). Even under constant boundary conditions, autogenic processes induce sediment storage and release over a range of spatio-temporal scales (Anderson & Konrad, 2019; Armitage *et al.,* 2011; East *et al.*, 2015; Hajek & Straub, 2017; Jerolmack, 2011; Kim & Jerolmack, 2008; Pelletier *et al.,* 2015; Powell *et al.,* 2012; Vercruysse *et al.,* 2017), from centimeter-scale bedforms migrating over seconds (Ganti *et al.,* 2013; Leary & Ganti, 2020; Muto *et al.,* 2007; Paola, 2016; Zlatanović *et al.,* 2017) to delta lobes avulsing hundreds of kilometers over millennia (Brooke *et al.,* 2022; Chadwick *et al.,* 2020; Ganti *et al.,* 2016; Paola, 2016). This stochasticity means that a one-to-one correlation between a singular or periodic environmental perturbation, and a sedimentary-proxy record for the associated environmental sediment flux signal, is not guaranteed (Jerolmack & Paola, 2010; Foreman & Straub, 2017; Hajek & Straub, 2017; Straub *et al.*, 2020). Autogenic processes are a natural physical phenomenon that are ubiquitous across many landscapes and occur in the absence of external environmental perturbations (Hajek & Straub, 2017; Swanson *et al.*, 2019; Scheingross *et al.*, 2020). Autogenic processes are commonly associated with a self-organised behavior of STSs over sufficiently long timescales (Swanson *et al.*, 2019), where the time required for a STS to self-organise is scaled to the size of the system in question and the nature of the interactions between internal system components (Hajek & Straub, 2017). The self-organization of a physical system can be viewed as a statistical property (Phillips, 1999) and as a measurable property. Examples of the latter include the regular spacing of point bars in meandering rivers (Hajek & Straub, 2017), the size distribution of sediment storage and release events from a time series of sediment flux, or the organization of surface topography and strata (Dodds & Rothman, 2000; Paola, 2016).

We note that many measurable attributes of STSs follow heavy-tailed distributions that are truncated at the upper end (e.g. the magnitude of erosional and depositional events, (Ganti *et al.*, 2011). The shape of this distribution is determined by the specific transport mechanisms and depositional dynamics, and the upper truncation is due to the bounding effect of system size that sets a physical limit on the spatiotemporal scales of autogenic processes (Ganti *et al.*, 2011). In the broadest sense, self-organization is an emergent property of a system that can be used to make predictions about the overall behavior of a system (Hajek & Straub, 2017;

Phillips, 1999). However, autogenic processes also contribute noise to a STS in the form of autogenic sediment flux or 'natural variability in sediment flux' (Kim & Jerolmack, 2008; Van Dijk *et al.*, 2009; Jerolmack & Paola, 2010; Van De Wiel & Coulthard, 2010; Ganti *et al.*, 2014; Castelltort *et al.*, 2015; Paola, 2016; Romans *et al.*, 2016; Hajek & Straub, 2017), which will also impart variability to strata (Burgess *et al.*, 2019; Burgess, 2006; Foreman & Straub, 2017; Kim & Jerolmack, 2008; Toby *et al.*, 2019; Wang *et al.*, 2021). This noise can severely limit the identification of an environmental sediment flux signal either by obscuring it, i.e. the power of autogenic noise is greater than the environmental signal itself (Morris *et al.*, 2015); or by interacting with it to such an extent that no trace remains of the original signal (Li *et al.*, 2016; Simpson & Castelltort, 2012; Toby *et al.*, 2019), i.e. the signal is shredded (*sensu 34*). These two mechanisms are in operation simultaneously and will act to reduce the detectability of environmental signals from a time-series of sediment flux. However, the concepts of signal shredding and detectability have become somewhat intertwined, where all undetectable signals are considered shredded (Jerolmack & Paola, 2010; Lazarus *et al.*, 2019; Tofelde *et al.*, 2021). The relationship between these concepts, and a framework to predict when signals are shredded and/or undetectable, is not yet established.

To do this we use a physical rice pile as a rudimentary and idealised STS. Rice piles have previously been shown to exhibit a complex behavior (Bak *et al.*, 1987; Frette *et al.*, 1996) and are drawn upon to understand autogenic processes and environmental signal propagation through STSs (Jerolmack & Paola, 2010)**.** The aim here is to characterise the full temporal structure of autogenic noise and associated timescales from a physical model; and to understand how the periodicity and amplitude of imposed environmental signal interacts with the autogenic noise. This will provide a robust theoretical framework that can be used as a starting point to explore the autogenic temporal structure of field-scale STSs and how this information can be used to generate confidence limits of environmental signal detectability and thresholds of signal shredding (Hajek & Straub, 2017) in STSs and associated strata. More broadly, this is crucial to the accurate reconstruction of past environmental signals and to our ability to predict how environmental signals will interact with STSs over a range of timescales to garner a detectable (or not) response.

3.2. Theoretical background

The timescale required for the largest landscape components of STS (e.g. rivers or delta systems) to self-organise is beyond the timescales of human observation and modern instrumental records (Paola *et al.*, 2009), and so field scale systems are unsuitable targets to fully characterise the autogenic structure of STS and the interaction of autogenic processes with environmental signals. To overcome this, physical experiments and numerical models are used (Paola *et al.,* 2009). One such numerical experiment, and pertinent here, is a numerical 1D avalanching rice pile, which has offered key insights into the structure of stochastic noise (Hwa & Kardar, 1992) and the role of autogenic processes in environmental signal shredding (Jerolmack & Paola, 2010). The 1D numerical rice pile models, although rudimentary, elucidate the nature of autogenic processes and provide a basis from which natural STSs and strata can be understood (Foreman & Straub, 2017; Hajek & Straub, 2017; Toby *et al.*, 2019), especially with regards to environmental signal shredding and detectability (Jerolmack & Paola, 2010). Although these models capture the nature of stochastic dynamics well, one drawback is that they rely on user-defined thresholds to control the propagation of individual particles through the model domain rather than natural physical thresholds (Bak *et al.,* 1987). Additionally, numerical rice pile models do not allow for transport of grains out of the model domain without experiencing storage on the surface and contributing to the construction of topography until a critical angle is exceeded whereby an avalanche occurs. In natural systems, sediment has the capacity to propagate through a system with minimal storage or deposition which could enhance propagation and detection (Benda & Dunne, 1997; Ganti *et al.,* 2014). A key example of this is suspended sediment flux in rivers, which experiences significantly less storage than its bedload counterpart. Physical 1D rice piles do not suffer from these limitations and offer a richer suite of autogenic statistics that arises from sediment storage and release along a 1D transport path, analogous to sediment transport in a 2D path in field scale systems (Frette *et al.,* 1996; Jerolmack & Paola, 2010).

Jerolmack & Paola (2010) determined the structure and timescales of autogenic noise using a time series of efflux generated from a numerical avalanching rice pile model, and proposed a framework for the propagation and storage of environmental signals. In their study, the structure of autogenic noise was found to exhibit two regimes. The first regime comprises temporal correlation (red noise) over short timescales, where spectral power increases as a function of period. The second regime comprises zero correlation (white noise) over all succeeding timescales, where the spectral power plateaus. The transition between the red noise and white noise regimes denotes a characteristic timescale T_x, which was hypothesised to scale as $\sim L^2/q_0$, where L is system length and q_0 is input rate. T_x represents the upper temporal limit on the ability of autogenic processes to "shred" environmental signals (Jerolmack & Paola, 2010). Environmental signals with periods greater than T_x are recorded in the discrete time power spectral density of the efflux (hereafter, called power spectra), whereas those with periods less than T_x are shredded as the periodicity of the input signal is within the scale of individual sediment transport events in the system, obliterating evidence of the signal (Jerolmack & Paola, 2010).

Whilst the presence of white noise in STS is expected to persist over all timescales greater than T_x (Jerolmack & Paola, 2010), the results of other numerical sandpile models find the presence of blue noise (anticorrelation) over the longest timescales (Hwa & Kardar, 1992; Kutnjak-Urbanc *et al.,* 1996), where spectral power decreases as a function of period. The presence of anticorrelation within STS is due to the size constraints of a system which places an upper limit on the size of the largest sediment transport event (finite size effects). This finite size effect is reflected by a gradient break in the resulting power spectra at the transition from white noise to blue noise (Hwa & Kardar, 1992; Korup *et al.,* 2010; Ganti *et al.*, 2011; Straub & Esposito, 2013; Bracken *et al.*, 2015). Within the correlated regime (red noise), the system continues to operate in the same way as the previous time step (e.g. stabilization of channel networks on a delta which allow the system to generate consistently high sediment fluxes). However anticorrelation relates to a behaviour where the largest events are always followed by small events as the system regenerates or regrades over these longer timescales (Hajek & Straub, 2017). Anti-correlation or blue noise is common in power spectra from numerical sand and rice piles (Hwa & Kardar, 1992; Kutnjak-Urbanc *et al.,* 1996), ecological models (Petchey, 2000), ice-core analysis (Fisher *et al.,* 1985) and population dynamics (Scheuring & Zeöld, 2001), hinting at a universal structure due to the finite-size behavior of stochastic systems over their longest timescales.

In the same manner as T_x was defined by spectral gradient breaks (Jerolmack & Paola, 2010), the spectral gradient break from white noise to blue noise denotes the presence of another autogenic timescale, which was suggested to scale with a system-wide discharge event ($\sim L^2$) (T_c of Hwa & Kardar, 1992). The numerical rice pile investigations of both Hwa & Kardar (1992) and Jerolmack & Paola (2010) report a short autogenic timescale (i.e. transition from red noise to white noise) but a discrepancy exists in the definition and scaling of this fundamental timescale. Hwa & Kardar (1992) suggest that the transition from red noise to white noise scales as the maximum duration of avalanches (Hwa & Kardar, 1992), whilst Jerolmack & Paola (2010) suggest that this timescale represents a wedge-filling timescale on the order of

L^2 (T_x, Jerolmack & Paola, 2010). The latter definition overlaps somewhat with the definition of the longer autogenic timescale by Hwa & Kardar (1992)

The structure of autogenic processes (Hwa & Kardar, 1992) and the original framework for signal shredding (Jerolmack & Paola, 2010) is yet to be duplicated within a physical rice pile that evolves under gravity and hence is more comparable to natural STS. The physical rice pile is analogous to a single sediment routing system (Allen, 2017)**,** and the associated temporal structure and timescales of autogenic processes incorporates all of the autogenic variability this single sediment routing system can offer. The analogy of a rice pile as a single sediment routing system is therefore a simple one, but still offers a crucial insight into the autogenic dynamics of natural systems and their ability to shred or transmit environmental signals. Here we set out to clarify the origin and scaling of these autogenic timescales by resolving the temporal structure of autogenic processes using, for the first time, a 1D physical rice pile. To do this, a time series of efflux from the rice pile at discrete time intervals is utilised (Figure 3.1). This efflux time series is generated from stochastic avalanche dynamics within the rice pile and is a proxy for the autogenic dynamics operating within the Earth's surface. The characterizing the structure and timescales of autogenic dynamics within a system run under constant input rate, and this is used to understand the controls on signal shredding, by imposing signals with periodicity over the full range of autogenic timescales.

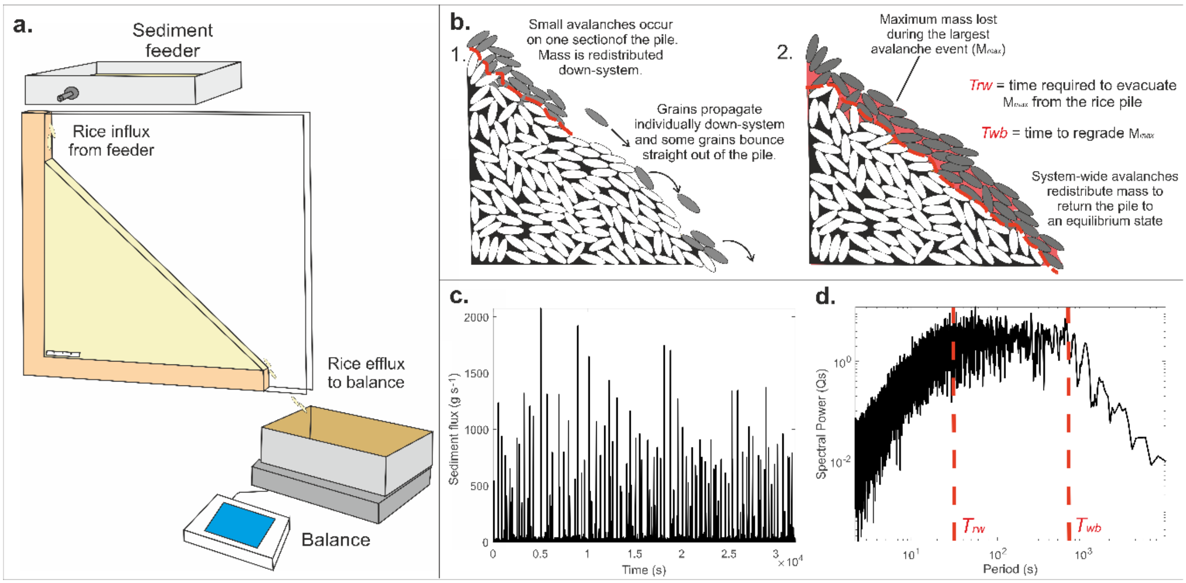

Figure 3.1: The geometry and nature of rice pile experiments.

(a) *Schematic diagram of the experimental rice pile set-up.* ***(b)*** *Spatiotemporal scales of avalanches within the rice pile; over short timescales* ***(b1)****, individual grains and small avalanches dominate the time series whereas over long timescales* ***(b2)****, avalanches on the order of system size occur.* ***(c)*** *Time series of efflux from the physical rice pile run under constant influx rate* ***(d)*** *Power spectra generated from the efflux time series. Autogenic timescales are defined according to spectral gradient breaks.*

3.3. Results

3.3.1. The temporal structure of autogenic processes

To understand how autogenic processes control signal propagation, we must first understand the inherent structure of autogenic processes and quantify the key autogenic timescales intrinsic to the physical rice pile. To do this, a time series of efflux measured at discrete time intervals is utilised, generated from multiple realizations of the control experiment (run under a constant feed rate of 0.37 g s^{-1}; ~18.5 grains s^{-1}). Constant influx to the physical rice pile generates a range of avalanche event sizes, from continuous small efflux events (e.g. 0.1 g s^{-1}; ~5 grains s^{-1}) to avalanches that span the entire length of the system (33-43 g s^{-1}; ~1650 – 2150 grains s^{-1}). The wide range of avalanche sizes that occur within the pile are generated from the pile fluctuating around a stationary critical state where localized, individual granular interactions can induce events of system scale. The probability distribution of these avalanches throughout the time series is heavy-tailed (Figure 3.2A), meaning that although the time series is dominated by small events (e.g. Figure 3.11, B1), an avalanche on the order of system size (e.g. a wedge failure event that returns the system to dynamic equilibrium; Figure 3.1, B2), has a small chance of occurring (Ganti *et al.*, 2011). The rich stochastic dynamics evident in the output from the physical system agree with the structure of the internal dynamics observed in numerical models (Bak *et al.*, 1987; Frette *et al.*, 1996; Malthe-Sørenssen *et al.*, 1999; Jerolmack & Paola, 2010).

The power spectra generated from the efflux time series from the constant influx experiment exhibit three noise regimes defined by two distinct changes in the gradient of the power spectra (Figure 3.2B). The first regime comprises red noise (temporal correlation), whereby spectral power increases as a function of period (with a spectral gradient, α, of 2.2), The upper temporal limit of red noise denotes a characteristic autogenic timescale, T_{rw}, which is approximately 30 seconds for this experiment. The second regime comprises white noise, which occurs over 30 to 650 seconds, where spectral power plateaus, indicating events over this timescale are temporally uncorrelated. The upper temporal limit of white noise denotes a characteristic autogenic timescale, T_{wb}, which occurs at approximately 650 seconds for this experiment. The third regime comprises blue noise over timescales greater than 650 seconds, whereby spectral power decreases as a function of period (with a spectral gradient, α, of -2), exhibiting anti-correlation in efflux.

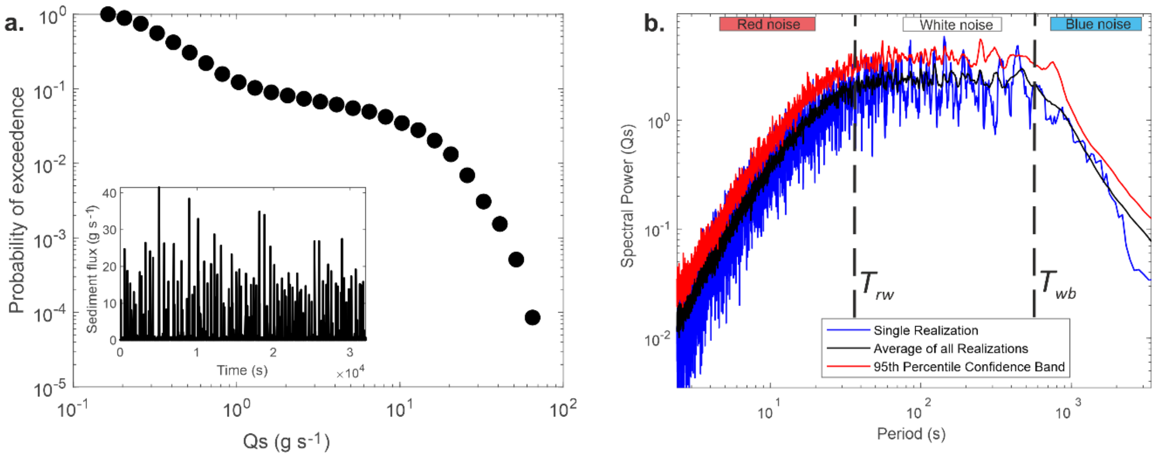

Figure 3.2: Time series analysis of mass efflux from the control experiment, where influx rate is 0.37 g s^{-1}.

(a) *Distribution of avalanche sizes throughout the time series, where the probability shows a heavy-tailed distribution.* ***(b)*** *Power spectra of the time series for one realization of the control experiment, generated by the multi-taper method, showing tripartite geometry composed of red, white and blue noise. Spectral gradient breaks between the regimes mark two timescales: T_{rw} and T_{wb}. This spectrum is compared to the mean spectra from all 25 realizations of the control experiment, with the 95% confidence band generated from the realizations displayed.*

These three noise regimes exist within the power spectra regardless of the absolute influx rate, Q_{in} (Figure 3.3A). However, we explore the controls on the absolute spectral duration of each regime and both autogenic timescales, T_{rw} and T_{wb}, using a suite of experiments run under a range of constant influx rates (Table S3.1). Firstly, we find that the red noise regime and the value of T_{rw} is insensitive to the influx rate and remain at a constant value of 30 seconds. In numerical sandpiles, this spectral regime was found to record the duration of individual avalanche events, where the duration of individual avalanches is directly proportional to avalanche size (e.g. mass effluxed). These individual events increase in duration until an upper cut off time is reached (Hwa & Kardar, 1992) which defines the maximum duration of an avalanche within the system and corresponds to the largest avalanche in terms of total mass liberated. Through examination of the efflux time series (Figure S3.1), this is also the case for the physical rice pile. The constancy of the value of T_{rw} reflects the fixed dimensions of the system and material properties of the rice material, which fixes the critical angle of repose and therefore sets the duration of the longest avalanche regardless of the influx rate. T_{rw} will vary between systems of different lengths (Hwa & Kardar, 1992). Over timescales greater than that of individual avalanche events (e.g. the white noise regime), avalanche of all sizes and duration coalesce, increasing the duration over which efflux occurs (Hwa & Kardar, 1992; Kutnjak-Urbanc *et al.*, 1996). In other words, the onset of one avalanche can instigate another avalanche, and so the efflux measured is the result of merged events. T_{wb} on the other hand, which sets the upper limit to the white noise regime, is influx rate dependent (Figure 3.3B). In numerical sandpiles, this longer timescale was suggested to scale with L^2 and influx rate, however the precise dependence was not determined (Hwa & Kardar, 1992; Kutnjak-Urbanc *et al.*, 1996). T_{wb} represents the time required for the influx to regrade the mass lost in the largest avalanche event (a regeneration timescale). The value of T_{wb} can be predicted by $T_{wb} = a.(M_{max}/Q_{in})$, where M_{max} is the maximum mass efflux over the longest avalanche event (defined by T_{rw}) and a is a parameter value that accounts for a bypass fraction of the efflux as the pile regrades; this is required as the rice pile is an open system and hence efflux still occurs whilst the mass regrades. Here, a has a value of 1.38±0.13 (n = 8). For this experiment, M_{max} is approximately 142 grams (Figure S3.1); this will be discussed later. Over timescales greater than T_{wb}, the rice pile experiences avalanches that are of the order of system size, which return the pile from the maximum to the minimum slope.

Figure 3.3: Time series analysis of efflux from four experiments compared to the control experiment. ***(a)*** *Power spectra of the time series, normalized by the mean spectral power from each experiment. Period is normalized by* T_{rw} *(~30 seconds).* ***(b)*** *Comparison of timescales* T_{rw} *and* T_{wb} *with changing input rate, where* T_{rw} *remains constant and* T_{wb} *decreases as a function of input rate. The dashed line shows the line of best fit for the variation in* T_{rw}*. The solid red line shows the fit of the equation* $T_{wb} = a*(M_{max}/Q_{in})$.

3.3.2. Shredding and detection of environmental signals

Given that autogenic processes can alter environmental signals, we explore how the sediment transport mechanics associated with each spectral noise regime control signal propagation and hence how both autogenic timescales, T_{rw} and T_{wb} set thresholds for signal shredding and signal detection. We define shredded environmental signals as those signals that have undergone a severe reduction in amplitude during propagation through the rice pile. From now on these will be referred to as degraded signals. We define detectable environmental signals as those signals

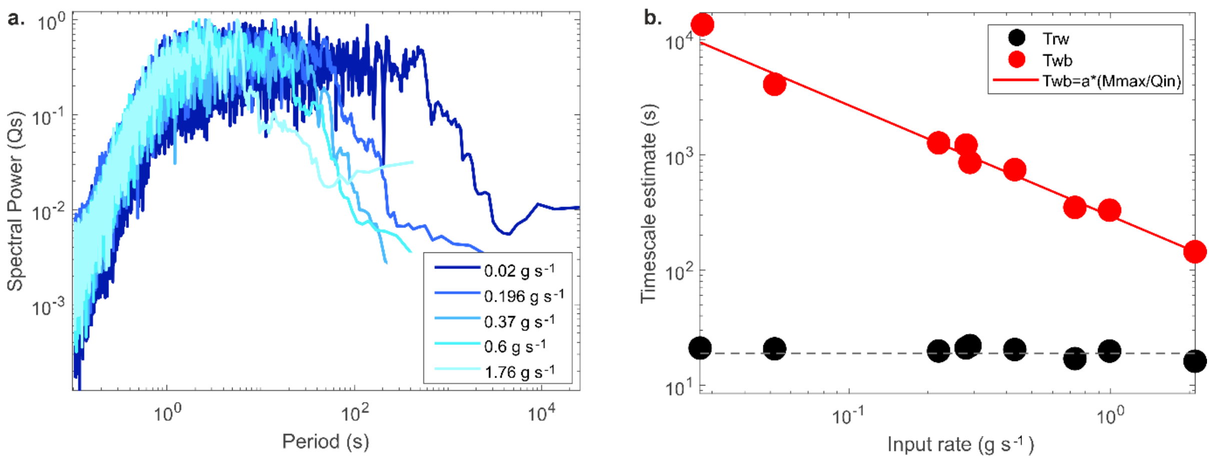

that produce a spectral peak within a power spectrum that exceeds the range of autogenic noise; this is defined statistically by the 95% confidence band. These concepts are defined separately as they describe different properties of environmental signals, but we emphasize that they do not always coincide; e.g. degradation does not define detectability. To understand thresholds for signal degradation and detection, we ran a suite of physical rice pile experiments with imposed sediment influx signals. The periodicities of the signals spanned the full temporal range of autogenic timescales, from below T_{rw} to above T_{wb} (Figure 3.4), to delimit the influence of both autogenic timescales. Furthermore, to understand the effect of signal amplitude on signal degradation and detectability, we systematically varied the signal amplitude for each periodicity. For parity with the control experiment, all the imposed signals share the same mean feed rate (0.37 g s^{-1}), but decrease in amplitude from 100% to 25% of the mean feed rate.

To quantify degradation, we require knowledge of the amplitude of the output signal relative to the known input signal. Here, degradation is comparable to the concept of “gain” used to analyse the propagation and preservation of environmental signals within diffusive systems (e.g. Braun *et al.*, 2015).

To quantify the output signal amplitude, the efflux time series from an experiment with imposed periodicity is first divided into lengths equal to the input period. Then, the mean efflux is taken every second over the input signal period; this mean efflux time series should approximately resemble the input signal. To this mean efflux, we then fit a sine wave where the period is pre-defined (the known input periodicity), but the amplitude and phase shift are returned depending on the output signal identified. We compare the amplitude of the signal evident in the output flux, to that of the known input signal and quantify a percentage similarity (Figure S3.2).

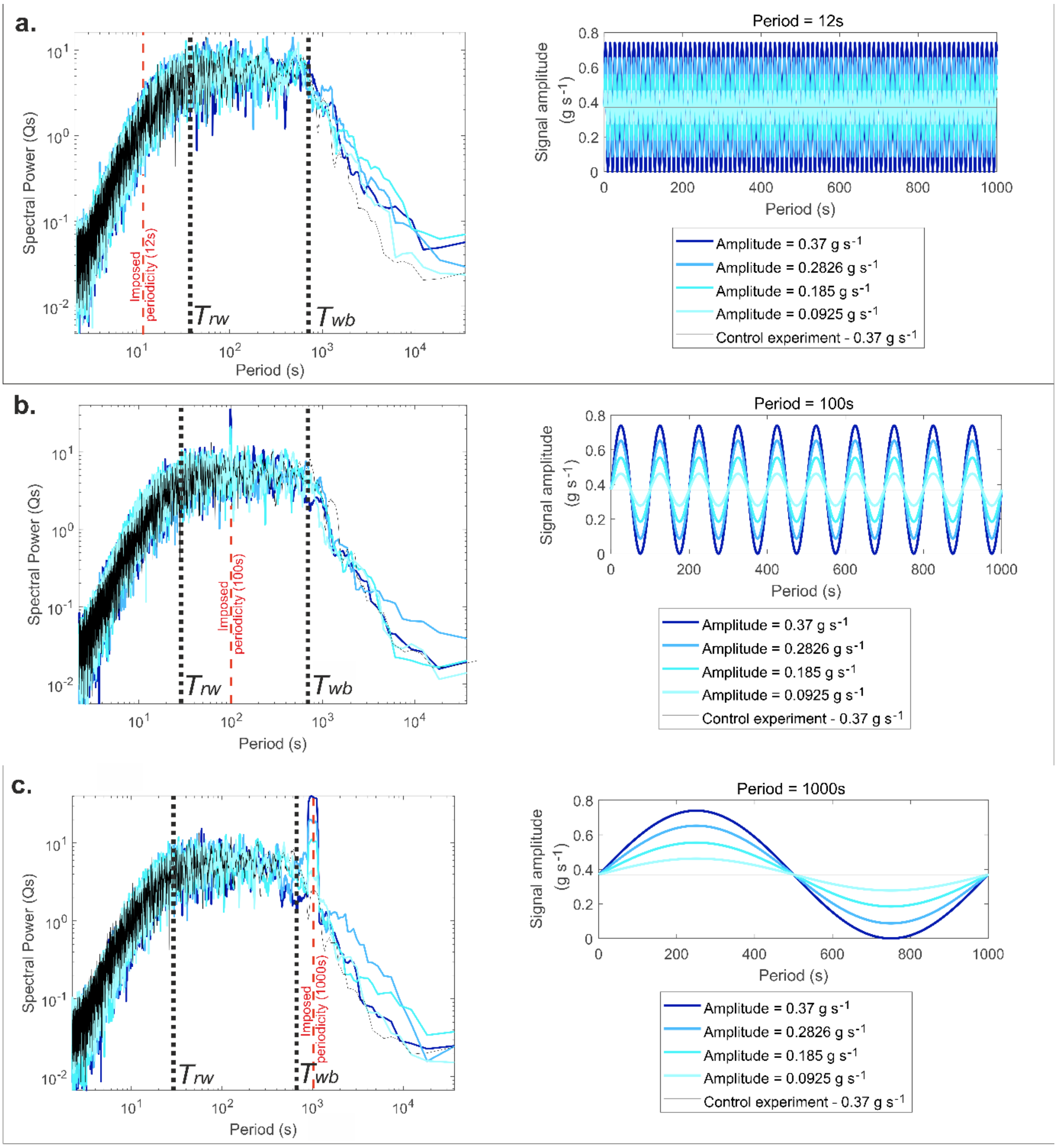

Figure 3.4: Power spectra generated from a suite of rice pile experiments with imposed signals in the form of cyclic rice influx. Spikes in power at the imposed periodicity highlight the presence of imposed signals. The power of the signal spike decreases as signal amplitude decreases.

Each panel contains 5 power spectra; 4 from rice pile experiments with imposed periodicity where the imposed periodicity is constant but signal amplitude decreases in reference to the mean feed rate, and also the spectra from the control experiment. ***(A)*** *Imposed periodicity of 12s.* ***(B)*** *Imposed periodicity of 100s.* ***(C)*** *Imposed periodicity of 1000s. We highlight that spectral structure is not influenced by the addition of external forcing. The imposed influx signals are shown in relation to both autogenic timescales (T_{rw} and T_{wb}) by the dashed red line.*

We find that input signal periodicity is the primary control on signal degradation and that the short autogenic timescale, T_{rw}, sets an upper-limit to the timescales over which signals experience degradation (Figure 3.5A). Over all periodicities, signal amplitude does not influence the amount of signal degradation. Signals with periodicity less than T_{rw} experience severe degradation, where the smaller the periodicity of the signal, the greater the amount of degradation experienced. We highlight these signals are not completely destroyed (i.e. shredded (Jerolmack & Paola, 2010) but are reduced in amplitude. In comparison, signals with periodicities greater than both T_{rw} and T_{wb} experience minimal degradation, where the output signal exhibits on average 90% similarity to the known input signal over all periodicities greater than T_{rw} (Figure 3.5A). We note that signal amplitude does not influence the amount of degradation a signal experiences; signals of the same periodicity are degraded by equal amounts regardless of their input amplitude (Figure S3.3). However, we acknowledge this may not be the case for signals with larger amplitudes (e.g., those on the order of M_{max}).

We also explore the relationship between the degradation of input signals and their detectability. To make a statistical statement about the presence of an influx signal within the power spectra, a confidence band was generated from the background structure of autogenic processes, which allows autogenic noise to be differentiated from imposed periodicity. We generate a 95th percentile confidence band from a suite of control experiments (Figure 3.2B), all sharing the same forcing conditions, by calculating the percentage of the power spectra that falls above a given power for each period. To quantify detectability, we compare the spectral power of the signal spike to the spectral power of the 95% confidence band at the imposed periodicity; detectable signals are those which breach the confidence band. We find that signals with periodicity less than T_{rw} do not generate a spectral response that exceeds the 95% confidence band and so are statistically undetectable in the output flux, regardless of amplitude (Figure 3.5B). We acknowledge this may not be the case for signals with larger amplitudes (e.g. those on the order of M_{max}). Above T_{rw}, signal amplitude influences the detectability of signals; the greater the amplitude of the signal, the greater the ratio of the spectral peak to the confidence band. Large amplitude signals with periodicity between T_{rw} and T_{wb} are easily detectable in the output flux, but small amplitude input signals can be rendered undetectable in the output flux. This is because the amplitude of the signal is of the same magnitude as autogenic fluctuations, i.e. the signals are obscured by autogenic noise. However, above T_{wb}, the amplitude of the resultant signal spike is much greater than that of the confidence showing enhanced detectability. Signals with periodicity over these long timescales are greater than the largest autogenic fluctuations and therefore overwhelm the noise produced by autogenic processes. Therefore, T_{wb} sets a temporal threshold beyond which the detectability of environmental signals is enhanced.

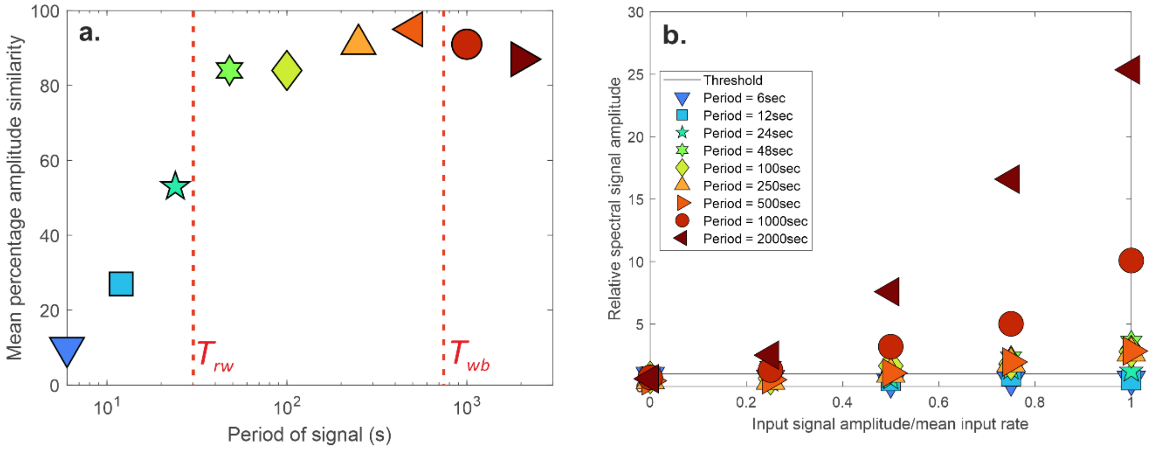

Figure 3.5: Degradation and detectability of environmental signals

(A) *Signal degradation as a function of input period, measured by comparing the known input signal, to the signal evident in the efflux from stacking multiple realizations (see Methods).* ***(B)*** *Signal detectability as a function of both input period and amplitude. Power of the signal spike at the imposed periodicity compared to the power of the 95% confidence band at the imposed periodicity. The data at 0 amplitude represents an experimental run with no imposed periodicity. Y-axis data points are calculated as power at imposed period/power of confidence band at imposed period, hence values greater than 1 breech the confidence band.*

3.4. Discussion

3.4.1. Separating thresholds for the shredding and detection of environmental signals

Our physical experiments show the presence of a short autogenic timescale, T_{rw}, denoting the red noise to white noise transition in the power spectra. T_{rw} in the physical rice pile is analogous to T_x found in numerical rice pile systems (Jerolmack & Paola, 2010), and our experiments confirm that T_{rw} provides an upper limit to the timescales over which signals experience shredding. Jerolmack & Paola (2010) found that short period input signals ($T<T_x$), with amplitudes below an exceedance that would otherwise induce system clearing events, were not detectable in the power spectra and were described as completely obliterated (i.e. shredded). However, we show that small amplitude influx signals can be reconstructed by stacking the output flux if the periodicity is known, suggesting that input signals are not obliterated but

rather severely degraded in amplitude. Small amplitude influx signals are of similar magnitude to autogenic fluctuations within STS, so storage and release processes can physically smear short period input signals out over a band of time (i.e. signal shredding (Jerolmack & Paola, 2010), which consequently reduces the amplitude of an input signal (degradation) and hence the power of the input periodicity. We modify the original definition of signal shredding to: the smearing of externally-driven signals by sediment transport processes across a range of spatiotemporal scales, resulting in the amplitude of the environmental signal at the system output being severely degraded when compared to the amplitude of the original signal. Although T_x provides a threshold for shredding in the numerical rice pile, Jerolmack & Paola (2010) did find that a separate threshold existed for the detectability of shredded signals, where the signal produced a measurable response in the power spectra. They found that only signals with periodicity T/T_x <0.6 are rendered undetectable in the output flux, whereas the output flux showed evidence of periodicity when the signal periodicity was T/T_x = 0.6-1. Our physical experiments show this is not the case. We find that all signals with periodicity less than T_{rw} are rendered undetectable in the output flux, and hence T_{rw} provides an upper limit for signal degradation, and a lower limit for signal detectability.

We also find that signals with periodicity greater than T_{rw} can be rendered undetectable if obscured by autogenic noise (Morris *et al.*, 2015). This finding augments earlier work that hypothesised that the red noise to white noise transition acts as 'a lower-limit on the ability to pass and record environmental signals' (Jerolmack & Paola, 2010). Instead, we find that signal detectability is amplitude dependent at timescales between T_{rw} and T_{wb}. We show that only at timescales greater than $T_{wb,}$ is faithful signal transfer expected over all amplitudes, as the signal period is greater than the longest timescale autogenic process. Therefore, we find that it is the truncation timescale T_{wb}, not T_{rw} (T_x) that is 'the lower-limit for the faithful propagation and recording of environmental signals within landscapes'; a definition originally given to T_x. This is also found to be the case for theoretical frameworks defining signal detectability for longer timescale stratigraphic analysis (Foreman & Straub, 2017; Toby *et al.*, 2019).

Jerolmack & Paola (2010) considered T_x (here T_{rw}) to be comparable to the 'basin filling timescale' or the 'equilibrium timescale' (T_{eq}) in a deterministic diffusional framework of landscapes, representing the time required to completely regrade surface topography to a steady state following a perturbation (Paola *et al.*, 1992). However, we suggest that T_{eq} is more appropriately approximated by the longer autogenic timescale T_{wb}, which comes about through the shared property of complete surface regrading or topographic filling, that takes place over these timescales. Whilst T_{wb} and T_{eq} are comparable regeneration timescales, T_{rw} and T_{eq} both denote upper limits to the timescales over which environmental signals experience degradation; signals propagating through a diffusional system do not experience a reduction in amplitude ("gain") when the signal period considerably exceeds T_{eq} (McNab *et al.*, 2023). However, the timescales over which signal degradation occurs in stochastic systems ($<T_{rw}$) could be up to an order of magnitude less than within diffusional systems (if T_{wb} is approximately equal to T_{eq}), but this is dependent on the mechanics of sediment transport within the system and the influx rate to the system, which governs the separation of T_{rw} and T_{wb}. The reason for this difference in behaviour is that a periodic sediment supply signal will pass unimpeded through a diffusive system (i.e. no degradation) once a system-wide topographic steady state is achieved (Straub *et al.*, 2020), whereas, in stochastic systems, the signal period must only exceed that of the largest autogenic event. As autogenic processes have no role within a diffusion framework due to the averaging of lateral stochastic system dynamics, T_{rw} does not exist and signals can therefore only be related to T_{eq}. This leads to a loss of predictive capability when evaluating the limits of environmental signal propagation across the Earth's surface, as only long timescale signals can be assessed (Toby *et al.*, 2022). As autogenic processes are inherent to 3D STS and set a lower limit for signal propagation and preservation, any theoretical framework must incorporate stochastic dynamics.

3.4.2. The detectability of shredded signals

At timescales less than T_{rw} we find signal amplitude to have no effect on the degree of signal degradation, but we acknowledge that a threshold must exist within the system beyond which high amplitude short-period input signals are detectable in the output flux. This amplitude or magnitude threshold (M) is expected to scale with the maximum size of autogenic events in the numerical rice pile , i.e. $M \sim L^2S_c$, where S_c is the critical threshold slope (Jerolmack & Paola, 2010). In the numerical rice pile, M represents the maximum volume of rice effluxed over the longest avalanche event (analogous to M_{max} in this study). M was defined on the basis that the short autogenic timescale scaled with sediment flux (e.g. a volume filling timescale, equivalent to T_{eq}; (Jerolmack & Paola, 2010), which we show not to be the case for $T_{rw,}$ but instead applies to the longer autogenic timescale, T_{wb}. Therefore, we postulate that the amplitude required for a degraded influx signal to be detectable is much lower than M, as the signal amplitude is only required to exceed that of individual autogenic events, rather than the mass required to achieve a system-wide topographic steady state. Furthermore, in the numerical rice pile, the model does not allow for grains to propagate through the model without experiencing storage (analogous to washload sediment in rivers). In this model, grains that enter the model at the top of the pile instantly 'stick' at the input location and remain in the model unless liberated by an avalanche. However, in the physical rice pile (and STS), grains have the ability to propagate through the system with minimal storage. Therefore, the inclusion of suspended and/or washload sediment increases the efficiency of signal propagation. These reasons allow us to anticipate that amplitude required for the detectability of degraded signals is much lower than M.

The amplitude of the largest signals $T<T_{rw}$ imposed onto the physical rice pile is equal to the mean feed rate, with a total influx much lower than M_{max}, and hence are severely degraded and undetectable in the output flux. However, we suggest that if the signal amplitude exceeded the mean feed rate, or the rate at which the influx rate varied was increased, the signal would be degraded by the same amount but would be detectable in the output flux. A square wave input signal with periodicity less than T_{rw} and an amplitude equal to the mean feed rate was imposed onto the physical rice pile and produced a detectable response in the output flux (Figure S3.4). We hypothesize this to be the case as the total mass influx of a square wave signal is greater than that of a sine wave signal over the same periodicity. This means that a signal can be both severely degraded in amplitude, but the spectral spike can exceed the 95% confidence band. Once the amplitude of the signal is equal to or greater than M_{max}, these signals will overwhelm the magnitude of the autogenic processes, and hence we hypothesize that these signals will pass through the system without experiencing degradation. A pathway for future work will be to quantify the amplitude threshold over which short-period signals experience no degradation and explore the nature of this threshold as a function of input periodicity.

While quantifying the effects of autogenic processes is important for understanding signal shredding, we note that quantifying the detectability of signals over all periodicities in landscapes and sedimentary layers takes precedence when reconstructing past environmental signals from landscapes and strata. Power spectra are the most common method used to search for evidence of environmental signals from a time series of stratigraphic measurables. However, the use of power spectra alone is insufficient if signals have been rendered undetectable due to degradation/obscuring by autogenic noise. In this case, the only way to truly show the presence of external signals is if one knows for certain the periodicity and can stack multiple realizations of the signal to reconstruct it. However, when working with time series generated from stratigraphic measurables, the messy conversion of space to time (e.g. the assumption of linear sedimentation rate) brings substantial error into a reconstructed time series over meso-timescales (~10^1 – 10^5 years) (Sheets *et al.* 2002; Straub & Wang, 2013;

Foreman & Straub, 2017; Straub *et al.*, 2020). This, alongside the lack of knowledge of the imposed periodicity to search for, makes this methodology generally unfeasible and hence we have to rely on power spectra. If environmental signals could be identified in a time series without the use of power spectra (e.g. the time series has excellent age control so the signal could be reconstructed by stacking the time series), this would remove the requirement to define appropriate statistical thresholds (i.e. confidence levels) to differentiate signal from noise in power spectra. This is beneficial, as the application of ill-fitting thresholds can generate false positives and promote misinterpretations regarding the presence of periodicity (Vaughan *et al.,* 2011). The identification of environmental signals from power spectra is aided by knowledge of key autogenic timescales, such as those presented here. For example, the interaction between an environmental signal of known periodicity and autogenic processes can guide scientific practitioners as to whether a signal is not detectable due to shredding ($T< T_{rw}$) or whether the signal has been obscured by autogenic noise ($T>T_{rw}$).

3.4.3. Rice piles to landscapes to strata

The specific sediment transport and storage mechanisms within an STS will determine the nature and timescales of autogenic processes, which mediates how STSs might transmit environmental signals (Hajek & Straub, 2017; Scheingross *et al.*, 2020; Toby *et al.*, 2022). In the physical rice pile, the temporal extent of correlation (i.e. red noise up to T_{rw}) is defined by the duration of individual avalanche events. The rice pile is analogous to an individual component or segment of a STS, such as a hillslope experiencing sediment transport events of all sizes, with the largest event being a landslide. In this example, it is the duration of individual sediment transport events (or autogenic processes) within a single segment that defines the temporal extent of correlation. However, when considering a STS with multiple, linked segments, the sediment efflux out of one segment becomes the sediment influx to the next (e.g. sediment transport from a hillslope segment to a fluvial segment in a catchment). Therefore, in order for the sediment flux from a hillslope to be measured at the catchment outlet, it must propagate from the hillslope into the fluvial network. This means that rather than the absolute duration of individual sediment transport events defining the extent of correlation, we hypothesize that it is instead the time required to evacuate the sediment from the hillslope to a valley and ultimately into the fluvial system and hence be measured at the catchment outlet. This means that the (dis)connectivity of STS segments could influence the extent of correlation and the timescales of autogenic processes evident from a time series of sediment flux at the catchment outlet (Wohl *et al.,* 2019). For linked segments of a hillslope-fluvial system, the timescales of correlation would relate to the time required to remove and redistribute sediment from the hillslope to the fluvial network. If the hillslope-fluvial system is well connected, sediment delivered from the hillslope segment is fed directly into the fluvial segment, hence we hypothesize that time required to evacuate sediment from the catchment is short, and hence T_{rw} is short. This also means that the STS could convey sediment flux signals effectively through consecutive STS segments (Tofelde *et al.*, 2021), depending on the autogenic processes and storage capacity of the STS segment in question (Toby *et al.*, 2022). On the other hand, if a hillslope-fluvial system is disconnected, sediment is stored on the hillslope where it is gradually removed and transported to the river network. This gradual liberation of sediment enhances the sediment flux exiting the catchment over long timescales (Clapuyt *et al.*, 2019). Many extremely large landslide deposits can remain in mountain landscapes for up to 10^4 years (Korup *et al.,* 2010), which contributes to sediment flux exiting the catchments over these timescales. This means that although the absolute landslide duration on the hillslope is short-lived, the time to evacuate the associated sediment from the catchment by fluvial processes is much longer, which we hypothesize will extend the timescales of temporal correlation (e.g. red noise) (Korup *et al.,* 2010) and hence the timescales over which signals will experience shredding. From the above it is evident that the interconnection of STS segments strongly influences the spectral geometry of influx at the outlet of the connected segments and controls how signals propagate between and through them (e.g. Toby *et al.*, (2022)).

We find that T_{rw} in the physical rice pile is independent of the rate of sediment supply, however the behavior of smaller avalanche dynamics is not. The greater the sediment supply rate, the more frequent the occurrence of smaller avalanches in the rice pile (Figure S3.5), however, the frequency of the largest avalanches converges at the size of the largest system-scale event. Conversely, for natural and experimental STSs this timescale is unlikely to be independent of the rate of sediment supply because topography can be built and filled faster with an increased sediment supply rate. For example, temporal correlation (red noise) in a cellular automata model of alluvial transport (Jerolmack & Paola, 2007) extends up to a maximum timescale of river avulsion, and within a single deltaic system, the maximum autogenic timescale is denoted by a system-wide, lobe movement event and associated compensational filling of topography (Straub, 2019). In each case, the maximum autogenic timescale is akin to T_{rw} in the physical rice pile, but unlike T_{rw} they are dependent on the rate of sediment supply (Bryant *et al.*, 1995). Further work is needed to investigate the mechanisms that contribute to the longest duration autogenic events, which will define the autogenic timescales in both experimental and field scale systems.

Limitations of stratigraphic datasets (e.g. limited outcrop exposure, incompleteness and the assumption of linear sedimentation rate) make it difficult for field practitioners to explore details of autogenic processes over geological timescales. High resolution time series of surface sediment fluxes and preserved deposition rates of an experimental delta run under constant boundary conditions (Straub *et al.*, 2015) allow us to study the structure and timescales of autogenic processes in a system more analogous to that of field scale systems, and one that contains morphodynamic behaviour. We create power spectra of surface sediment flux from the terrestrial delta top to the marine, analogous to the efflux of rice from the rice pile (Figure 3.6), which reveals temporal correlation (red noise) over all timescales up to the compensation timescale, T_c (Wang *et al.*, 2011). T_c represents the truncation timescale of depositional processes in natural systems (Ganti *et al.*, 2011), analogous to T_{wb} that represents the largest autogenic event in the rice pile, and defines the maximum timescale of autogenic organization in stratigraphy (Sheets *et al.*, 2002; Wang *et al.*, 2011). As with T_{wb} in the rice pile, the compensation timescale denotes a detectability timescale for signals within channelized systems, whereby input signal periodicity greater than T_c are more likely to be recorded in both landscapes and strata (Li *et al.*, 2016; Foreman & Straub, 2017; Toby *et al.*, 2019). At timescales greater than T_c, anti-correlation (blue noise) persists over all subsequent timescales. This spectral geometry is maintained within spectra generated from a time series of preserved deposition rates generated from the same experiment (Figure 3.6).

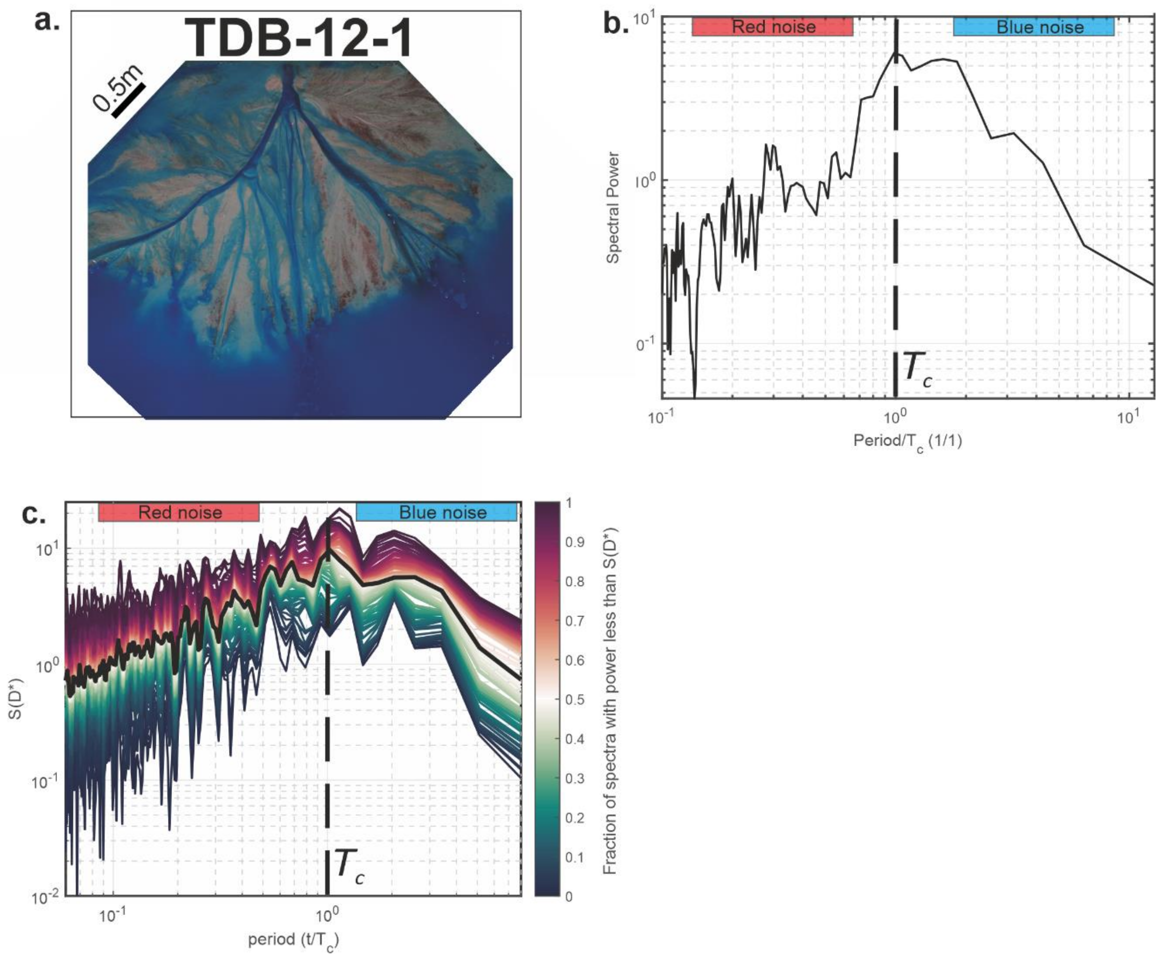

Figure 3.6: Surface morphology and power spectral analysis from delta basin experiment TDB-12-1 (Straub et al., 2015).

(A) *Overhead photo from the delta basin experiment. Power spectra for preserved deposition rates were generated at every point (5mm spacing) from the centre portion of the radial white line, from which an average spectrum was generated.* ***(B)*** *Power spectra generated from a time series of sediment flux to the marine using the multi-taper method. Time is normalized by the compensation timescale, Tc (~49 hours).* ***(C)*** *Power spectra generated from a time series of preserved deposition rates (Figure S6), using the multi-taper method. The black line defines the ensemble average power spectra. normalized by the long-term accommodation generation rate (0.25mm h^{-1}). Time is normalized by the compensation timescale, Tc (~49 hours).*

Unlike the rice pile, power spectra generated from the experimental delta do not exhibit a white noise regime. Building on our understanding of physical rice pile processes and their contribution to autogenic spectral structure, we note that a white noise regime will not be present when the timescale of the longest correlated event (i.e. T_{rw}) is equal to or exceeds the regeneration timescale (T_{wb}). The convergence of these timescales in the power spectra of the experimental delta defines only one spectral rollover from red to blue noise. We hypothesize this to be because the duration of the maximum autogenic timescales (i.e. a system-wide, lobe movement event) and the compensation timescale (T_c; approximately 49 hours for this experiment (Hajek & Straub, 2017)) are of the same order of magnitude. Therefore, we emphasize that the spectra produced from a time series of landscape or stratigraphic measurables may not necessarily exhibit tripartite geometry, as this is dependent on system size and sediment supply rate which controls the relationship between T_{rw} and T_{wb} and so therefore the presence and duration of white noise. However, a long time series generated from landscape or stratigraphic measurables that is of sufficient temporal resolution should reveal both red and blue noise. The convergence of timescales could also happen in other geomorphic systems, such as landsliding in mountain catchments, whereby a tripartite spectral geometry would be prevalent when the reoccurrence interval of landslides exceeds the time needed to evacuate the landslide sediment from the catchment by fluvial processes. However, if the time to evacuate landslide sediment exceeds the reoccurrence interval, we expect this would result in a condensed spectral geometry showing one spectral rollover between red and blue noise (i.e. no white noise).

Within the rice pile T_{rw} and T_{wb} are linked by the maximum-size autogenic event, whereby T_{rw} represents the longest avalanche duration to evacuate this rice mass and T_{wb} represents the time required to regrade the rice-wedge with this same amount of mass. To investigate whether this parity of mass or volume might exist in close analogues of field scale systems, we use volume fluxes from the experimental delta. Specifically, we calculate the volume of sediment exported between large scale lobe movement events, representing the largest avalanche, to be approximately 0.030 m^3; and the volume of sediment required to regrade delta topography by one channel depth, representing the regrading of the sediment wedge, to be approximately 0.024 m^3. The large-scale lobe movement events analysed on the delta were limited to timescales less than T_c, which is defined on the basis of the time taken to deposit one channel depth across the delta. We once again advocate that T_c is analogous to the wedge filling timescale T_{wb}.

3.4.4. The severity of the signal shredder

Although autogenic processes within landscapes and strata show comparable temporal structure containing both red and blue noise, we have evidence that the shredding process may operate with differing severity. The spectral growth index (e.g. gradient of red noise) varies between the spectra, with the deposition rate power spectra following a much lower index value than the surface delta fluxes or rice pile ($\alpha = 0.8$ versus $\alpha = 1.3$ and $\alpha = 2.2$ respectively).

Systems which evolve towards a critically self-organised state are defined as having spectral growth at 1/f (e.g. pink noise, $\alpha = 1$) (Bak *et al.*, 1987), where noise in the system is moderately correlated (Grumbacher *et al.*, 1993). We find that over short timescales, the surface delta fluxes have moderate correlation, with spectral growth at approximately 1/f ($\alpha = 1.3$), whereas the rice pile has strong correlation, with spectral growth is approximately $1/f^2$ (e.g. red noise, $\alpha = 2$) (Grumbacher *et al.*, 1993). Over these timescales, the strength in the correlation of the system indicates the frequency of erratic behaviour away from the mean state; the stronger the correlation, the less frequent the chance of erratic behaviour. To explain this, we refer to the dynamics present within a delta. When a channel network is stable on a delta top, the fluxes to the marine are consistent at high rates until the channel network collapses. The consistency of the channel network allows for the efficient propagation of sediment down system. However, during this period of stability, events such as infrequent breaches may occur that divert water and sediment to the delta-top for short time periods, but do not trigger an avulsion event. This is defined as erratic behaviour; e.g. a rapid, temporary change in the system. This long-term stability intermixed with short term temporary fluctuations manifests as approximately 1/f noise in surface delta fluxes. However, we find that depositional fluxes have weak correlation, with spectral growth less than $\alpha = 1$, indicating that the system has a considerable chance of being driven in a different direction at any time. Within the delta system, we hypothesize that the correlation in the system is defined by periods of no-deposition, and hence during a period of stasis, the system will tend to remain in stasis up to a maximum timescale of T_c. However, periods of deposition and erosion (over a range of spatiotemporal scales) interrupt periods of no-deposition (e.g. long-term erratic behaviour) which weakens the temporal correlation.

The differences in the strength of the correlation between surface and stratigraphic records could suggest variations in the intensity of the shredding process. Within pink noise ($\alpha \sim 1$) and red noise ($\alpha \sim 2$) systems, the stability of the STS could suggest short-period signals propagate more effectively. Whilst these signals would still experience some degradation, as they do not overwhelm autogenic fluctuations, their propagation is relatively uninterrupted. For example, when the channel is stabilized on a delta top, consistently high sediment flux rates allow for effective sediment transport down system. This would result in overall less degradation and possibly allow the imposed signal to be reconstructed by stacking records at the known periodicity. However, the erratic correlation present in systems where $\alpha < 1$ (e.g. interruptions in sediment transport and deposition) suggests a stronger ability to smear signals through space and time. In these systems, the balance between deposition, erosion and stasis is highly variable. Hence, the greater the lateral mobility of the system, the greater the chance of hiatuses and/or reworking of previously deposited sediment by erosion (e.g. the occurrence of long-term erratic behaviour) and hence the lower the rate of spectral growth. This may result in a signal being completely obliterated (i.e. no returnable amplitude in a time series of sediment flux). If the severity of the degradation process does inversely scale with alpha, our results suggest that the depositional filter could act as a "super shredder" of environmental signals.

Signals with periodicity less than T_{rw} can sometimes be reconstructed from stacking landscape records, but this requires the record to be many multiples of the imposed periodicity allowing the transport system noise to be averaged. Furthermore, signals with periodicity between T_{rw} and T_{wb} can be detected or obscured within a landscape depending on the amplitude of the signal. However, any signal detectable within landscape records may not be of sufficient periodicity or magnitude to overcome the longer, harsher stratigraphic shredding regime. Therefore any resemblance of a signal would be completely removed within a time-series of stratigraphic measurables (Toby *et al.*, 2019; Straub *et al.*, 2020).

3.4.5. The nature of autogenic processes

The longest autogenic timescales evident in landscapes and strata (T_{wb} or T_c) define rollovers to a blue noise regime within power spectra. Although the presence of this spectral regime is intuitive, it is rarely acknowledged in spectra generated from stratigraphic measurables; instead, spectra are described to be dominated by the presence of commonly known red and white noise (Weedon, 2003; Vaughan *et al.*, 2011). The lack of identification could be a result of how power spectra are commonly plotted; plotting power spectra as a function of frequency renders blue noise more difficult to identify than if plotted as a function of period. However if blue noise is simply not present, this could result from the lack of availability of long-time series datasets (either due to insufficient duration of the instrumental record or due to the availability of outcrop exposure), the incompleteness of the stratigraphic record favouring high-frequency fluctuations (Straub *et al.*, 2020), the messy conversion of space to time from stratigraphic measurables (e.g. the assumption of linear sedimentation rates) (Barefoot *et al.*, 2023), or the lack of dynamic equilibrium in STSs, generating non-stationary statistics and therefore rendering blue noise unobservable (Muto *et al.*, 2007). The unknown presence of blue noise within power spectra generated from stratigraphic measurables has implications for generating statistical tests to detect the presence of environmental signals (Hajek & Straub, 2017). The application of the autoregressive lag 1 (AR1) model (Pemberton & Priestley, 1990), typically for paleo-climatic studies, does not fully represent the spectral background structure generated by geomorphic variability (Foreman & Straub, 2017), which could produce false positives and spurious signals. To ensure accurate detection of environmental signals, spectral estimations must provide a strong fit to the background structure. The potential universality of the presence of blue noise within the temporal structure of autogenic processes highlights the requirement to generate a statistical model to fit power spectra of this structure, which will allow the accurate detection of environmental signals over all autogenic timescales.

Overall, two key timescales emerge from the study of autogenic dynamics within a physical rice pile experiment which provide thresholds for both signal degradation (T_{rw}: the event duration timescale) and enhanced signal detection (T_{wb}: the system regrading timescale). The autogenic timescales presented provide a framework to predict the severity of signal shredding across the Earth's surface and to strata, and establish robust confidence limits of signal detectability in landscapes and strata. We highlight the applicability of this framework to all segments of a sediment routing system (for example, erosive catchments experiencing land sliding or fluxes to the deep marine) alongside systems that experience environmental stochasticity (e.g. earthquakes, storms and floods; (Straub *et al.,* 2020)).

3.5. Materials and methods

3.5.1. Experimental design

A suite of rice pile experiments were conducted in the Sediment Dynamics Laboratory at Tulane University, to characterise the nature of the autogenic dynamics and assess the degree to which key autogenic timescales provide thresholds for signal shredding and detection.

The experimental apparatus is constructed of two vertical, parallel glass sheets 37.5cm long, positioned 2.6cm apart. Rice was fed (influx) to the pile from a dry particle feeder (Schenk Accurate) positioned 8mm from the top surface, allowing a rice pile to form at a critical angle so that a dynamic topographic equilibrium was achieved. Over the suite of experiments, influx was defined between a minimum and maximum range (0 g s^{-1} and 0.78 g s^{-1}), controlled at 1 second intervals via a computer connected to the sediment feeder which directly feeds the pile. Efflux was measured at approximately 1 second intervals using an Ohaus EX12002 balance (accuracy and precision of 0.1 grams). The balance has a maximum mass of 12kg, and all experiments were run until the balance was saturated. The dimensions of rice grains used in the experiments have a diameter of 2.5±0.5 mm, length of 8±0.5 mm and a mass of 0.02 grams (Table S2:). The experimental set-up used here is similar to that of the physical rice pile of Frette *et al.*, (1996).

To ensure the efflux data are driven only by the internal autogenic dynamics of the rice pile and not triggered by external noise, we analysed accelerations within the room when the sediment feeder was on and off, when sediment feeder was on but with no rice delivery, and when rice was delivered (Figure 2.2). Accelerations were measured using the Phyphox application on an iPad, which records x, y and z accelerations at an increment of ~0.05 seconds to two significant digits of acceleration with SI units. The raw acceleration data, alongside power spectra of the time series, were analysed to confirm external vibrations were not triggering avalanches, or that external vibrations did not occur at repeating frequencies.

A series of experiments were conducted where rice was fed directly from the sediment feeder to the scale, to confirm we had high temporal control over the influx rates and cycles imposed. We generated power spectra from the time series, which confirms white noise was present across all frequencies, except a spike in power if periodicity was imposed (Figure 2.3).

Firstly, a control experiment was run for 9 hours with a constant influx rate of 0.37 g s^{-1}. The influx rate denotes the mean rate of the sediment feeder, and experimental run time was defined by the time to saturate the balance at the defined influx rate. This experiment was used to define the full spectral structure generated by a physical rice pile and quantify autogenic timescales evident from rollovers between spectral regions. Using this baseline behaviour, a suite of 9 experiments (Table S1). were used to explore the influence of influx rate on the autogenic dynamics and timescales found in the control experiment. These experiments varied systematically in intervals of approximately 0.1 g s^{-1} from the minimum to the maximum influx rates available on the sediment feeder.

To explore limits of signal shredding and signal detection, a matrix of 36 experiments were run with cyclic influx of different periods and amplitudes. To achieve parity with the control experiment, a mean influx rate of 0.37 g s^{-1} was attained for all cyclic experiments. 9 periodicities were chosen to cover the range of autogenic timescales evident in the control experiment: 6s, 12s, 24s, 48s, 100s, 250s, 500s, 1000s and 2000s. The amplitude of the cycles were chosen as percentages of the mean feed rate (0.37 g s^{-1}), increasing in 25% intervals from 25% (0.0925 g s^{-1}) to 100% (0.37 g s^{-1}).

3.5.2. Signal detection from power spectra

Discrete time-power spectral densities of efflux time series (power spectra) were generated using the multi-taper method (MTM) with 2 tapers. Key autogenic timescales can be observed by eye on the power spectra as ‘roll-overs’ or ‘gradient-breaks’. To delimit these timescales accurately we use the ‘findchangepts’ function in MATLAB. This function is controlled by two key input parameters: the maximum number of changes and the type of change to detect (e.g. variations in mean, standard deviation, gradient). For our spectra, we specify 2 changes (to account for the presence of two rollovers in the spectra) and use linear as the type of change to detect, applied on log transformed spectral data. This method detects changes in the mean and slope of the input spectra, which can be inverse log transformed to solve for the power-law exponent of the fit.

To make a statistical statement about the presence or not of an influx signal in the power spectra, a confidence band for the discrete time-power spectral densities is required. Using 25 realizations of the control experiment, we generated power spectra for each realization. For each periodicity, we rank the associated power values from all 25 spectra into ascending order to calculate the percentage of the realizations that fall above a given power for each period. From this, we calculate an estimate of the 95th percentile confidence band.

3.5.3. Signal degradation

To quantify the amount of degradation a signal experiences during propagation, we stack the efflux time series into lengths equal to the input period, and take the mean of the efflux for each second over the imposed periodicity. From this, we gain a mean ensemble efflux to which we fit a sine wave with a period equal to the known input, and are returned an amplitude and phase based on the signal present in the mean ensemble efflux. We compare the amplitude of the signal evident in the ensemble efflux, to that of the known input signal and quantify a percentage similarity (Figure S3.2)

Acknowledgements

Funding We gratefully acknowledge support from the University of Liverpool and the International Association of Sedimentologists (Postgraduate Research Grant).

Author contributions

R.A.D and K.M.S conceived initial idea of the study

C.G. lead development of experimental matrix with input from R.A.D and K.M.S

C.G. and K.M.S. ran the suite of rice pile experiments.

All authors contributed to the data analysis and interpretations

C.G. wrote the manuscript with edits provided by R.A.D and K.M.S

C.G. revised the manuscript after review with edits provided by R.A.D and K.M.S

Competing interests

The authors declare they have no competing interests.

Data and materials availability

All data needed to evaluate the conclusions in the paper are present in the paper and/or the Supplementary Materials. Data from the suite of experiments discussed in the manuscript are accessible through the Harvard Dataverse. All data can be accessed at https://dataverse.harvard.edu/dataset.xhtml?persistentId=doi:10.7910/DVN/SO5XJP under the dataset Rice Pile Experiments conducted at Tulane University in 2022.

This chapter characterises the temporal spectral of autogenic processes within the physical rice pile (an idealised STS) and provides a theoretical framework for the degradation and detection of environmental signals based on the autogenic timescales present within a STS (Research Question 1). The temporal structure of autogenic noise within the physical rice pile is found to contain three regimes: red noise over short timescales, white noise over intermediate timescales, and blue noise over long timescales. The breaks in the noise regimes delimit two autogenic timescales: T_{rw} and T_{wb} (Objective 1.1). T_{rw} is found to delimit the duration of the largest sediment flux event, whereas T_{wb} is found to be a regrading timescale that scales with influx rate (Objective 1.2). These two timescales denote thresholds for the occurrence of signal degradation and detection. T_{rw} provides an upper limit to signal degradation and a lower limit to signal detection, whereas T_{wb} provides a lower limit to enhanced signal detection (Objective 1.3).

Supplementary information to chapter 3

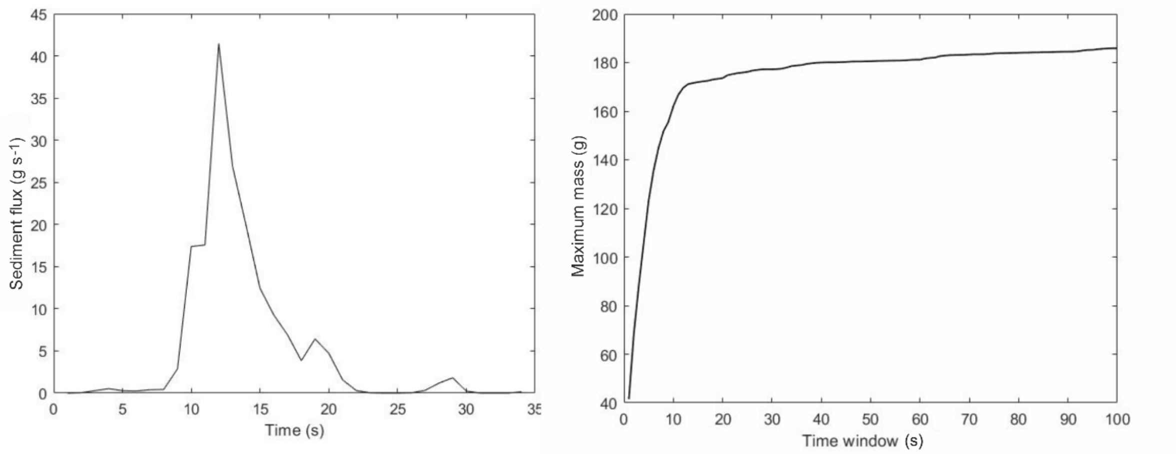

Figure S3.1: Calculation of M_{max}.

Left: Time series of efflux over the duration of the largest avalanche in the rice pile. Right: Maximum mass effluxed over increasing time windows of observation, where at timescales greater than T_{rw}, maximum mass plateaus

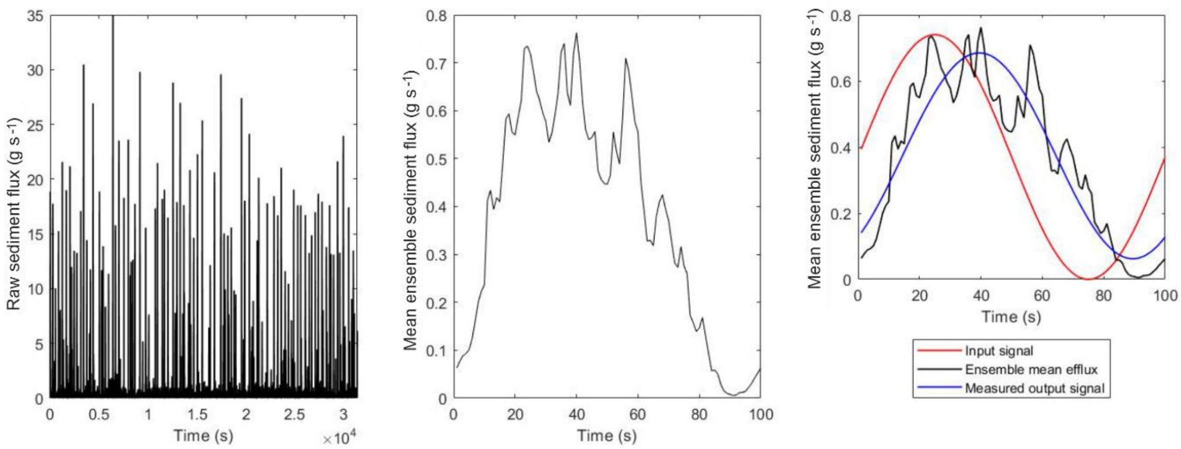

Figure S3.2: Methodology to determine the amount of degradation a signal has experienced during propagation.

The raw efflux time series is generated for an experiment with imposed cyclicity (here, period 100s, amplitude 0.37 g s^{-1}). Then, the efflux is divided into lengths equal to the period of the input signal and the mean efflux over each second of the imposed periodicity is calculated. After this, a sine wave is fitted to the stacked data, where the periodicity is defined and the amplitude and phase is calculated based on the individual dataset. The amplitude of the output signal is then compared to the amplitude of the known input signal to calculate percentage similarity.

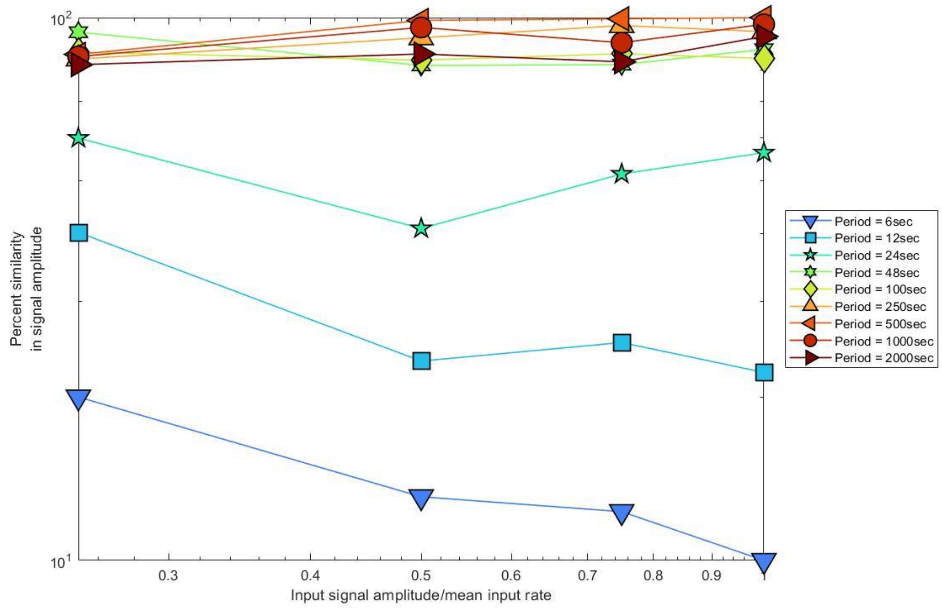

Figure S3.3: Signal degradation as a function of both input period and amplitude.

Signals with periodicity below T_{rw} experience severe degradation, whereas signals with periodicity greater than T_{rw} experience minimal degradation.

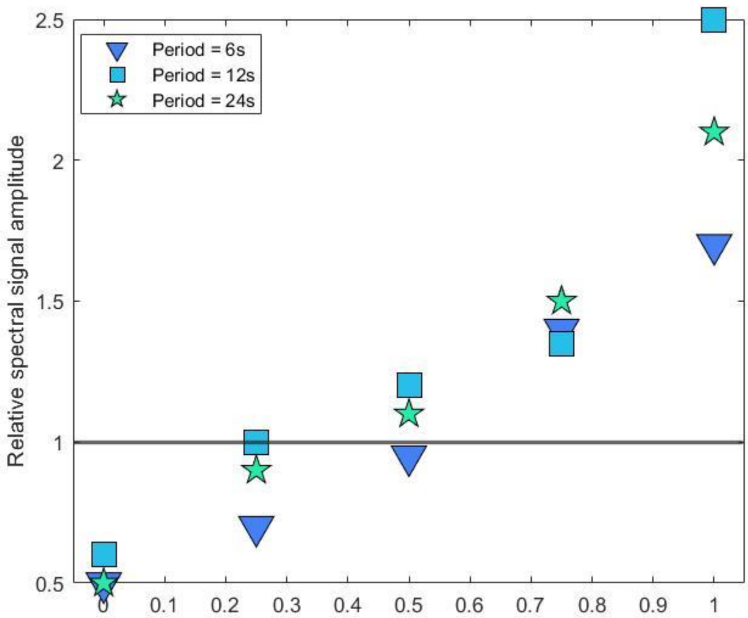

Figure S3.4: Detectability of square wave input signals with periodicity less than T_{rw} and with an amplitude equal to or below the mean feed rate.

Power of the signal spike at the imposed periodicity compared to the power of the 95% confidence band at the imposed periodicity. The data at 0 amplitude represents an experimental run with no imposed periodicity. Y-axis data points are calculated as power at imposed period/power of confidence band at imposed period, hence values greater than 1 breech the confidence band.

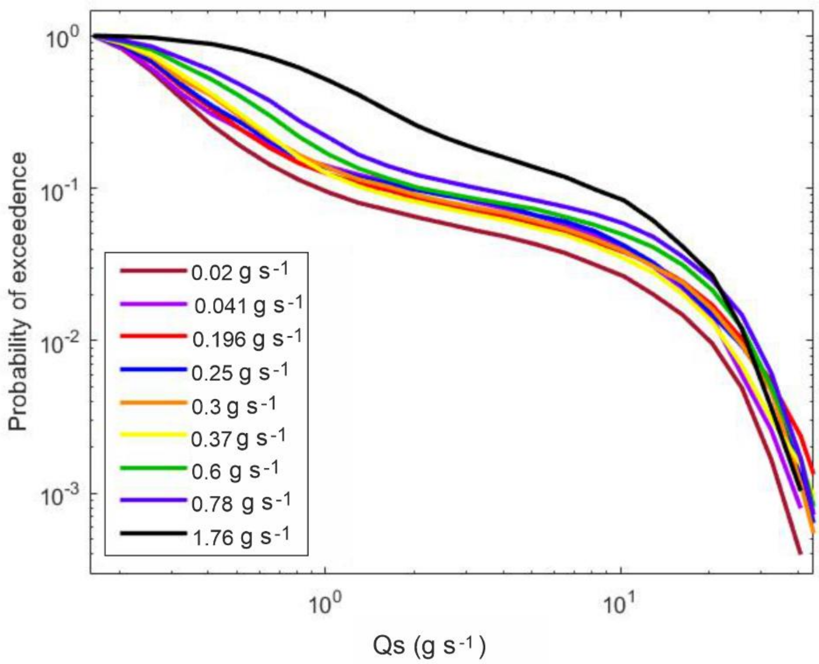

Figure S3.5: Distribution of avalanche sizes within the efflux time series from nine experiments with increasing influx rate.

All the time series show a heavy-tailed distribution, however as the influx rate increases, there is an increased probability of a certain sized event occurring, but the distributions converge at the largest event

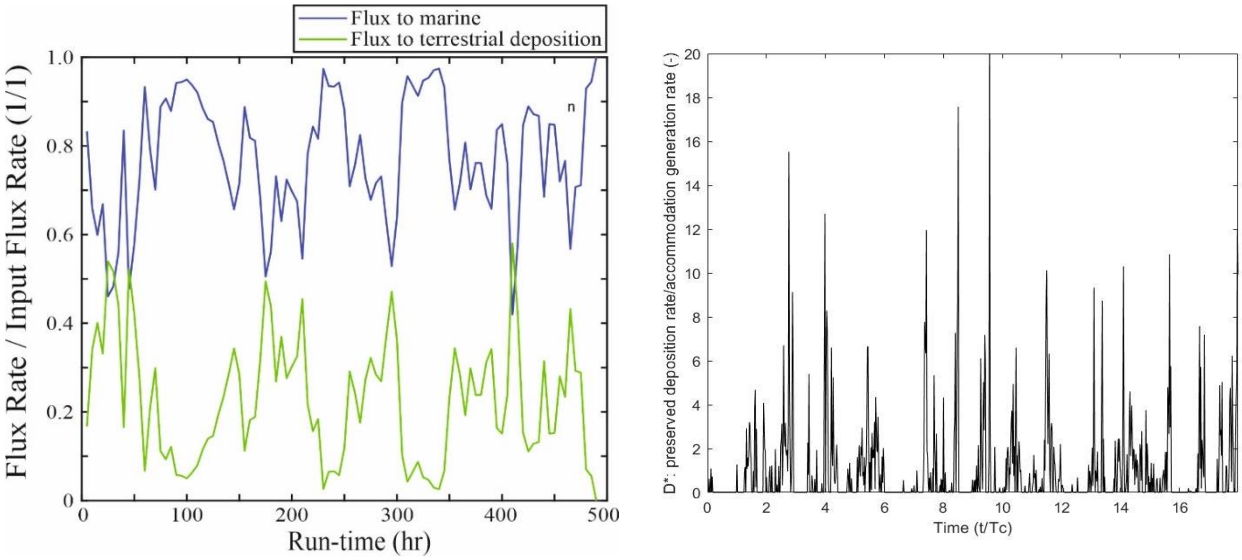

Figure S3.6: Time series of surface and stratigraphic dynamics from the delta basin

Left: Time series of sediment flux to the marine realm, versus sediment flux to the terrestrial deposit within the experimental delta basin. The time series is generated from experiment TDB-12-1 (Straub et al., 2015). The time series of sediment flux to the marine was generated as follows. Topographic maps were taken over the duration of the experiment. Successive topographic maps were differenced to generate an isopach map (map of sediment thickness). Using the measured and imposed sea level each hour, all pixels in the terrestrial realm on the isopach map were summed, and this was multiplied by the x and y node spacing on the map to get a bulk volume of sediment deposit in the terrestrial over this time period. Then, a bulk sediment flux to terrestrial deposition was calculated by dividing by the time between the maps, and then converted to a volumetric sediment flux to terrestrial deposition by multiplying the bulk sediment flux by the fraction of the deposit which is sediment (1-porosity). This has been previously measured as 0.5 with the same mixture of sediment. To get a mass flux to terrestrial deposition, the volumetric flux was multiplied by sediment density (2650 kg m^{-3}). The mass flux to terrestrial deposition was then subtracted from the known mass input flux (1.41 kg $hour^{-1}$) to get the flux to the marine. Right: Time series of preserved deposition rates measured from data points spaced 5mm apart along a radial arc within the experimental delta basin.

Table S3.1: Supply characteristics for the individual rice pile experiments, both constant and cyclic feed rates

Experiment	Stage	Desired mean feed rate (g s^{-1})	Actual mean feed rate (g s^{-1})	Period of forcing (s)	Amplitude of forcing (g s^{-1})
1	Control	0.37	0.358	-	-
2.1	Steady	0.02	0.027	-	-
2.2	Steady	0.041	0.052	-	-
2.3	Steady	0.196	0.22	-	-
2.4	Steady	0.25	0.28	-	-
2.5	Steady	0.3	0.29	-	-
2.6	Steady	0.6	0.73	-	-
2.7	Steady	0.78	0.99	-	-
2.8	Steady	1.76	2.1	-	-
3.1	Cyclic	0.37	0.358	6	0.37
3.2	Cyclic	0.37	0.358	6	0.2826
3.3	Cyclic	0.37	0.358	6	0.185
3.4	Cyclic	0.37	0.358	6	0.0925
3.5	Cyclic	0.37	0.358	12	0.37
3.6	Cyclic	0.37	0.358	12	0.2826
3.7	Cyclic	0.37	0.358	12	0.185
3.8	Cyclic	0.37	0.358	12	0.0925
3.9	Cyclic	0.37	0.358	24	0.37
3.10	Cyclic	0.37	0.358	24	0.2826
3.11	Cyclic	0.37	0.358	24	0.185
3.12	Cyclic	0.37	0.358	24	0.0925
3.13	Cyclic	0.37	0.358	48	0.37
3.14	Cyclic	0.37	0.358	48	0.2826
3.15	Cyclic	0.37	0.358	48	0.185
3.16	Cyclic	0.37	0.358	48	0.0925
3.17	Cyclic	0.37	0.358	250	0.37
3.18	Cyclic	0.37	0.358	250	0.2826
3.19	Cyclic	0.37	0.358	250	0.185
3.2	Cyclic	0.37	0.358	250	0.0925
3.21	Cyclic	0.37	0.358	500	0.37
3.22	Cyclic	0.37	0.358	500	0.2826
3.23	Cyclic	0.37	0.358	500	0.185
3.24	Cyclic	0.37	0.358	500	0.0925
3.25	Cyclic	0.37	0.358	1000	0.37
3.26	Cyclic	0.37	0.358	1000	0.2826
3.27	Cyclic	0.37	0.358	1000	0.185
3.28	Cyclic	0.37	0.358	1000	0.0925
3.29	Cyclic	0.37	0.358	2000	0.37
3.3	Cyclic	0.37	0.358	2000	0.2826
3.1	Cyclic	0.37	0.358	2000	0.185
3.2	Cyclic	0.37	0.358	2000	0.0925

4. The incomplete record of autogenic processes sets limits on signal detectability.

This chapter has been published as: Griffin., C., Duller, R.A., & Straub, K.M (2024). The incomplete record of autogenic processes sets limits on signal detectability. *Journal of Geophysical Research: Earth Surface,* v 129 (4), e2023JF007538

When this thesis was initially submitted, Chapter 4 was in review at *JGR: Earth Surface*. This has now been published in *JGR: Earth Surface* as of 01/04/2024. Since review, the only significant changes have been clarifying section 4.4.2 and rewriting section 4.4.3 to add clarity to the workflow.

Abstract

Spectral analysis is a central tool regularly used by the scientific community to identify the presence of periodic processes within a time series of information, as spectral peaks at an imposed periodicity can be differentiated from internal (autogenic) variance. In scientific disciplines, such as seismology, the time series of information is of high temporal resolution. Hence, although temporal gaps are present, they do not impact the overall noise structure, meaning the full spectrum of autogenic variance can be reconstructed. However, power spectra generated from stratigraphic information are affected by temporal incompleteness due to varying episodes of erosion and geomorphic stasis which generate gaps over a range of scales. This removes information related to the natural, autogenic, variability present within sediment-transport systems which makes it challenging to accurately reconstruct the structure and strength of paleo-surface processes, which defines the detectability of past environmental signals. We explore how incompleteness impacts the temporal structure of autogenic noise within power spectra, and how this influences the detectability of spectral spikes related to environmental signals. We utilise a sediment flux time series from a physical rice pile and progressively degrade this data to mimic varying degrees of stratigraphic incompleteness. We find that incompleteness strongly influences the timescales and spectral structure of autogenic noise evident, and can render signals over all periodicities undetectable within a highly incomplete time series. This offers the ability to confidently justify the interpretation of subtle environmental signals from field measurements and understand the records that may best preserve paleoenvironmental variability.

4.1. Introduction

The internal dynamics within sediment-transport systems (STSs) are characterised by local episodes of sediment storage and release that occur naturally, known as autogenic processes, which are ubiquitous across all landscapes and generate stochastic fluctuations in sediment transport in the absence of external (allogenic) forcing (Hajek & Straub, 2017; Jerolmack, 2011; Jerolmack & Paola, 2010; Kim & Jerolmack, 2008a; Paola, 2016; Pelletier *et al.*, 2015; Romans *et al.,* 2016; Straub *et al.,* 2020). Stochastic sediment transport resulting from autogenic processes generates noise within a STS, and the resultant stratigraphy, and limits the predictability of STS dynamics (Ganti *et al.,* 2014; Hajek & Straub, 2017; Jerolmack, 2011; Jerolmack & Paola, 2010; Paola, 2016; Romans *et al.*, 2016; Van De Wiel *et al.,* 2011). The duration and magnitude of autogenic processes within STSs determines the structure and timescales of autogenic noise present (Griffin *et al.,* 2023; Hwa & Kardar, 1992; Jerolmack & Paola, 2010). Autogenic noise has a distinct tripartite structure composed of three noise regimes, delimited by two autogenic timescales. The first regime comprises temporal correlation (red noise) over short timescales, where spectral power increases as a function of period. The second comprises no correlation (white noise) over intermediate timescales, where spectral power plateaus. The third regime comprises anti-correlation (blue noise) over long timescales, where spectral power decreases of a function of period (Griffin et al., 2023; Hwa & Kardar, 1992). Whilst the tripartite structure should be evident in all stochastic natural systems, the presence of all three noise regimes depends on the relationship between the autogenic timescales; where these timescales converge, power spectra may only display red and blue noise (Griffin *et al.*, 2023).

The two autogenic timescales denote temporal thresholds for the degradation and detectability of sediment flux signals, generated by external environmental perturbations (Griffin *et al.,* 2023; Jerolmack & Paola, 2010). Whilst signal degradation severely reduces the amplitude in comparison to the input signal ('shredding'), signals can undergo no modification but be rendered undetectable, if the signal magnitude is similar to that of autogenic processes (Griffin *et al.,* 2023; Jerolmack & Paola, 2010). Therefore, characterizing the temporal structure of autogenic processes from a time series of stratigraphic information enables the accurate reconstruction of paleo-surface processes, and allows theoretical frameworks which predict the degradation and detectability of sediment flux signals in both landscapes and strata to be fully utilised (Jerolmack & Paola, 2010; Toby *et al.,* 2019).

Theoretical frameworks for signal degradation and detection rely on the full characterization of the structure of autogenic processes within a specific STS. This has been achieved for an exquisitely preserved time series of sediment flux and preserved deposition rates measured from physical experiments (Griffin *et al.,* 2023; Hajek & Straub, 2017; Jerolmack & Paola, 2010; Toby *et al.,* 2019). However, a time series of stratigraphic information is inherently incomplete, owing to the presence of hiatuses over a variety of spatiotemporal scales from laminae to basin-scale unconformities, which reduce the preservation of autogenic processes within vertical sections (Ager, 1973; Davies *et al.,* 2019; Foreman & Straub, 2017; Jerolmack & Sadler, 2007; Kemp, 2012; Sadler, 1981; Schumer & Jerolmack, 2009; Sommerfield, 2006). Within all geomorphic environments, variations exist in the duration of depositional, stasis (non-deposition) and erosional events, driven by autogenic reorganization, which generates hiatal surfaces with a range of frequencies and durations (Hajek & Straub, 2017; Kim & Jerolmack, 2008b; Sadler, 1981; Sommerfield, 2006; Straub *et al.,* 2020; Straub & Foreman, 2018; Strauss & Sadler, 1989; Tipper, 2015; Trampush *et al.*, 2017). As a result, part of the original autogenic signal is removed and imposed sediment flux signals can be distorted (e.g. Burgess *et al.,* 2019; Foreman & Straub, 2017; Trampush & Hajek, 2017), making it challenging to accurately reconstruct sediment-transport processes and detect environmental signals from landscapes and strata (Kemp, 2012, 2016; Kemp & Sexton, 2014; Miall, 2015; Paola *et al.,* 2018; Straub *et al.,* 2020; Tofelde *et al.,* 2021). Furthermore, limits on our ability to date strata mean sediment age is often assigned by linear interpolation between dated horizons (Abels *et al.,* 2010; Ramos-Vázquez *et al.*, 2017), providing additional challenges to the incompleteness problem by distorting the apparent representation of time in strata, relative to true time (Barefoot *et al.,* 2023; Trampush & Hajek, 2017). Hence, fundamental questions exist regarding the reliability of strata as an archive of past and future environmental change.

Analysis of a time series of stratigraphic information assumes *a priori* that the original, full signal of autogenic noise is present and can be reconstructed, without deeply considering the impact of incompleteness. Instead, the preserved noise is measured and assumed to accurately characterise the full spatiotemporal scales of autogenic processes within landscapes and strata. Griffin *et al.,* (2023) find a time series of surface processes generate power spectra with tripartite spectral structure, however, it is hypothesised that the lack of blue noise in stratigraphic measurables could result from incompleteness, and/or the assumption of linear sedimentation rate (Figure 1). This means that the punctuated chronology generated as a result of stratigraphic incompleteness could significantly distort the record of autogenic processes

(Davies *et al.*, 2019). This has secondary consequences for the detectability of environmental signals, which could be significantly reduced due to incompleteness, meaning periodic signals could be defined as statistically insignificant, or missed entirely (Foreman & Straub, 2017; Griffin *et al.,* 2023; Straub *et al.,* 2020). Although this is predicted, the relationship between signal detectability and stratigraphic incompleteness, and a framework to predict signal detectability as a function of incompleteness and input signal properties is not yet established (Burgess *et al.*, 2019; Foreman & Straub, 2017; Trampush & Hajek, 2017). Understanding how incompleteness affects the preserved structure of autogenic processes is of fundamental importance for establishing robust confidence limits for signal detectability within environmental measurables.

Here, we quantify 1) how incompleteness modifies the preserved record of autogenic surface processes and 2) how incompleteness influences the detectability and apparent degradation of environmental signals from a time series of sediment flux. To do this, we utilise a physical rice pile as an idealised STS, from which a time series of sediment flux is generated at discrete time intervals. The rice pile can provide a basis from which natural STSs and strata can be understood, as the complex internal dynamics which arise from storage and release along a 1D path elucidate the nature of autogenic processes in field scale systems (Bak *et al.,* 1987; Frette *et al.,* 1996; Griffin *et al.,* 2023; Jerolmack & Paola, 2010). The distribution of these sediment flux events within the rice pile is heavy tailed, which has also been measured and theorized for many field scale systems. However, the statistics of these fluxes are not linked to the same processes at play in field-scale systems, hence we do not focus on the specific processes but rather the ramifications of having a stochastic time series of sediment flux, bound by process timescales and finite size effects. Although the rice pile does not directly generate strata, it produces a time series of sediment flux from a single location, which is a measurable attribute that links both Earth surface processes and strata (Toby *et al.*, 2022). The time series generated is comparable to a time series of stratigraphic measurables collected from a 1D vertical section, which provides insight into the complex internal dynamics operating up-system of this location (Figure 4.1). Physical rice piles have been utilised to generate theoretical frameworks for the signal degradation and detection in STSs (Griffin *et al.,* 2023; Jerolmack & Paola, 2010). Here, we advance this framework to understand the effect of incompleteness on the structure of autogenic noise and the detectability of environmental signals. This will provide a robust framework that can be used to predict the ability of various geomorphic environments to record evidence of external environmental perturbations.

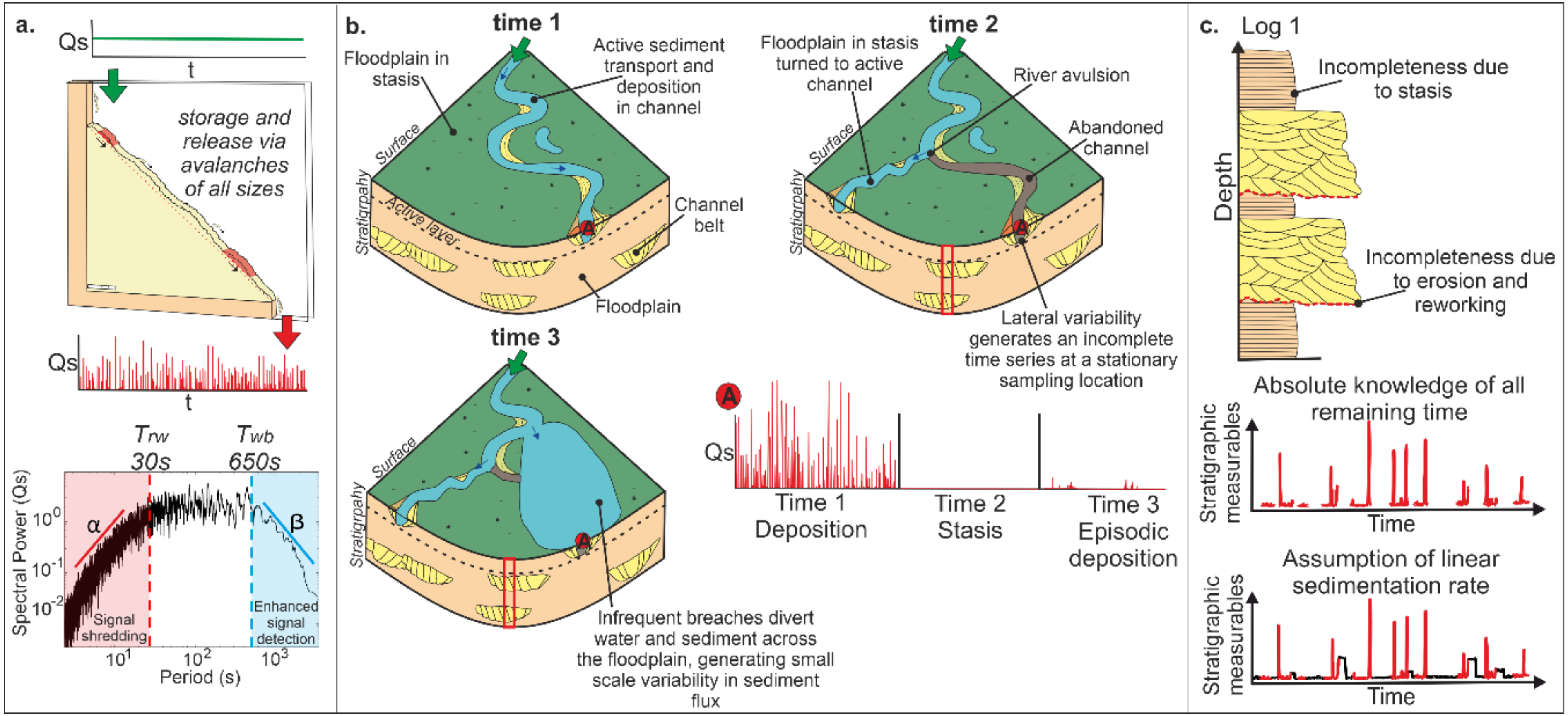

Figure 4.1: The nature of autogenic processes and the generation of an incomplete stratigraphic record

(a) *Schematic illustration of the physical rice pile run under a constant input rate, highlighting the stochastic sediment flux time-series generated, comparable to a time-series of preserved deposition rates produced from natural systems. This generates power spectra with tripartite spectral structure defining two autogenic timescales,* T_{rw} *and* T_{wb}*.* ***(b)*** *Autogenic dynamics within the Earth's surface promote constant system reorganization, causing episodes of deposition, erosion and stasis (non-deposition), generating an incomplete time series of sediment flux at a stationary sampling location, defined by the red circle.* ***(c)*** *Sedimentary log taken from the red rectangle in Figure 1B. Time series of stratigraphic information, containing temporal gaps and accumulating under variable sedimentation rates. If the absolute ages of all remaining sediment are known, the time series contains gaps of varying duration. To overcome this, the time series is bound by sparsely dated horizons under the assumption of a linear sedimentation rate between these points.*

4.2. Materials and methods

4.2.1. Experimental design

We use a suite of rice pile experiments presented in Griffin *et al.,* (2023). These experiments have precisely controlled boundary conditions and generate a time series of efflux which is 100% complete, compared to the incomplete time series generated from stratigraphic measurables. The experimental apparatus is constructed of two vertical, parallel glass sheets 0.37 m long, positioned 0.026 m apart (Figure 4.1A). Rice was fed (influx) to the pile from a dry particle feeder (Schenk Accurate) positioned 0.008 m from the top surface, allowing a rice pile to form at a critical angle so that a dynamic topographic equilibrium was achieved. Over the suite of experiments, influx was defined between a minimum and maximum range (0 g s^{-1} and 0.78 g s^{-1} controlled at 1 second intervals via a computer connected to the sediment feeder which directly feeds the pile. Efflux was measured at approximately 1 second intervals using an Ohaus EX12002 balance (accuracy and precision of 0.1 g). The balance has a maximum mass of 12 kg, and all experiments were run until the balance was saturated. The dimensions of rice grains used in the experiments have a diameter of 0.0025 ±0.5 m, length of 0.008 ±0.5 m and an average mass of 0.02 g. The experimental set-up is similar to that of the physical rice pile of (Frette *et al.* 1996)

We first utilize the control experiment, run with a constant influx rate of 0.37 g s^{-1}. The influx rate denotes the mean rate of the sediment feeder, and the experimental run time (nine hours) defines the time to saturate the balance at the specified influx rate. This experiment was used to quantify the effect of stratigraphic incompleteness on the spectral structure of autogenic processes and to generate confidence bands to quantify signal detectability within power spectra of tripartite geometry.

To quantify the effect of incompleteness on signal detectability and apparent signal degradation, we utilize 36 experiments run with cyclic influx (where influx rate follows a sinusoid) of different periods and amplitudes. To achieve parity with the control experiment, a mean influx rate of 0.37 g s^{-1} was attained for all cyclic experiments. 9 periodicities were chosen to cover the range of autogenic timescales present (Figure 4.1): 6s, 12s, 24s, 48s, 100s, 250s, 500s, 1000s and 2000s. Signal amplitude was chosen as percentages of the mean feed rate (0.37 g s^{-1}), increasing in 25% intervals from 25% (0.0925 g s^{-1}) to 100% (0.37 g s^{-1}).

4.2.2. The removal and interpolation of time within a time series

4.2.2.1. Removing time from a time series

The spectral structure of autogenic processes has been quantified from a 100% complete time series (Griffin *et al.*, 2023); we explore the implications of imperfect sampling on the temporal by systematically removing data from the time series. The sediment flux time series generated from the rice pile is limited to positive values and zeros; positive values are analogous to depositional events and zeros are analogous to stasis events. This is comparable to a time series of preserved deposition rates generated from natural systems.

Physical experimental results suggest the duration of depositional events (t_k) on deltas exhibit an exponential distribution (Ganti *et al.*, 2011):

$$PDF(t_k) = \lambda e^{-\lambda t_k}$$

Where λ is a rate parameter which defines the mean number of events in an interval, here set to 0.5 so the mean duration of depositional episodes is generally lower than the mean duration of temporal gaps (Ganti *et al.,* 2011). This distribution defined the amount of time kept at each iteration.

Conversely, stasis events (t_r) within a system exhibit a truncated Pareto distribution (Ganti *et al.*, 2011):

$$PDF(t_r) = \frac{\tau \gamma^{\tau} {t_r}^{-\tau-1}}{1-(\frac{\gamma}{\upsilon})^{\tau}}$$

Where τ is the tail index which controls the shape of the distribution, γ is the smallest time step removed (here, set to 1) and υ is the truncation parameter, which defines the largest time step removed (here, set to 650s, which is equivalent to the longest autogenic timescale, T_{wb}, which is 650s in the rice pile control experiment (Griffin *et al.,* 2023). This distribution defines the amount of time removed at each iteration.

To generate an incomplete time series, a random number from within the limits of the exponential distribution is generated, defining the number of time steps kept. Following this, a random number from within the limits of the truncated Pareto distribution was generated, defining the number of time steps removed. This pattern was repeated for the full length of the time series. Completeness was systematically varied between 100% and 1% by changing the tail index (τ) of the truncated Pareto distribution between 3 and 0.05 respectively. We acknowledge this is not exactly akin to how stratigraphy is generated; as we utilise the overall percentage completeness of a time series, we believe this is comparable to natural systems that produce time series with similar overall completeness. This method allows us to explore the impact of incompleteness on both the spectral structure of autogenic processes and signal detectability.

The new discrete time series, generated by removing proportions of time contains gaps of varying duration. This variable discretization of time resembles the record of autogenic processes recorded in stratigraphy that could be produced if the absolute ages of all sediment present were known. To generate power spectra from a time series containing gaps of varying duration, we use the Lomb-Scargle Periodogram which is the best available technique to compute periodicity directly from unevenly sampled data (VanderPlas, 2018).

4.2.2.2. Interpolation using an assumption of linear sedimentation rate

The lack of age constraint within stratigraphy means that generating a time series with absolute knowledge of time is improbable. Instead, the section in question can be bound by sparsely dated horizons under the assumption of a linear sedimentation rate between these points. This method is applied to produce linearly sampled time series from many environmental measurables (Sadler, 1981; Hofstra *et al.*, 2008; Wu *et al.*, 2013; Martínez-Graña *et al.*, 2016). We utilize both these methods in order to compare the spectral structure of autogenic processes and signal detectability generated from a time series containing temporal gaps to the record influenced by the assumption of linear sedimentation. We interpolate the degraded time series onto a time interval of 1 second between the first- and last-time step using the nearest neighbour method, where the interpolated value at the query point is the value at the nearest sample grid point. If a linear sedimentation rate is assumed in a time series of stratigraphic measurables, beds bounding significant temporal gaps are thicker than average and are hence overrepresented in the apparent time. The method of interpolation chosen in this work aims to mimic this. To generate power spectra from the linear time series, we utilise the multi-taper method (MTM) with 2 tapers (Thomson, 1982).

4.2.3. Signal detectability and apparent signal degradation

To make a statistical statement about the presence or not of an influx signal in the power spectra generated from a time series of efflux, a statistical model with a good fit to the background noise spectrum must be applied from which confidence bands can be generated (Vaughan *et al.*, 2011).

As blue noise is present within the power spectra, the commonly utilised autoregressive lag 1 (AR1) model provides a poor approximation of the spectral structure (Figure S4.1). We overcome this by constructing a spectral model and suite of associated confidence bands for power spectra of tripartite structure through adaptation of the bending power law (BPL) model (McHardy *et al.*, 2004; Vaughan, 2010; Vaughan *et al.*, 2011) to account for two spectral gradient breaks. The BPL model optimizes a best fit of the function to the data and smoothly changes from one power law to another (McHardy *et al.*, 2004):

$$S_{BPL} = \frac{Nf^{-\alpha 1}}{1 + \left(\frac{f}{f_b}\right)^{\alpha 2 - \alpha 1}}$$

Where S is the power at a given frequency, f, N is a power-law normalization factor, f_b is the frequency associated with the bend in the power-law from one trend described with a slope of $\alpha 1$ to a second trend described by a slope of $\alpha 2$.

We augment this equation to account for two bends in the power spectra and generate the double bending power law (DBPL) model;

$$S_{DBPL} = \frac{Nf^{-\alpha 1}}{1 + \left(\frac{f}{f_{b1}}\right)^{-\alpha 1} + \left(\frac{f}{f_{b2}}\right)^{\alpha 2 - \alpha 1}}$$

Where S_{DBPL} is the spectral power at a given frequency, f. N is a power law normalization factor, $\alpha 1$ is the slope of the power law at high frequencies, $\alpha 2$ is the slope of the power law at low frequencies and f_{b1} and f_{b2} are the frequencies of the two bends. This equation assumes the slope of the power law at intermediate frequencies is zero (white noise). This spectral model provides a strong statistical fit to the power spectra generated from the physical rice pile (Figure S4.2).

To quantify signal detectability, the 95% confidence band generated from the DBPL model was applied to the power spectra of the efflux. The ratio between the power of the signal spike and the power of the 95% confidence band at the imposed periodicity was quantified: if this ratio exceeds 1, a signal is considered statistically detectable.

To quantify the amount of apparent degradation a signal experiences due to incompleteness, we stack the efflux time series into lengths equal to the input period, and take the mean of the efflux for each second over the imposed periodicity. From this, we gain a mean ensemble efflux to which we fit a sine wave with a period equal to the known input, and are returned an amplitude and phase based on the signal present in the mean ensemble efflux. We compare the amplitude of the signal evident in the ensemble efflux, to that of the known input signal and quantify a percentage similarity (Griffin *et al.,* 2023)

Data is removed from the time series randomly, hence the detectability and apparent degradation of a sinusoidal sediment flux signal is dependent on the exact data points removed. Whilst two time series may have the same completeness, different parts of a sinusoidal signal may be removed each time which influences signal degradation and detectability. To quantify a representative detectability and apparent degradation for each incompleteness interval, the time series was degraded randomly 5 times and an average detectability and apparent degradation was quantified. 5 iterations are the minimum number required to stabilize the trends seen in Figures 4.4 and 4.5.

4.3. Results

4.3.1. Incompleteness on the structure of autogenic processes

Firstly, we quantify the temporal structure of autogenic processes evident within stratigraphy using a time series containing temporal gaps of varying duration (Figure 4.2). This provides understanding of how incompleteness alone influences the spectral structure of autogenic processes. When power spectra are generated from a time series which is between 100% and 35% complete, all three noise regimes (red, white and blue noise) are present. As completeness decreases beyond 50% the temporal range of the red noise regime is gradually reduced, as short time scales are progressively removed from the power spectra; this is indicated by T_{rw} moving progressively to the left as completeness decreases (Figure 4.2A). In contrast, the timescales over which blue noise persists are consistently present. As completeness decreases, the gradient of spectral growth (red noise) and spectral decay (blue noise) both decrease at a linear rate, meaning the structure of these noise regimes becomes increasingly difficult to distinguish. When completeness is reduced to 50%, the structure of blue noise is lost, rendering the power spectra to white noise over all timescales greater than T_{rw}. This is indicated by T_{wb} disappearing as completeness decreases below 50% (Figure 4.2A). As completeness is reduced to below

35%, short timescales continue to be removed from the power spectra; at 15% complete, all timescales less than T_{rw} are removed, rendering the power spectra to solely white noise.

Secondly, we quantify the structure of these processes evident within an incomplete time series where the temporal gaps have been removed through interpolation using the assumption of linear sedimentation rate. This is analogous to a time series of stratigraphic information (Figure 4.3). When the time series is between 100% and 35% complete, all three noise regimes (red, white and blue noise) are present within the power spectra. The timescales over which both red noise and blue noise persist are consistently present. Although the structure of the red noise regime remains easily distinguishable with decreasing completeness, identifying blue noise is difficult when completeness is reduced to 50% as the gradient of spectral decay (blue noise) decreases. When completeness is below 50%, the structure of blue noise is lost, rendering the time series to white noise over all timescales greater than T_{rw}. This is indicated by T_{wb} disappearing as completeness decreases below 50% (Figure 4.3A). As completeness is reduced to below 35%, T_{rw} gradually increases from 30 seconds to more than 1000 seconds, as high-frequency noise is added to the time series via interpolation. This is indicated by T_{rw} moving progressively to the right as completeness decreases (Figure 4.3A).

.

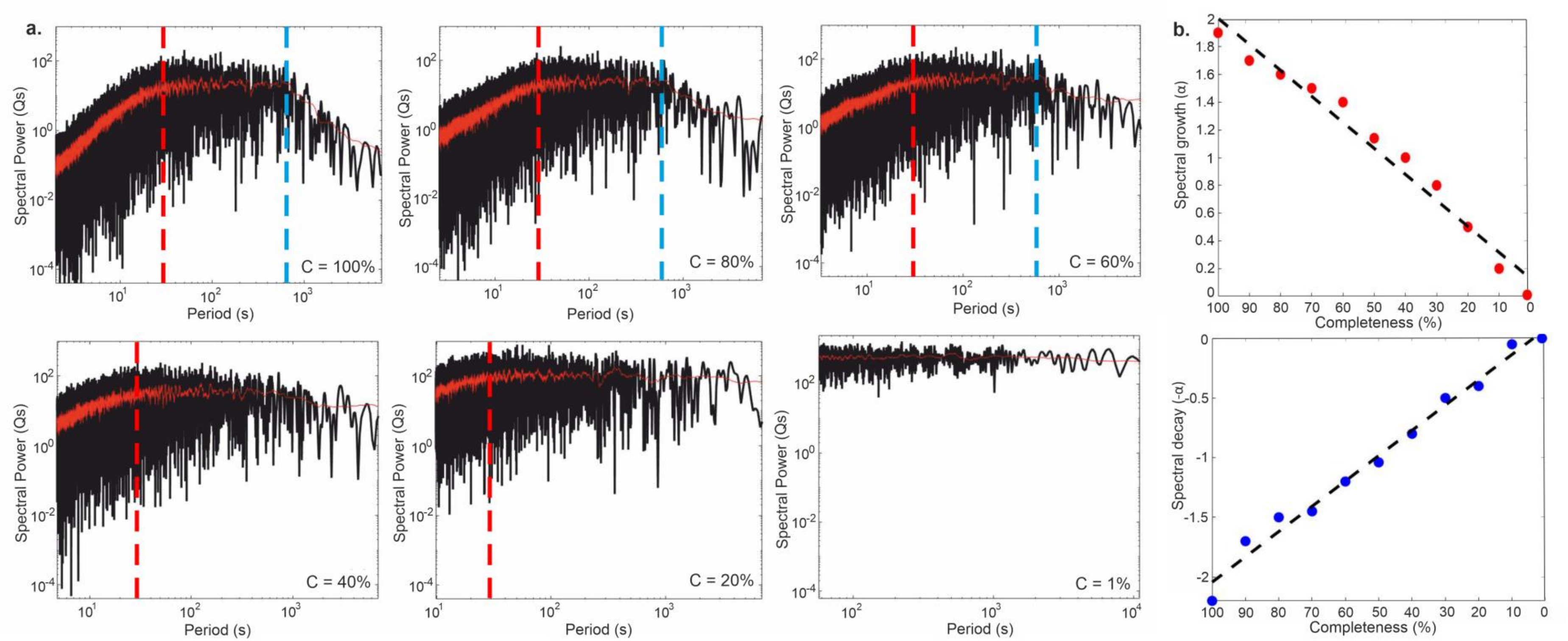

Figure 4.2: The temporal structure of autogenic processes evident from a time series containing temporal gaps of varying duration

(a). *Power spectra generated from a time series of efflux from the control experiment (influx rate of 0.37 g s^{-1}), where time has been systematically removed in approximately 10% intervals as a proxy for stratigraphic incompleteness. The full spectrum is shown in black, with the mean spectra shown in red. The vertical dashed lines denote the autogenic timescales, T_{rw} (red) and T_{wb} (blue). The percentages in the bottom right corner of each panel denote the percentage completeness (C). The time series utilised is non-linear, to resemble the record of autogenic processes in stratigraphy that could be reproduced if the ages of all sediment were known. Due to the temporal gaps within the time series, power spectra have been generated using the Lomb-Scargle periodogram.* ***(b)*** *Variations in the spectral gradient (see Figure 4.1) of the red noise regime (top) and the blue noise regime (bottom) as a function of completeness.*

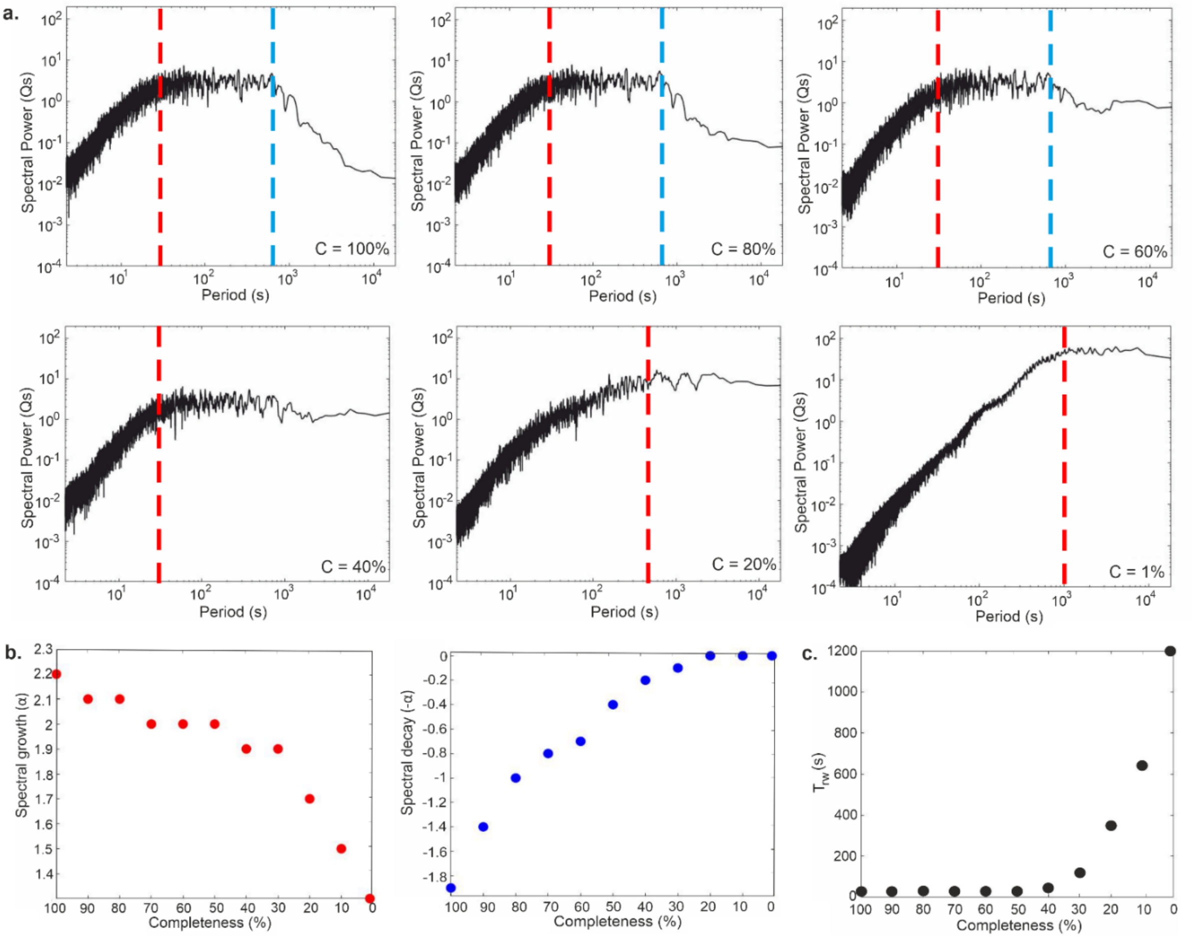

Figure 4.3: The temporal structure of autogenic processes is evident from a time series where the temporal gaps have been removed through interpolation using the assumption of linear sedimentation rate

***(a)** Power spectra generated from a time series of efflux from the control experiment (influx rate of 0.37 g s^{-1}), where time has been systematically removed in approximately 10% intervals as a proxy for stratigraphic incompleteness. The vertical dashed lines denote the autogenic timescales, T_{rw} (red) and T_{wb} (blue). The percentages in the bottom right corner of each panel refer to the completeness (C) of the time series. The time series has been interpolated onto a regular time interval to resemble a time series produced from stratigraphic measurables where a linear sedimentation rate is assumed. Power spectra have been generated using the multi-taper method (MTM) with 2 tapers. **(b)** Variations in the spectral gradient of the red noise regime (left) and the blue noise regime (right) as a function of completeness. **(c)** Variations in T_{rw} as a function of completeness.*

4.3.2. Incompleteness on the detectability of environmental signals

Firstly, we quantify signal detectability from a time series containing temporal gaps of varying duration (Figure 4.4), which provides insight into how incompleteness alone influences signal preservation. Signals with periodicity less than T_{rw} are undetectable over all amplitudes within a complete time series due to signal shredding and are therefore undetectable over all amplitudes within a time series which is incomplete to any degree (Griffin et al. 2023). High amplitude signals (100% of the mean feed rate) with periodicity between T_{rw} and T_{wb} are detectable within a complete time series. As completeness decreases, signal detectability also decreases, but high amplitude signals over these periodicities remain detectable within a time series over all levels of completeness (Figure 4.4). As the amplitude of these influx signals are reduced, signal detectability decreases and medium amplitude signals (50% of the mean feed rate) with periodicity between T_{rw} and T_{wb} can be rendered undetectable in a time series with low completeness. Low amplitude input signals (25% of the mean feed rate) with periodicity between T_{rw} and T_{wb} are undetectable within a complete time series as they are obscured by autogenic noise (Griffin et al. 2023), hence these signals are undetectable within a time series which is incomplete to any degree (Figure 4.4). Long period signals with periodicity greater than T_{wb} show enhanced detectability (Griffin et al. 2023), hence high amplitude, long period influx signals remain highly detectable within time series over all levels of completeness.

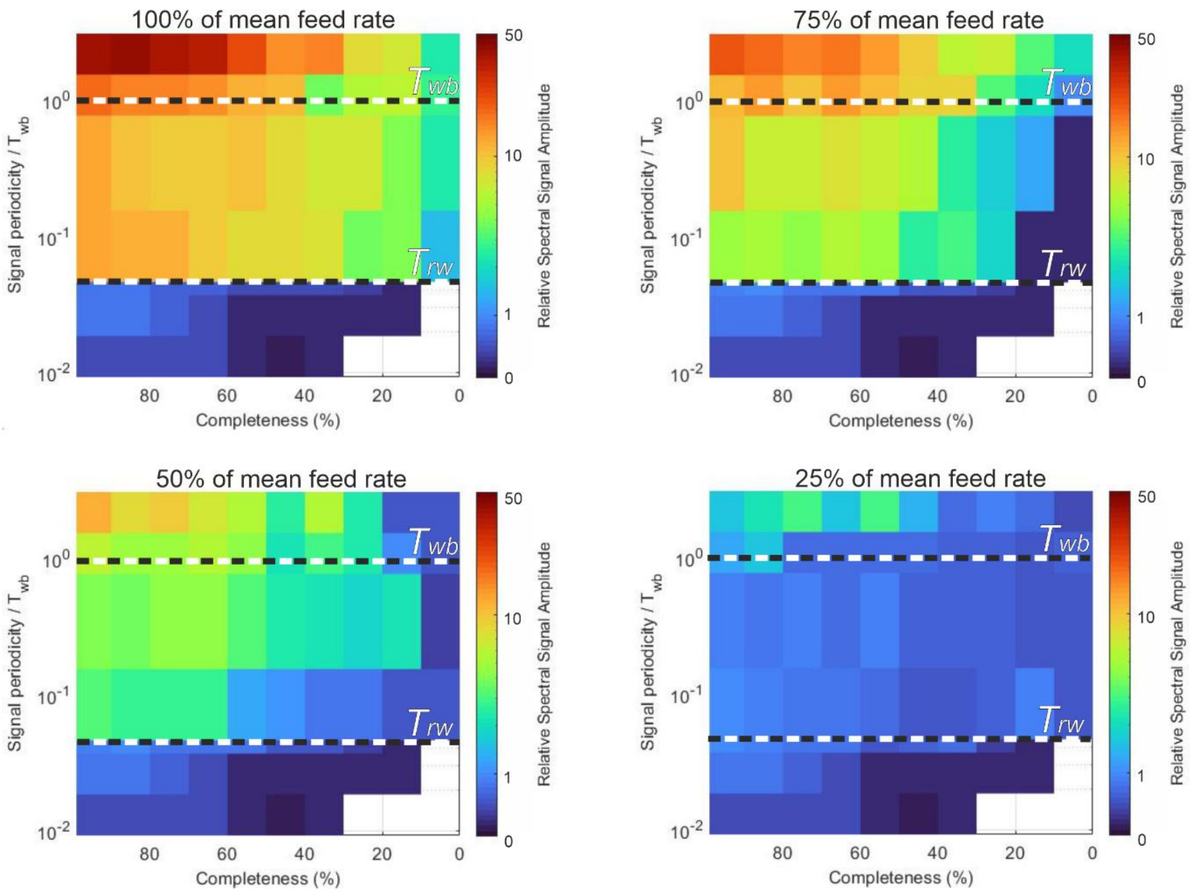

Figure 4.4: Signal detectability from a time series containing temporal gaps of varying duration

The combined effects of signal periodicity, amplitude and stratigraphic completeness on signal detectability. Signal amplitude decreases in 25% intervals.

Secondly, we quantify the detectability of signals from a time series where the temporal gaps have been removed through interpolation using the assumption of linear sedimentation rate. This is analogous to a time series of stratigraphic information (Figure 4.5). Overall, a divide in signal detectability is evident when completeness is approximately 50%. This is intuitive, as approximately half the time series, and hence the influx signal, is removed and replaced with high-frequency noise. Signals with periodicity less than T_{rw} are undetectable over all amplitudes within a complete time series due to signal shredding by autogenic processes and are therefore undetectable over all amplitudes within a time series which is incomplete to any degree (Griffin *et al.* 2023) (Figure 4.5). High amplitude signals with periodicity between T_{rw} and T_{wb} are detectable within complete time series. As completeness decreases, signal detectability also decreases, but high amplitude signals over these periodicities remain detectable within a time series overall levels of completeness (Figure 4.5) . As the amplitude of the influx signal is reduced, signal detectability reduces dramatically, where medium amplitude signals show minimal detectability even within a highly complete time series. Low amplitude input signals are undetectable within a complete time series as they are obscured by autogenic noise (Griffin et al. 2023), hence these signals are undetectable within a time series which is incomplete to any degree. Signals with periodicity greater than T_{wb} show enhanced detectability when completeness is high (Griffin et al., 2023), however as completeness is reduced to below 50%, signals become difficult to differentiate from autogenic noise. As the amplitude of the influx signal is reduced, the detectability of these long-period signals significantly reduces, where low amplitude long-period signals are rendered undetectable when completeness is below 80% (Figure 4.5).

4.3.3. Incompleteness on the apparent degradation of environmental signals

Autogenic processes degrade sediment flux signals when the amplitude of the signal is less than T_{rw} (Jerolmack & Paola, 2010; Griffin *et al.,* 2023). Given this, we explore the apparent degradation experienced by environmental signals as a result of incompleteness. Here, apparent degradation refers to the reduction in signal amplitude experienced due to incompleteness. This is analogous to the reduction in signal amplitude which occurs due to signal shredding (Griffin *et al.,* 2023).

For both time series containing temporal gaps of varying duration, and time series in which these gaps have been moved by interpolation, signals with periodicity less than T_{rw} experience a severe degradation in amplitude as a result of shredding by autogenic processes and therefore are severely degraded within a time series which is incomplete to any degree (Griffin *et al.,* 2023) (Figure 4.6).

Signals with periodicity greater than, but close to T_{rw} experience a gradual increase in degradation as completeness decreases, where they are severely degraded when completeness is low (<30%). Although degraded, these signals can still be reconstructed by stacking the time series over all levels of completeness. Long period signals above T_{rw} and T_{wb} experience minimal degradation until completeness is low (<30%) where the recoverable signal amplitude is approximately than half of the known input amplitude.

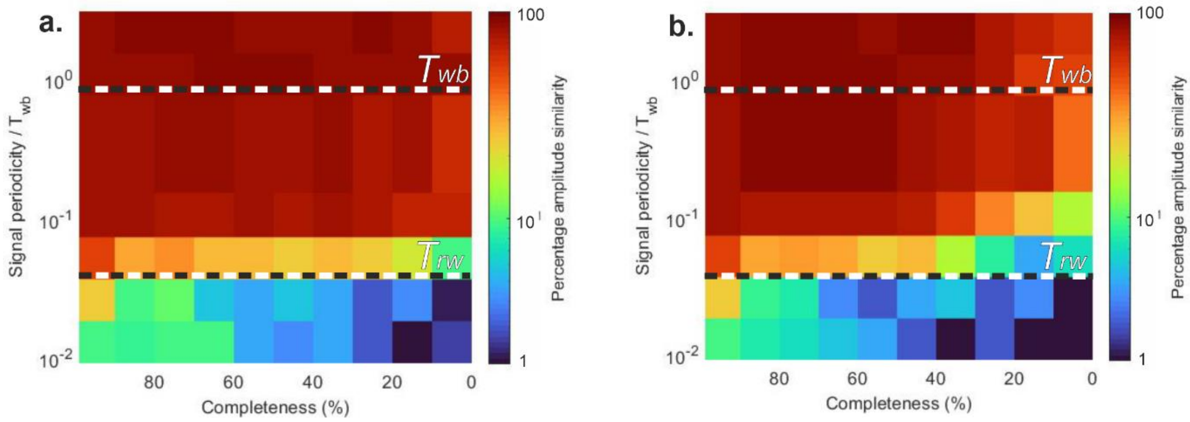

Figure 4.6: The dual role of signal periodicity and stratigraphic incompleteness on apparent signal degradation.

(a). *Apparent signal degradation from time series containing temporal gaps of varying duration.* ***(b)*** *apparent signal degradation from time series where the temporal gaps have been removed through interpolation using the assumption of linear sedimentation rate. Signal degradation is not influenced by signal amplitude (Griffin et al. 2023), hence apparent signal degradation has only been quantified for signals with amplitudes equivalent to 100% of the mean feed rate.*

4.4. Discussion

4.4.1. The apparent colours of noise in sediment transport systems

The tripartite spectral structure of autogenic processes is evident from a time series of high temporal resolution (Griffin *et al.*, 2023), however the spectral structure of these processes preserved in stratigraphy is rarely representative of their true character. Whilst we turn to strata as an archive of Earth's surface processes and environments, this record is inevitably incomplete (Paola *et al.*, 2018; Sadler, 1981; Schumer & Jerolmack, 2009; Straub & Esposito, 2013; Straub & Foreman, 2018; Vendettuoli *et al.*, 2019), which hinders and warps our interpretation of the spatiotemporal scales of autogenic dynamics present within a STS.

Stratigraphers have long known that all stratigraphic sections are incomplete (Ager, 1973; Hutton, 1788; Sadler, 1981), hence efforts have been made to understand the circumstances which allow for the reconstruction of environmental signals from incomplete records, encompassing both autogenic timescales and the properties of environmental signals (e.g. Foreman & Straub, 2017; Kemp & Sexton, 2014; Trampush *et al.*, 2017). However, the impact of incompleteness on the spectral structure of autogenic processes has not been deeply considered, as the preserved noise is assumed to accurately characterise the full spatiotemporal scales of autogenic processes within landscapes and strata. We show the importance of also understanding the noise removed in the process. As completeness decreases, the preserved record is less faithful to the full spectrum of autogenic processes, hindering our ability to reconstruct paleo-surface processes. However, the structure of the resulting power spectra can provide stratigraphers with an approximate evaluation of completeness, from which the full spectral structure can be estimated. Quantifying the change in spectral growth and decay as a function of completeness allows us to infer the structure and strength of paleo-surface processes from an incomplete record and hence to some extent recreate the autogenics within a STS.

Although blue noise is common in power spectra generated from a time series of Earth surface processes with sufficient duration (e.g. Benavides *et al.,* 2022; Lazarus *et al.,* 2019; McKean & Roering, 2004;), evidence of this regime within power spectra generated from stratigraphic measurables is generally rarer (e.g. Aziz *et al.,* 2008; Perron & Huybers, 2009; Vaughan *et al*., 2011) (Figure 6). Our results suggest this is predominantly due to stratigraphic incompleteness filtering the preservation of surface processes, where one effect is to remove evidence of blue noise. The magnitude of the autogenic events associated with this spectral regime generates a system-scale response (e.g. the largest autogenic events within a system of a defined size). However, the rarity of these events within a STS renders them more likely to be removed (Ganti *et al*., 2020), or at least significantly reduced in scale, from a time series of stratigraphic measurables. The removal of the Elwha Dam in Washington, USA released 20 million tons of sediment, generating a huge sediment wave downstream and initiating a rapid aggredational response (Ritchie *et al.*, 2018). Although the response to this event was large, the associated geomorphic imprint rapidly waned, and channel incision dispersed the deposits of the initial sediment wave (East *et al.*, 2018), which could massively reduce the stratigraphic evidence of this event. Furthermore, the sedimentary record at one locality in a STS may not record evidence of all sediment-transport events, as the signal may not be of sufficient magnitude to propagate and deposit downstream. For example, a 500 million ton sediment pulse generated in response to knickpoint collapse on the Rio Coca, Ecuador occurred in the upstream reach but is undetectable at the mouth of the Amazon (Crespo *et al.,* 2024). Field evidence over a range of scales suggests stratigraphy is more likely to record mundane, common transport conditions (Ganti *et al.,* 2020). This means small-scale sediment-transport events can be removed entirely from the record, but their high frequency allows for regularity in preservation. Although the time series in question may not record the full extent of autogenic processes, this does not mean they are absent within the system; care must be taken to differentiate these concepts. To ensure the most accurate reconstruction of autogenic dynamics within a STS, we must aim to reduce the requirement to interpolate a time series as much as possible. Absolute knowledge of time is unattainable; instead a high sampling resolution allows temporal gaps to be minimized and result, as much as possible, from incompleteness alone. This will allow scientists the ability to identify and account for as many unconformities as possible, as well as develop techniques to improve the messy conversion from space to time (Barefoot *et al.*, 2023).

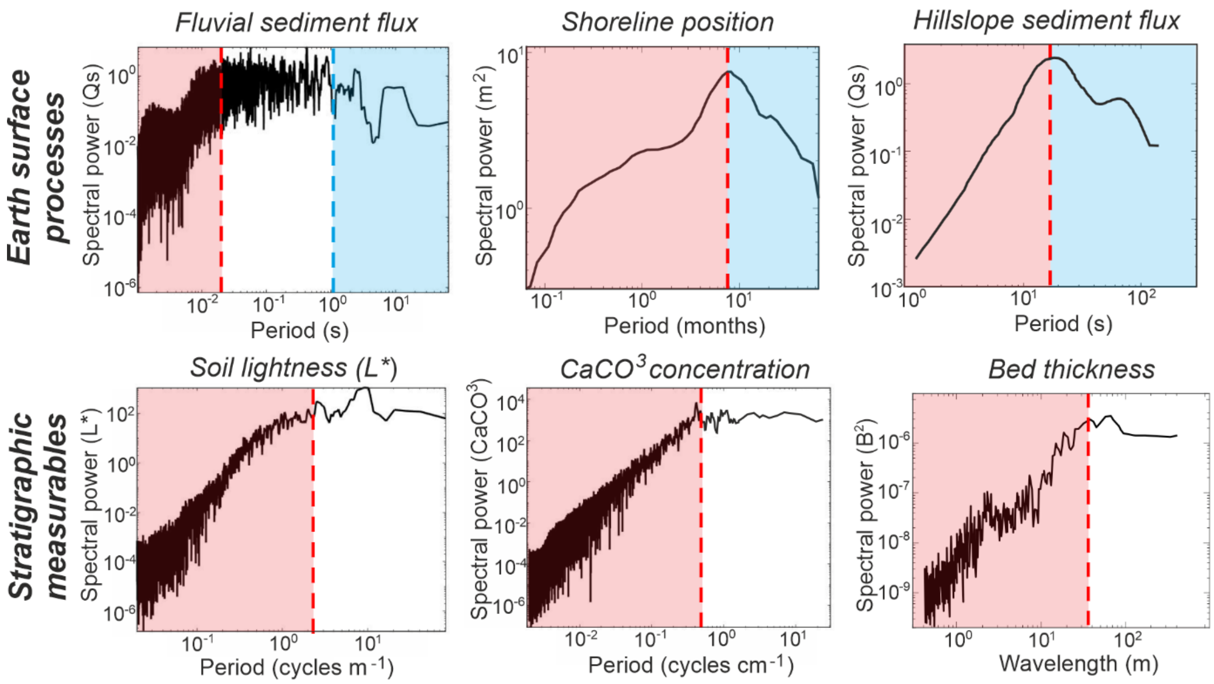

Figure 4.7: The spectral structure of autogenic processes preserved within surface and stratigraphic measurables.

Top: *Power spectra generated from time series of surface processes, where all spectra show evidence of red and blue noise, hypothesised to be universal. Data taken from: Benavides et al., (2022); Lazarus et al., (2019); McKean & Roering (2019).* ***Bottom:*** *Power spectra generated from a time series of stratigraphic measurables, where the full spectral structure of autogenic processes is not present in the* *majority of the spectra shown. Data taken from: Aziz et al., (2008), Vaughan et al., (2011), Perron & Huybers (2009).*

The preservation of blue noise within power spectra generated from a time series of stratigraphic information (either physical measures or chemical data as a proxy for an environmental change) is infrequent, but we highlight that some studies find evidence of blue noise (Figure 4.7) (Abels *et al.*, 2013; Dunkley Jones *et al.*, 2018; Kurokawa *et al.*, 2019; Liu *et al.*, 2023; Pas *et al.*, 2020). However, blue noise is often discounted to apply the autoregressive lag 1 (AR1) spectral estimation model. The ease of visually identifying the noise regimes present within power spectra is dependent on how the data is displayed (Figure 4.8). Power spectra generated from stratigraphic measurables are commonly displayed with a linear frequency axis, which allows alleged periodicity to be equated to cycles per meter. This impedes the identification of the noise regimes present. In this case, blue noise appears as a sharp drop in power at low frequencies that is easily missed, especially when the rest of the power spectra appear to resemble a sloping continuum from low to high frequencies common with a red noise process (Weedon, 2003). This can explain the common thought that stochastic variations in sediment transport are characterised in power spectra by red noise, where the spectral rollover to white noise is thought to define the upper limits of stochasticity within a STS (Jerolmack & Paola, 2007, 2010; Meyers, 2012; Vaughan *et al.*, 2011; Weedon, 2003). Instead, displaying the same data with a logarithmic period axis allows the full spectral structure to be visualized and interpreted with more clarity (Figure 4.8). Therefore, the tripartite spectral structure of autogenic processes may not be as rare as thought, but instead, misinterpreted. We must now look beyond the traditionally assumed Gaussian noise models and instead establish realistic expectations of the structure of autogenic variability produced and also preserved in the stratigraphic record (Grove *et al.*, 2022; Tu *et al.*, 2023). This highlights the requirement to understand the true temporal structure of autogenic processes within a system, and how to best analyse the data before inverting spectra for paleo-surface process interpretation and signal detectability. Accounting for blue noise within power spectra generated from stratigraphic measurables has significant implications for generating estimates of spectral background structure from which confidence bands are produced to determine the presence of environmental signals (Hajek & Straub, 2017; Vaughan *et al.*, 2011). The AR1 model, which assumes the power spectra only contain red noise over high frequencies and white noise over low frequencies, is commonly applied to all power spectra generated for paleoclimate analysis, as the presence of blue noise is often overlooked. If the AR1 model is applied to power spectra that contain blue noise, the model would generate confidence bands where the expected power at low frequencies will be underestimated relative to the true power of the spectra. This means the transition to blue noise could be confused with a statistically significant periodicity, resulting in false positives and spurious signals (Hajek & Straub, 2017).

Although incompleteness has minimal impact on the spectral structure of autogenic processes until a time series is less than 50% complete at common discretization timescales, we do not include other time-reducing effects. Alongside incompleteness, low measurement resolution and/or the utilization of short temporal records can further hinder the preservation of autogenic processes. Although blue noise should be evident within a time series of moderate completeness, in reality, evidence of the full tripartite spectral structure may be removed if the time interval of measurement is shorter than the maximum autogenic timescale, or due to the short time series studied. Whilst the length of the time series available from stratigraphic measurables is bound by outcrop availability or the length of core extracted, to achieve the best estimate of autogenic spectral structure the measurement resolution utilised should be considered carefully to allow for the most thorough temporal sampling. Although we can control these factors to some extent, a time series of stratigraphic measurables is already substantially hindered if the time series is significantly incomplete. Further work should focus on understanding the effects of measurement resolution on the structure of autogenic processes and work to define an optimal measurement resolution for stratigraphic time series analysis.

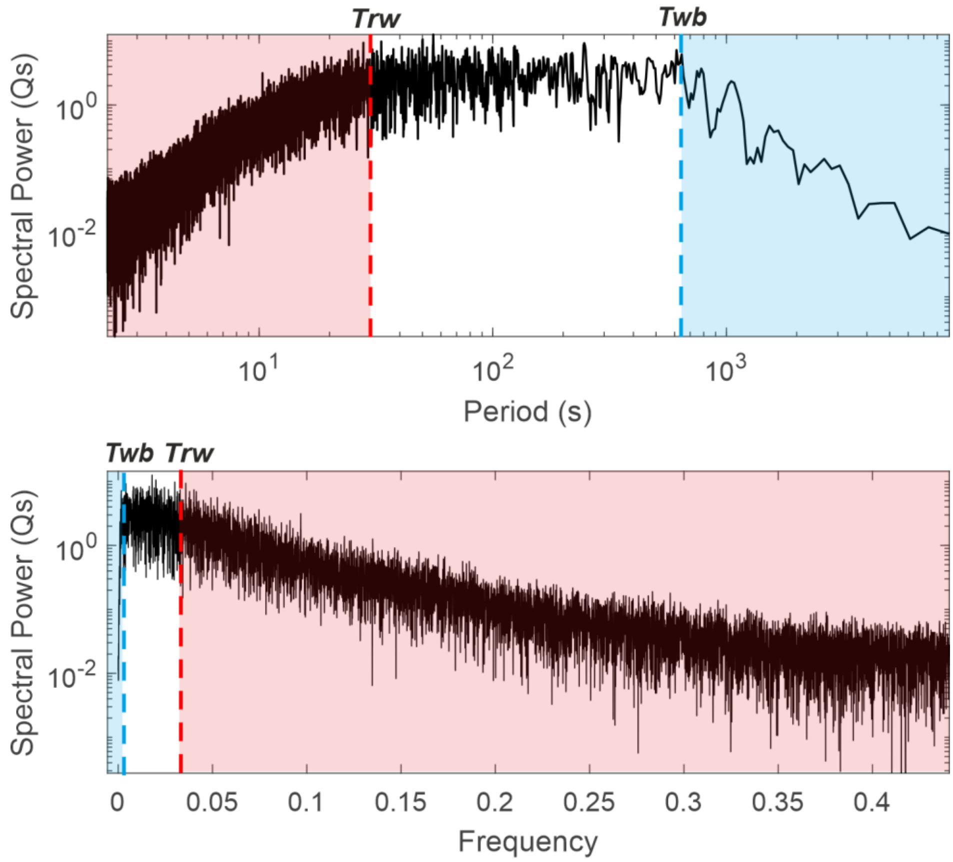

Figure 4.8: Power spectra generated from the control experiment (influx rate of 0.37 g s^{-1}) with both autogenic timescales, T_{rw} and T_{wb}, highlighted.

Top: *Power spectra plotted as a function of period, where the x-axis is displayed logarithmically. The tripartite spectral structure is evident.* ***Bottom:*** *Power spectra plotted as a function of frequency, where the x-axis is displayed linearly. The spectra appear to resemble a sloping continuum from low to high frequencies common with a red noise process, however the presence of blue noise is evident at low frequencies by the sharp drop-off in spectral power.*

4.4.2. Quantifying signal detection and degradation from an incomplete record

To overcome poor age constraints within stratigraphic sections, sediment age is linearly interpolated between sparsely dated horizons (Abels *et al.*, 2013; Ramos-Vázquez *et al.*, 2017); however, incompleteness and substantial interpolation can hinder our ability to differentiate signal degradation and detection timescales. The loss of blue noise from power spectra due to incompleteness impedes our ability to quantify T_{wb}. This means the maximum timescale of autogenic organization and the timescales of faithful signal preservation over all amplitudes cannot be quantified (Griffin *et al.*, 2023). However, this timescale has been predicted to be of similar magnitude as the compensation timescale, T_c (Griffin *et al.*, 2023). T_c can be defined from stratigraphy (Wang *et al.*, 2011), hence allowing for approximation of T_{wb}. The substantial interpolation of stratigraphic time series can drive the red-to-white noise transition (e.g. T_{rw}) to longer timescales (Figure 3), extending the duration of apparent correlation due to the addition of high-frequency noise via interpolation. This generates an apparent spectral T_{rw}, which can be over an order of magnitude larger than the true T_{rw}, and hence an apparent shredding regime. If T_{rw} is known, this extended red noise regime can be differentiated into true and apparent red noise and the true shredding timescales can be defined. However, the reliance on power spectra to quantify T_{rw} means signals with periodicity over all apparent red noise timescales will appear shredded when instead incompleteness renders them undetectable.

Incompleteness also has direct ramifications for the detectability and reconstruction of environmental signals from stratigraphic measurables. Incompleteness has been described as having power-limiting effects on signals (Kemp, 2012), where the power of the signal spike is significantly diminished when compared to the signal spike from a complete time series. Therefore, a signal that only just breaches the 90% confidence band is the best we can hope for (Hilgen *et al.*, 2015; Kemp, 2012). We show that when the absolute ages of all sediment present in the time series are known, the impact of incompleteness on signal detectability is minimal. The direct effects of incompleteness are less than previously described (e.g. Hilgen *et al.*, 2015; Kemp, 2012) and instead, poor geochronology and the assumption of a linear sedimentation rate causes a significant reduction in signal detectability. The assumption of linear sedimentation rate can cause signals to be undetectable from within a highly incomplete time series unless the signal is of high amplitude or the periodicity exceeds T_{wb}. This means that many meso-timescale environmental forcings (those with periodicity less than $T_{wb,}$ and span timescales between 10^1 and 10^4 years (Sheets *et al.*, 2002), may experience a severe detectability decrease, and hence be difficult to detect within a time series.

Furthermore, Blum & Hattier-Womack (2009) calculate that a change in temperature due to Milankovitch scale climatic forcing may result in a change in sediment yield of 20-50% according to the empirical BQART model (Syvitski & Milliman, 2007). This would generate a low amplitude sediment flux signal with an amplitude of 25% of the mean feed rate; we show that such signals are rendered undetectable within highly incomplete time series. If the time series of interest becomes incomplete over timescales comparable to known environmental signals, the assumption of a linear sedimentation rate causes a severe detectability decrease where these signals may be rendered undetectable in the time series. This challenges our ability to extract subtle environmental signals from field measurements with limited exposure and current methods (Straub *et al.,* 2020; Toby *et al.,* 2019).

However, we highlight that the amplitude of the spectral peak present within an incomplete time series will always be the minimum spectral amplitude for the signal in question. This could result in evidence of signals being missed within a power spectrum, as the signal power has been reduced to similar magnitude to the power of autogenic noise. Due to the detectability reduction with decreasing completeness, if a measurable response is produced from an incomplete time series, the true signal would naturally produce a much larger response. Although true, this must still be treated with caution. The 95% confidence band denotes the 95th percentile of the data, hence 5% of the noise will consistently breach the confidence band. If part of the transport system noise occurs at a periodicity of known external forcing (e.g. Milankovitch-forced climatic periodicity) then it could be assumed as periodicity and justified due to the spectral amplitude reduction. To overcome this, a simplistic remedy was proposed by defining a detection threshold where the probability of false detections is low; the global (99.95%) confidence band (Vaughan *et al.,* 2011). This is a strong statistical solution, however, the power reduction due to incompleteness could mean signals cannot always be detectable at this level (Meyers, 2019). Whilst low significance levels may lead to false positive signals, high significance levels could lead to false negative signals, and generate competing problems (Hilgen *et al.,* 2015). We highlight the use of T_{wb} as the timescale of faithful signal transfer, even from highly incomplete stratigraphic sections (Griffin *et al.,* 2023). However, a pathway for future work is to quantify from field data whether the raised detection threshold is too harsh for detecting signals from incomplete records, and how much this threshold should be raised by to produce a realistic and accurate signal detectability threshold.

Incompleteness impacts signal degradation less than signal detectability, but removing time from a time series still has consequences for reconstructing environmental signals. Although we show that signals with periodicity above T_{rw} still resemble the known input signal over all degrees of completeness, when completeness is low (e.g. below 20%) the reconstructed signal amplitude can be degraded to half of the true signal amplitude. This amplitude reduction is not as severe as the amplitude reduction caused by signal shredding, but this apparent degradation combined with the apparent increase in T_{rw} could allow these signals to appear shredded. We highlight these signals have not experienced shredding by autogenic processes, but have been degraded in amplitude by incompleteness, which affects the structure of the signal recorded in a time series. These signals could potentially be reconstructed if the signal periodicity (e.g. the periodicity of Milankovitch-scale orbital forcing) was known. Therefore, multiple realizations of the time series could be stacked at this periodicity, which could aid the reconstruction of environmental signals rendered undetectable by incompleteness. However, interpolation onto a linear sedimentation rate brings significant error into the reconstructed time series, as the proportions of the input signal preserved in each time interval are not linear, making this method generally unfeasible. Methods to improve the signal detectability from a time series of stratigraphic information without using linear interpolation have been suggested (e.g. Trampush & Hajek, 2017), however a pathway for future work is to investigate the effect of various methods of interpolation on signal detectability.

4.4.3. Detection and reconstruction of sediment supply signals form stratigraphic measurables

The theoretical framework can be used to guide the interpretation of sediment-supply signals from a time series of stratigraphic measurables, providing we have knowledge of stratigraphic completeness, the properties of the input signal and the compensation timescale, T_c. Over short timescales (10^1 - 10^3 years), completeness is set by the maximum magnitude of fluctuations in sedimentation, controlled by the internal, stochastic dynamics of a STS. However, over long timescales (10^4 - 10^5 years), completeness shows little variation as sedimentation is controlled by subsidence, resulting in a completeness exponent close to 1 (Jerolmack & Sadler, 2007). To highlight differences between STS, we note that channelized depositional environments generally have shallower short-term completeness exponents than non-channelized depositional environments; by concentrating sedimentation into a narrow zone, channels increase the rapidity and noisiness of sediment accumulation (Jerolmack & Sadler, 2007). using the short-term completeness exponents for different depositional environments, and using half the period of the imposed signal as the minimum discretization timescale (according to the Nyquist sampling theorem), we can ascertain an estimated completeness for a time series of stratigraphic measurables that might contain an imposed signal.

This framework can be applied in two ways depending on whether the information sought is an estimate of signal detectability (forward application) or signal properties (inverse application). Both applications can be applied to time series of information which contain temporal gaps (Figure 4.4) and those which have undergone interpolation (Figure 4.5). The rice pile only allows for the analysis of surface fluxes due to the lack of subsidence. When applying this framework to a time series of stratigraphic information we suggest normalizing the 3D space by the compensation timescale, T_c, which represents the maximum timescale of autogenic organization within stratigraphy and marks the transition from transient to persistent rates of sedimentation (Straub *et al.,* 2020). Hence, T_c is the smallest discretization timescale necessary to obtain a complete stratigraphic record (Straub *et al.,* 2020).

The forward application of this framework provides an estimate of signal detectability and the ratio of the signal spike to the 95% confidence band. This provides more certainty when identifying potential signals from a time series of stratigraphic information. The estimated ratio of the signal spike to the 95% confidence band generated can be for either a time series which contains temporal gaps (e.g. Figure 4.4), or a time series where temporal gaps have been removed by linear interpolation (e.g. Figure 4.5). The benefit of this, is that it allows for the detectability of the original signal to be compared to the expected detectability after linear interpolation. As an example, we can utilise Figure 4.5 to approximate whether a 40kyr Milankovitch signal will be detectable within a power spectrum generated from a linearly interpolated time series of stratigraphic measurables from the Mississippi Delta. The y-axis of Figure 4.5 requires knowledge of signal periodicity (40kyr). To quantify signal amplitude, and hence utilise the correct amplitude subplot, we assume a change in sediment input flux (signal amplitude) of approximately 50% (Blum & Hattier-Womack, 2009). The x-axis of Figure 4.5 requires an estimate of stratigraphic completeness. The database of depositional environments provides a short-term incompleteness exponent for delta's of $\propto = 0.44$, allowing us to estimate completeness as: $C = a(\frac{discretization\ dt}{T_C})^{\propto}$, where a is approximately 1, the discretization dt is half input signal periodicity, (20kyr), and T_c is the compensation timescale; 200kyr for the Mississippi Delta (Li *et al.*, 2016).Using these values, we calculate a completeness of C = 36% for the Mississippi Delta. We can then place the signal within all 3 axis of the framework to estimate the expected ratio of the signal spike to the confidence band. We estimate this ratio as ~1.5; this signal would breach the confidence band but detectability is low.

The inverse application of this framework provides an estimate of the true amplitude of the imposed signal, which is generally difficult to quantify first-hand. Although identification of signal periodicity takes precedence in cyclostratigraphy, we provide a novel method to quantify the imposed signal amplitude which is commonly unknown. As an example, we can utilise the trends in Figure 4.5 to approximate the absolute amplitude of a Milankovitch signal identified within a power spectrum generated from a linearly interpolated time series of soil lightness taken from the Bighorn Basin, USA (Abels *et al.*, 2013), where a spectral spike that breaches the 99% confidence band is evident. Due to the linear interpolation of stratigraphic information onto a regular time series, we emphasize that the ratio input will be the minimum signal detectability. The y-axis of Figure 4.5 requires knowledge of signal periodicity (20kyr). To place the signal within the coloured matrix, we utilise the known ratio of the signal spike to the confidence band (~2). The x-axis of Figure 4.5 requires an estimate of stratigraphic completeness. The depositional environment of this strata has been interpreted as channelized alluvial plain (Abels *et al.*, 2013), providing a short-term completeness exponent of $\propto = 0.17$, allowing us to estimate completeness as: $C = a(\frac{discretization\ dt}{T_C})^{\propto}$, where a is approximately 1, the discretization dt is half the input signal periodicity, (10 kyr), and T_c is the compensation timescale; 67kyr for the Bighorn Basin (Straub *et al.*, 2020). Using these values, we calculate a completeness of C=72% for the Bighorn Basin. We can then place the signal on the correct amplitude subplot to estimate the expected signal amplitude. We estimate this to be 25% of the mean feed rate.

We stress that the framework presented is merely a guide for the signal detectability within stratigraphic measurables. Time series of stratigraphic information from different locations within the same STS may have similar estimated completeness, but the instances of time preserved may differ, and hence change the exact signal preserved. In the framework presented the time series was degraded randomly 5 times to stabilize the trends and an average detectability and apparent degradation was quantified. Although we utilise the average detectability and apparent degradation for this framework, we find that for the same degree of completeness, signal detectability can range by ±7% and signal degradation by ±10% depending on the time intervals removed in each iteration. Hence, we highlight the uncertainty in these estimations. This framework can provide a conceptual path forward for signal detection from stratigraphic measurables, however, this needs to be tested within field scale systems. Application of this framework allows stratigraphers the ability to quantitatively justify the interpretation of environmental signals in landscapes and strata and also offers a new direction for defining robust confidence limits for signal detectability.

4.5. Conclusions

- Incompleteness and the linear interpolation of time between dated horizons distort the true autogenic signal, hence defining the true nature and timescales of autogenic processes can be improbable when completeness is low.

- The preservation of the true autogenic signal within stratigraphic measurables is problematic, however the ease of visually identifying the structure of autogenic noise can be impeded by how the data is displayed. This highlights the requirement to understand how to analyse stratigraphic data before inverting spectra for paleo-surface process interpretation and signal detectability
- Incompleteness has consequences for signal detectability, where signals over all periodicities can be rendered undetectable if completeness is low. However poor constraints on time hinder signal detectability further.
- We develop a framework that can predict signal detectability and reconstruct signal properties using an estimate of completeness, which enables stratigraphers to quantitatively justify the presence of environmental signals within stratigraphic measurables. This provides better constraints on the structure of autogenic processes evident from landscapes and strata, but also improves understanding of the records in which information about paleoenvironmental variability may be best preserved.

Acknowledgements

We gratefully acknowledge support from the University of Liverpool and the International Association of Sedimentologists (Postgraduate Research Grant).

This chapter advances on the theoretical framework presented in Chapter 3 and investigates how stratigraphic incompleteness controls the preservation of Earth surface processes and the detectability of environmental signals from the stratigraphic record (Research Question 2). The removal of time from the stratigraphic record influences the temporal structure of autogenic processes preserved, where blue noise and eventually red noise is removed from the power spectra under low levels of completeness (Objective 2.1). However, interpolation of a time series using the assumption of linear sedimentation rate has much stronger influences on the structure and timescales of surface processes preserved, where blue noise is removed from the power spectra and the short autogenic timescale, T_{rw}, is modified due to the addition of high frequency noise (Objective 2.2). This influences the detectability of environmental signals, where signals over all periodicities and amplitudes can be rendered undetectable when completeness is low, however signal detectability is further hindered by interpolation (Objective 2.3).

Supplementary material for chapter 4

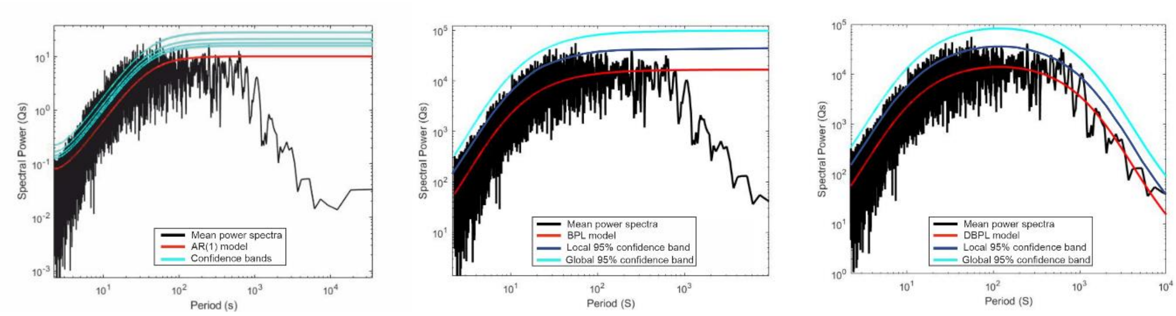

Figure S4.1: The fit of various spectral models to the power spectra generated from the physical rice pile control experiment, where influx rate is 0.37 g s^{-1}.

(Left) *The poor fit of the autoregressive lag 1 (AR(1)) model to the power spectra generated from the physical rice pile.* ***(Middle)*** *The strong fit of the bending power law (BPL) model to the red and white portions of the power spectra generated from the physical rice pile.* ***(Right)*** *The strong fit of the double bending power law (DBPL) model to the full power spectra generated from the physical rice pile.*

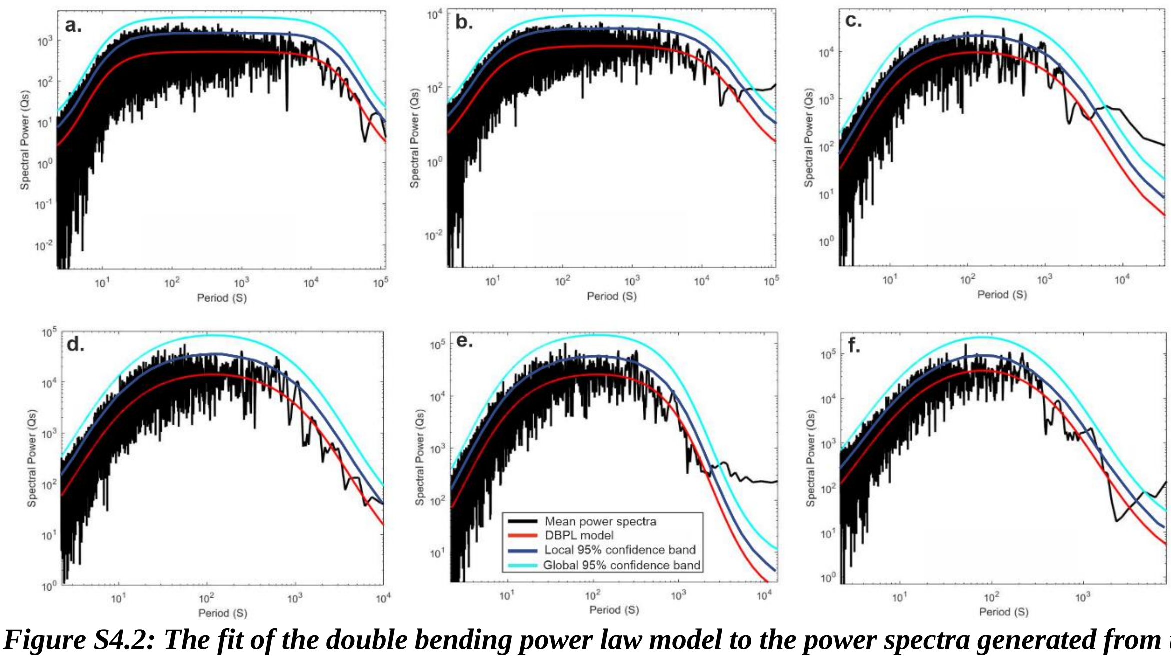

Figure S4.2: The fit of the double bending power law model to the power spectra generated from the physical rice pile under different rates of constant input.

The strong fit of the double bending power law (DBPL) model to power spectra run under input rates of: ***(a)*** *0.02 g s^{-1},* ***(b)*** *0.041 g s^{-1},* ***(c)*** *0.25 g s^{-1},* ***(d)*** *0.37 g s^{-1},* ***(e)*** *0.6 g s^{-1} and* ***(f)*** *0.78 g s^{-1}.*

5. Turning the volume down: How does the magnitude of autogenic noise in a sediment transport system influence the preservation of environmental signals?

This chapter is currently in preparation for submission: Griffin, C., Duller, R.A., Straub, K.M., & Higham, J.E. Turning the volume down: How does the magnitude of autogenic noise in a sediment transport system influence the preservation of environmental signals?

Abstract

Internal (autogenic) processes generate noise within sediment transport systems, where the frequency and magnitude of autogenic noise sets thresholds for the degradation and detectability of environmental sediment flux signals in landscapes and strata. The nature and timescales of autogenic noise, and hence signal propagation thresholds, have been quantified for sediment transport systems with strong sediment storage and release dynamics. However, the magnitude of autogenic processes varies across and within landscapes, which may influence the thresholds for the degradation and detectability of sediment flux signals. We explore how the magnitude of autogenic noise within a sediment transport system controls the temporal structure of autogenic processes within power spectra, and how this influences the degradation and detectability of periodic external environmental perturbations. To do this, a time series of sediment flux generated from an idealised numerical granular pile, which experiences minimal variation in sediment transport rates, is compared to that of a physical rice pile, which experiences large fluctuations in sediment transport rate. The magnitude of autogenic noise does not affect the structure and timescales of autogenic processes within a sediment transport system. However, it is evident that the detectability of environmental signals is dependent on the magnitude of noise within the system. Evidence of stochastic resonance is also found, evidenced by signals experiencing no degradation and heightened detectability when the periodicity of the input signal is equal to the maximum duration of autogenic processes. This can provide a theoretical basis that can be used to understand how signal detectability varies between sediment transport system segments. This also provides understanding as to the environments and records which may best preserve evidence of palaeo-surface processes and environmental variability.

5.1. Introduction

Sediment transport rates across the Earth's surface experience fluctuations over a range of spatiotemporal scales, which arise due to local episodes of sediment storage and release and are known as autogenic processes. Autogenic processes are pervasive within all geomorphic environments (Murray *et al.,* 2014; Paola, 2016; Allen, 2017), including but not limited to palaeosol development, alluvial fan development, bed and bar form migration, shoreline progradation, delta growth and the morphology of submarine fans (Kraus & Aslan, 1995; Muto *et al.,* 2007; Kim & Jerolmack, 2008; Clarke *et al.,* 2010; Fick *et al.,* 2017; Hajek & Straub, 2017; Lazarus *et al.*, 2019). Even in the absence of external (allogenic) forcing, autogenic processes cause variations in sediment transport capacity across a landscape which generates STS instability and triggers landscape reorganisation (Kim & Jerolmack, 2008; DeAngelis, 2012; Hajek & Straub, 2017; Kwang & Parker, 2019). This generates noise within a time series of sediment flux over a wide range of autogenic frequencies; from minutes to millions of years (Coulthard & Van De Wiel, 2007; Jerolmack & Sadler, 2007; Kim & Jerolmack, 2008; Jerolmack & Paola, 2010; Jerolmack, 2011; Romans *et al.*, 2016; Hajek & Straub, 2017). The duration and magnitude of autogenic processes within a specific segment of a sediment transport system (STS) determine the structure and timescales of autogenic noise present (Jerolmack & Paola, 2010; Griffin *et al.*, 2023; Tu *et al.*, 2023), where autogenic noise has a tripartite spectral structure composed of three noise regimes (Hwa & Kardar, 1992; Griffin *et al.*, 2023). Two autogenic timescales (T_{rw} and T_{wb}) delimit the temporal extent of each noise regime, and set temporal thresholds for the degradation and detectability of environmental sediment flux signals (Jerolmack & Paola, 2010; Griffin *et al.*, 2023). Degradation of environmental signals refers to the ability of autogenic processes to severely reduce the amplitude of short period input signals (e.g., signal shredding), whereas detectability refers to our ability to differentiate the presence of a signal spike from autogenic noise. Signals which are of similar magnitude to autogenic processes are described as obscured (Morris *et al.*, 2015), as they have undergone no direct modification. Understanding the extent and structure of autogenic noise within a STS provides a basis from which to extract and reconstruct paleo-surface processes, and quantify the ability of a STS to propagate and preserve evidence of environmental signals (Jerolmack & Paola, 2010; Straub *et al.*, 2020; Toby *et al.*, 2022).

The structure and timescales of autogenic processes have been hypothesised to be universal within all STSs (Griffin *et al.*, 2023). However spatial variations in sediment properties mean the thresholds for sediment transport within and across the Earth's surface are landscape dependant (Jerolmack, 2011; Bracken *et al.*, 2015; Harries *et al.*, 2019; Benavides *et al.*, 2022). For example, the initiation of sediment transport on hillslopes requires the slope and pore pressure to surpass specific thresholds (Rustomji & Prosser, 2001; Schneider *et al.,* 2008; DiBiase *et al.*, 2017), which generally generates large magnitude, infrequent sediment transport events (Roering *et al.*, 2001). In contrast, sediment transport in channelized systems (e.g. rivers and deltas) occurs if critical flow strengths for a particular grain size are exceeded (Schneider *et al.*, 2008). As the frequency of sediment transport events increases, and the magnitude of these events decreases, as sediment transport switches from bedload to suspended load (Kleinhans & van Rijn, 2002; Benavides *et al.*, 2022). The more infrequent the sediment transport events, the greater the magnitude of sediment transport fluctuations (and noise) within a STS (Benavides *et al.*, 2023). Therefore, every geomorphic environment, and sub-environments within these, will have its own bounds on the magnitude and duration of sediment transport fluctuations experienced (Trampush & Hajek, 2017; Toby *et al.*, 2022).

Previous work has highlighted the existence and importance of autogenic magnitude thresholds for predicting the detectability of environmental signals within landscapes and strata (e.g. (Jerolmack & Paola, 2010; Trampush & Hajek, 2017; Toby *et al.*, 2019; Hein & Ashton, 2020). Jerolmack & Paola, (2010) utilised a numerical rice pile to propose a magnitude threshold (M) above which short period input signals are detectable within a time series of sediment flux. M is expected to scale with the maximum size of autogenic events within the system, i.e., $M \sim L^2S_c$, where S_c is the critical slope. In the numerical rice pile, M represents the maximum volume of rice effluxed over the longest avalanche. Hence for a short period signal to be detectable, the signal amplitude must exceed this volume. Furthermore, Toby *et al.,* (2019) developed this theory and found that the threshold for the storage of sediment flux signals in stratigraphy is governed by a time-dependant magnitude threshold. This threshold is set by the maximum scales of autogenic storage, bypass and release within a STS over the time window of interest. Therefore, the longer the signal duration, the smaller the amplitude required for the signal to be detectable. Both these studies highlight that when the magnitude of a sediment flux variation is not sufficiently greater than the natural autogenic variability within a STS, the signal will be rendered unidentifiable at the terminus of a STS or in the resulting strata.

The specific sediment transport mechanics within a STS determine the magnitude of autogenic noise present (Tresch & Strasser, 2011; Ganti *et al.*, 2014; Harries *et al.*, 2019; Toby *et al.*, 2022). However, a current bias exists towards quantifying autogenic processes within geomorphic environments where large-scale sediment transport fluctuations are dominant (Jerolmack, 2011), e.g. hillslopes (Hasbargen & Paola, 2000; McKean & Roering, 2004), bedload sediment transport in fluvial systems (Singh *et al.*, 2010; Benavides *et al.*, 2022), deltaic systems (Kim & Jerolmack, 2008; Van Dijk *et al.*, 2009) and alluvial fans (Goehring *et al.*, 2021). Consequently, defining the spatiotemporal scales of sediment transport, and hence thresholds for signal detectability, in environments with less sediment storage potential is in its infancy, for example, suspended sediment dominant systems. The inclusion of suspended sediment within a STS is hypothesised to increase the efficiency of signal propagation, which may lower the amplitude required for degraded signal to be detectable (Pizzuto *et al.*, 2017), however this is yet to be quantified. Importantly, anthropogenic impact (i.e. dam building, deforestation land use variations) causes dramatic alterations in the volume of suspended sediment transported. This has consequences for both the morphology of STS and also the ability of a STS to propagate and record sediment flux signals (Weltje & von Eynatten, 2004; Dai *et al.*, 2009; Restrepo *et al.*, 2015; Dethier *et al.*, 2022).

Here, the full temporal structure of autogenic processes is characterised and the associated timescales quantified within a STS where the magnitude of sediment transport fluctuations, and hence autogenic noise, is low. This will provide understanding as to how sediment storage potential within a STS influences the thresholds for the degradation and detectability of environmental sediment flux signals. A theoretical framework for the degradation and detection of environmental signals over the full range of autogenic timescales has been generated using a physical rice pile. In this study, this is expanded to understand how systems with less sediment storage potential propagate and degrade high frequency signals, which influences signal detectability. This is crucial for understanding which environments allow for the accurate reconstruction of past environmental signals, and to predict the response of STSs to current and future anthropogenically induced change. To do this, an idealised numerical granular pile is utilised, generated as a discrete element model (DEM) containing weak stick-slip dynamics, as an analogue for a STS with less sediment storage potential. Like a rice pile, a numerical granular pile can provide a basis from which natural STS are understood, as these granular systems can elucidate the nature of autogenic processes in a variety of field scale systems, depending on the nature of the granular medium used. Whilst 1D cellular automata sandpiles have been heavily utilised to understand avalanche dynamics (e.g Bak *et al.*, 1987; Hwa & Kardar, 1992; Frette *et al.*, 1996; Kutnjak-Urbanc *et al.*, 1996; Manna, 1999; Malthe-Sørenssen *et al.*, 2001; Carreras *et al.*, 2002; Pradhan, 2021) this is yet to be studied using a DEM that bridges the gap between numerical and physical granular experiments (Ajmal *et al.*, 2020). The results of the DEM are compared to that of a physical rice pile, where the magnitude of stick-slip dynamics, and hence autogenic noise, is much greater. From this, the ability of DEM's to replicate the dynamics present within physical experimental systems can be evaluated.

5.2. Methods

5.2.1. MFiX-DEM set-up

This study employs MFiX (Multiphase Flow with Interphase eXchanges) version 21.4, developed by the National Energy Technology Laboratory (NETL), freely available from the U.S. Department of Energy (DOE) at https://mfix.netl.doe.gov. MFiX is an open-source, multiphase flow solver written in FORTRAN that can be used to study the complex flow behaviours present in fluid-solid systems (Darabi *et al.*, 2011). In MFiX-DEM, the discrete element method (DEM) is used to describe solids at a particle level. The solid phase is represented by individual particles (Lagrangian approach), each with a defined diameter and density (Garg *et al.*, 2012). In the DEM, particle-particle and particle-wall interactions are resolved and the time integration is undertaken using Newton's second law of motion (Gopalakrishnan and Tafti, 2013). Particle collisions within the model are resolved using the soft-sphere model of Cundall and Strack, (1979). In the soft-sphere model, particle collisions are treated as a continuous process that occurs over a finite time. These collisions are based on physically realistic interaction laws using empirical values for the spring stiffness coefficient, dissipation constant and friction coefficient (Li *et al.*, 2012). The gas phase of the DEM is treated as a continuum (Eulerian approach), allowing it to be modelled using the continuum conservation equations of mass, momentum and energy (Li *et al.,* 2012). The full details of the model are outlined in Chapter 2, and the governing equations and a detailed verification study of the MFiX-DEM was undertaken by Garg *et al.*, (2012).

In this work, a quasi-2D idealised granular pile was generated as a DEM in order to utilise the pure granular model as the fluid phase is not considered. The granular pile in the computational domain was constructed of two vertical, parallel walls 0.03 m long, positioned 0.002 m apart (Figure 2.4), to resemble the physical rice pile set-up. Grains were fed (influx) to the pile via a point source inlet, generated as a 0.08 x 0.06 m region, allowing only individual particles to enter the domain increasing accuracy in the influx rate. Influx rate can be precisely defined over an infinite range by defining an influx rate in kg s^{-1} using the MFiX GUI. The grains utilised in the model are spherical, with a diameter and density of 0.003 m and 1250kg m^{-3} respectively; the properties of these particles can be found in Table 1. Grains can leave the domain via a defined outlet region; efflux cannot be measured directly in the DEM but the number of particles in the model can be recorded. Throughout the model run, the evolution of the pile was monitored by saving data in .csv files at a defined time interval (here defined at

0.001 s). The data saved in the output files include: particle ID, X, Y and Z velocity and X, Y and Z coordinates for each particle present.

To reduce the computational time, an initial run was completed to pre-assign particles into a granular pile. This consisted of inputting 11,311 particles into the model domain to form a small granular pile. After the run was completed, the particle coordinates were saved and velocities reset to 0, generating an input file used in all the numerical granular pile experiments. Although the granular pile geometry was partially pre-defined within the model domain, at the start of each run the particles within the model needed to stabilise and build the pile to the maximum angle of repose which took approximately 2000s of model time. The total model run time for all experiments was set to 32,000s; comparable to the time required to saturate the balance during the control experiment of the physical rice pile experiments.

Firstly, a control experiment was run with a constant influx rate of 0.00018 kg s^{-1}, equivalent to 10 grains s^{-1}. This influx rate is comparable to the control experiment of the physical rice pile. This experiment was used to define the full spectral structure generated by the numerical granular pile and quantify autogenic timescales evidence from rollovers between spectral regions.

To explore how the numerical granular pile shreds high-frequency signals and hence render them undetectable in the output flux, a matrix of 10 experiments were run with cyclic influx of different periods and amplitudes. To achieve parity with the control experiment, a mean influx rate of 0.00018 kg s^{-1} (10 grains s^{-1}) was attained for all cyclic experiments. The periods of the influx signals were chosen to only span the range of red noise timescales within the control experiment. This is because efforts are focused on understanding how the stochasticity of sediment transport dynamics influences signal shredding potential. The periodicities chosen increased in 10-second intervals from 10 s to 70 s. To explore the effect of signal amplitude on signal degradation and detectability, a signal with a period of 40 s was imposed, but gradually decreased signal amplitude. For parity with the control experiment, all the imposed signals share the same mean feed rate (0.00018 kg s^{-1}) but decrease in amplitude from 0.00018 kg s^{-1} (10 grains s^{-1}) to 0.0000035 kg s^{-1} (2 grains s^{-1}).

5.2.2. Physical rice pile experiments

The suite of rice pile experiments presented in Griffin *et al.,* (2023) were utilised. As the idealised numerical granular pile was built to the same specification as the physical rice pile, this allows for direct comparison between the temporal structure of the power spectra and associated autogenic timescales.

The experimental apparatus is constructed of two vertical, parallel glass sheets 0.37 m long, positioned 0.26 m apart. Rice was fed (influx) to the pile from a dry particle feeder (Schenk Accurate) positioned 0.008 m from the top surface, allowing a rice pile to form at a critical angle so that a dynamic topographic equilibrium was achieved. Over the suite of experiments, influx was defined between a minimum and maximum range (0 g s^{-1} and 0.78 g s^{-1} controlled at 1 s intervals via a computer connected to the sediment feeder which directly feeds the pile. Efflux was measured at approximately 1 second intervals using an Ohaus EX12002 balance (accuracy and precision of 0.1 g). The balance has a maximum mass of 12 kg, and all experiments were run until the balance was saturated. The dimensions of rice grains used in the experiments have a diameter of 0.0025 ±0.5 m, length of 0.008 ±0.5 m and a mass of 0.02 g. The experimental set-up is similar to that of the physical rice pile of Frette *et al.,* (1996).

The control experiment, run with a constant influx rate of 0.37 g s^{-1}, was first used. The influx rate denotes the mean rate of the sediment feeder, and the experimental run time (9 hours) was defined by the time to saturate the balance at the defined influx rate. This experiment was used to compare the sediment transport dynamics and the structure of autogenic processes between the physical rice pile and numerical granular pile.

To explore how the limits of signal shredding and signal detection vary with the stochasticity of sediment transport dynamics, 12 experiments run with cyclic influx (where influx rate follows a sinusoidal pattern) of different periods and amplitudes were utilised. To achieve parity with the control experiment, a mean influx rate of 0.37 g s^{-1} was attained for all cyclic experiments. 3 periodicities were chosen to cover the range of autogenic timescales evident within the red noise regime: 6s, 12s and 24s. The amplitude of the cycles were chosen as percentages of the mean feed rate (0.37 g s^{-1}), increasing in 25% intervals from 25% (0.0925 g s^{-1}) to 100% (0.37 g s^{-1}).

5.2.3. Time series analysis for signal detectability and degradation

Power spectra were generated from the efflux time series from each set of experiments using the multi-taper method (MTM) with 2 tapers. Key autogenic timescales can be observed by eye on the power spectra as ‘roll-overs’ or ‘gradient-breaks’. To delimit these timescales accurately the ‘findchangepts’ function in MATLAB was employed. This function is controlled by two key input parameters: the maximum number of significant changes and the type of change to detect (e.g. variations in mean, standard deviation, gradient). For the spectra, 2 changes are specified (to account for the presence of two rollovers in the spectra) and use linear as the type of change to detect, applied on log-transformed spectral data. This method detects changes in the mean and slope of the input spectra, which can be inverse log transformed to solve for the power-law exponent of the fit.

To make a statistical statement about the presence or not of an influx signal in the power spectra of the efflux from the end of the pile, a confidence band is required. To quantify signal detectability from the numerical granular pile, the 95% confidence band generated from the DBPL model (see Chapter 4) was applied to the power spectra of the efflux. To quantify signal detectability from the physical rice pile experiments, a 95% confidence band was generated using 25 realizations of the control experiment (see Chapter 3). The ratio between the power of the signal spike and the power of the 95% confidence band at the imposed periodicity was quantified: if this ratio exceeds 1, a signal is detectable.

To quantify the amount of degradation a signal experiences within both the numerical and physical experiments, the efflux time series is stacked from the end of the pile into lengths equal to the input period, and take the mean of the efflux for each second over the imposed periodicity. From this, a mean ensemble efflux is gained to which a sine wave is fitted with a period equal to the known input signal and return an amplitude and phase based on the signal present in the mean ensemble efflux. The amplitude of the signal evident in the ensemble efflux is compared to that of the known input signal and quantify a percentage similarity. Within both the numerical and physical experiments, the degradation of signals within the efflux time series taken from the end of the granular pile is quantified.

5.3. Sensitivity analysis for parameter calibration within the numerical granular pile

One limitation of the MFiX-DEM is that it is only capable of modelling perfectly spherical grains. However, whilst the system cannot exactly replicate a rice pile, it offers the opportunity to study a system with different sediment transport mechanics, and hence variations in the magnitude of storage and release processes. To accurately achieve this, the rest of the domain and granular material properties must be comparable between both systems. Sensitivity analysis methods are commonly employed to determine the influence of different individual parameters and how combinations of parameters affect target performance. This can then be used to match the properties of a DEM to those of the related physical system (Guo *et al.*, 2023). Although these methods are generally utilised to calibrate microscale properties of granular materials, sensitivity analysis methods can be used to quantify the influence of individual properties on the macroscopic behaviour of the bulk material (Katterfeld *et al.*, 2019).

The granular pile in the computational domain was built to the same specification as the physical rice pile apparatus. The diameter and density of the grains within the numerical granular pile were set to correspond to those of the rice used in the physical experiments. However, other microscale physical parameters were difficult to quantify directly, namely those controlling grain contacts and interactions. Here, those parameters which simultaneously influence intergranular contacts as well as the contact between the grains and the domain boundaries are the friction coefficient (FC) and the coefficient of restitution (CoR) (Figure S5.1). The FC combines both the rolling and sliding resistance of individual grains during motion, which impacts strain localization and the thresholds for granular motion (e.g. the stickiness of a grain, to both other grains and the walls of the domain) (Tang *et al.*, 2019). The greater the FC, the 'stickier' the grains and hence the more resistance between the particles. The CoR is the material property which indicates the ratio of the normal relative velocity before a granular collision to the normal relative velocity after a granular collision (Tang *et al.*, 2019). In the numerical granular pile, this will affect the dissipation of kinetic energy during granular collisions (e.g. how bouncy grains are). The greater the CoR, the lower the energy dissipation during a granular collision as the grains do not bounce.

To quantify the effect of both parameters on the dynamics of the granular pile, two key variables were analysed: granular temperature (GT) and the number of particles within the model as an analogue for avalanche size. Firstly, the GT provides an index of the level of collisional activity within a granular flow (Gollin *et al.*, 2015; Taylor-Noonan *et al.*, 2021), where the higher the GT, the greater the number of interparticle collisions (Duan & Feng, 2017). This provides a quantitative measure of the ability of a granular material to flow, and an understanding of how energy is passed through a granular medium (Gollin *et al.*, 2015; Higham *et al.*, 2019). Although the flow in question will have a bulk mean velocity, collisions between neighbouring particles will cause random fluctuations in particle velocity away from a group mean. For a field of particles each with a known velocity per time step, the GT of a particle is calculated by comparing the velocity of each individual particle to the group mean, and averaging the square of these velocity fluctuations (Taylor-Noonan *et al.*, 2021):

$$GT_{(particle)} = \sqrt{Vx^2 + Vy^2 + Vz^2}$$

Where *Vx* is the x component of particle velocity, *Vy* is the y component of particle velocity and *Vz* is the z component of particle velocity. Due to the high computational power required to record the velocities of individual particles, in this analysis, an ensemble mean GT per experiment is generated, where the mean x, y and z velocities of the whole system are recorded per second, from which GT is calculated. To do this, the mean x, y and z velocities of all the particles in the computational domain per time step were measured, from which a bulk GT per second is calculated. This is then averaged to generate a singular GT value, which describes the mean GT over the whole duration of the experiment. Secondly, a time series of the number of particles within the computational domain is analysed, which provides us with information on the size of avalanches and hence the magnitude of storage and release processes, as a function of both FC and CoR.

To analyse the effect of both parameters on GT and avalanche distributions, a matrix of 625 experiments were run, where the coefficient of restitution and the friction coefficient were both varied between 0.1 and 1.0 in intervals of 0.0038 (Figure 5.1). A short run time of 1000s was utilised for this initial matrix; this was chosen to reduce computational time whilst capturing a broad overview of system dynamics from which a reduced matrix can be defined for more detailed analysis.

Firstly, GT variations as a function of FC and CoR were studied. A region of very high granular temperature is present when the CoR is high (Figure 5.1A). Comparison of this with the avalanche dynamics reveals this is caused by the instantaneous collapse of the granular pile, where over 90% of the grains left the system after the model run began (Figure 5.1B,C). This was therefore defined as the upper limit of the CoR which could be used in the numerical granular pile experiments. A region of high GT is also evident when the FC is low (e.g. less than 0.25), where above this threshold GT is consistently low across the matrix (Figure 5.1A). The avalanche dynamics reveal that this region of high GT is generated due to the occurrence of systematic large avalanches approximately every 150 s (Figure 5.1C). As these runs contained minimal small avalanches due to the system constantly regrading, this was defined as the lower limit of the FC which could be used in the numerical granular pile experiments. The rest of the matrix shows minimal variation in granular temperature. Here, avalanche dynamics show stronger storage and release potential evidenced by a constant pile accumulation (ramping up geometry) and the occurrence of small avalanches (Figure 5.1C). These model runs do not show evidence of any system-clearing events.

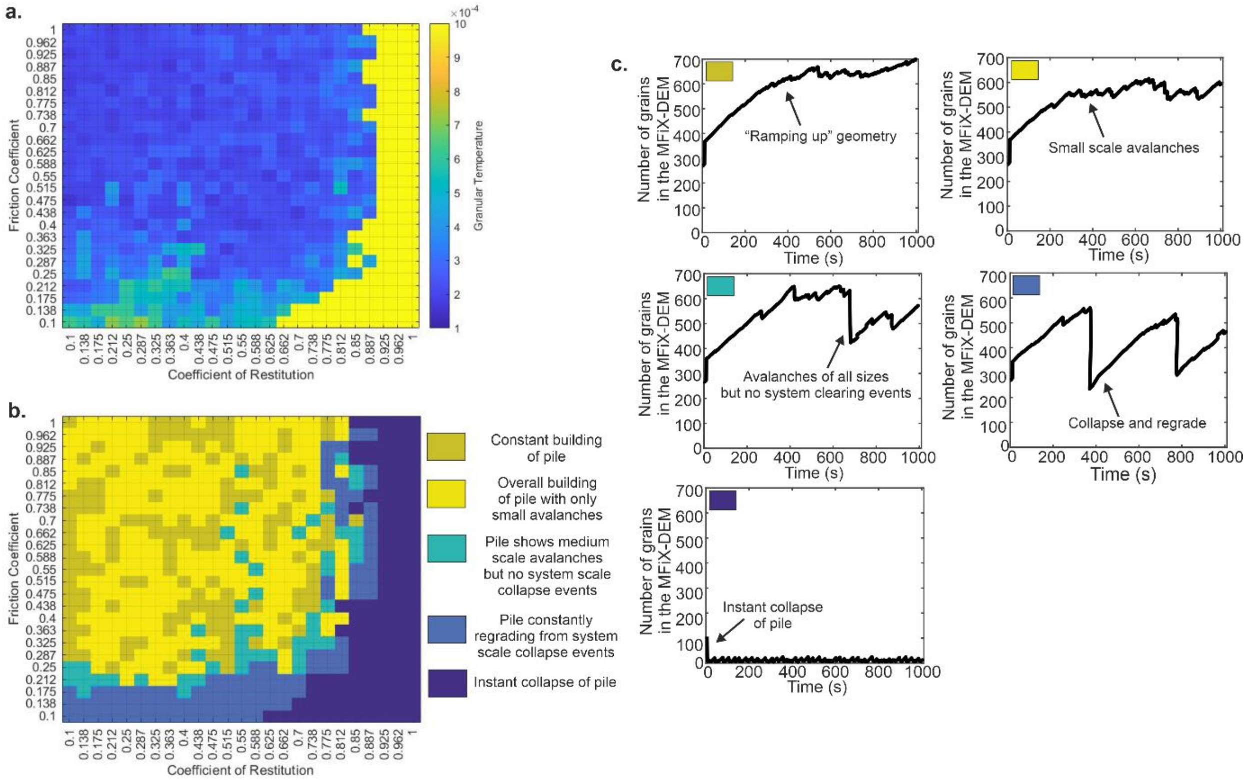

Figure 5.1: Large-scale sensitivity analysis of the MFiX-DEM numerical granular pile.

(a) *Variations in granular temperature (GT) as a function of both the friction coefficient (FC) and the coefficient of restitution (CoR), for all 625 possible combinations of the parameters.* ***(b)*** *Classification of each of the 625 experiments runs according to the magnitude of avalanche dynamics within the model. All the experimental runs were classified according to 5 categories, dependant on the magnitude and frequency of the avalanches experienced over the duration of the experiment.* ***(c)*** *Examples of the avalanche dynamics within the five categories defined in (b).*

This large-scale sensitivity analysis allowed combinations of FC and CoR to be eliminated that produced unrealistic dynamics, for example the instant collapse of the pile. However, this also revealed a large region of consistently low GT which needed a longer experimental run time to reveal the full range of dynamics. This encompasses all the experiments which only experienced small avalanches or show ramping up geometry (Figure 5.1C). Due to limits on computational time, the size of the experimental matrix was reduced further to significantly increase the run time. To provide more constraint on both parameters, estimates of both the FC and CoR were utilised from previous work on physical rice piles. Firstly, the CoR for the rice used in the physical experiments was estimated to range between 0.5 and 0.55 (Wang *et al.*, 2021). Secondly, estimates of the FC can be made from the angle of repose of the granular material (Beakawi Al-Hashemi & Baghabra Al-Amoudi, 2018; Madrid *et al.*, 2022), which was found to range between 32 to 38 degrees, hence providing a FC in the range of 0.62 and 0.8. This allowed a smaller matrix of 28 experiments to be defined which was run for 20,000s.

For the smaller experimental matrix with increased run time, variations in GT were re-analysed and the avalanche dynamics present (Figure 5.2). Across the matrix, GT showed minimal variation even with significantly increased run time, where the standard deviation of the GT was only 3x10^{-5}. To understand this, the variations in GT were compared to the avalanche dynamics present. Comparing all the parameter combinations, a clear cluster of runs were evident showing similar internal dynamics and sharing similar mean ensemble GT. Due to this lack of variation, a combination of parameters that fell in this range were chosen: a CoR of 0.5 and a FC of 0.7.

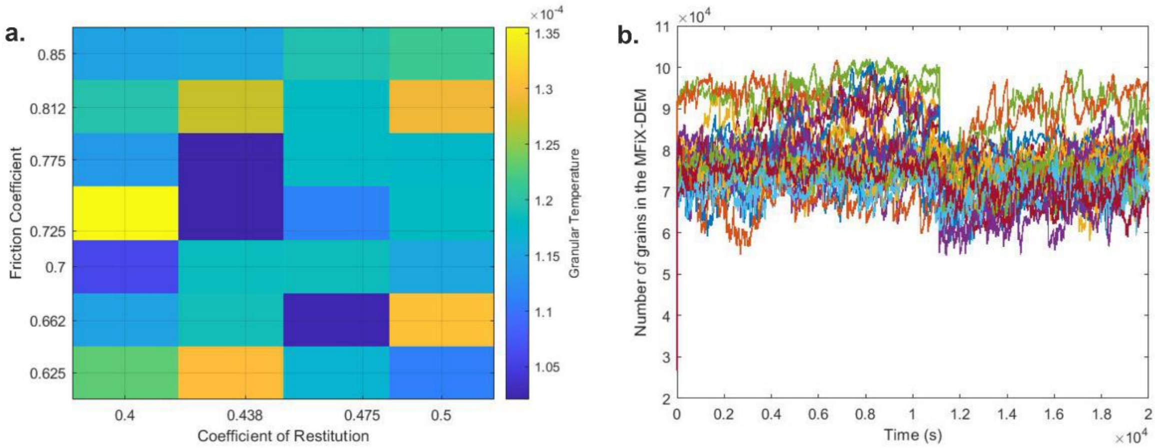

Figure 5.2: Reduced scale sensitivity analysis of the MFiX-DEM numerical granular pile.

(a) *Variations in granular temperature with changing friction coefficient and coefficient of restitution across the 28 parameter combinations used in the reduced matrix.* ***(b)*** *Stochastic avalanche dynamics within the 28 experiments showing a cluster of experiments with similar internal dynamics.*

5.4. Results

5.4.1. The temporal structure of autogenic processes

To understand the ability of the numerical granular pile to degrade environmental signals and also influence their detectability, the magnitude of the storage and release processes must first be characterised. This allows the temporal structure and timescales of autogenic processes intrinsic to the MFiX-DEM to be quantified.

Constant influx to the numerical granular pile generates a range of avalanche event sizes, from 1 grain sec^{-1} to 90 grains s^{-1}. The probability distribution of these avalanches throughout the time series is exponential (light-tailed) (Figure 5.3A), highlighting that small events are dominant, and the chance of occurrence of an extreme event is nearly zero (Ganti *et al.*, 2011). Although the system has a different probability distribution to that of the physical rice pile, the distribution evident in the output from the numerical granular pile agrees with the distribution of avalanche sizes observed within physical sandpile models (Malthe-Sørenssen *et al.*, 1999; Carreras *et al.*, 2002). Whilst the efflux from both the numerical granular pile and physical rice pile is similar to the influx (Figure 5.3B), highlighting both systems evolve to an equilibrium state, the granular systems achieve this through different internal dynamics. The physical rice pile experiences repeated cycles composed of long periods of aggradation, followed by rapid system-scale avalanches. Instead, the numerical granular pile experiences consistently small avalanche events of the same magnitude as the influx, and does not experience avalanche events on the order of system size (Figure 5.3B).

Although the systems show differences in the distribution of avalanche sizes, the power spectra generated from both the MFiX-DEM and the physical rice pile show parity in structure when run under a similar rate of constant influx (Griffin *et al.*, 2023). Both experimental systems exhibit three noise regimes defined by two distinct changes in the gradient of the power spectra (Figure 5.3C). The first regime comprises red noise (temporal correlation), whereby spectral power increases as a function of period. The spectral gradient, α, of the correlated noise regime generated from the numerical granular pile is 0.56, in comparison to 2.2 for the physical rice pile. The upper temporal limit of correlated noise denotes a characteristic autogenic timescale, T_{rw} (Griffin *et al.*, 2023), which is approximately 30 seconds for both granular systems. The second regime comprises white noise, where spectral power plateaus, indicating events over this timescale are temporally uncorrelated. The upper temporal limit of white noise denotes a characteristic autogenic timescale T_{wb} (Griffin *et al.*, 2023) , which occurs at comparable timescales within both granular systems; 550 seconds for the numerical granular pile and 650 seconds for the physical rice pile. The third regime comprises anti-correlated noise over timescales greater than T_{wb}, whereby spectral power decreases as a function of period. The spectral gradient, α, of the anti-correlated noise regime generated from the numerical granular pile is -0.58, in comparison to -2 for the physical rice pile.

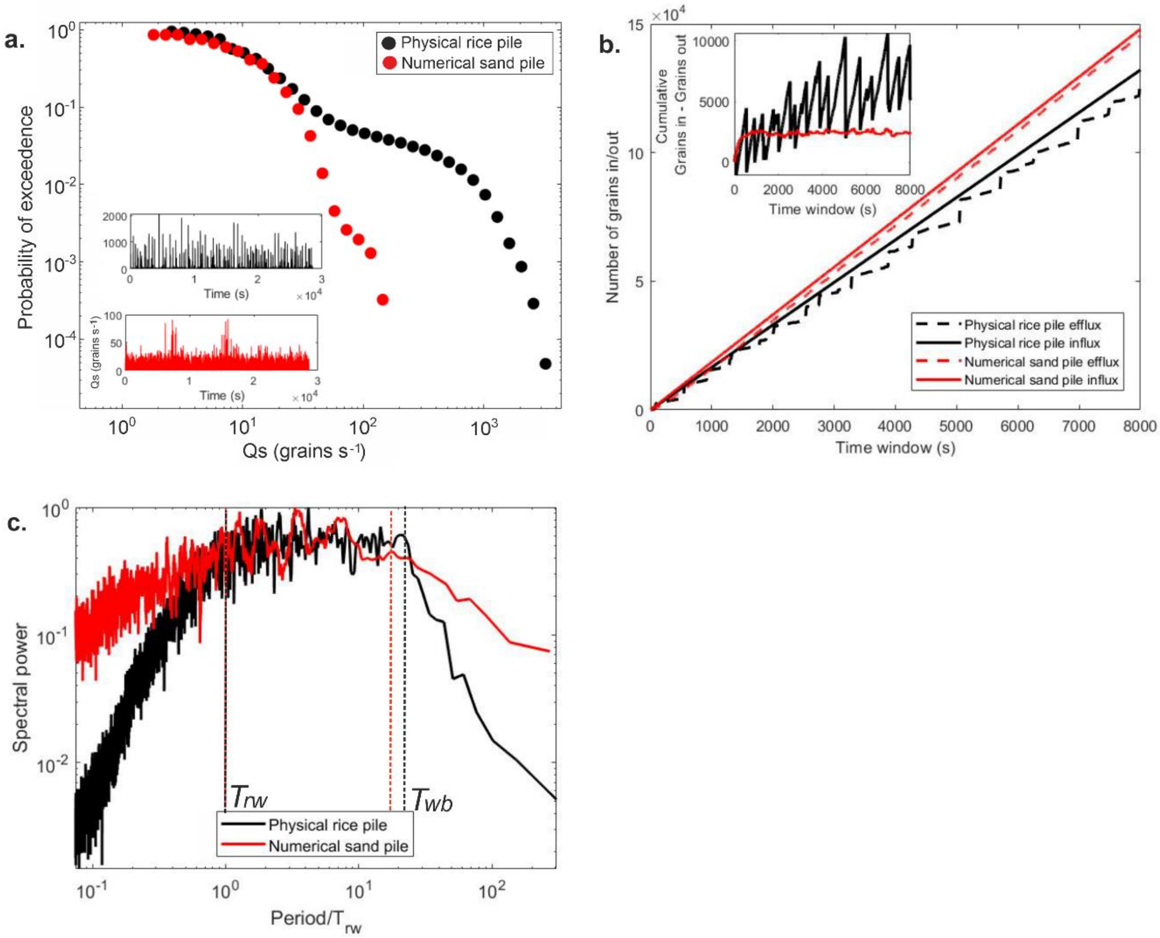

Figure 5.3: Time series of mass efflux from the MFiX-DEM numerical granular pile control experiment (10 grains s^{-1}) versus the physical rice pile control experiment (~10 grains s^{-1}).

__(a)__ Distribution of avalanche sizes throughout the time series, where the numerical granular pile shows an exponential distribution and the physical rice pile shows a heavy-tailed distribution. We highlight the difference in y-axis on the efflux plots, where the efflux from the MFiX-DEM is up to an order of magnitude less than the physical rice pile __(b)__ Comparison of the internal dynamics of both the numerical granular pile and physical rice pile under constant influx rate. The physical rice pile undergoes cycles of aggradation followed by rapid efflux, whereas the numerical granular pile only experiences a continuous, low variance flux __(c)__ Power spectra generated from a time series of efflux measured from the end of the numerical granular pile and the physical rice pile using the multi-taper method. Both power spectra show tripartite geometry composed of red, white and blue noise, where spectral gradient breaks between the regimes mark two timescales: T_{rw} and T_{wb}.

5.4.2. The degradation and detectability of environmental signals

Autogenic processes have the ability to degrade signals and/or render them undetectable in the output flux (Jerolmack & Paola, 2010; Griffin *et al.*, 2023). Degraded signals are those that have experienced a severe reduction in amplitude during propagation through the granular system. Detectable signals are those signals that produce a peak within a power spectrum that exceeds the 95% confidence band. Here, the focus is solely on the degradation and detectability of high-frequency input signals, hence the periodicities of the signals were limited to below 70 seconds (Figure 5.4).

Input signal periodicity is the primary control on signal degradation, in the same manner as the physical rice pile. T_{rw} sets an upper limit to the timescales over which signals experience significant degradation (Figure 5.5A). Here, the smaller the signal periodicity below T_{rw}, the greater the amount of degradation a signal experiences. It is noted that signal amplitude does not influence the amount of degradation a signal experiences; signals of the same periodicity are degraded by equal amounts regardless of their input amplitude (Figure 5.5A, inset figure). In comparison, signals with periodicity greater than T_{rw} experience significantly less degradation, where the output signal amplitude is more than 70% similar to the known input signal. However, within the numerical granular pile, evidence of a signal bump when the input signal periodicity is equal to T_{rw} is present, highlighting stochastic resonance. At this periodicity, the input signal experiences no degradation.

Within the numerical granular pile, signals over all periodicities above and below T_{rw} are highly detectable in the output flux (Figure 5.5B). However, signal detectability also increases as a function of input signal period. This directly contrasts the results from the physical rice pile, where signals with periodicity less than T_{rw} are statistically undetectable in the output flux over all amplitudes (Griffin *et al.*, 2023). In the numerical granular pile, signal amplitude influences the detectability of signals. The greater the amplitude of the signal, the greater the ratio of the spectral peak to the confidence band (Figure 5.5, inset figure). When the signal periodicity is equal to T_{rw}, signals also experience significantly enhanced detectability as a result of stochastic resonance.

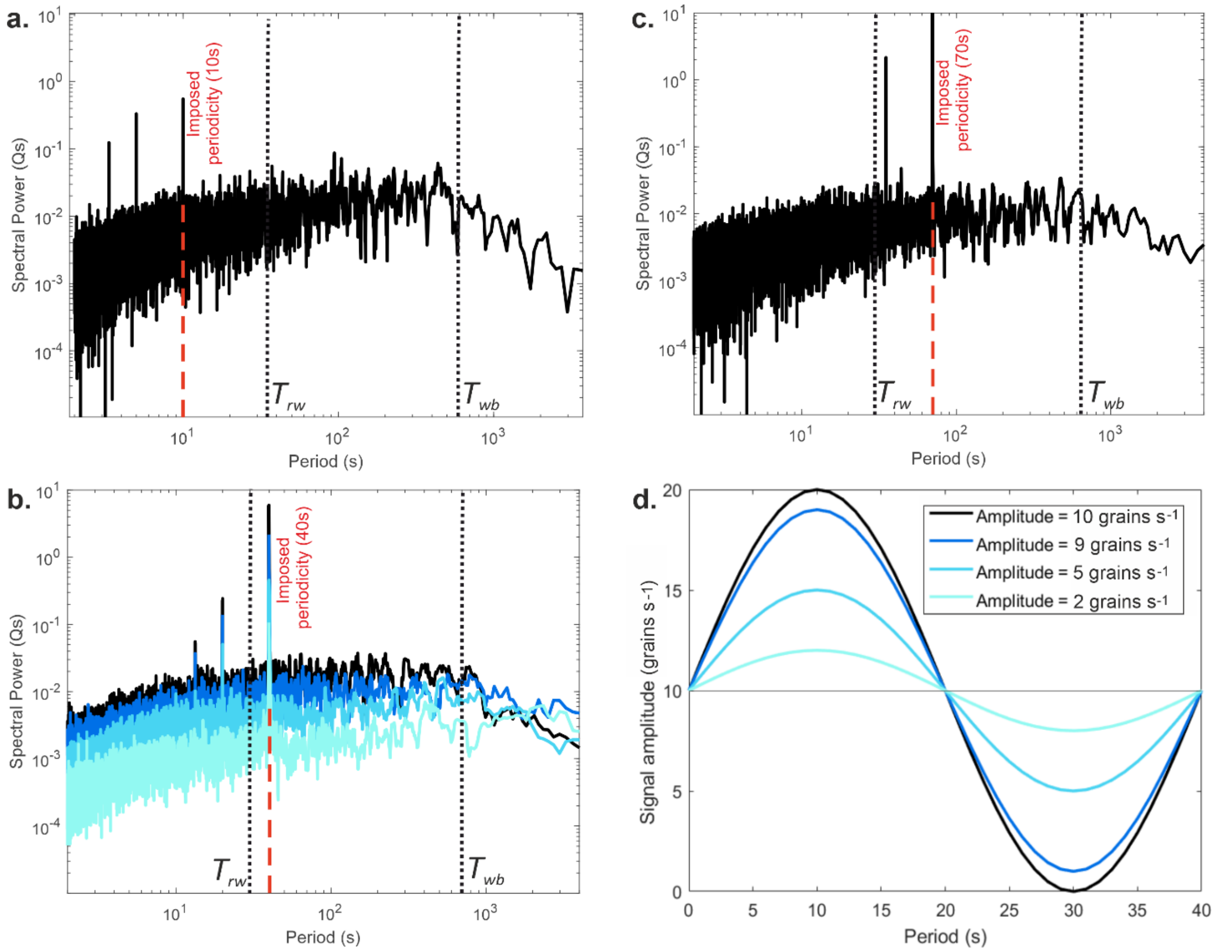

Figure 5.4: Power spectra generated from a suite of numerical granular pile experiments with imposed signals in the form of cyclic grain influx. Spikes in power spectra at the imposed periodicity highlight the presence of imposed signals.

*Power spectra from 3 numerical granular pile experiments with imposed periodicity of 10 seconds **(a)** 40 s **(b)** and 70 s **(c).** Whilst the period of the input signals was systematically increased, the amplitude was held constant at 10 grains s^{-1}. However, to understand the effect of amplitude, 3 experiments were run with a period of 40 s, but with decreasing amplitude (c); the structure of these imposed signals is shown in **(d)**. We highlight that the spectral structure is not influenced by the additional of external forcing, however the absolute power of the spectra is influenced by the addition of external forcing; the greater the signal amplitude, the greater the power over all periodicities. The imposed influx signals are shown in relation to both autogenic timescales T_{rw} and T_{wb} by the dashed red lines.*

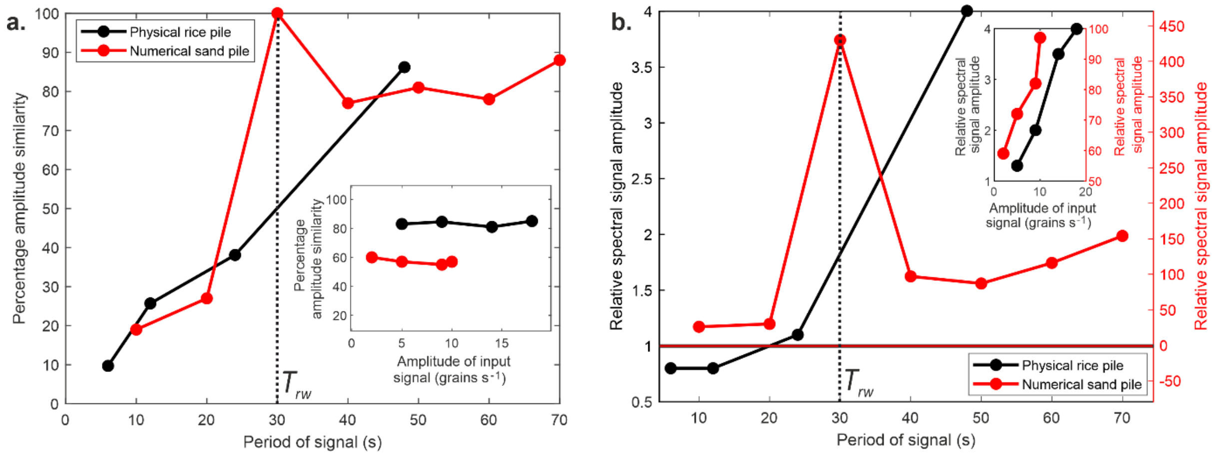

Figure 5.5: Degradation and detectability of environmental signals within the numerical granular pile and physical rice pile.

(a) *Signal degradation as a function of input period, measured by comparing the known input signal to the signal evident in the efflux. Inset figure shows signal degradation as a function of signal amplitude, utilising signals with a periodicity of 40 s and 48 s for the numerical granular pile and physical rice pile respectively.* ***(b)*** *Signal detectability as a function of input period, is measured by comparing the power of the spectral spike and the power of the 95% confidence ban at the imposed periodicity. If the ratio of signal spike to confidence band is greater than 1, define by the horizontal line, the signal is detectable in the output flux. Inset figure shows signal detectability as a function of signal amplitude, utilising signals with a periodicity of 40 s and 48 s for the numerical granular pile and physical rice pile respectively.*

5.5. Discussion

5.5.1. Signal degradation and detectability in systems with low transport system noise

The magnitude of the storage and release dynamics, and hence autogenic noise, is small within the numerical granular pile. However, power spectra generated from a time series of sediment flux maintain the tripartite spectral structure previously quantified (e.g. Griffin *et al.*, 2023; Hwa & Kardar, 1992; Kutnjak-Urbanc *et al.*, 1996). This distinctive spectral structure was advocated to arise from autogenic processes in numerous STSs due to finite size effects (Ganti *et al.*, 2011). Whilst the size of the avalanche events may be up to an order of magnitude smaller within the numerical granular pile compared to the physical rice pile, the geometry of the domain still sets limits on the duration and size of the largest avalanche (Jerolmack & Paola, 2010; Ganti *et al.*, 2011; Griffin *et al.*, 2023). However, the largest avalanche within the numerical granular pile is not on the order of system size (e.g. a wedge failure event) due to the lack of strong stick-slip dynamics which results in minimal internal storage. Instead, this event is more localized, where one large region within the granular pile system may fail at a given time. Nonetheless, correlation within both systems is defined by the duration of individual avalanche events (Hwa and Kardar, 1992). Hence it is unsurprising that the autogenic timescales, T_{rw} and T_{wb} are of similar absolute value due to the identicality in system geometry and rate of influx. Hence, further evidence is provided for the potential universality of the temporal structure of autogenic processes. The tripartite spectral structure and key timescales should be present within STSs with different sediment storage potential.

T_{rw} within the numerical granular pile provides an upper limit to the timescales over which signals experience shredding in the same manner as the physical rice pile. These short period input signals ($T<T_{rw}$) experience a severe reduction in amplitude during propagation as they are of similar magnitude to the natural autogenic fluctuations within the system. Although the sediment storage potential varies considerably between granular systems, the amount of degradation experienced by signals of similar periodicity is comparable. This suggests that the fractional amount of degradation an environmental signal experiences could be solely dependent on the input signal periodicity. However, this needs further testing within natural and experimental STS. From this knowledge, a database of expected signal degradation could be constructed as a function of both signal periodicity and the length of the STS in question. To achieve this, future work should investigate signal degradation as a function of STS length and aim to test if this theory holds for STS of differing lengths.

Whilst the fractional degradation of high-frequency signals is comparable between the granular systems, the detectability of imposed signals differs significantly, where severely degraded signals $T<T_{rw}$ are highly detectable within the output flux of the numerical granular pile. Therefore, within systems with lower sediment storage potential, T_{rw} does not provide a lower temporal threshold for signal detection as it does in the physical rice pile. This means that although high frequency signals still experience severe degradation, they need not be of large amplitude to exceed the magnitude of transport system noise to be detectable. Alongside this, low amplitude signals $T>T_{rw}$ are unlikely to be obscured in the output flux, as likewise to degraded signals, any imposed periodicity will likely be greater than background noise levels within a STS. As the magnitude of the autogenic processes within a STS sets the threshold for signal detectability (Toby *et al.*, 2019), this could vary significantly between segments of a

STS depending on the nature of the autogenic processes present (Toby *et al.*, 2022). Therefore, this could aid or hinder the detectability of high frequency signals.

Previous work has hypothesised that a method to maximize the preservation of sediment flux signals is to eliminate nonlinearity from the system, hence reducing the noise and the ability of the system to mix up signals (Jerolmack & Paola, 2010). In this analogy, high sediment storage potential (generating high transport system noise) could be equated to turbulent flows with significant mixing. On the other hand, low sediment storage potential (generating low transport system noise) are more analogous to laminar flows, which promote the linear convolution of an input signal but with added noise (Jerolmack & Paola, 2010). The numerical granular pile does not produce completely linear dynamics. However, sediment storage potential is significantly reduced compared to the physical rice pile or 1D cellular models of granular systems with strict sediment transport thresholds (e.g. Bak *et al.,* 1987; Hwa & Kardar, 1992; Malthe-Sørenssen *et al.*, 1999; Manna, 1999). Minimising sediment storage capacity does not reduce the amount of degradation a signal experiences as previously suggested. Instead, this maximises the detectability of environmental signals and guarantees faithful signal transfer over all periods and amplitudes. However, this has implications when interpreting the influence of autogenic processes on signal preservation. As severely degraded signals produce a highly detectable response, the process of signal shredding could be overlooked. In previous work, detecting the presence of environmental signals from a time series of stratigraphic measurables has taken precedence over reconstructing signal properties (Vaughan *et al.*, 2011; Meyers, 2012; Tjiputra *et al.*, 2023), especially when searching for evidence of well-studied environmental forcing (e.g. Milankovitch scale climatic forcing). However, it can be highlighted that signal detectability does not guarantee the accurate reconstruction of paleo-signal magnitude. For example, the Palaeocene-Eocene Thermal Maximum (PETM) was a significant, mesotimescale global climate change event (McInerney & Wing, 2011), where the signal periodicity was likely shorter or equal to T_{rw} for many stratigraphic records (Trampush & Hajek, 2017; Straub *et al.*, 2020). The signal of this event may be detectable within stratigraphy (Dunkley Jones *et al.*, 2018; Duller *et al.*, 2019). However, using the absolute record of this event would underpredict the magnitude of Earth-surface process change that should be expected from future global warming events. Therefore, the use of T_{rw} to accurately describe the preservation of short-period input signals is emphasised. By comparing the input signal periodicity to T_{rw}, it can be ascertained as to whether the signal periodicity and amplitude have been preserved (i.e., the signal has not been shredded), or just the periodicity (i.e., the signal has been shredded).

This work focuses on the propagation and preservation of high-frequency input signals. However, the similarity of the results between both granular systems allows us to hypothesize that T_{wb} will provide a timescale over which signals experience heightened detectability in the same manner as the physical rice pile. A pathway for future work will be to understand the detectability of long-period input signals within systems with low transport system noise and explore the nature of T_{wb} as a threshold for enhanced signal detection.

5.5.2. Stochastic resonance within sediment transport systems

Whilst all signals with periodicity $T<T_{rw}$ experience significant degradation, for influx signals $T=T_{rw}$ evidence of a stochastic resonance behaviour is found (Benzi *et al.*, 1981; Gammaitoni *et al.*, 1998; Wellens *et al.*, 2004). This behaviour was not observed within the physical rice pile as an influx signal with $T=T_{rw}$ was not imposed. However, Jerolmack & Paola, (2010) found hints of this behaviour within a 1D cellular rice pile model but the effect was never fully quantified. The occurrence of resonance at $T=T_{rw}$ is rational as the signal periodicity is of the same duration and magnitude as the largest avalanche within the numerical granular pile. At this periodicity, the imposed sediment flux signal experiences no degradation during propagation down-system, and the spectral spike at the imposed periodicity is amplified by approximately 500%. This behaviour has been identified previously during the saltating of sand grains by wind in desertified territories, resulting in a spectral amplification of approximately 700% (Gorchakov *et al.*, 2013). However, resonance is a common phenomenon with numerous applications in physics, chemistry, biomedical science, engineering, climatology and more recently the response of landscapes to climatic forcing (Benzi *et al.*, 1982; Nicolis, 1993; Ganopolski & Rahmstorf, 2002; Andersson *et al.*, 2011; Godard *et al.*, 2013; Falanga *et al.*, 2020; Alkhayuon *et al.*, 2023).

Noise is generally viewed as inconvenient when transferring and detecting environmental signals. However, stochastic noise can play a useful role in enhancing detection of weak periodic signals in nonlinear systems (Hänggi, 2002). This finding hints that some landscapes can respond, and sometimes amplify, the preservation and detectability of sediment flux signals (Godard *et al.*, 2013; Romans *et al.*, 2016). Nevertheless, the potential for a system to amplify the preservation of an external signal will depend on the timescales of autogenic processes within the system and the duration of the imposed forcing. The short autogenic timescale, T_{rw}, has been hypothesised to equate to the maximum timescale of river avulsion, T_a, or within a single deltaic system, a system-wide lobe movement event and associated compensational filling of topography (Jerolmack & Paola, 2007; Straub, 2019; Griffin *et al.,* 2023). The avulsion frequency of many natural delta systems has been found to vary between 10 years (e.g. the Huanghe Delta) and 140 kyr (e.g. the Mississippi Delta) (Jerolmack & Mohrig, 2007; Chadwick *et al.,* 2020), highlighting the potential for signals generated by Milankovitch scale climatic forcing to experience resonance. Due the long periodicity of Milankovitch forcing, resonance is most likely to occur in larger river systems, where the aggradation thickness necessary for avulsion is large. This would extend the avulsion frequency to the order of thousands of years (Chadwick *et al.,* 2020). Resonance within STS would result in the external signal exhibiting enhanced detectability within a time series of Earth surface processes (Godard *et al.,* 2013). Therefore, if these sediment flux signals generate sedimentary deposits of greater thickness (Foreman & Straub, 2017), this would suggest a stronger likelihood of signal preservation within the resulting strata. This may allow the signal to be detectable despite the spectral power reducing effects of stratigraphic incompleteness (Kemp, 2012; Hilgen *et al.,* 2015).

It is not explored as to how either granular system responds to a signal with periodicity $T=T_{wb}$. This timescale has been hypothesised to equate to the equilibrium timescale, T_{eq} (Paola *et al.,* 1992), and the compensation timescale, T_c (Wang *et al.,* 2011) within field scale systems. Resonance at this periodicity is unlikely as T_{wb} represents a topographic filling timescale rather than an event duration timescale, however future work must quantify the interaction of imposed periodicity with this longer autogenic timescale. T_c of many natural delta systems has been found to vary between 6 kyr (e.g. The Rhine) and 370 kyr (e.g. the Orinoco) (Li *et al.,* 2016; Supplementary Material), which could also resonate with external environmental perturbations (e.g. Milankovitch scale climatic forcing) and amplify the response. Evidence for, and the understanding of, resonance in field scale STS is in its infancy. However, if this phenomenon exists in STS, this could aid the reconstruction of certain paleo-environmental signals from both landscapes and strata. This would provide crucial insights to predict how future anthropogenic environmental signals will interact with autogenic processes within STS to garner a detectable response in strata.

5.5.3. Signal detectability within different geomorphic environments

The scale of autogenic noise within a STS is determined by the frequency and magnitude of sediment storage and release processes which determines the transmission and hence detectability of environmental signals within landscapes and strata (Blum *et al.*, 2018; Swanson *et al.*, 2019; Savi *et al.*, 2020; Tofelde *et al.*, 2021). In both the physical rice pile and numerical granular pile, the temporal extent of correlation (red noise less than T_{rw}) is defined by the duration of individual avalanche events. This is also found within 1D granular cellular automata models that evolve by stochastic toppling rules, which are a common method used to study the avalanche dynamics within granular systems (e.g. Bak *et al.*, 1987; Christensen *et al.*, 1996; Hwa & Kardar, 1992; Jerolmack & Paola, 2010). Whilst all three granular systems may share events of similar duration and magnitude (providing domain size and input conditions are comparable) the sediment storage potential, levels of autogenic noise produced and hence signal detection thresholds differ significantly.

Jerolmack & Paola (2010) utilised a 1D cellular automata model to understand the propagation and detectability of high-frequency sediment flux signals. This system employs strict sediment transport thresholds where grains entering the model instantly 'stick' at the input location and only move when the stability threshold at each specific point is exceeded. Jerolmack & Paola (2010) found a strict signal detectability threshold, where shredded signals ($T<T_{rw}$) were obliterated and hence rendered undetectable in the output flux. The significant fluctuations between long episodes of stasis and large sediment release events in the model generate high-magnitude autogenic noise within the system, meaning signals must be of even larger amplitude to be detectable (Jerolmack & Paola, 2010). This system has high sediment storage potential, of which a natural analogue is hillslopes (Figure 5.6) (Benda *et al.*, 2005; DiBiase *et al.*, 2017; Eekhout *et al.*, 2023). Hillslopes experience sediment transport events of all sizes (Stark & Hovius, 2001), with the largest being a landslide, that occur after the threshold for failure has been exceeded (Medwedeff *et al.*, 2020). However, hillslope sediment is likely to be temporarily sequestered by topographic variability, which then remains in storage and eventually fuels subsequent landslides (DiBiase *et al.*, 2017; Clapuyt *et al.*, 2019; Tilahun *et al.*, 2022). This high sediment storage potential means that the sediment associated with periodic influx signals is not conveyed efficiently down-system and is instead only liberated

by large events, obliterating evidence of cyclicity (Schmidt, 2009). Therefore, for a signal to be detectable, the amplitude must be on the order of, or greater than, the magnitude of the largest autogenic event e.g. a landslide.

As the sediment storage potential within a STS decreases, the potential detectability of sediment flux signals increases. Unlike the numerical system, the physical rice pile evolves under gravity, removing the requirement for strict sediment transport thresholds. Alongside this, some grains propagate through the system with minimal storage, analogous to suspended sediment (Bouchaud *et al.*, 1994). Whilst sediment storage and release are still prominent within this system, sediment retention times may be reduced as the thresholds for failure are less strict. This means that the chance of smaller flux events occurring is much higher and hence some severely degraded signals $T<T_{rw}$ can produce a low-level detectable response within the output flux (Griffin *et al.,* 2023). The rice pile with moderate sediment storage potential could be thought of as analogous to bedload dominant fluvial systems, which experience high temporal variability in sediment transport rates (Elgueta-Astaburuaga *et al.*, 2018; Bakker *et al.*, 2019). Within bedload-dominated fluvial systems, phases of aggradation and degradation of the channel bed and bar forms results in punctuated episodes of sediment storage and release over a variety of spatiotemporal scales (Hassan *et al.*, 2007; Luzi *et al.*, 2021). This causes continuous evolution of the fluvial network and hence a highly dynamic STS (Hoey & Sutherland, 1991; Wheaton *et al.*, 2013; Bakker *et al.*, 2019), where the scales of sediment storage and release vary considerably from minutes to thousands of years (Wheaton *et al.*, 2013; Tofelde *et al.*, 2021; Greenberg & Ganti, 2024). Whilst the sediment flux at the outlet may relate to the input signal, sediment storage and remobilization dilute the imposed sediment flux signal and hence reduce its detectability (Tofelde *et al.,* 2021). Therefore, depending on the spatiotemporal dynamics of the system, high-frequency input signals can sometimes produce a detectable response at the system outlet.

Contrastingly, when the capacity for sediment storage is low, sediment flux signals are consistently detectable, evidenced by the results of the numerical granular pile. This system evolves via continuous sediment transport in the form of small-magnitude avalanches, but many grains also propagate through the system with minimal storage analogous to a suspended sediment dominant system. The low sediment storage potential within this system could be equated to a suspended sediment dominated fluvial system (Vercruysse *et al.,* 2017), which generally have more linear particle trajectories compared to bedload dominated systems (Lauer & Parker, 2008). The nature of suspended sediment transport is still stochastic (Shojaeezadeh *et al.*, 2018), and hence signals still experience the same amount of degradation. However, the reduction in autogenic noise due to the more continuous sediment transport mechanics allows severely degraded signals to still be detectable at the system outlet. This highlights the importance of understanding the nature of suspended sediment transport within STS, as they have greater preservation potential for environmental signals. Anthropogenic impact (i.e. dam building and land use variations) causes dramatic alterations in the volume of suspended sediment within fluvial systems, which has consequences for both the morphology of STS and the preservation of sediment flux signals (Dethier *et al.*, 2022; Gardner *et al.*, 2023). Some anthropogenic alterations within fluvial systems (e.g. punctuated sediment storage behind dams) may have the effect of completely shredding high frequency sediment flux signals, rendering them undetectable at the system outlet. In other scenarios, such as the channelization of fluvial systems, signal propagation and hence detectability may be enhanced by anthropogenic influence.

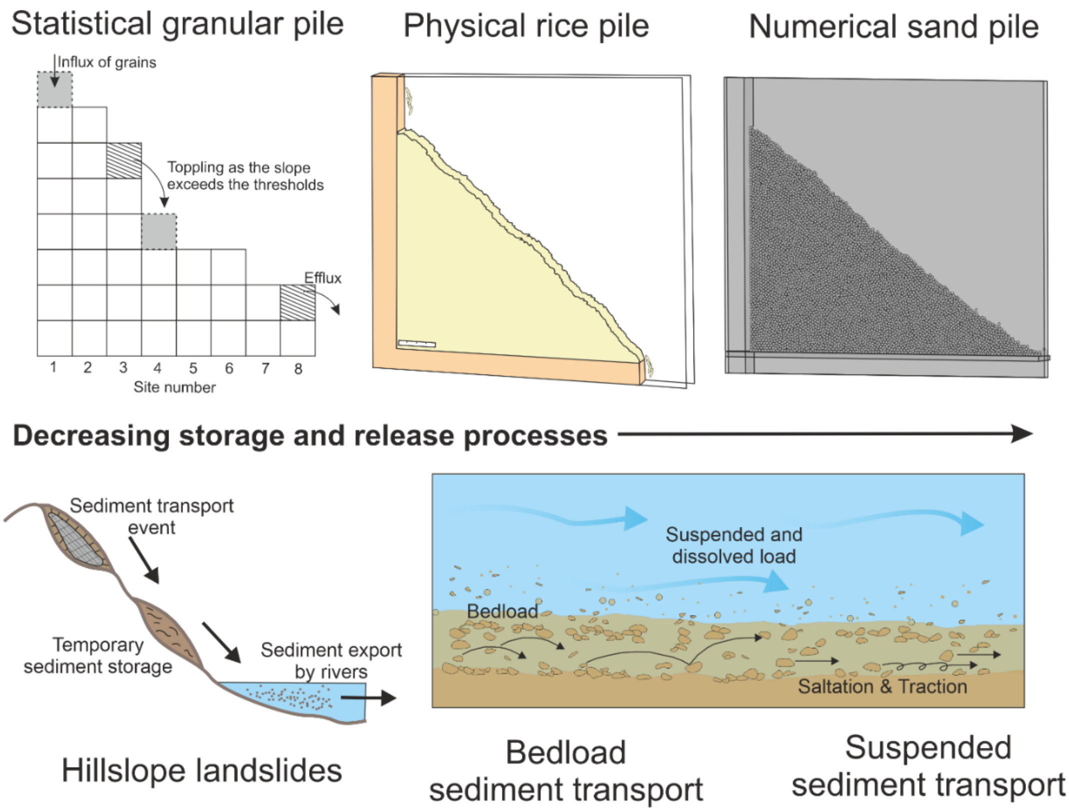

Figure 5.6: Relating granular avalanching systems to segments of sediment transport systems.

The mechanisms of sediment transport in each of the granular avalanching systems are analogous to sediment transport in a variety of STS. The strong storage and release dynamics within a 1D cellular rice pile can be equated to hillslopes where topographic variations store sediment. Schematic adapted *from (Rhoads, 2020). The moderate storage and release processes within the physical rice pile can be analogous to the high spatiotemporal variability present within the bedload sediment transport in fluvial systems. The more continuous sediment transport dynamics in the numerical granular pile can equate to suspended sediment transport in fluvial systems, with continuous flow but punctuated storage. Schematic adapted from (Teng et al., 2020).*

Whilst influx signals into and out of each individual STS is the focus, a STS has multiple linked segments where the sediment efflux out of one segment becomes the sediment influx into the next (Allen, 2017). Therefore, although the first segment of a STS may have a low autogenic noise level and allow signals to be highly detectable, the next may contain a much higher level of noise which obliterates evidence of high-frequency signals (Toby *et al.*, 2022). This highlights the requirement to understand the specific mechanisms of sediment transport present within the STS segment in question, rather than applying the same autogenic thresholds to every geomorphic environment. This is especially important when considering the role of $T_{rw.}$ Whilst this timescale is always an upper limit to signal degradation, it is only a lower limit to signal detection if the magnitude of autogenic noise is sufficiently large. A pathway for future work is to understand how signals propagate through consecutive STS segments with different magnitudes of autogenic noise. The forcing conditions applied to these systems are strictly controlled whereas in natural systems, the input to the next segment is not solely the output of the previous (Toby *et al.*, 2022). Additional forcing can be added to STS segments, for example, sea-level oscillations at the terrestrial/marine boundary, which may add additional noise and/or overprint the sediment flux signal. Future work should aim to understand how the superposition of signals influences the detectability of both periodicities involved.

5.5.4. Defining the magnitude of autogenic noise within sediment transport systems

Quantifying the magnitude of noise present within a specific STS segment of interest is necessary to predict the potential for signal propagation and detection. Comparison of time series, and the associated analysis of avalanche dynamics is utilised to compare the dynamics in this study. However, this may not be possible from field scale systems and hence quantitative classifications must be defined to determine and differentiate the magnitude of autogenic noise within all geomorphic environments.

Firstly, the general class of distributions (i.e. heavy versus thin tail) of autogenic events within a STS may provide one method of classifying the degree of noise present (Ganti *et al.*, 2011). Systems with large sediment transport fluctuations generate a heavy-tailed distribution, whereas a light-tailed distribution is evident from systems with small sediment transport fluctuations. Although this hypothesis is based on two systems alone, future work should generate probability distribution functions for sediment transport in a variety of geomorphic environments, with the aim to determine if the nature of this distribution. However, it has been found that the stratigraphic record does not preserve the heavy tails in magnitude of depositional events, resulting instead in the preservation of false exponential distributions (Ganti *et al.*, 2011). This highlights the importance of understanding the nature and temporal structure of autogenic processes within Earth surface processes, which can provide greater understanding of how to invert the stratigraphic record to reconstruct paleo-Earth surface processes.

Secondly, although autogenic processes within both granular systems show comparable temporal structure with evidence of all three spectral regimes, it is hypothesised that the magnitude of autogenic noise within these systems can be differentiated by the spectral growth index (e.g. gradient of red noise respectively) within the power spectra (Figure 5C). The spectral growth index defines the strength of the correlation within a system. Strong correlation is defined by $1/f^2$ noise (e.g. red noise, $\alpha > 2$), and weak correlation is defined by noise that less than 1/f (e.g. pink noise, $\alpha < 1$) (Grumbacher *et al.*, 1993). The spectral growth index varies between the power spectra, where the physical rice pile power spectra follow a much higher index value than the numerical granular pile ($\alpha = 2.2$ and $\alpha = 0.56$ respectively). The strength of the correlation present indicates how frequently and erratically a system can be driven away from the mean state; the stronger the correlation, the stronger the ability of a system to resist erratic behaviour. Erratic behaviour is defined as a rapid, temporary change within the system; in granular systems, the mean state of a system is consistently small sediment fluxes, hence examples of erratic behaviour within these systems include system-scale avalanche events or periods of stasis (no deposition). Therefore, long-term stability intermixed with temporary fluctuations manifests as approximately 1/f noise.

Sediment fluxes from the numerical granular pile display weak correlation, with spectral growth of $\alpha = 0.56$, indicating that the system is frequently driven away from the mean state. However, although this system experiences frequent erratic behaviour, the recurrence of these rapid, temporary changes means that the variations away from the mean state are small in magnitude and short-lived, before the system is changed rapidly but temporarily in the opposite direction. For example, if the numerical granular pile experiences stasis (no deposition), it is likely that this stasis is short-lived before fluxes restart, and it is likely that a large avalanche event will occur in quick succession after the onset of sediment flux. The frequency in changes of behaviour within the system could mean that the noise caused by any one shift in behaviour may be of small magnitude. This would cause the overall noise levels in the system to be lower than a system where the shifts in behaviour are more sustained (e.g., the rice pile). This has implications for the degradation of environmental signals, meaning that signals are severely degraded in amplitude as they are smeared through space and time by autogenic processes. However, the low noise levels within the system may allow the detectability of sediment flux signals to be enhanced over all periodicities, as the magnitude of imposed signals will exceed the noise produced within the STS.

5.5.5. Evaluating the use of discrete element models to simulate physical granular avalanching systems.

Analysis and comparison of the efflux time series between the numerical granular pile and the physical rice pile show relatively poor agreement, even though the microscopic parameters of the grains used in the DEM (excluding grain shape) were set to replicate the microparameters of the rice used in the physical experiments. The statistics of the avalanche dynamics differ significantly between the systems where the DEM is found to strongly replicate the dynamics previously found in physical sandpile experiments rather than rice piles (Frette *et al.*, 1996; Paguirigan *et al.*, 2015). This was somewhat expected due to the spherical geometry of the particles in the system (a current limitation of MFiX) and hence was not a limiting factor to this study as it allowed different sediment transport dynamics to be compared. However, this is generally not the case when trying to realistically and accurately simulate materials for industrial applications i.e. agricultural materials (Zhao *et al.*, 2021), pharmaceuticals (Yeom *et al.*, 2019), mining stability (Radhakanta & Debashish, 2010), food processing technology (Suehr *et al.*, 2021) and chemical mixing (Blais *et al.*, 2019). This highlights the importance of experimental validation when utilising DEM simulations (Zhang & Vu-Quoc, 2000; Grima & Wypych, 2011; Coetzee, 2016), however, this is still a relatively uncommon practice (Li *et al.*, 2005). Without validating the results, it is easy to accept that the dynamics present within a DEM will accurately replicate the properties of the physical system (Coetzee & Scheffler, 2023). However, a DEM with carefully assigned micro properties may not produce the same level of accuracy on a bulk level, or the bulk behaviours may be comparable and the micro parameters may not (Quist & Evertsson, 2015; Simons *et al.*, 2015). This emphasizes the difficulty in the numerical modelling of complex granular systems and the relative practicality and ease of physical experiments.

When conducting a sensitivity analysis to calibrate the MFiX-DEM to the physical rice pile, measures of GT were utilised. As this gives a measure of collisional activity within a system (Taylor-Noonan *et al.*, 2021), it has been hinted that this could also provide a strong measure of variations in the scale of internal system dynamics (Kasper *et al.*, 2021). However, GT is a poor parameter to use when calibrating the bulk behaviour of a granular system. In Figure 5.1, it is evident that two MFiX-DEM experiments which produce different avalanche statistics can yield a similar mean ensemble GT. Therefore, reliance on this parameter alone without further understanding of the system could lead to erroneous model calibration. Whilst this GT value is heavily averaged in this study, this is necessary when comparing GT over a large suite of sensitivity analysis experiments. This reason makes GT a difficult and inaccurate parameter to utilise for DEM calibration. The most common and important macroscopic parameter in characterising the behaviour of granular materials is the angle of repose (Zhou *et al.*, 2002; Yan *et al.*, 2015; Roessler & Katterfeld, 2019; Müller *et al.*, 2021). MFiX does not record the angle of repose directly throughout experimental runs, and measurement of this parameter is time-consuming and comes at a high computational cost. This was unfeasible for the long total simulation time and short time step utilised in the sensitivity analysis experiments. This issue is usually averted as DEMs utilise short simulation times, on the order of seconds to minutes (Siegmann *et al.*, 2021), whereas the nature of these experiments required run times on the order of hours. Therefore, experiments of this nature are generally impractical to simulate using a DEM and physical experiments are favoured. To gain an idea of the angle of repose throughout the run, a time series of the number of grains in the experiment was utilised. This was useful to gain an understanding of the temporal variation. However, a measure of the static angle of repose of the MFiX-DEM when at dynamic equilibrium during each of the sensitivity analysis experiments would have provided early insight as to which combination of FC and CoR described the bulk properties best. This would also provide insight as to whether utilising spherical particles could truly reproduce the dynamics of a rice pile.

Spherical grains, such as those used in MFiX, are widely used within DEM's for computational simplicity. It has been suggested that an accurate geometrical representation of a granular material does not lead to an accurate prediction of bulk behaviour and that often, simple representations of spheres can produce similar results whilst reducing computational time (e.g. Chung & Ooi, 2006). Within a granular avalanching pile this is not the case; the micro properties of the grains in MFiX (e.g. grain density, grain size, FC and CoR) are equivalent to the rice used in the physical experiments, but the spherical geometry naturally leads to a lower rolling resistivity and ensemble internal friction angle that cannot be overcome (Ting *et al.*, 1993). When using DEM's it is assumed that the shape of the material is the least important factor in the model; hence instead of accurately simulating grain shape in DEM's, studies precisely constrain the macro and microscopic properties of the material being simulated. For example, it would be assumed that assigning the correct macro and micro properties to spherical particles would generate the same granular interlocking potential as elongated rice grains and therefore the same magnitude of stick-slip dynamics would be produced. However, this is not the case. Whilst the spherical grains in the MFiX-DEM were microscopically prescribed to reproduce the dynamics rice, the system cannot ignore the effects of particle geometry as commonly thought and hence the stick-slip dynamics produced were akin to that of near spherical particles. Recent advances in DEMs have allowed the creation of non-spherical particles by rigidly connecting multiple spherical grains in different orientations (e.g. Favier & Kremmer, 2001; Elskamp *et al.*, 2017). Whilst a better alternative than using individual spherical grains, it has been shown that connected particles may capture qualitative experimental features of granular materials, but cannot accurately reproduce quantitative results (Qu *et al.*, 2022). For the most accurate results, it may be advised that DEM's are only utilised when the geometry of the physical material can be accurately simulated.

To form a stable granular pile from spherical particles which has a realistic profile and a greater angle of repose, enhanced rolling resistivity was incorporated into the MFiX-DEM to prevent excess particle rolling and rotation (Zhou & Ooi, 2009; Wensrich & Katterfeld, 2012). Whilst a simple and effective prevention method that may allow the alignment of bulk measurements, the macroscopic shape of a granular pile is the result of various internal mechanisms involving many physical factors (Li *et al.*, 2005; Coetzee, 2017). Although estimates of rolling resistance should be physically meaningful estimates (Marigo and Stitt, 2015), this parameter is often not measured and instead arbitrarily increased to combat the issue of spherical particles (Asaf *et al.*, 2007; Coetzee, 2017). Similar issues also occur with other micro parameters such as particle stiffness or particle damping (Kačianauskas *et al.*, 2015). Difficulty arises when estimating these parameters as in many circumstances, microparameters are determined by trial and error rather than accurate measurements (Belheine *et al.*, 2009; Ma *et al.*, 2020), and how these parameter values were obtained is not mentioned. This instigates a vicious cycle; scientists search for measured parameter estimates, are unsuccessful in obtaining these, and resort to utilising previous inaccurate estimates. The result of this is that the final model is often invalid and the physical meaning of these parameters is lost (Marigo & Stitt, 2015). Therefore, a more robust set of calibration procedures may be required that are more experimentally and numerically efficient (Coetzee, 2016).

Although only a simple time series of efflux from the outlet of the MFiX-DEM was utilised, DEM’s can provide more in-depth insights at both a system and a particle level which are impossible to gain from physical experiments (Neto and Wriggers, 2022). MFiX has the capability to record the trajectories of individual particles through the model. This would allow the residence times of grains within the model to be quantified, and also the trajectories of signal propagation through a STS at grain level. Information from DEM’s which may be hard to get from physical experiments can also be retrieved. For example, a time series of efflux at different locations down the system to quantify the trends in signal degradation and detection with distance from the inlet. Finally, the use of DEM’s can bridge the gap between the cellular automata models of granular piles used previously (e.g. Bak *et al.*, 1987; Hwa & Kardar, 1992; Manna, 1999; Jerolmack & Paola, 2010) and physical granular avalanching experiments. Whilst DEM’s are not completely free from user defined thresholds and parameters, they can produce a realistic experiment using open-source numerical software and without expensive laboratory equipment.

5.6. Conclusions

- A numerical granular pile model built as a discrete element model is utilised to understand the nature and timescales of autogenic processes, and the resultant degradation and detection of environmental signals, within a STS where the magnitude of autogenic noise is low.
- Whilst the internal dynamics of the numerical granular pile differ considerably in comparison to the physical rice pile, power spectra generated from efflux from the numerical granular pile shows a clear tripartite spectral structure, where the autogenic timescales, T_{rw} and T_{wb}, show identicality with the physical rice pile.
- Although the magnitude of autogenic noise is considerably less in the numerical granular pile, T_{rw} still provides an upper limit to the timescales over which signal degradation is

experienced. However, T_{rw} does not provide a lower limit for signal detectability, as the low magnitude of autogenic noise means high-frequency signals are detectable over all periodicities and amplitudes.

- Evidence of resonance is present in the numerical sandpile when the periodicity of the input signal is equal to T_{rw}. This finding hints that landscapes can respond and amplify the preservation and detectability of environmental signals, but also the increased likelihood for these signals to be preserved in strata.
- This will provide a theoretical basis that can be used to understand how signal detectability varies between segments of a STS and how the magnitude of autogenic noise within suspended sediment dominated geomorphic environments controls signal propagation and detection.

Acknowledgements

We gratefully acknowledge support from the University of Liverpool and the International Association of Sedimentologists (Postgraduate Research Grant).

This chapter explores how the efficiency of sediment transport and the magnitude of autogenic noise within a STS influences signal degradation and detectability (Research Question 3). The temporal structure of autogenic noise within a numerical granular system is found to also contain three spectral regimes and two autogenic timescales (T_{rw} and T_{wb}), however the overall levels of noise within the system are much lower (Objective 3.1). This chapter focuses on high frequency signals and finds that T_{rw} still denotes a threshold for the occurrence of signal degradation. However, this timescale does not provide a lower limit to signal detection, as signals over all periodicities and amplitudes are detectable (Objective 3.2). However, stochastic resonance behaviour is present when the period of the signal is equal to T_{rw} (Objective 3.3). Overall, whilst the DEM is not able to replicate the behaviour of the physical rice pile due to limits on the geometry of the grains used, it can provide insight into systems with different internal dynamics (Objective 3.4).

Supplementary materials for chapter 5

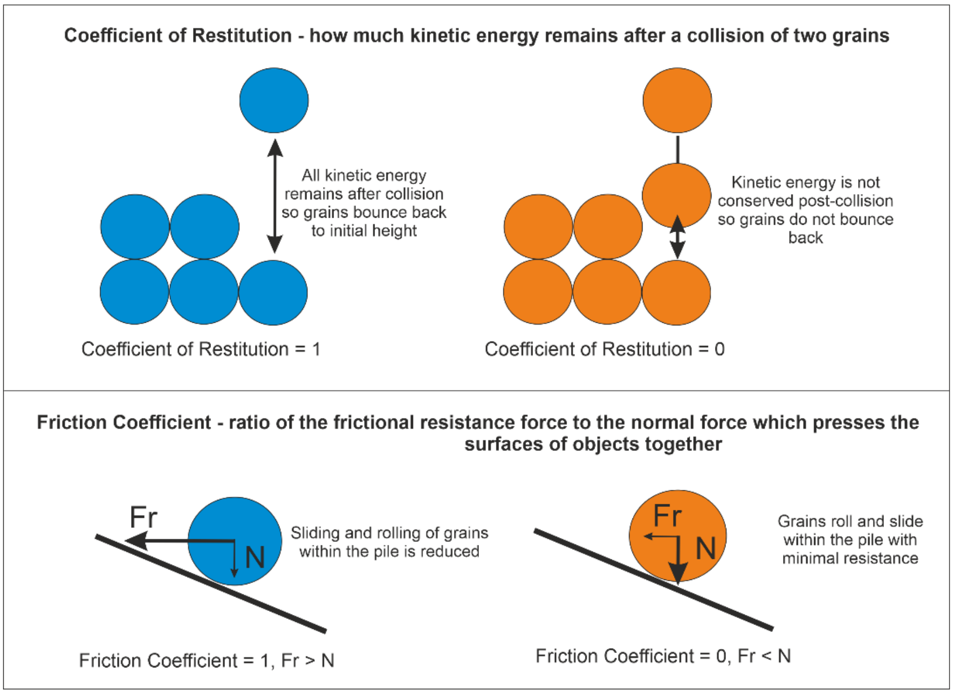

Figure S5.1: Schematic diagram highlighting the differences in granular mechanics resulting from variations in the coefficient of restitution and the friction coefficient.

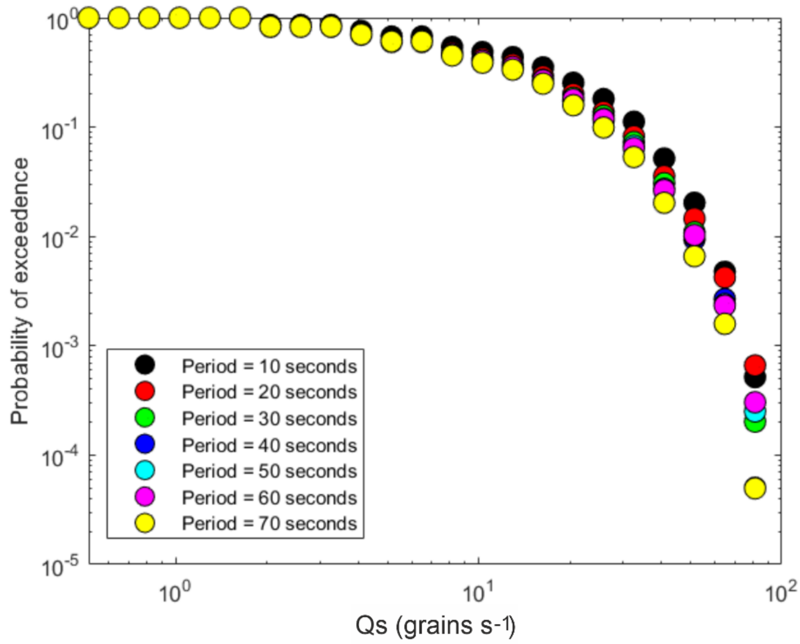

Figure S5.2: Distribution of avalanche sizes within the efflux time series from seven experiments with increasing periodicity.

The time series show an exponential distribution, however as the influx rate increases, there is an increased probability of a certain sized event occurring, but the distributions converge at the largest event.

Table S5.1: Supply characteristics for the individual numerical granular pile experiments, both constant and cyclic feed rates.

Experiment	Stage	Mean feed rate (grains s^{-1})	Periodicity of signal (s)	Amplitude of signal (grains s^{-1})
1	Control	10	-	-
2	Cyclic	10	10	10
3	Cyclic	10	20	10
4	Cyclic	10	30	10
5	Cyclic	10	40	10
6	Cyclic	10	50	10
7	Cyclic	10	60	10
8	Cyclic	10	70	10
9	Cyclic	10	40	9
10	Cyclic	10	40	5
11	Cyclic	10	40	2

6. Summary, implications and further work

In this chapter, the results of Chapters 3, 4 and 5 are summarised and discussed in relation to the overall thesis aim, and individual research questions outlined in section 1.6. Each one of these chapters covers one of the presented research questions and is presented as an individual research paper. The implications of the work are then expanded on in broader context and suggestions for further research that have developed from the outcomes of this thesis are discussed.

6.1. Summary of results

Chapter 3 utilises a physical avalanching rice pile to quantify the full temporal structure of autogenic processes and define key autogenic timescales present within STS. Whilst numerical sand and rice piles are commonly used to answer questions regarding the mechanics of granular systems, these questions were yet to be addressed using a physical rice pile. The true spectral structure of autogenic processes generated from a time series of sediment flux was ambiguous and unquantified. In some experiments, three noise regimes are present (red, white and blue noise), where the spectral gradient breaks define the existence of two autogenic timescales (e.g. Hwa & Kardar, 1992). However other experiments only delimit two noise regimes (red and white noise) and hence one autogenic timescale, T_{x}, which provides an upper limit to the occurrence of signal shredding (e.g. Jerolmack & Paola, 2010). Hence, the aim of these experiments was to define the true temporal structure and timescales of autogenic processes within STS, and quantify how this structure delimits periods of signal shredding from those which are masked by autogenic noise. The temporal structure of autogenic processes is characterised using a rice pile experiment run under constant influx, and then a subsequent suite of experiments run under different rates of constant input was utilised to understand the controls on the autogenic timescales. Cyclic sediment flux signals were then imposed onto the rice pile with different combinations of period and amplitude. Signals over all amplitudes with periodicity less than the short autogenic timescale ($<T_{rw}$) show a severe reduction in amplitude as a result of signal shredding and are hence rendered undetectable in the output flux. Large amplitude signals with periodicity between the autogenic timescales ($T_{rw}<T<T_{wb}$) are detectable within the output flux. However, detectability scales with signal amplitude, where low amplitude signals are of the same magnitude as autogenic noise and are hence obscured. Signals with periodicity greater than the longest autogenic timescale ($>T_{wb}$) show enhanced detectability as the signal period is greater than the longest timescale autogenic process. This framework will allow us to predict how environmental signals interact with STSs over a range of timescales to garner a detectable (or not) response.

Chapter 4 quantifies the effect of stratigraphic incompleteness on the temporal structure of autogenic processes and consequently the detectability and apparent degradation of environmental signals. The reconstruction of environmental signals is challenging from a temporally complete record due to the effect of autogenic processes (Chapter 3). However, the geological record is temporally incomplete due to the existence of time gaps over a variety of scales, generated by unsteady geomorphic processes, which further complicates signal detection and reconstruction. Whilst stratigraphers have long known that all stratigraphic sections are incomplete, the impact of incompleteness on the spectral structure of autogenic processes that can be recovered and hence the detectability of environmental signals was yet to be established. As the temporal structure of autogenic processes and signal detectability has been quantified from a physical rice pile, time is artificially removed from the rice pile time series (generated from both constant and cyclic influx) to mimic stratigraphic incompleteness and the later assumption of linear sedimentation rate. Incompleteness strongly influences the scales and spectral structure of autogenic processes preserved, where the tripartite spectral structure can be distorted, making both autogenic timescales challenging to quantify. Due to this, signals over all autogenic timescales can be rendered undetectable if completeness is low, and environmental perturbations can appear to be degraded in amplitude as a result of incompleteness. This provides improved understanding regarding the records in which information about paleoenvironmental variability may be best preserved.

In Chapter 5, the temporal structure of autogenic processes is characterised within a system where the sediment transport dynamics are less stochastic and the degradation and detectability of environmental signals is quantified as a function of autogenic noise. Every geomorphic environment has its own bounds on the magnitude and duration of sediment transport fluctuations, defined by the thresholds for sediment transport. The magnitude of sediment transport events within a system have been found to provide thresholds for the detectability of environmental signals within landscapes and strata (e.g. Jerolmack & Paola, 2010; Toby *et al.*, 2019). Whilst efforts have been focused on understanding the nature of sediment transport and environmental signal propagation within systems with strong storage and release processes (e.g. bedload dominant systems), quantifying these thresholds within systems where sediment transport is more continuous (e.g. suspended sediment dominant systems) is in its infancy. As an analogue for a system with less stochastic dynamics, a numerical sandpile was utilised and the results compared to that of the physical rice pile. The temporal structure of autogenic processes and associated timescales is established using a experiment run under constant influx, and then cyclic sediment flux signals were imposed onto the numerical granular pile with different combinations of periods and amplitude. Signals over all amplitudes with periodicity less than the short autogenic timescale ($<T_{rw}$) show a severe reduction in amplitude as a result of signal shredding, where signals of similar periodicity experience the same amount of degradation no matter the magnitude of transport system noise. Signals over all periodicity and amplitude (even those which experience shredding) are highly detectable in the output flux. Evidence of resonance is also present when the periodicity of the input signal is equal to T_{rw}; this results in the signal experiencing no degradation, and heightened detectability. This is important for predicting how high-frequency signals interact within autogenic noise in different geomorphic environments and to understand the consequences of anthropogenic activity, which influences the volume of suspended sediment, on the ability of a STS to propagate and record sediment flux signals.

6.2. Discussion of results in relation to the thesis aim

The overall aim of this thesis is to understand the nature of autogenic processes within STSs and how these processes influence the ability of landscapes and strata to record evidence of external sediment flux signals. Together, the individual research questions presented in Chapters 3, 4 and 5 generate a workflow for understanding the propagation, preservation, extraction and interpretation of external sediment supply signals across landscapes and to strata. The three main research questions are:

Research Question 1: *What is the spectral structure of autogenic processes in a STS and how do autogenic timescales control signal propagation and preservation?* (Chapter 1).

Research Question 2: *How does stratigraphic incompleteness influence the preserved structure of autogenic processes and influence signal detectability?* (Chapter 2).

Research Question 3: *How does the magnitude of autogenic noise within a STS influence the degradation and detectability of environmental signals?* (Chapter 3).

The objectives defined to answer the 3 questions have been achieved, and hence the research questions have been answered. Therefore, the results of all three papers provide quantitative understanding of the mechanisms by which autogenic processes operate within the Earth surface active layer (landscapes) and within the Earth's surface inactive layer (stratigraphy).

This theory provides a pathway to understand how the combination of depositional, non-depositional (stasis) and erosional dynamics operating over different spatiotemporal scales governs the preservation and detectability of environmental signals.

The theoretical advances in Chapter 3 (Research Question 1) were fundamental to the subsequent work presented in this thesis (Chapters 4 and 5; Research Questions 2 and 3) as it provides the theoretical foundation on which these papers were based. However, collating the results of Chapters 3 to 5 provides insight into autogenic processes within different individual segments within an entire STS (Figure 6.1), and hence signal propagation potential from upland catchments to deep sea basins (overall thesis aim).

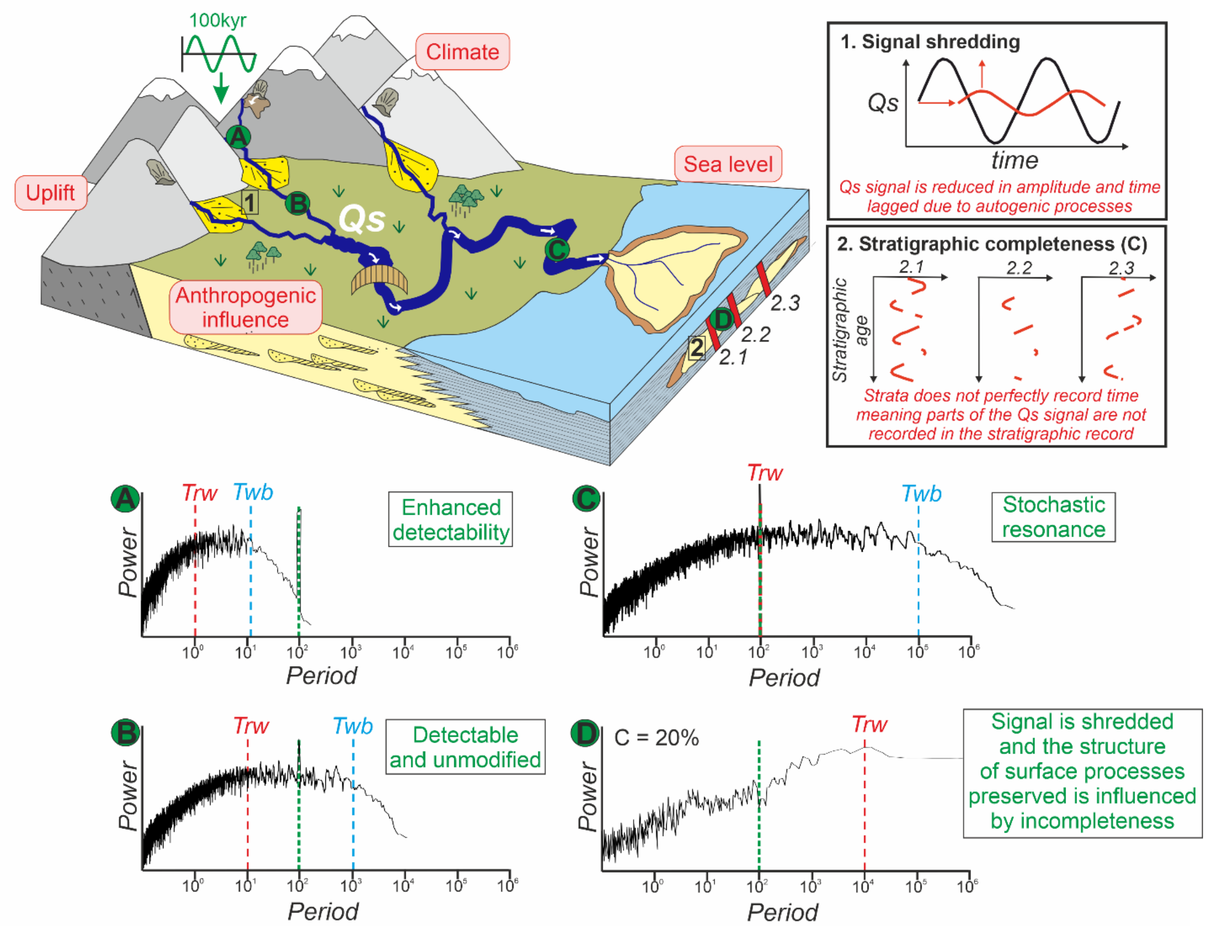

Figure 6.1: Conceptual diagram of a sediment transport system (STS), highlighting the major impediments to the propagation and storage of environmental signals.

STSs transport sediment from erosional sources to depositional sinks and are sensitive to environmental forcings (climate, tectonic, eustatic or anthropogenic change). Propagation of environmental signals across the Earth's surface and into the stratigraphic record is influenced by two primary impediments resulting from autogenic processes: signal shredding and stratigraphic incompleteness. These *impediments can affect any section of a STS, but for simplicity, these are separated into the transfer zone and the depositional sink. 100kyr climatic variability associated with Milankovitch forcing generates sinusoidal variations in sediment flux in upland catchments. Autogenic processes within hillslope catchments operate over short timescales (<10^1 years; McKean & Roering (2004)), hence the signal periodicity exceeds the duration of the longest autogenic process and the signal is preserved and highly detectable in the output flux (A). The signal propagates into the mountain front alluvial fan system. Autogenic processes on alluvial fans operate on longer timescales (10^2-10^4 years; Straub & Wang 2013)), but the propagation of an unmodified signal is dependent on the coupling of the fan/fluvial systems. When fully coupled, the signal will be detectable at the inlet of the trunk fluvial system (B). The compensation timescale (T_c) of large river systems can be on the order of 10^5 years (Li et al., 2016), meaning that autogenic timescales can overlap with many mesotimescale environmental forcings. Where signal periodicity is of equal duration to the short autogenic timescale (T_{rw}), stochastic resonance may amplify the spectral amplitude of the signal (C). The preservation of sediment flux signals in the stratigraphic record is complicated by both the harsher stratigraphic shredding regime and incompleteness, reducing both signal detectability and the preservation of Earth surface processes (D).*

Chapter 3 characterises the spectral structure and timescales of autogenic processes within an idealised STS (Research Question 1) and highlights the potential universality of this temporal structure within all segments of STSs (Figure 6.1). Chapter 5 advances on this framework to show that this spectral structure is present within STSs with different sediment transport mechanics and sediment storage potential (Research Question 3). Hence, these two papers provide key theory to predict what the characteristic autogenic distribution shape should be for a given landscape (overall research question). The size constrains of the system in question place upper bounds on the largest autogenic process (Ganti *et al.*, 2011), where different properties of the same event define the two autogenic timescales present (Ganti *et al.*, 2011). Whilst all three noise regimes will arise in each STS segment, the absolute duration of these regimes will vary due to an array of factors including the length of the STS, sediment storage potential and the rate/efficiency of sediment transport (linked to water discharge). Therefore, whilst this structure is likely inherent to geomorphic processes, evidence of the full spectral structure may be unobtainable from a time series due to incompleteness, insufficient duration of the instrumental record or measurement resolution (Chapter 4; Research Question 2). These papers highlight the importance of establishing realistic expectations of the structure of autogenic variability that can be recorded in landscapes versus the structure that can be extracted from strata and, importantly, scientists can look beyond the traditionally assumed Gaussian noise models can be (overall thesis aim).

The advancements in understanding and characterising autogenic processes made in all three papers provide key insight into the ability of landscapes and strata to record evidence of external sediment flux signals (overall thesis aim). The autogenic timescales (T_{rw} and T_{wb}) provide temporal limits for signal shredding (T_{rw}) and signal detection (T_{wb}). Hence, comparison of the signal periodicity to both timescales provides knowledge of signal detectability within a given STS (Chapters 3 and 5; Research Questions 1 and 3) or the resultant stratigraphy (Chapter 4; Research Question 2). Although this thesis utilises two granular systems to understand individual STS segments, links can be made as to how signals would propagate from source to sink through multiple segments where the duration and magnitude of autogenic processes varies (Figure 6.1). In a STS, the efflux of one segment becomes the influx to the next, hence signal propagation potential depends on both the timescales of autogenic processes (Toby *et al.*, 2022) and landscape connectivity (Wohl *et al.*, 2019). In an ideal scenario, an environmental signal would propagate unmodified from an erosional catchment to a deep-sea basin, and then be preserved in the stratigraphic record. However, this is highly unlikely. The nature and timescales of autogenic processes will vary significantly between segments, where the autogenic timescales would likely increase with distance down system, as the length of the STS segments increases. Hence, a signal that was highly detectable in the erosional zone could be rendered undetectable by the time it has reached the marine realm, and hence has no chance of stratigraphic preservation even before the effects of incompleteness (Figure 6.1). Overall, this thesis establishes a suite of theoretical frameworks that provide robust confidence limits for signal detectability within environmental parameters and offers novel insight into the ability of various geomorphic environments and strata to record evidence of external environmental perturbations (overall thesis aim).

This thesis has been able to make significant theoretical advances in understanding the nature of autogenic processes and the mechanics of sediment transport within STS. For the first time, this project utilised a physical avalanching rice pile which contains no strict user-defined thresholds (e.g. Hwa & Kardar, 1992; Jerolmack & Paola, 2010). This allowed the full structure of these processes to be quantified, and provided insight into how these processes propagate, modify and preserve evidence of external sediment flux signals at the terminus of individual STS segments (Chapters 3 and 5) and in the strata of depositional sinks (Chapter 4). It has therefore contributed to addressing significant data, theory and knowledge gaps outlined in

Chapter 1, by providing understanding and insight into the internal mechanics of STS (overall thesis aim).

6.3. Implications and future work

In depositional landscapes, on which this thesis focuses, the importance of defining the spatiotemporal scales of autogenic processes has been increasingly recognised (Murray, 2007; Murray *et al.*, 2014; Paola, 2016). To define these, a mechanistic understanding of the depositional processes which drive autogenic dynamics has been achieved. However, this is yet to be achieved to the same extent within erosional landscapes (Whipple & Tucker, 1999), where the mechanisms that cause autogenic dynamics and their interaction with allogenic forcing are scarcely characterised (Merritts *et al.*, 1994; Limaye & Lamb, 2014; Grimaud *et al.*, 2016; Baynes *et al.*, 2018; Scheingross *et al.*, 2020). Internal feedback between erosional processes and landscape components causes fluctuations in erosion rate, topography and consequently downstream sediment flux under constant external forcing but these processes also remain active as landscapes respond to external environmental perturbations (Malatesta *et al.*, 2017). Despite ongoing work examining how erosional landscapes respond to allogenic forcing (Wobus *et al.*, 2006; Whittaker & Boulton, 2012) defining quantitative frameworks to define the scales of autogenic processes present remains a pressing issue for future work (Scheingross *et al.*, 2020). The ubiquity of autogenic processes within landscapes allows it to be hypothesised that the temporal structure of autogenic processes in erosional environments will display a similar tripartite spectral structure as found in depositional systems due to the presence of finite size effects within erosional processes, in the same manner as depositional processes (Ganti *et al.*, 2011). However, whilst the short autogenic timescale (T_{rw}) in depositional environments is defined by the duration of sediment deposition, within an erosional landscape this would most likely equate to the time required for the removal and redistribution of sediment from a system (e.g. erosion and evacuation of sediment from hillslopes by a fluvial system). Whilst this would still be governed by system length (e.g. the length of a hillslope), it is also controlled by the connectivity of STS segments which controls the timescales of sediment storage within landscapes (Clapuyt *et al.*, 2019). Similarly, whilst the long autogenic timescale (T_{wb}) in depositional environments is defined by topographic filling, in erosional landscapes this will most likely equate to the time required for the landscape to steepen to a similar elevation profile after a large erosional event. This means that variations in the frequency of landslide events and/or uplift rate would potentially cause variations in T_{wb} in the same manner as sediment influx rate within depositional environments. The linkage between erosional and depositional landscapes within a STS highlights the requirement to understand how the mechanics driving autogenic processes evolve down a STS which will enable a quantitative understanding of signal propagation potential from source to sink (Allen, 2008).

When quantifying the propagation and preservation of sediment flux signals, simple cyclical signals with sine wave structure are generally employed (Overeem *et al.*, 2001; Zabel *et al.*, 2001; Kirby & Whipple, 2012; D'Arcy *et al.*, 2017; Foreman & Straub, 2017; Toby *et al.*, 2019; Mancini *et al.*, 2023). This is also the case when studying other signals of environmental change, including but not limited to water discharge (Simpson & Castelltort, 2012; Moragoda & Cohen, 2020), geochemical variations (Newton & Bottrell, 2007; Berner & Berner, 2012), or palynological variations (Jiménez-Moreno *et al.*, 2005; Utescher *et al.*, 2009). However, the geometry of the input signal may influence its detectability, due to the variations in the volume of sediment supplied over the same periodicity and/or the rate of change in sediment supply (Toby *et al.*, 2019). This has been somewhat investigated, but mainly focused on rapid, instantaneous variations (e.g. signal spikes; Armitage *et al.*, 2011) rather than differences in overall signal structure (e.g. square waves, saw tooth waves or superimposed cyclical signals). Whilst this thesis also utilises cyclic signals for simplicity, the influence of short-period square wave signals is quantified where the rate of change in supply (e.g. acceleration; Toby *et al.,* 2019) is found to influence detectability. The exact nature of this acceleration threshold is yet to be quantified in the surface or strata, but improving our understanding regarding the nature of this threshold could provide another pathway which would allow high frequency, degraded signals to be detectable. However, when considering a signal of set periodicity, changing the rate of sediment input also causes a variation in the total sediment mass input to the system. Whilst square wave signals were detectable in the rice pile in comparison to signals with sine wave structure, whether the variation in mass or input rate caused this detectability difference has not currently been isolated. Nevertheless, all signals imposed on natural sediment routing systems are unlikely to exactly follow these geometries. Although perfect sine wave signals are utilised for experimental convenience, signals in nature are more likely to be stepped, e.g. tectonic signals (Sharman *et al.*,, 2019), asymmetrical e.g. relative sea level fluctuations (Ritchie *et al.*, 2004), or in the form of a sharp increase/decrease in sediment flux that returns to a steady state condition e.g. precipitation (Armitage *et al.*, 2011; Van De Wiel *et al.*, 2011) or glacial cycles (Watkins *et al.*, 2018). The common trend with these signals is the sharp increase in sediment flux at the onset of environmental change, followed by a decrease either to a new, or mean steady state condition. In these scenarios, the rapid change in sediment flux, or the larger sediment mass supplied over the same periodicity, may allow the signal to overwhelm the magnitude of the autogenic noise and hence be detectable within landscapes, but not necessarily in strata. In contrast, stratigraphic preservation of environmental signals generally favours those of longer duration (Foreman & Straub, 2017; Toby *et al.*, 2019; Zhang *et al.*, 2020; Trampush & Hajek 2016), and it may be the long, slow decline in sediment flux resulting from the same environmental forcing that is preserved in strata. Whilst environmental perturbations that are natural in origin (e.g. Milankovitch-forced climatic cycles) tend to generate longer, slower responses, the recent increase in anthropogenic forcing mechanisms comes with much faster rates of change (Syvitski, 2003; Blum & Roberts, 2009). This is more analogous to the square wave sediment flux signals imposed onto the physical rice pile, however, the amplitude of anthropogenically generated sediment flux signals will most likely be much greater than those imposed in this thesis (East *et al.*, 2022). For example, the installation or removal of dams can trigger an instantaneous decline or increase in sediment yield down-system (Hu *et al.*, 2009), or variations in sediment load can result from urbanization, deforestation and agricultural practices (Syvitski & Kettner, 2011; Hao *et al.*, 2016; Ibáñez *et al.*, 2019). However, whilst anthropogenic activity can directly influence sediment flux, it can also have secondary consequences in the form of inducing faster rates of environmental change (Rosa *et al.*, 2015). Hence, the theory presented in this thesis can provide insight as to whether sediment flux signals generated by different types of anthropogenic perturbations will be detectable within STSs and survive the effects of incompleteness to be detectable within strata.

When generating thresholds for the propagation and detectability of periodic sediment flux signals, all other external conditions are held constant to isolate impacts (Simons & Senturk, 1992). Whilst frameworks have been developed based on sediment supply, the threshold for the preservation and detectability of allogenic water discharge signals may differ. Whilst granular avalanching systems do not allow water discharge signals to be investigated, the thresholds for the preservation of discharge variations should be explored, especially due to the effects of the current warming climate (Hao *et al.*, 2016; Hirabayashi *et al.*, 2021). Furthermore, whilst the propagation of sediment flux signals is widely studied, sedimentary signals in the form of grain size variations must be advanced on. It has been shown that deposit texture should vary as a response to allogenic forcing (Fedele & Paola, 2007), however assessing this in field scale systems may be complex due to local variability imparted by autogenic processes which causes problems when spatially averaging trends (D'Arcy *et al.*, 2017). STS can also experience the simultaneous occurrence of other allogenic forcings (e.g. base level change), which may influence the thresholds for signal transfer. Whilst research has focused on the influence of down-system sediment flux/water discharge signals or up-system base level signals the impacts of these have successfully been isolated and an understanding of how a sediment routing system responds to the superposition of these signals must be achieved. This could be attained using a physical rice pile system which was constructed to include accommodation generation (e.g. a subsiding base), or by a more natural experimental system such as an experimental delta subjected to simultaneous allogenic forcing. Furthermore, to advance on this, the thresholds for preserving superimposed signals must be understood, as although signals with one periodicity have been imposed for simplicity, natural allogenic variations can contain evidence of more than one periodicity. For a more rounded understanding of the propagation of all types of environmental signal, it must be understood when, where and how different types of signals influence the autogenic processes within a sediment routing system, and how these signals become degraded and/or rendered undetectable during propagation downstream. Whilst a time series of sediment flux from the system outlet is utilised for ease of measurement from both experimental and field scale systems, extracting time series from various locations down a STS would allow us to understand the rate of signal degradation/obscuring within an STS, and the potential locations where signal preservation is most likely. This would enable both geomorphologists and stratigraphers the opportunity to find evidence of environmental signals before concluding the lack of periodicity from a time series gained from the system outlet or depositional sink.

To quantify the detectability of external environmental signals within power spectra, the most common method to generate confidence bands, typically for paleo-climatic studies, is the application of the AR(1) model (Pemberton & Priestley, 1990; Weedon, 2003). This model is applied due to the assumption that the temporal structure of power spectra generated from environmental and stratigraphic measurables contains only red and white noise (Husson *et al.*, 2014; Hajek & Straub, 2017). Although commonly utilised, the AR(1) model has been previously quantified as a poor fit to any dataset that does not strictly follow an AR(1) process, even if the spectra show the presence of red and white noise (Meyer & Kantz, 2019; Shi *et al.*, 2022). This is because if the spectral model utilised does not fully represent the spectral background structure generated by autogenic variability, the model would generate confidence bands where the expected power at low frequencies would be underestimated relative to the true power of the spectra. This could result in false positives and spurious signals (Vaughan *et al.*, 2011; Hajek & Straub, 2017). A likely reason the AR(1) model is a poor fit to power spectra generated from autogenic processes, is that the power spectra generated from the natural variability present in environmental measurables contain evidence of blue noise over long timescales. Whilst evidence of blue noise may be uncommon, due to the lack of long time series available or the incompleteness of strata, as sediment transport dynamics do not follow an AR(1) process, this model will consistently be a poor fit to power spectra generated from surface or stratigraphic measurables. This highlights the implications of not quantifying the temporal structure of autogenic processes, which influences the choice data analysis methods utilised before inverting power spectra for paleo-surface process interpretations and for signal detection. Due to the importance of spectral model fit for accurate signal detection, future work should focus on generating a model which can produce a strong statistical fit to power spectra of this structure over all autogenic timescales. The theory presented in this thesis will aid stratigraphers to look beyond the traditionally assumed Gaussian noise models and establish realistic expectations of the structure of autogenic variability produced and also those preserved in the stratigraphic record (Grove *et al.*, 2022; Tu *et al.*, 2023).

An exciting attribute of research surrounding signal propagation and the thresholds for signal shredding and detectability is that they can be reasonably estimated using measurable parameters in field-scale systems. However, although these thresholds are well-known to field scientists, applying existing theories to STSs and the resulting stratigraphy can be difficult. Whilst the short autogenic timescale (T_{rw}) will be present in each segment of a STS, this timescale will be defined by the precise mechanisms that contribute to the longest-duration autogenic event. For example, on hillslopes, this may equate to the largest sediment transport event (e.g. a landslide), whereas in a river, this may equate to a channel avulsion timescale (Jerolmack & Paola, 2007). Therefore, to truly quantify the nature of autogenic processes within a STS and how signals are shredded during propagation, future work should aim to define the processes that describe the extent of correlation in different STS segments. From this, a database could be constructed in a similar manner to the database of incompleteness exponents by Jerolmack & Sadler, (2007), which would provide estimates of these timescales for a range of modern STS. Furthermore, whilst this timescale in the rice pile is sediment supply independent, in field scale systems this timescale is likely to be influenced by sediment supply and potentially other factors including but not limited to grain size, cohesion and water discharge. Delimiting the precise controls on this timescale in different STS segments would improve understanding of how these additional factors influence the rate of spectral growth, the nature of autogenic processes and hence the degree of shredding experienced by environmental signals. This would also allow the nature of the relationship between T_{rw} and T_{wb} in a variety of different STSs to be established (Figure 6.1). Both of these timescales generate a framework that can be used when potential evidence for environmental signals are present in power spectra, or to reconstruct the supply conditions of the signal based on the preserved record. This means that the interpretation of environmental signals within a time series of stratigraphic measurables can be quantitatively justified and field studies where no evidence of expected signals was found can test if this is likely due to the signal shredding/obscuring, the degree of autogenic noise within a STS, stratigraphic incompleteness, or a combination of these issues.

Whilst a signal may not be recovered from a time series of surface sediment flux, the imposed variation in sediment supply will influence the internal dynamics of autogenic processes and the resultant stratigraphy. Whilst this thesis starts to explore the preservation of signals in strata, it is acknowledged that this theory does not include signal loss caused by vertical cut and fill processes associated with the autogenic reworking of sediment, hence a major challenge remaining is to integrate surface and stratigraphic timescales and test these in field scale systems. Achieving this will allow scientists the ability to identify specific geomorphic or stratigraphic records, the sampling resolution or scale of enquiry required or to establish a null hypothesis for the presence of external environmental signals. Whilst the thresholds for the transfer and detectability of sediment supply signals to landscapes and strata are not the same, understanding the relationship between surface and stratigraphic timescales is important for defining autogenic thresholds. For example, whilst in the experimental delta the maximum avulsion timescale is of the same order of magnitude as T_c, in field scale systems this need not be the case and the maximum avulsion timescale may be much shorter. This influences the structure of autogenic processes and the timescales over which signals experience shredding. Furthermore, it has been suggested that T_{eq} and T_c are of the same order of magnitude (Straub *et al.*, 2020; Toby *et al.*, 2022). This thesis suggests that the longest surface autogenic timescale, T_{wb}, should also be of the same order of magnitude and related to these other autogenically derived timescales. Whilst connections between these timescales have been hypothesised, future work should aim to quantify the nature of the theoretical relationships between these timescales in different sediment routing system segments, which would enable better predictions on which information can be stored in both landscapes and strata.

One of the largest, but most rewarding challenges of this research still remains: the application of theoretical knowledge gained through experiments and numerical models to field scale systems and outcrops (Paola *et al.*, 2009; Straub *et al.*, 2020). Whilst the spatial resolution of datasets has increased significantly through modern geophysical techniques and the use of UAV's, resolution limitations in geochronometers mean that accurately quantifying all missing time in stratigraphic sections is next to impossible (Smith *et al.*, 2015). Due to this, our understanding of autogenic processes and thresholds for signal propagation is limited to experimental predictions. The theory presented in this thesis could be used to outline field localities where specific environmental signals may be preserved. This could either be the preservation of modern signals within specific landscapes or the preservation of ancient signals within stratigraphy. Whilst this theory utilises measurable parameters from field scale systems meaning a first workflow can be developed for the application to field scale systems, a large amount of work remains to integrate field and experimental data in order for the specific controls on autogenic timescales, and hence thresholds for signal propagation, to be denoted for different STS segments. Once achieved, this will allow for qualitative reconstructions of palaeo-Earth surface processes, and environmental change, to be accurately achieved from the stratigraphic record.

6.4. Concluding remarks

This thesis aimed to develop a quantitative theoretical basis, established using an understanding of autogenic processes, that can be used to assess the potential of geomorphic environments and the resulting strata to record external environmental signals of varying sediment flux. To achieve this, two 2D granular avalanching experiments were developed to bridge the gap between simplified 1D cellular automata models and complex, 3D field scale systems, and enabled detailed measurements of sediment flux to be made, providing quantitative insight into autogenic processes. As a result, this thesis: (1) contributes a quantitative understanding of the temporal structure and key timescales of autogenic processes operating within various sediment transport systems, which is used to develop a framework that can predict the degradation and detectability of environmental signals within landscapes and strata, (2) quantifies how stratigraphic incompleteness and the assumption of linear sedimentation rate can hinder the reconstruction of palaeo-surface processes and environmental signals from time series of stratigraphic information, and (3) provides insight into how the degradation and detectability o environmental signals varies with the magnitude of autogenic noise within a STS. Thus, this thesis contributes to the scientific understanding of autogenic processes and how they govern signal propagation across landscapes and preservation in strata.

Appendices

1. Physical rice pile datasets

This thesis utilises a suite of physical rice pile experiments conducted at Tulane University. A description of these experiments is outlined in Chapter 2. A total of 41 physical experiments have been used in this thesis. The control experiment refers to the rice pile experiment run under a constant input rate of 0.37 g s^{-1}. Eight further rice pile experiments run under constant input rate were conducted, where the input rate increased systematically in 0.1 g s^{-1} intervals from 0.02 g s^{-1} to 1.78 g s^{-1}. Based on this, 32 experiments with cyclic input rate were conducted. The periodicities of the imposed cycles varied from 6s to 2000s. The amplitude of the imposed cycles all shared a mean feed rate of 0.37 g s^{-1}, but varied as a function of the mean feed rate from 25% (0.009 g s^{-1}) to 100% (0.37 g s^{-1}).

Datasets from the physical rice pile experiments are available online through the Harvard Dataverse online repository. Here the reference for these experiments is provided. Metadata of these experiments can be accessed on the Harvard Dataverse online repository.

1.1. Physical rice pile metadata

Reference:

Griffin, C., Straub, K.M., 2023, Rice Pile Experiments Conducted at Tulane University in 2022, https://dataverse.harvard.edu/dataset.xhtml?persistentId=doi:10.7910/DVN/SO5XJP

Name:

Rice Pile Experiments Conducted at Tulane University in 2022

Link:

https://dataverse.harvard.edu/dataset.xhtml?persistentId=doi:10.7910/DVN/SO5XJP

See the dataset on the Harvard Dataverse online repository for metadata.

1.2. MFiX-DEM sandpile datasets

A suite of numerical sandpile experiments was conducted using MFiX open-source code. A description of these experiments is outlined in Chapter 2. A total of 11 numerical experiments have been used in this thesis. The control experiment refers to the sandpile experiment run under a constant input rate of 10 grains s^{-1}. Ten further numerical sandpile experiments were run with cyclic input rate. Seven experiments varied the periodicity of the imposed cycles from

10s to 70s, with a constant amplitude of 10 grains s^{-1}. Three experiments varied the amplitude of the imposed cycles from 10 grains s^{-1} to 2 grains s^{-1}, with a constant periodicity of 40 seconds. Here I provide metadata for the MFiX-DEM sandpile experiments.

1.3.MFiX-DEM sandpile metadata

Name:

MFiX-DEM numerical sandpile experiments conducted in 2022/2023

Dates run:

June 2022 – June 2023

Primary individual responsible for experiments:

Chloe Griffin, Jonathan Higham

Purpose of experiments:

To understand the temporal spectral structure of autogenic dynamics within the numerical sandpile and to define the storage conditions of sediment supply signals within the sandpile. Sediment supply cycles in this experiment followed a sine wave pattern with variations in periodicity and amplitude.

General description:

The granular pile was built using a 3D computational domain replicating the physical experiment, with dimensions of 0.3 x 0.3 x 0.02m (Figure 4). The domain geometry is discretised by a non-uniform grid of 20, 10 and 5 cells in the X, Y and Z directions respectively. The walls of the domain utilise the non-slip boundary condition. Particles enter and leave the domain via a defined inlet and outlet region. The point-source inlet is generated as a 0.008 x 0.006m region, allowing only individual particles to enter the domain, increasing accuracy in the input rate. The inlet has a mass flow boundary condition and the outlet has a pressure outflow boundary condition which spans the open down-system end of the domain. Spherical grains with a diameter and density of 0.003m and 1500kg m^{-3} respectively are used as the granular medium. The particle input parameters utilised in the DEM can be found in Table 2. Grains are fed into the system from the inlet at the mass flow rate defined in the GUI. Input conditions to the system can be precisely controlled by defining an input rate in kg s^{-1}.

Control experiment input conditions:

Total run time: 30,000 seconds

Input rate: 10 grains s^{-1} (0.00018 kg s^{-1})

<u>Cyclic experiment input conditions:</u>

Total run time: 30,000 seconds

Periodicities: 10s, 20s 30s 40s 50s 60s 70s (amplitude held constant at 10 grains s^{-1} (0.00018 kg s^{-1}).

Amplitudes: 10 grains sec^{-1} (0.00018 kg s^{-1}), 9 grains sec^{-1} (0.00016 kg s^{-1}), 5 grains s^{-1} (0.00009 kg s^{-1}), 2 grains s^{-1} (0.00004 kg s^{-1}) (periodicity held constant at 40 seconds).

<u>Data collection:</u>

Frequency of data collection: 0.001 seconds

Data collected: particle ID, X, Y and Z velocity, resultant velocity, X, Y and Z coordinates

2. Table of symbols and acronyms

α	Spectral gradient
a	Parameter value accounting for bypass efflux
AR(1)	Autoregressive lag 1
β	1
BPL	Bending power law model
C	Stratigraphic completeness
CDM	Continuum discrete methods
CoR	Coefficient of restitution
d	Diameter
DBPL	Double bending power law model
DEM	Discrete element model
f	Frequency
f_b	Frequency of the spectral rollover
FC	Friciton coefficient
$F_{c,a}$	Collisional force
γ	Smallest time step removed
GT	Granular temperature
GUI	Graphical user interface
H_{max}	Channel depth
$\propto$	Short term completeness exponent (Jerolmack & Sadler 2007).
I	Moment of inertia
Kyr	Thousand years
L	System length
λ	Rate parameter
LSP	Lomb-Scargle Periodogram
m	Mass
M	Maximum autogenic sediment release event
MFiX	Multiphase Flow with Interphase eXchanges
M_{max}	Maximum mass effluxed over the longest avalanche event
MTM	Multi-taper method
N	Power law normalization factor
ω_a	Angular velocity
PETM	Paleocene-Eocene Thermal Maximum
Q_{in}	Sediment input rate (flux)
Q_s	Sediment input rate (volume)
q_o	Sediment input rate (mass)
r	Particle coordinate
ρ	Density
φ	Truncation parameter
S	Power at a given frequency
S_c	Critical threshold slope
SOC	Self-organised criticality
STS	Sediment transport system
T	Periodicity of the input signal
τ	Tail index
T_c	Compensation timescale
T_{cp}	Torque acting on the centre of mass of the particle
T_{eq}	Equilibrium timescale
TFM	Two fluid model
t_k	Duration of depositional events
t_r	Duration of stasis events

T_{rw}	Short autogenic timescale in a physical rice pile
T_{wb}	Long autogenic timescale in a physical rice pile
T_x	Equilibrium timescale in a numerical rice pile
UAV	Unmanned aerial vehicle
v	Diffusivity
V_x	X component of particle velocity
Vy	Y component of particle velocity
Vz	Z component of particle velocity
W	Width

References

Abels, H. A., Aziz, H. A., Krijgsman, W., Smeets, S. J. B., & Hilgen, F. J. (2010). Long-period eccentricity control on sedimentary sequences in the continental Madrid Basin (middle Miocene, Spain). *Earth and Planetary Science Letters*, *289*(1–2), 220–231. https://doi.org/10.1016/j.epsl.2009.11.011

Abels, H. A., Kraus, M. J., & Gingerich, P. D. (2013). Precession-scale cyclicity in the fluvial lower Eocene Willwood Formation of the Bighorn Basin, Wyoming (USA). *Sedimentology*, *60*(6). https://doi.org/10.1111/sed.12039

Ager, D. . (1973). *The Nature of the Stratigraphical Record* (3rd Edition). Wiley-Blackwell.

Ajmal, M., Roessler, T., Richter, C., & Katterfeld, A. (2020). Calibration of cohesive DEM parameters under rapid flow conditions and low consolidation stresses. *Powder Technology*. https://doi.org/10.1016/j.powtec.2020.07.017

Alkhayuon, H., Marley, J., Wieczorek, S., & Tyson, R. C. (2023). Stochastic resonance in climate reddening increases the risk of cyclic ecosystem extinction via phase-tipping. *Global Change Biology*, *29*(12), 3347–3363. https://doi.org/10.1111/gcb.16679

Allen, P. A. (2008). From landscapes into geological history. *Nature*. https://doi.org/10.1038/nature06586

Allen, P. A. (2017). *Sediment Routing Systems: The Fate of Sediment from Source to Sink*. *Sediment Routing Systems*.

Allen, P. A., & Densmore, A. L. (2000). Sediment flux from an uplifting fault block. *Basin Research*. https://doi.org/10.1111/j.1365-2117.2000.00135.x

Anderson, R. S. (1990). Eolian ripples as examples of self-organization in geomorphological systems. *Earth Science Reviews*. https://doi.org/10.1016/0012-8252(0)90029-U

Anderson, S. W., & Konrad, C. P. (2019). Downstream-Propagating Channel Responses to Decadal-Scale Climate Variability in a Glaciated River Basin. *Journal of Geophysical Research: Earth Surface*. https://doi.org/10.1029/2018JF004734

Andersson, B., Andersson, R., Håkansson, L., Mortensen, M., Sudiyo, R., & Van Wachem, B. (2011). *Computational fluid dynamics for engineers*. *Computational Fluid Dynamics for Engineers*. https://doi.org/10.1017/CBO9781139093590

Armitage, J. J., Duller, R. A., Whittaker, A. C., & Allen, P. A. (2011). Transformation of tectonic and climatic signals from source to sedimentary archive. *Nature Geoscience*. https://doi.org/10.1038/ngeo1087

Armitage, J. J., Dunkley Jones, T., Duller, R. A., Whittaker, A. C., & Allen, P. A. (2013). Temporal buffering of climate-driven sediment flux cycles by transient catchment response. *Earth and Planetary Science Letters*. https://doi.org/10.1016/j.epsl.2013.03.020

Asaf, Z., Rubinstein, D., & Shmulevich, I. (2007). Determination of discrete element model parameters required for soil tillage. *Soil and Tillage Research*, *92*(1–2), 227–242. https://doi.org/10.1016/j.still.2006.03.006

Aziz, H. A., Hilgen, F. J., van Luijk, G. M., Sluijs, A., Kraus, M. J., Pares, J. M., & Gingerich, P. D. (2008). Astronomical climate control on paleosol stacking patterns in the upper Paleocene-lower Eocene Willwood Formation, Bighorn Basin, Wyoming. *Geology*, *36*(7), 531–534. https://doi.org/10.1130/G24734A.1

Bak, P., Tang, C., & Wiesenfeld, K. (1987). Self-organised criticality: An explanation of the 1/f noise. *Physical Review Letters*, *59*(4), 381–384. https://doi.org/10.1103/PhysRevLett.59.381

Bakker, M., Antoniazza, G., Odermatt, E., & Lane, S. N. (2019). Morphological Response of an Alpine Braided Reach to Sediment-Laden Flow Events. *Journal of Geophysical Research: Earth Surface*, *124*(5), 1310–1328. https://doi.org/10.1029/2018JF004811

Barefoot, E. A., Nittrouer, J. A., & Straub, K. M. (2023). Sedimentary Processes and the Temporal Resolution of Sedimentary Strata. *Geophysical Research Letters*, *50*(13). https://doi.org/10.1029/2023GL103925

Baynes, E. R. C., Lague, D., Attal, M., Gangloff, A., Kirstein, L. A., & Dugmore, A. J. (2018). River self-organisation inhibits discharge control on waterfall migration. *Scientific Reports*. https://doi.org/10.1038/s41598-018-20767-6

Beakawi Al-Hashemi, H. M., & Baghabra Al-Amoudi, O. S. (2018). A review on the angle of repose of granular materials. *Powder Technology*. https://doi.org/10.1016/j.powtec.2018.02.003

Beerbower, J. R. (1964). Cyclothems and cyclic depositional mechanisms in alluvial plain sedimentation. In: D.F. Merriam (Ed.), Symposium on Cyclic Sedimentation. *Kansas Geological Survey Bulletin, 169:31-42.*, 31–42. Retrieved from http://www.kgs.ku.edu/Publications/Bulletins/169/Beerbower/

Belheine, N., Plassiard, J. P., Donzé, F. V., Darve, F., & Seridi, A. (2009). Numerical simulation of drained triaxial test using 3D discrete element modeling. *Computers and Geotechnics*. https://doi.org/10.1016/j.compgeo.2008.02.003

Benavides, S. J., Deal, E., Rushlow, M., Venditti, J. G., Zhang, Q., Kamrin, K., & Perron, J. T. (2022). The Impact of Intermittency on Bed Load Sediment Transport. *Geophysical Research Letters*, *49*(5), 1–10. https://doi.org/10.1029/2021GL096088

Benavides, S. J., Deal, E., Venditti, J. G., Bradley, R., Zhang, Q., Kamrin, K., & Perron, J. T. (2023). How Fast or How Many? Sources of Intermittent Sediment Transport. *Geophysical Research Letters*. https://doi.org/10.1029/2022GL101919

Benda, L., & Dunne, T. (1997). Stochastic forcing of sediment routing and storage in channel networks. *Water Resources Research*. https://doi.org/10.1029/97WR02387

Benda, L., Hassan, M. A., Church, M., & May, C. L. (2005). GEOMORPHOLOGY OF STEEPLAND HEADWATERS: THE TRANSITION FROM HILLSLOPES TO CHANNELS. *Journal of the American Water Resources Association*. https://doi.org/10.1111/j.1752-1688.2005.tb03773.x

Benzi, R., Sutera, A., & Vulpiani, A. (1981). The mechanism of stochastic resonance. *Journal of Physics A: Mathematical and General*, *14*(11). https://doi.org/10.1088/0305-

4470/14/11/006

Benzi, R., Parisi, G., Sutera, A., & Vulpiani, A. (1982). Stochastic resonance in climatic change. *Tellus A: Dynamic Meteorology and Oceanography*. https://doi.org/10.3402/tellusa.v34i1.10782

Berner, E. K., & Berner, R. . (2012). *Global Environment: Water, Air, and Geochemical Cycles* (Second Edi). Princeton: Princeton University Press. https://doi.org/https://doi.org/10.1515/9781400842766

Bhattacharya, J. P., Copeland, P., Lawton, T. F., & Holbrook, J. (2016). Estimation of source area, river paleo-discharge, paleoslope, and sediment budgets of linked deep-time depositional systems and implications for hydrocarbon potential. *Earth-Science Reviews*, *153*, 77–110. https://doi.org/10.1016/j.earscirev.2015.10.013

Blais, B., Vidal, D., Bertrand, F., Patience, G. S., & Chaouki, J. (2019). Experimental Methods in Chemical Engineering: Discrete Element Method—DEM. *Canadian Journal of Chemical Engineering*, *97*(7), 1964–1973. https://doi.org/10.1002/cjce.23501

Blöthe, J. H., & Korup, O. (2013). Millennial lag times in the Himalayan sediment routing system. *Earth and Planetary Science Letters*. https://doi.org/10.1016/j.epsl.2013.08.044

Blum, M., & Hattier-Womack, J. (2009). Climate change, sea-level change, and fluvial sediment supply to deepwater depositional systems: external controls on deep-water depositional systems. *SEPM Spec. Publ*, *92*, 15–39.

Blum, M., Rogers, K., Gleason, J., Najman, Y., Cruz, J., & Fox, L. (2018). Allogenic and Autogenic Signals in the Stratigraphic Record of the Deep-Sea Bengal Fan. *Scientific Reports*. https://doi.org/10.1038/s41598-018-25819-5

Blum, M. D., & Roberts, H. H. (2009). Drowning of the Mississippi Delta due to insufficient sediment supply and global sea-levelrise. *Nature Geoscience*. https://doi.org/10.1038/ngeo553

De Boer, D. H. (2001). Self-organization in fluvial landscapes: Sediment dynamics as an emergent property. *Computers and Geosciences*. https://doi.org/10.1016/S0098-3004(00)00137-0

Bouchaud, J.-P., Cates, M. E., Prakash, J. R., & Edwards, S. F. (1994). A model for the dynamics of sandpile surfaces. *Journal de Physique I*. https://doi.org/10.1051/jp1:1994195

Boulesteix, K., Poyatos-Moré, M., Flint, S. S., Taylor, K. G., Hodgson, D. M., & Hasiotis, S. T. (2019). Transport and deposition of mud in deep-water environments: Processes and stratigraphic implications. *Sedimentology*. https://doi.org/10.1111/sed.12614

Bracken, L. J., Turnbull, L., Wainwright, J., & Bogaart, P. (2015). Sediment connectivity: A framework for understanding sediment transfer at multiple scales. *Earth Surface Processes and Landforms*, *40*(2). https://doi.org/10.1002/esp.3635

Braun, J., Voisin, C., Gourlan, A. T., & Chauvel, C. (2015). Erosional response of an actively uplifting mountain belt to cyclic rainfall variations. *Earth Surface Dynamics*, *3*(1), 1–14.

https://doi.org/10.5194/esurf-3-1-2015

Brooke, S., Chadwick, A. J., Silvestre, J., Lamb, M. P., Edmonds, D. A., & Ganti, V. (2022). Where rivers jump course. *Science, 376*(6596). https://doi.org/10.1126/science.abm1215

Brooke, S. A. S., Whittaker, A. C., Armitage, J. J., D'Arcy, M., & Watkins, S. E. (2018). Quantifying Sediment Transport Dynamics on Alluvial Fans From Spatial and Temporal Changes in Grain Size, Death Valley, California. *Journal of Geophysical Research: Earth Surface*. https://doi.org/10.1029/2018JF004622

Bryant, M., Falk, P., & Paola, C. (1995). Experimental study of avulsion frequency and rate of deposition. *Geology*, *23*(4), 365–368. https://doi.org/10.1130/0091-7613(1995)023<0365:ESOAFA>2.3.CO;2

Budd, D. A., Hajek, E. A., & Purkis, S. J. (2016). Introduction to autogenic dynamics and self-organization in sedimentary systems. *SEPM Special Publications*. https://doi.org/10.2110/sepmsp.106.14

Burgess, P. ., Masiero, I., Toby, S. C., & Duller, R. . (2019). A Big Fan of Signals? Exploring Autogenic and Allogenic Process and Product In a Numerical Stratigraphic Forward Model of Submarine-Fan Development. *Journal of Sedimentary Research*, *89*(1), 1–12. https://doi.org/10.2110/jsr.2019.3

Burgess, P. M. (2006). The Signal and the Noise: Forward Modeling of Allocyclic and Autocyclic Processes Influencing Peritidal Carbonate Stacking Patterns. *Journal of Sedimentary Research*. https://doi.org/10.2110/jsr.2006.084

Butt, T., & Russell, P. (1999). Suspended sediment transport mechanisms in high-energy swash. *Marine Geology*. https://doi.org/10.1016/S0025-3227(99)00043-2

Caracciolo, L. (2020). Sediment generation and sediment routing systems from a quantitative provenance analysis perspective: Review, application and future development. *Earth-Science Reviews*. https://doi.org/10.1016/j.earscirev.2020.103226

Carreras, B. A., Lynch, V. E., Newman, D. E., & Sanchez, R. (2002). Avalanche structure in a running sandpile model. *Physical Review E - Statistical Physics, Plasmas, Fluids, and Related Interdisciplinary Topics*. https://doi.org/10.1103/PhysRevE.66.011302

Castelltort, S., & Van Den Driessche, J. (2003). How plausible are high-frequency sediment supply-driven cycles in the stratigraphic record? *Sedimentary Geology*. https://doi.org/10.1016/S0037-0738(03)00066-6

Castelltort, S., Whittaker, A., & Vergés, J. (2015). Tectonics, sedimentation and surface processes: From the erosional engine to basin deposition. *Earth Surface Processes and Landforms*. https://doi.org/10.1002/esp.3769

Cazelles, B. (2004). Symbolic dynamics for identifying similarity between rhythms of ecological time series. *Ecology Letters*. https://doi.org/10.1111/j.1461-0248.2004.00629.x

Cendrero, Antonio, Juan Remondo, Achim A. Beylich, Piotr Cienciala, Luis M. Forte, Valentin N. Golosov, Artyom V. Gusarov et al. "Denudation and geomorphic change in the

Anthropocene; a global overview." *Earth-Science Reviews* 233 (2022), https://doi.org/10.1016/j.earscirev.2022.104186

Chadwick, A. J., & Lamb, M. P. (2021). Climate-Change Controls on River Delta Avulsion Location and Frequency. *Journal of Geophysical Research: Earth Surface*. https://doi.org/10.1029/2020JF005950

Chadwick, A. J., Lamb, M. P., & Ganti, V. (2020). Accelerated river avulsion frequency on lowland deltas due to sea-level rise. *Proceedings of the National Academy of Sciences of the United States of America*, *117*(30). https://doi.org/10.1073/pnas.1912351117

Chin, A., & Phillips, J. D. (2007). The self-organization of step-pools in mountain streams. *Geomorphology*. https://doi.org/10.1016/j.geomorph.2006.02.021

Christensen, K., Corral, Á., Frette, V., Feder, J., & Jøssang, T. (1996). Tracer dispersion in a self-organized critical system. *Physical Review Letters*. https://doi.org/10.1103/PhysRevLett.77.107

Church, M., 2002. Geomorphic thresholds in riverine landscapes. *Freshwater biology*, *47*(4), pp.541-557.

Chung, Y. C., & Ooi, J. Y. (2006). Confined Compression and Rod Penetration of a Dense Granular Medium: Discrete Element Modelling and Validation. https://doi.org/10.1007/978-3-540-35724-7_14

Cislaghi, A. and Bischetti, G.B., 2019. Source areas, connectivity, and delivery rate of sediments in mountainous-forested hillslopes: A probabilistic approach. *Science of the Total Environment*, *652*, pp.1168-1186. https://doi.org/10.1016/j.scitotenv.2018.10.318

Clapuyt, F., Vanacker, V., Christl, M., Van Oost, K., & Schlunegger, F. (2019). Spatio-temporal dynamics of sediment transfer systems in landslide-prone Alpine catchments. *Solid Earth*, *10*(5). https://doi.org/10.5194/se-10-1489-2019

Clar, S., Drossel, B., & Schwabl, F. (1996). Forest fires and other examples of self-organized criticality. *Journal of Physics Condensed Matter*. https://doi.org/10.1088/0953-8984/8/37/004

Clarke, L., Quine, T. A., & Nicholas, A. (2010). An experimental investigation of autogenic behaviour during alluvial fan evolution. *Geomorphology*, *115*(3–4). https://doi.org/10.1016/j.geomorph.2009.06.033

Clarke, L. E. (2015). Experimental alluvial fans: Advances in understanding of fan dynamics and processes. *Geomorphology*. https://doi.org/10.1016/j.geomorph.2015.04.013

Clifford, N. J. (1993). Formation of riffle-pool sequences: field evidence for an autogenetic process. *Sedimentary Geology*. https://doi.org/10.1016/0037-0738(93)90074-F

Coetzee, C. J. (2016). Calibration of the discrete element method and the effect of particle shape. *Powder Technology*, *297*, 50–70. https://doi.org/10.1016/j.powtec.2016.04.003

Coetzee, C. J. (2017). Review: Calibration of the discrete element method. *Powder Technology*, *310*, 104–142. https://doi.org/10.1016/j.powtec.2017.01.015

Coetzee, C. J., & Scheffler, O. C. (2023). Review: The Calibration of DEM Parameters for the Bulk Modelling of Cohesive Materials. *Processes*, *11*(1). https://doi.org/10.3390/pr11010005

Colombera, L., Arévalo, O.J. and Mountney, N.P., 2017. Fluvial-system response to climate change: the Paleocene-Eocene Tremp group, Pyrenees, Spain. *Global and Planetary Change*, *157*, pp.1-17. https://doi.org/10.1016/j.gloplacha.2017.08.011

Corcoran, P. L., Norris, T., Ceccanese, T., Walzak, M. J., Helm, P. A., & Marvin, C. H. (2015). Hidden plastics of Lake Ontario, Canada and their potential preservation in the sediment record. *Environmental Pollution*. https://doi.org/10.1016/j.envpol.2015.04.009

Coulthard, T. J., & Van De Wiel, M. J. (2007). Quantifying fluvial non linearity and finding self organized criticality? Insights from simulations of river basin evolution. *Geomorphology*. https://doi.org/10.1016/j.geomorph.2007.04.011

Covault, J. A., Craddock, W. H., Romans, B. W., Fildani, A., & Gosai, M. (2013). Spatial and temporal variations in landscape evolution: Historic and longer-term sediment flux through global catchments. *Journal of Geology*. https://doi.org/10.1086/668680

Croke, J., Denham, R., Thompson, C., & Grove, J. (2015). Evidence of Self-Organized Criticality in riverbank mass failures: A matter of perspective? *Earth Surface Processes and Landforms*. https://doi.org/10.1002/esp.3688

Cundall, P. A., & Strack, O. D. L. (1979). A discrete numerical model for granular assemblies. *Geotechnique*. https://doi.org/10.1680/geot.1979.29.1.47

Curtis, K.E., Renshaw, C.E., Magilligan, F.J. and Dade, W.B., 2010. Temporal and spatial scales of geomorphic adjustments to reduced competency following flow regulation in bedload-dominated systems. *Geomorphology*, *118*(1-2), pp.105-117.

D'Arcy, M., Whittaker, A. C., & Roda-Boluda, D. C. (2017). Measuring alluvial fan sensitivity to past climate changes using a self-similarity approach to grain-size fining, Death Valley, California. *Sedimentology*. https://doi.org/10.1111/sed.12308

Dade, W. B., & Friend, P. F. (1998). Grain-size, sediment-transport regime, and channel slope in alluvial rivers. *Journal of Geology*. https://doi.org/10.1086/516052

Dai, S. B., Yang, S. L., & Li, M. (2009). The sharp decrease in suspended sediment supply from China's rivers to the sea: Anthropogenic and natural causes. *Hydrological Sciences Journal*. https://doi.org/10.1623/hysj.54.1.135

Daniels, J. M. (2008). Distinguishing allogenic from autogenic causes of bed elevation change in late Quaternary alluvial stratigraphic records. *Geomorphology*. https://doi.org/10.1016/j.geomorph.2008.05.022

Darabi, P., Pougatch, K., Salcudean, M., & Grecov, D. (2011). DEM investigations of fluidized beds in the presence of liquid coating. *Powder Technology*, *214*(3), 365–374. https://doi.org/10.1016/j.powtec.2011.08.032

Darby, S.E., Alabyan, A.M. and Van de Wiel, M.J., 2002. Numerical simulation of bank erosion and channel migration in meandering rivers. *Water Resources Research*, *38*(9), pp.2-1. https://doi.org/10.1029/2001WR000602

Davies, N. S., Shillito, A. P., & McMahon, W. J. (2019). Where does the time go? Assessing the chronostratigraphic fidelity of sedimentary geological outcrops in the pliocene–pleistocene red crag formation, eastern england. *Journal of the Geological Society*, *176*(6), 1154–1168. https://doi.org/10.1144/jgs2019-056

DeAngelis, D. L. (2012). Self-Organizing Processes in Landscape Pattern and Resilience: A Review. *ISRN Ecology*. https://doi.org/10.5402/2012/274510

Densmore, A. L., Allen, P. A., & Simpson, G. (2007). Development and response of a coupled catchment fan system under changing tectonic and climatic forcing. *Journal of Geophysical Research: Earth Surface*. https://doi.org/10.1029/2006JF000474

Dethier, E. N., Renshaw, C. E., & Magilligan, F. J. (2022). Rapid changes to global river suspended seidment flux by humans. *Science*, *1452*(June), 1447–1452.

DiBiase, R. A., Lamb, M. P., Ganti, V., & Booth, A. M. (2017). Slope, grain size, and roughness controls on dry sediment transport and storage on steep hillslopes. *Journal of Geophysical Research: Earth Surface*, *122*(4), 941–960. https://doi.org/10.1002/2016JF003970

Van Dijk, M., Postma, G., & Kleinhans, M. G. (2009). Autocyclic behaviour of fan deltas: An analogue experimental study. *Sedimentology*. https://doi.org/10.1111/j.1365-3091.2008.01047.x

Dodds, P. S., & Rothman, D. H. (2000). Scaling, universality, and geomorphology. *Annual Review of Earth and Planetary Sciences*, *28*. https://doi.org/10.1146/annurev.earth.28.1.571

Duan, Y., & Feng, Z. G. (2017). Incorporation of velocity-dependent restitution coefficient and particle surface friction into kinetic theory for modeling granular flow cooling. *Physical Review E*. https://doi.org/10.1103/PhysRevE.96.062907

Duller, R. A., Armitage, J. J., Manners, H. R., Grimes, S., & Jones, T. D. (2019). Delayed sedimentary response to abrupt climate change at the Paleocene-Eocene boundary, northern Spain. *Geology*. https://doi.org/10.1130/G45631.1

Dunkley Jones, T., Manners, H. R., Hoggett, M., Turner, S. K., Westerhold, T., Leng, M. J., et al. (2018). Dynamics of sediment flux to a bathyal continental margin section through the Paleocene-Eocene Thermal Maximum. *Climate of the Past*, *14*(7), 1035–1049. https://doi.org/10.5194/cp-14-1035-2018

East, A. ., Clift, P. ., Carter, A., Alizai, A., & VanLaningham, S. (2015). Fluvial–Eolian Interactions In Sediment Routing and Sedimentary Signal Buffering: An Example From the Indus Basin and Thar Desert. *Journal of Sedimentary Research*. https://doi.org/10.2110/jsr.2015.42

East, A. ., Warrick, J. ., Li, D., Sankey, J. ., Redsteer, M. ., Gibbs, A. ., et al. (2022). Measuring and Attributing Sedimentary and Geomorphic Responses to Modern Climate Change: Challenges and Opportunities. *Earth's Future*. https://doi.org/10.1029/2022EF002983

East, A. E., Logan, J. B., Mastin, M. C., Ritchie, A. C., Bountry, J. A., Magirl, C. S., & Sankey, J. B. (2018). Geomorphic Evolution of a Gravel-Bed River Under Sediment-Starved Versus Sediment-Rich Conditions: River Response to the World's Largest Dam Removal. *Journal of Geophysical Research: Earth Surface*, *123*(12), 3338–3369. https://doi.org/10.1029/2018JF004703

Edmonds, D. A., & Slingerland, R. L. (2010). Significant effect of sediment cohesion on deltamorphology. *Nature Geoscience*. https://doi.org/10.1038/ngeo730

Eekhout, J. P. C., Jódar-Abellán, A., Carrillo-López, E., Boix-Fayos, C., & de Vente, J. (2024). Assessing the hillslope-channel contributions to the catchment sediment balance under climate change. *Environmental Modelling & Software*, *171*(June 2023), 105890. https://doi.org/10.1016/j.envsoft.2023.105890

Elgueta-Astaburuaga, M. A., Hassan, M. A., Saletti, M., & Clarke, G. K. C. (2018). The Effect of Episodic Sediment Supply on Bedload Variability and Sediment Mobility. *Water Resources Research*, *54*(9), 6319–6335. https://doi.org/10.1029/2017WR022280

Elskamp, F., Kruggel-Emden, H., Hennig, M., & Teipel, U. (2017). A strategy to determine DEM parameters for spherical and non-spherical particles. *Granular Matter*. https://doi.org/10.1007/s10035-017-0710-0

Fairchild, I. J., Smith, C. L., Baker, A., Fuller, L., Spötl, C., Mattey, D., & McDermott, F. (2006). Modification and preservation of environmental signals in speleothems. *Earth-Science Reviews*. https://doi.org/10.1016/j.earscirev.2005.08.003

Falanga, M., De Lauro, E., & de Martino, S. (2020). Stochastic resonance observed in aerosol optical depth time series. *Atmosphere*, *11*(5), 502.

Faulkner, D.J., Larson, P.H., Jol, H.M., Running, G.L., Loope, H.M. and Goble, R.J., 2016. Autogenic incision and terrace formation resulting from abrupt late-glacial base-level fall, lower Chippewa River, Wisconsin, USA. *Geomorphology*, *266*, pp.75-95. https://doi.org/10.1016/j.geomorph.2016.04.016

Favier, J. F., Abbaspour-Fard, M. H., & Kremmer, M. (2001). Modeling Nonspherical Particles Using Multisphere Discrete Elements. *Journal of Engineering Mechanics*. https://doi.org/10.1061/(asce)0733-9399(2001)127:10(971)

Fedele, J. J., & Paola, C. (2007). Similarity solutions for fluvial sediment fining by selective deposition. *Journal of Geophysical Research: Earth Surface*. https://doi.org/10.1029/2005JF000409

Fick, C., Manica, R., & Junior, E. E. T. (2017). Autogenic influence on the morphology of submarine fans: An approach from 3D physical modelling of turbidity currents. *Brazilian Journal of Geology*, *47*(3), 345–368. https://doi.org/10.1590/2317-4889201720170066

Fisher, D. A., Reeh, N., & Clausen, H. B. (1985). Stratigraphic Noise in Time Series Derived from Ice Cores. *Annals of Glaciology*, *7*, 76–83. https://doi.org/10.3189/s0260305500005942

Flemings, P. B., & Jordan, T. E. (1989). A synthetic stratigraphic model of foreland basin development. *Journal of Geophysical Research*.

https://doi.org/10.1029/JB094iB04p03851

Fonstad, M., & Marcus, W. A. (2003). Self-organized criticality in riverbank systems. *Annals of the Association of American Geographers*. https://doi.org/10.1111/1467-8306.9302002

Foreman, B. Z., & Straub, K. M. (2017). Autogenic geomorphic processes determine the resolution and fidelity of terrestrial paleoclimate records. *Science Advances*, *3*(9), 1–11. https://doi.org/10.1126/sciadv.1700683

Forzoni, A., Storms, J. E. A., Whittaker, A. C., & de Jager, G. (2014). Delayed delivery from the sediment factory: Modeling the impact of catchment response time to tectonics on sediment flux and fluvio-deltaic stratigraphy. *Earth Surface Processes and Landforms*. https://doi.org/10.1002/esp.3538

Frette, V., Christensen, K., Malthe-Sørenssen, A., Feder, J., Jøssang, T., & Meakin, P. (1996). Avalanche dynamics in a pile of rice. *Nature*. https://doi.org/10.1038/379049a0

Fryirs, K. A., Brierley, G. J., Preston, N. J., & Kasai, M. (2007). Buffers, barriers and blankets: The (dis)connectivity of catchment-scale sediment cascades. *Catena*. https://doi.org/10.1016/j.catena.2006.07.007

Gagen, M., Battipaglia, G., Daux, V., Duffy, J., Dorado-Liñán, I., Hayles, L. A., et al. (2022). Climate Signals in Stable Isotope Tree-Ring Records. https://doi.org/10.1007/978-3-030-92698-4_19

Gammaitoni, L., Hänggi, P., Jung, P., & Marchesoni, F. (1998). Stochastic resonance. *Reviews of Modern Physics*. https://doi.org/10.1103/revmodphys.70.223

Ganopolski, A., & Rahmstorf, S. (2002). Abrupt Glacial Climate Changes due to Stochastic Resonance. *Physical Review Letters*, *88*(3), 4. https://doi.org/10.1103/PhysRevLett.88.038501

Ganti, V., Straub, K. M., Foufoula-Georgiou, E., & Paola, C. (2011). Space-time dynamics of depositional systems: Experimental evidence and theoretical modeling of heavy-tailed statistics. *Journal of Geophysical Research: Earth Surface*. https://doi.org/10.1029/2010JF001893

Ganti, V., Paola, C., & Foufoula-Georgiou, E. (2013). Kinematic controls on the geometry of the preserved cross sets. *Journal of Geophysical Research: Earth Surface*, *118*(3). https://doi.org/10.1002/jgrf.20094

Ganti, V., Lamb, M. P., & McElroy, B. (2014). Quantitative bounds on morphodynamics and implications for reading the sedimentary record. *Nature Communications*. https://doi.org/10.1038/ncomms4298

Ganti, V., Chadwick, A. J., Hassenruck-Gudipati, H. J., & Lamb, M. P. (2016). Avulsion cycles and their stratigraphic signature on an experimental backwater-controlled delta. *Journal of Geophysical Research: Earth Surface, 121*(9). https://doi.org/10.1002/2016JF003915

Ganti, V., Hajek, E. A., Leary, K., Straub, K. M., & Paola, C. (2020). Morphodynamic Hierarchy and the Fabric of the Sedimentary Record. *Geophysical Research Letters*, *47*(14). https://doi.org/10.1029/2020GL087921

Gardner, J., Pavelsky, T., Topp, S., Yang, X., Ross, M. R. V., & Cohen, S. (2023). Human activities change suspended sediment concentration along rivers. *Environmental Research Letters*. https://doi.org/10.1088/1748-9326/acd8d8

Garg, R. (2013). Documentation of open-source MFIX–DEM software for gas-solids flow. *Géotechnique*.

Garg, R., Galvin, J., Li, T., & Pannala, S. (2012). Open-source MFIX-DEM software for gas-solids flows: Part I-Verification studies. *Powder Technology*, *220*. https://doi.org/10.1016/j.powtec.2011.09.019

Gilman, D. L., Fuglister, F. J., & Mitchell, J. M. (1963). On the Power Spectrum of "Red Noise." *Journal of the Atmospheric Sciences*. https://doi.org/10.1175/1520-0469(1963)020<0182:otpson>2.0.co;2

Giri, S., Arbab, N. N., & Lathrop, R. G. (2019). Assessing the potential impacts of climate and land use change on water fluxes and sediment transport in a loosely coupled system. *Journal of Hydrology*. https://doi.org/10.1016/j.jhydrol.2019.123955

Glade, R. C., Shobe, C. M., Anderson, R. S., & Tucker, G. E. (2019). Canyon shape and erosion dynamics governed by channel-hillslope feedbacks. *Geology*, *47*(7), 650-654..

Godano, C., Alonzo, M. L., & Caruso, V. (1993). Self-organized criticality and earthquake predictability. *Physics of the Earth and Planetary Interiors*. https://doi.org/10.1016/0031-9201(93)90042-8

Godard, V., Tucker, G. E., Burch Fisher, G., Burbank, D. W., & Bookhagen, B. (2013). Frequency-dependent landscape response to climatic forcing. *Geophysical Research Letters*. https://doi.org/10.1002/grl.50253

Goehring, B. M., Brown, N., Moon, S., & Blisniuk, K. (2021). The Transport History of Alluvial Fan Sediment Inferred From Multiple Geochronometers. *Journal of Geophysical Research: Earth Surface*, *126*(9), 1–17. https://doi.org/10.1029/2021JF006096

Goldstein, Evan B., A. Brad Murray, and Giovanni Coco. "Sorted bedform pattern evolution: Persistence, destruction and self-organized intermittency." *Geophysical Research Letters* 38.24 (2011). https://doi.org/10.1029/2011GL049732

Gollin, D., Bowman, E., & Shepley, P. (2015). Granular temperature field of monodisperse granular flows. *Deformation Characteristics of Geomaterials*, *17*(July 2017), 6652.

Gomez, B., Carter, L., & Trustrum, N. A. (2007). A 2400 yr record of natural events and anthropogenic impacts in intercorrelated terrestrial and marine sediment cores: Waipaoa sedimentary system, New Zealand. *Bulletin of the Geological Society of America*, *119*(11–12), 1415–1432. https://doi.org/10.1130/B25996.1

Gopalakrishnan, P., & Tafti, D. (2013). Development of parallel DEM for the open source code MFIX. *Powder Technology*, *235*. https://doi.org/10.1016/j.powtec.2012.09.006

Gorchakov, G. I., Karpov, A. V., Kopeikin, V. M., Zlobin, I. A., Buntov, D. V., & Sokolov, A. V. (2013). Study of the dynamics of saltating sand grains over desertified territories. *Doklady Earth Sciences*, *452*(2), 1067–1073.

https://doi.org/10.1134/S1028334X1309002X

Grant, G.E., 2012. The geomorphic response of gravel-bed rivers to dams: perspectives and prospects. *Gravel-bed Rivers: Processes, tools, environments*, pp.165-181.

Greenberg, E., & Ganti, V. (2024). The pace of global river meandering influenced by fluvial sediment supply. *Earth and Planetary Science Letters*, *634*, 118674.

Griffin, C., Duller, R. A., & Straub, K. M. (2023). The degradation and detection of environmental signals in sediment transport systems. *Science Advances*, *9*(44), 1–11. https://doi.org/10.1126/sciadv.adi8046

Grima, A. P., & Wypych, P. W. (2011). Investigation into calibration of discrete element model parameters for scale-up and validation of particle-structure interactions under impact conditions. *Powder Technology*, *212*(1), 198–209. https://doi.org/10.1016/j.powtec.2011.05.017

Grimaud, J. L., Paola, C., & Voller, V. (2016). Experimental migration of knickpoints: Influence of style of base-level fall and bed lithology. *Earth Surface Dynamics*, *4*(1), 11–23. https://doi.org/10.5194/esurf-4-11-2016

Grove, M., Timbrell, L., Jolley, B., Polack, F., & Borg, J. M. (2022). The Importance of Noise Colour in Simulations of Evolutionary Systems. *Artificial Life*, *27*. https://doi.org/10.1162/artl_a_00354

Grumbacher, S. K., McEwen, K. M., Halverson, D. A., Jacobs, D. T., & Lindner, J. (1993). Self-organized criticality: An experiment with sandpiles. *American Journal of Physics*, *61*(4), 329–335. https://doi.org/10.1119/1.17264

Guo, L., Ye, J. J., & Zhang, J. (2023). Sensitivity Analysis of the Maximal Value Function with Applications in Nonconvex Minimax Programs. *Mathematics of Operations Research*, 1–35. https://doi.org/10.1287/moor.2023.1366

De Haas, T., Van Den Berg, W., Braat, L., & Kleinhans, M. G. (2016). Autogenic avulsion, channelization and backfilling dynamics of debris-flow fans. *Sedimentology*. https://doi.org/10.1111/sed.12275

Ewing, Ryan C., Gary Kocurek, and Larry W. Lake. "Pattern analysis of dune-field parameters." *Earth Surface Processes and Landforms: The Journal of the British Geomorphological Research Group* 31.9 (2006): 1176-1191.

Hajek, E. A., & Straub, K. M. (2017). Autogenic Sedimentation in Clastic Stratigraphy. *Annual Review of Earth and Planetary Sciences*, *45*, 681–709. https://doi.org/10.1146/annurev-earth-063016-015935

Hajek, E. A., Heller, P. L., & Sheets, B. A. (2010). Significance of channel-belt clustering in alluvial basins. *Geology*, *38*(6), 535–538. https://doi.org/10.1130/G30783.1

Hajek, E. A., Heller, P. L., & Schur, E. L. (2012). Field test of autogenic control on alluvial stratigraphy (Ferris Formation, Upper Cretaceous-Paleogene, Wyoming). *Bulletin of the Geological Society of America*, *124*(11–12). https://doi.org/10.1130/B30526.1

Han, Z., Liu, D., & Hovan, S. A. (2002). Lightness timescale for terrestrial sediments in the past 500,000 years. *Paleoceanography*, *17*(3), 20-1-20–7. https://doi.org/10.1029/2001PA000731

Hänggi, P. (2002). Stochastic resonance in biology: How noise can enhance detection of weak signals and help improve biological information processing. *ChemPhysChem*. https://doi.org/10.1002/1439-7641(20020315)3:3<285::AID-CPHC285>3.0.CO;2-A

Hao, Y., Zhang, J., Wang, J., Li, R., Hao, P., & Zhan, H. (2016). How does the anthropogenic activity affect the spring discharge? *Journal of Hydrology*, *540*, 1053–1065. https://doi.org/10.1016/j.jhydrol.2016.07.024

Harries, R. M., Kirstein, L. A., Whittaker, A. C., Attal, M., & Main, I. (2019). Impact of recycling and lateral sediment input on grain size fining trends—Implications for reconstructing tectonic and climate forcings in ancient sedimentary systems. *Basin Research*. https://doi.org/10.1111/bre.12349

Hasbargen, L. E., & Paola, C. (2000). Landscape instability in an experimental drainage basin. *Geology*. https://doi.org/10.1130/0091-7613(2000)028<1067:LIIAED>2.3.CO;2

Hassan, M. A., Smith, B. J., Hogan, D. L., Luzi, D. S., Zimmermann, A. E., & Eaton, B. C. (2007). 18 Sediment storage and transport in coarse bed streams: scale considerations. *Developments in Earth Surface Processes*. https://doi.org/10.1016/S0928-2025(07)11137-8

Hasselmann, K. (1976). Stochastic climate models: Part I. Theory. *Tellus A: Dynamic Meteorology and Oceanography*. https://doi.org/10.3402/tellusa.v28i6.11316

Hecht, H., & Oguchi, T. (2017). Global evaluation of erosion rates in relation to tectonics. *Progress in Earth and Planetary Science*. https://doi.org/10.1186/s40645-017-0156-3

Hentschke, U., & Milkert, D. (1996). Power spectrum analyses of storm layers in marine silty sediments: A tool for a paleoclimatic reconstruction? *Journal of Coastal Research*, *12*(4).

Hessler, A. M., & Fildani, A. (2019). Deep-sea fans: Tapping into Earth's changing landscapes. *Journal of Sedimentary Research*. https://doi.org/10.2110/jsr.2019.64

Higham, J. E., Shepley, P., & Shahnam, M. (2019). Measuring the coefficient of restitution for all six degrees of freedom. *Granular Matter*. https://doi.org/10.1007/s10035-019-0871-0

Hilgen, F. J., Hinnov, L. A., Abdul Aziz, H., Abels, H. A., Batenburg, S., Bosmans, J. H. C., et al. (2015). Stratigraphic continuity and fragmentary sedimentation: The success of cyclostratigraphy as part of integrated stratigraphy. *Geological Society Special Publication*, *404*. https://doi.org/10.1144/SP404.12

Hirabayashi, Y., Alifu, H., Yamazaki, D., Imada, Y., Shiogama, H., & Kimura, Y. (2021). Anthropogenic climate change has changed frequency of past flood during 2010-2013. *Progress in Earth and Planetary Science*, *8*(1). https://doi.org/10.1186/s40645-021-00431-w

Hoey, T. B., & Sutherland, A. J. (1991). Channel morphology and bedload pulses in braided rivers: a laboratory study. *Earth Surface Processes and Landforms*, *16*(5), 447–462.

https://doi.org/10.1002/esp.3290160506

Hoffmann, T. (2015). Sediment residence time and connectivity in non-equilibrium and transient geomorphic systems. *Earth-Science Reviews*. https://doi.org/10.1016/j.earscirev.2015.07.008

Hofstra, N., Haylock, M., New, M., Jones, P., & Frei, C. (2008). Comparison of six methods for the interpolation of daily, European climate data. *Journal of Geophysical Research Atmospheres*, *113*(21). https://doi.org/10.1029/2008JD010100

Hooke, J. M. (2007). Complexity, self-organisation and variation in behaviour in meandering rivers. *Geomorphology*. https://doi.org/10.1016/j.geomorph.2007.04.021

Hooke, R. L. (2000). On the history of human as geomorphic agents. *Geology*, *28*(9), 843–846. https://doi.org/10.1130/0091-7613(2000)028<0843:OTHOHA>2.3.CO;2

Hovius, N. (1996). Regular spacing of drainage outlets from linear mountain belts. *Basin Research*. https://doi.org/10.1111/j.1365-2117.1996.tb00113.x

Hoyal, D. C. J. D., & Sheets, B. A. (2009). Morphodynamic evolution of experimental cohesive deltas. *Journal of Geophysical Research: Earth Surface*, *114*(2), 1–18. https://doi.org/10.1029/2007JF000882

Hu, B., Yang, Z., Wang, H., Sun, X., Bi, N., & Li, G. (2009). Sedimentation in the Three Gorges Dam and the future trend of Changjiang (Yangtze River) sediment flux to the sea. *Hydrology and Earth System Sciences*. https://doi.org/10.5194/hess-13-2253-2009

Husson, D., Thibault, N., Galbrun, B., Gardin, S., Minoletti, F., Sageman, B., & Huret, E. (2014). Lower Maastrichtian cyclostratigraphy of the Bidart section (Basque Country, SW France): A remarkable record of precessional forcing. *Palaeogeography, Palaeoclimatology, Palaeoecology*. https://doi.org/10.1016/j.palaeo.2013.12.008

Hutton, J. (1788). Theory of the Earth; or an investigation of the laws observable in the composition, dissolution, and restoration of land upon the globe. *Earth and Environmental Science Transactions of the Royal Society of Edinburgh*, *1*(1), 209–304.

Hwa, T., & Kardar, M. (1992). Avalanches, hydrodynamics, and discharge events in models of sandpiles. *Physical Review A*. https://doi.org/10.1103/PhysRevA.45.7002

Ibáñez, C., Alcaraz, C., Caiola, N., Prado, P., Trobajo, R., Benito, X., et al. (2019). Basin-scale land use impacts on world deltas: Human vs natural forcings. *Global and Planetary Change*, *173*(December 2018), 24–32. https://doi.org/10.1016/j.gloplacha.2018.12.003

J. Hein, C., & D. Ashton, A. (2020). *Long-term shoreline morphodynamics: Processes and preservation of environmental signals*. *Sandy Beach Morphodynamics*. Elsevier Ltd. https://doi.org/10.1016/B978-0-08-102927-5.00021-7

Jerolmack, D. J. (2009). Conceptual framework for assessing the response of delta channel networks to Holocene sea level rise. *Quaternary Science Reviews*, *28*(17–18). https://doi.org/10.1016/j.quascirev.2009.02.015

Jerolmack, D. J. (2011). Causes and effects of noise in landscape dynamics. *Eos*.

https://doi.org/10.1029/2011EO440001

Jerolmack, D. J., & Mohrig, D. (2005). A unified model for subaqueous bed form dynamics. *Water Resources Research*, *41*(12). https://doi.org/10.1029/2005WR004329

Jerolmack, D. J., & Mohrig, D. (2007). Conditions for branching in depositional rives. *Geology*, *35*(5), 463–466. https://doi.org/10.1130/G23308A.1

Jerolmack, D. J., & Paola, C. (2007). Complexity in a cellular model of river avulsion. *Geomorphology*. https://doi.org/10.1016/j.geomorph.2007.04.022

Jerolmack, D. J., & Paola, C. (2010). Shredding of environmental signals by sediment transport. *Geophysical Research Letters*, *37*(19), 1–5. https://doi.org/10.1029/2010GL044638

Jerolmack, D. J., & Sadler, P. (2007). Transience and persistence in the depositional record of continental margins. *Journal of Geophysical Research: Earth Surface*. https://doi.org/10.1029/2006JF000555

Jiménez-Moreno, G., Rodríguez-Tovar, F. J., Pardo-Igúzquiza, E., Fauquette, S., Suc, J. P., & Müller, P. (2005). High-resolution palynological analysis in late early-middle Miocene core from the Pannonian Basin, Hungary: Climatic changes, astronomical forcing and eustatic fluctuations in the Central Paratethys. *Palaeogeography, Palaeoclimatology, Palaeoecology*, *216*(1–2), 73–97. https://doi.org/10.1016/j.palaeo.2004.10.007

Jones, R. T., Reinhardt, L. J., Dearing, J. A., Crook, D., Chiverrell, R. C., Welsh, K. E., & Vergès, E. (2013). Detecting climatic signals in an anthropogenically disturbed catchment: The late-Holocene record from the Petit Lac d'Annecy, French Alps. *Holocene*, *23*(9), 1329–1339. https://doi.org/10.1177/0959683613486940

Kačianauskas, R., Kruggel-Emden, H., Markauskas, D., & Zdancevičius, E. (2015). Critical assessment of visco-elastic damping models used in DEM simulations. *Procedia Engineering*, *102*, 1415–1425. https://doi.org/10.1016/j.proeng.2015.01.274

Kao, S. J., Hilton, R. G., Selvaraj, K., Dai, M., Zehetner, F., Huang, J. C., et al. (2014). Preservation of terrestrial organic carbon in marine sediments offshore Taiwan: Mountain building and atmospheric carbon dioxide sequestration. *Earth Surface Dynamics*, *2*(1), 127–139. https://doi.org/10.5194/esurf-2-127-2014

Kasper, J. H., Magnanimo, V., de Jong, S. D. M., Beek, A., & Jarray, A. (2021). Effect of viscosity on the avalanche dynamics and flow transition of wet granular matter. *Particuology*, *59*, 64–75. https://doi.org/10.1016/j.partic.2020.12.001

Katterfeld, A., Coetzee, C., Donohue, T., Fottner, J., Grima, A., Ramirez Gomez, A., et al. (2019). Calibration of DEM Parameters for Cohesionless Bulk Materials under Rapid Flow Conditions and Low Consolidation, (July). https://doi.org/DOI: 10.13140/RG.2.2.26318.31048/1

Kemp, D. B. (2012). Stochastic and deterministic controls on stratigraphic completeness and fidelity. *International Journal of Earth Sciences*, *101*(8), 2225–2238. https://doi.org/10.1007/s00531-012-0784-1

Kemp, D. B. (2016). Optimizing significance testing of astronomical forcing in cyclostratigraphy. *Paleoceanography*, *31*(12). https://doi.org/10.1002/2016PA002963

Kemp, D. B., & Sexton, P. F. (2014). Time-scale uncertainty of abrupt events in the geologic record arising from unsteady sedimentation. *Geology*, *42*(10), 891–894. https://doi.org/10.1130/G35783.1

Kim, W., & Jerolmack, D. J. (2008). The pulse of calm fan deltas. *Journal of Geology*, *116*(4), 315–330. https://doi.org/10.1086/588830

Kim, W., & Paola, C. (2007). Long-period cyclic sedimentation with constant tectonic forcing in an experimental relay ramp. *Geology*. https://doi.org/10.1130/G23194A.1

Kirby, E., & Whipple, K. X. (2012). Expression of active tectonics in erosional landscapes. *Journal of Structural Geology*, *44*, 54–75. https://doi.org/10.1016/j.jsg.2012.07.009

Kleinhans, M. G., & van Rijn, L. C. (2002). Stochastic Prediction of Sediment Transport in Sand-Gravel Bed Rivers. *Journal of Hydraulic Engineering*, *128*(4), 412–425. https://doi.org/10.1061/(asce)0733-9429(2002)128:4(412)

Knight, J., & Harrison, S. (2013). The impacts of climate change on terrestrial Earth surface systems. *Nature Climate Change*. https://doi.org/10.1038/nclimate1660

Korup, O., Densmore, A. L., & Schlunegger, F. (2010). The role of landslides in mountain range evolution. *Geomorphology*, *120*(1–2). https://doi.org/10.1016/j.geomorph.2009.09.017

Kraus, M. J., & Aslan, A. (1995). Palaeosol Sequences in Floodplain Environments: A Hierarchical Approach. In *Palaeoweathering, Palaeosurfaces and Related Continental Deposits*. https://doi.org/10.1002/9781444304190.ch12

Kurokawa, S., Tada, R., Matsuzaki, K. M., Irino, T., & Johanna, L. (2019). Cyclostratigraphy of the Late Miocene to Pliocene sediments at IODP sites U1425 and U1430 in the Japan Sea and paleoceanographic implications. *Progress in Earth and Planetary Science*, *6*(1), 1–20. https://doi.org/10.1186/s40645-018-0250-1

Kutnjak-Urbanc, B., Havlin, S., & Stanley, H. E. (1996). Temporal correlations in a one-dimensional sandpile model. *Physical Review E - Statistical Physics, Plasmas, Fluids, and Related Interdisciplinary Topics*, *54*(6). https://doi.org/10.1103/PhysRevE.54.6109

Kwang, J. S., & Parker, G. (2019). Extreme Memory of Initial Conditions in Numerical Landscape Evolution Models. *Geophysical Research Letters*. https://doi.org/10.1029/2019GL083305

Lai, J., Wang, G., Wang, S., Cao, J., Li, M., Pang, X., et al. (2018). Review of diagenetic facies in tight sandstones: Diagenesis, diagenetic minerals, and prediction via well logs. *Earth-Science Reviews*. https://doi.org/10.1016/j.earscirev.2018.06.009

Lambert, C.P. and Walling, D.E., 1988. Measurement of channel storage of suspended sediment in a gravel-bed river. *Catena*, *15*(1), pp.65-80. https://doi.org/10.1016/0341-8162(88)90017-3

Lane, S. N., Bakker, M., Costa, A., Girardclos, S., Loizeau, J. L., Molnar, P., et al. (2019). Making stratigraphy in the Anthropocene: climate change impacts and economic conditions controlling the supply of sediment to Lake Geneva. *Scientific Reports*. https://doi.org/10.1038/s41598-019-44914-9

Lauer, J. W., & Parker, G. (2008). Modeling framework for sediment deposition, storage, and evacuation in the floodplain of a meandering river: Application to the Clark Fork River, Montana. *Water Resources Research*. https://doi.org/10.1029/2006WR005529

Lazarus, E. D., Harley, M. D., Blenkinsopp, C. E., & Turner, I. L. (2019). Environmental signal shredding on sandy coastlines. *Earth Surface Dynamics*. https://doi.org/10.5194/esurf-7-77-2019

Leary, K. C. P., & Ganti, V. (2020). Preserved Fluvial Cross Strata Record Bedform Disequilibrium Dynamics. *Geophysical Research Letters*, *47*(2). https://doi.org/10.1029/2019GL085910

Leng, M. J., & Marshall, J. D. (2004). Palaeoclimate interpretation of stable isotope data from lake sediment archives. In *Quaternary Science Reviews*. https://doi.org/10.1016/j.quascirev.2003.06.012

Li, J., Ganti, V., Li, C., & Wei, H. (2022). Upstream migration of avulsion sites on lowland deltas with river-mouth retreat. *Earth and Planetary Science Letters*. https://doi.org/10.1016/j.epsl.2021.117270

Li, Q., Yu, L., & Straub, K. M. (2016). Storage thresholds for relative sea-level signals in the stratigraphic record. *Geology*, *44*(3), 179–182. https://doi.org/10.1130/G37484.1

Li, Q., Matthew Benson, W., Harlan, M., Robichaux, P., Sha, X., Xu, K., & Straub, K. M. (2017). Influence of Sediment Cohesion on Deltaic Morphodynamics and Stratigraphy Over Basin-Filling Time Scales. *Journal of Geophysical Research: Earth Surface*. https://doi.org/10.1002/2017JF004216

Li, Q., Gasparini, N. M., & Straub, K. M. (2018). Some signals are not the same as they appear: How do erosional landscapes transform tectonic history into sediment flux records? *Geology*. https://doi.org/10.1130/G40026.1

Li, T., Garg, R., Galvin, J., & Pannala, S. (2012). Open-source MFIX-DEM software for gas-solids flows: Part II - Validation studies. *Powder Technology*, *220*. https://doi.org/10.1016/j.powtec.2011.09.020

Li, Y., Xu, Y., & Thornton, C. (2005). A comparison of discrete element simulations and experiments for "sandpiles" composed of spherical particles. *Powder Technology*, *160*(3). https://doi.org/10.1016/j.powtec.2005.09.002

Limaye, A. B. S., & Lamb, M. P. (2014). Numerical Simulations of bedrock valley evolution by meandering rivers with variable bank material. *Journal of Geophysical Research: Earth Surface*. https://doi.org/10.1002/2013JF002997

Liu, G., Zhang, R., He, X., Wei, R., Zhu, R., Tang, Y., et al. (2023). Cyclostratigraphy and high-frequency sedimentary cycle framework for the Late Paleozoic Fengcheng Formation, Junggar Basin. *Frontiers in Earth Science*, *11*(May), 1–13.

https://doi.org/10.3389/feart.2023.1206835

Lu, L., Gao, X., Dietiker, J. F., Shahnam, M., & Rogers, W. A. (2022). MFiX based multi-scale CFD simulations of biomass fast pyrolysis: A review. *Chemical Engineering Science*. https://doi.org/10.1016/j.ces.2021.117131

Luzi, D., Hassan, M. A., Papangelakis, E., & Eaton, B. (2021). Cycles of aggradation and degradation in gravel-bed rivers mediated by sediment storage and morphologic evolution. *Geomorphology*. https://doi.org/10.1016/j.geomorph.2021.108001

Ma, C., Yang, J., Zenz, G., Staudacher, E. J., & Cheng, L. (2020). Calibration of the microparameters of the discrete element method using a relevance vector machine and its application to rockfill materials. *Advances in Engineering Software*. https://doi.org/10.1016/j.advengsoft.2020.102833

Madrid, M. A., Fuentes, J. M., Ayuga, F., & Gallego, E. (2022). Determination of the Angle of Repose and Coefficient of Rolling Friction for Wood Pellets. *Agronomy*, *12*(2). https://doi.org/10.3390/agronomy12020424

Mahon, R. C., Shaw, J. B., Barnhart, K. R., Hobley, D. E. J., & McElroy, B. (2015). Quantifying the stratigraphic completeness of delta shoreline trajectories. *Journal of Geophysical Research: Earth Surface*. https://doi.org/10.1002/2014JF003298

Malatesta, L. C., Prancevic, J. P., & Avouac, J. P. (2017). Autogenic entrenchment patterns and terraces due to coupling with lateral erosion in incising alluvial channels. *Journal of Geophysical Research: Earth Surface*. https://doi.org/10.1002/2015JF003797

Malthe-Sørenssen, A., Feder, J., Christensen, K., Frette, V., & Jøssang, T. (1999). Surface fluctuations and correlations in a pile of rice. *Physical Review Letters*. https://doi.org/10.1103/PhysRevLett.83.764

Malthe-Sørenssen, A., Feder, J., Christensen, K., Frette, V., & Jøssang, T. (2001). Structure and Dynamics of the Surface in a Pile of Rice, 1–35.

Mancini, D., Dietze, M., Müller, T., Jenkin, M., Miesen, F., Roncoroni, M., et al. (2023). Filtering of the Signal of Sediment Export From a Glacier by Its Proglacial Forefield. *Geophysical Research Letters*, *50*(21), 1–12. https://doi.org/10.1029/2023GL106082

Mann, M. E., & Lees, J. M. (1996). Robust estimation of background noise and signal detection in climatic time series. *Climatic Change*, *33*(3). https://doi.org/10.1007/BF00142586

Manna, S. S. (1999). Sandpile models of self-organized criticality. *Current Science*, *77*(3), 388–393.

Marchelli, F., & Di Felice, R. (2021). A comparison of ansys fluent and mfix in performing cfd-dem simulations of a spouted bed. *Fluids*. https://doi.org/10.3390/fluids6110382

Marigo, M., & Stitt, E. H. (2015). Discrete element method (DEM) for industrial applications: Comments on calibration and validation for the modelling of cylindrical pellets. *KONA Powder and Particle Journal*. https://doi.org/10.14356/kona.2015016

Martínez-Graña, A. M., Boski, T., Goy, J. L., Zazo, C., & Dabrio, C. J. (2016). Coastal-flood risk management in central Algarve: Vulnerability and flood risk indices (South Portugal). *Ecological Indicators*, *71*, 302–316. https://doi.org/10.1016/j.ecolind.2016.07.021

Masson-Delmotte, V., Dreyfus, G., Braconnot, P., Johnsen, S., Jouzel, J., Kageyama, M., et al. (2006). Past temperature reconstructions from deep ice cores: Relevance for future climate change. *Climate of the Past*. https://doi.org/10.5194/cp-2-145-2006

McElroy, B., & Mohrig, D. (2009). Nature of deformation of sandy bed forms. *Journal of Geophysical Research: Earth Surface*, *114*(F3). https://doi.org/10.1029/2008JF001220

McHardy, I. M., Papadakis, I. E., Uttley, P., Page, M. J., & Mason, K. O. (2004). Combined long and short time-scale X-ray variability of NGC 4051 with RXTE and XMM-Newton. *Monthly Notices of the Royal Astronomical Society*, *348*(3). https://doi.org/10.1111/j.1365-2966.2004.07376.x

McInerney, F. A., & Wing, S. L. (2011). The paleocene-eocene thermal maximum: A perturbation of carbon cycle, climate, and biosphere with implications for the future. *Annual Review of Earth and Planetary Sciences*, *39*, 489–516. https://doi.org/10.1146/annurev-earth-040610-133431

McKean, J., & Roering, J. (2004). Objective landslide detection and surface morphology mapping using high-resolution airborne laser altimetry. *Geomorphology*, *57*(3–4), 331–351. https://doi.org/10.1016/S0169-555X(03)00164-8

McNab, F., Schildgen, T. F., Turowski, J. M., & Wickert, A. D. (2023). Diverse Responses of Alluvial Rivers to Periodic Environmental Change. *Geophysical Research Letters*, *50*(10), 1–12. https://doi.org/10.1029/2023GL103075

Medwedeff, W. G., Clark, M. K., Zekkos, D., & West, A. J. (2020). Characteristic landslide distributions: An investigation of landscape controls on landslide size. *Earth and Planetary Science Letters*. https://doi.org/10.1016/j.epsl.2020.116203

Merritts, D. J., Vincent, K. R., & Wohl, E. E. (1994). Long river profiles, tectonism, and eustasy: a guide to interpreting fluvial terraces. *Journal of Geophysical Research*. https://doi.org/10.1029/94jb00857

Métivier, F. (1999). Diffusivelike buffering and saturation of large rivers. *Physical Review E - Statistical Physics, Plasmas, Fluids, and Related Interdisciplinary Topics*. https://doi.org/10.1103/PhysRevE.60.5827

Métivier, F., & Gaudemer, Y. (1999). Stability of output fluxes of large rivers in south and east Asia during the last 2 million years: Implications on floodplain processes. *Basin Research*. https://doi.org/10.1046/j.1365-2117.1999.00101.x

Meyer, P. G., & Kantz, H. (2019). Inferring characteristic timescales from the effect of autoregressive dynamics on detrended fluctuation analysis. *New Journal of Physics*, *21*(3). https://doi.org/10.1088/1367-2630/ab0a8a

Meyers, S. R. (2012). Seeing red in cyclic stratigraphy: Spectral noise estimation for astrochronology. *Paleoceanography*, *27*(3). https://doi.org/10.1029/2012PA002307

Meyers, S. R. (2019). Cyclostratigraphy and the problem of astrochronologic testing. *Earth-*

Science Reviews. https://doi.org/10.1016/j.earscirev.2018.11.015

Miall, A. D. (2015). Updating uniformitarianism: Stratigraphy as just a set of "frozen accidents." *Geological Society Special Publication*, *404*(2), 11–36. https://doi.org/10.1144/SP404.4

Mohrig, D., Heller, P. L., Paola, C., & Lyons, W. J. (2000). Interpreting avulsion process from ancient alluvial sequences: Guadalope-Matarranya system (Northern Spain) and Wasatch formation (Western Colorado). *Bulletin of the Geological Society of America*, *112*(12). https://doi.org/10.1130/0016-7606(2000)112<1787:IAPFAA>2.0.CO;2

Moragoda, N., & Cohen, S. (2020). Climate-induced trends in global riverine water discharge and suspended sediment dynamics in the 21st century. *Global and Planetary Change*, *191*(April), 103199. https://doi.org/10.1016/j.gloplacha.2020.103199

Morris, P. J., Baird, A. J., Young, D. M., & Swindles, G. T. (2015). Untangling climate signals from autogenic changes in long-term peatland development. *Geophysical Research Letters*, *42*(24). https://doi.org/10.1002/2015GL066824

Mouchené, M., Van Der Beek, P., Carretier, S., & Mouthereau, F. (2017). Autogenic versus allogenic controls on the evolution of a coupled fluvial megafan-mountainous catchment system: Numerical modelling and comparison with the Lannemezan megafan system (northern Pyrenees, France). *Earth Surface Dynamics*. https://doi.org/10.5194/esurf-5-125-2017

Müller, D., Fimbinger, E., & Brand, C. (2021). Algorithm for the determination of the angle of repose in bulk material analysis. *Powder Technology*, *383*, 598–605. https://doi.org/10.1016/j.powtec.2021.01.010

Murray, A. B. (2007). Reducing model complexity for explanation and prediction. *Geomorphology*. https://doi.org/10.1016/j.geomorph.2006.10.020

Murray, A. B., Coco, G., & Goldstein, E. B. (2014). Cause and effect in geomorphic systems: Complex systems perspectives. *Geomorphology*. https://doi.org/10.1016/j.geomorph.2014.03.001

Muto, T., & Steel, R. J. (2004). Autogenic response of fluvial deltas to steady sea-level fall: Implications from flume-tank experiments. *Geology*. https://doi.org/10.1130/G20269.1

Muto, T., Steel, R. J., & Swenson, J. B. (2007). Autostratigraphy: A Framework Norm for Genetic Stratigraphy. *Journal of Sedimentary Research*. https://doi.org/10.2110/jsr.2007.005

Neto, A. G., & Wriggers, P. (2022). Discrete element model for general polyhedra. *Computational Particle Mechanics*, *9*(2), 353–380. https://doi.org/10.1007/s40571-021-00415-z

Newton, R., & Bottrell, S. (2007). Stable isotopes of carbon and sulphur as indicators of environmental change: Past and present. *Journal of the Geological Society*. https://doi.org/10.1144/0016-76492006-101

Nicholas, A. P., & Quine, T. A. (2007). Modeling alluvial landform change in the absence of external environmental forcing. *Geology*. https://doi.org/10.1130/G23377A.1

Nicolis, C. (1993). Long-term climatic transitions and stochastic resonance. *Journal of Statistical Physics*. https://doi.org/10.1007/BF01053950

Overeem, I., Weltje, G. J., Bishop-Kay, C., & Kroonenberg, S. B. (2001). The Late Cenozoic Eridanos delta system in the Southern North Sea Basin: A climate signal in sediment supply? *Basin Research*, *13*(3), 293–312. https://doi.org/10.1046/j.1365-2117.2001.00151.x

Paguirigan, A. A., Monterola, C. P., & Batac, R. C. (2015). Loss of criticality in the avalanche statistics of sandpiles with dissipative sites. *Communications in Nonlinear Science and Numerical Simulation*, *20*(3), 785–793. https://doi.org/10.1016/j.cnsns.2014.06.020

Paola, C. (2000). Quantitative models of sedimentary basin filling. *Sedimentology*. https://doi.org/10.1046/j.1365-3091.2000.00006.x

Paola, C. (2016). A mind of their own: recent advances in autogenic dynamics in rivers and deltas. *Autogenic Dynamics and Self-Organization in Sedimentary Systems*. https://doi.org/10.2110/sepmsp.106.04

Paola, C., Heller, P. L., & Angevine, C. L. (1992). The large-scale dynamics of grain-size variation in alluvial basins, 1: Theory. *Basin Research*. https://doi.org/10.1111/j.1365-2117.1992.tb00145.x

Paola, C., Foufoula-Georgiou, E., Dietrich, W. E., Hondzo, M., Mohrig, D., Parker, G., Power, M. E., Rodriguez-Iturbe, I., Voller, V., & Wilcock, P. (2006). Toward a unified science of the Earth's surface: Opportunities for synthesis among hydrology, geomorphology, geochemistry, and ecology. *Water Resources Research*, 42, W03S10. https://doi.org/10.1029/2005WR004336

Paola, C., Straub, K., Mohrig, D., & Reinhardt, L. (2009). The “unreasonable effectiveness” of stratigraphic and geomorphic experiments. *Earth-Science Reviews*, *97*(4), 1–43. https://doi.org/10.1016/j.earscirev.2009.05.003

Paola, C., Ganti, V., Mohrig, D., Runkel, A. C., & Straub, K. M. (2018). Time Not Our Time: Physical Controls on the Preservation and Measurement of Geologic Time. *Annual Review of Earth and Planetary Sciences*. https://doi.org/10.1146/annurev-earth-082517-010129

Pas, D., Silva, Anne-Christine DaOver, J., Carlton, B., Brandt, L., Jin-Si, O., Hilgen, F. J., & Dekkers, M. J. (2020). Cyclostratigraphic Calibration of the Eifelian Stage (Middle Devonian, Appalachian Basin, Western New York, USA). *Bulletin of the Geological Society of America*, *133*(1), 277–286. https://doi.org/10.1130/B35589.1

Pelletier, J. D., Sherman, D. J., Ellis, J. T., Farrell, E. J., Jackson, N. L., Li, B., et al. (2015). Dynamics of sediment storage and release on aeolian dune slip faces: A field study in Jericoacoara, Brazil. *Journal of Geophysical Research: Earth Surface*. https://doi.org/10.1002/2015JF003636

Pemberton, J., & Priestley, M. B. (1990). Non-Linear and Non-Stationary Time Series Analysis. *Applied Statistics*, *39*(2). https://doi.org/10.2307/2347773

Petchey, O. L. (2000). Environmental colour affects aspects of single-species population dynamics. *Proceedings of the Royal Society B: Biological Sciences*, *267*(1445), 747–754. https://doi.org/10.1098/rspb.2000.1066

Phillips, C. B., & Jerolmack, D. J. (2016). Self-organization of river channels as a critical filter on climate signals. *Science*, *352*(6286). https://doi.org/10.1126/science.aad3348

Phillips, J. D. (1999). Divergence, convergence, and self-organization in landscapes. *Annals of the Association of American Geographers*, *89*(3), 466–488. https://doi.org/10.1111/0004-5608.00158

Pizzuto, J., Keeler, J., Skalak, K., & Karwan, D. (2017). Storage filters upland suspended sediment signals delivered from watersheds. *Geology*, *45*(2), 151–1654. Retrieved from https://pubs.geoscienceworld.org/gsa/geology/article/45/2/151/[XSLTDownloadPPT]

Powell, E. J., Kim, W., & Muto, T. (2012). Varying discharge controls on timescales of autogenic storage and release processes in fluvio-deltaic environments: Tank experiments. *Journal of Geophysical Research: Earth Surface*. https://doi.org/10.1029/2011JF002097

Pradhan, P. (2021). Time-Dependent Properties of Sandpiles. *Frontiers in Physics*. https://doi.org/10.3389/fphy.2021.641233

Qu, T., Wang, M., & Feng, Y. (2022). Applicability of discrete element method with spherical and clumped particles for constitutive study of granular materials. *Journal of Rock Mechanics and Geotechnical Engineering*. https://doi.org/10.1016/j.jrmge.2021.09.015

Quist, J., & Evertsson, M. (2015). Framework for DEM Model Calibration and Validation. *Proceedings of the 14th European Symposium on Comminution and Classification*, (September), 103–108.

Radhakanta, K., & Debashish, C. (2010). Discrete element approach for mine dump stability analysis. *Mining Science and Technology*, *20*(6), 809–813. https://doi.org/10.1016/S1674-5264(09)60286-6

Ramos-Vázquez, M. A., Armstrong-Altrin, J. S., Rosales-Hoz, L., Machain-Castillo, M. L., & Carranza-Edwards, A. (2017). Geochemistry of deep-sea sediments in two cores retrieved at the mouth of the Coatzacoalcos River delta, western Gulf of Mexico, Mexico. *Arabian Journal of Geosciences*, *10*(6). https://doi.org/10.1007/s12517-017-2934-z

Reitz, M. D., & Jerolmack, D. J. (2012). Experimental alluvial fan evolution: Channel dynamics, slope controls, and shoreline growth. *Journal of Geophysical Research: Earth Surface*. https://doi.org/10.1029/2011JF002261

Restrepo, J. D., Kettner, A. J., & Syvitski, J. P. M. (2015). Recent deforestation causes rapid increase in river sediment load in the Colombian Andes. *Anthropocene*. https://doi.org/10.1016/j.ancene.2015.09.001

Rhoads, B. L. (2020). Sediment Transport Dynamics in Rivers. In *River Dynamics*. https://doi.org/10.1017/9781108164108.005

Ritchie, A. C., Warrick, J. A., East, A. E., Magirl, C. S., Stevens, A. W., Bountry, J. A., et al. (2018). Morphodynamic evolution following sediment release from the world's largest dam removal. *Scientific Reports*. https://doi.org/10.1038/s41598-018-30817-8

Ritchie, B. D., Gawthorpe, R. L., & Hardy, S. (2004). Three-dimensional numerical modeling of deltaic depositional sequences 1: Influence of the rate and magnitude of sea-level change. *Journal of Sedimentary Research*. https://doi.org/10.1306/091303740203

Roering, J. J., Kirchner, J. W., Sklar, L. S., & Dietrich, W. E. (2001). Hillslope evolution b

Rodríguez-Iturbe, I., Rinaldo, A., Rigon, R., Bras, R.L., Marani, A. and Ijjász-Vásquez, E., 1992. Energy dissipation, runoff production, and the three-dimensional structure of river basins. *Water Resources Research*, *28*(4), pp.1095-1103.y nonlinear creep and landsliding: An experimental study. *Geology*, *29*(2), 143–146. https://doi.org/10.1130/0091-7613(2001)029<0143:HEBNCA>2.0.CO;2

Roessler, T., & Katterfeld, A. (2019). DEM parameter calibration of cohesive bulk materials using a simple angle of repose test. *Particuology*, *45*, 105–115. https://doi.org/10.1016/j.partic.2018.08.005

Rohais, S., Bonnet, S., & Eschard, R. (2012). Sedimentary record of tectonic and climatic erosional perturbations in an experimental coupled catchment-fan system. *Basin Research*. https://doi.org/10.1111/j.1365-2117.2011.00520.x

Romans, B. W., & Graham, S. A. (2013). A Deep-Time Perspective of Land-Ocean Linkages in the Sedimentary Record. *Annual Review of Marine Science*. https://doi.org/10.1146/annurev-marine-121211-172426

Romans, B. W., Castelltort, S., Covault, J. A., Fildani, A., & Walsh, J. P. (2016). Environmental signal propagation in sedimentary systems across timescales. *Earth-Science Reviews*. https://doi.org/10.1016/j.earscirev.2015.07.012

Rosa, E. A., Rudel, T. K., York, R., Jorgenson, A. K., & Dietz, T. (2015). The Human (Anthropogenic) Driving Forces of Global Climate Change. In *Climate Change and Society*. https://doi.org/10.1093/acprof:oso/9780199356102.003.0002

Rustomji, P., & Prosser, I. (2001). Spatial patterns of sediment delivery to valley floors: Sensitivity to sediment transport capacity and hillslope hydrology relations. *Hydrological Processes*. https://doi.org/10.1002/hyp.231

Sadler, P. M. (1981). Sediment accumulation rates and the completeness of stratigraphic sections. *Journal of Geology*. https://doi.org/10.1086/628623

Sadler, P. M., & Strauss, D. J. (1990). Estimation of completeness of stratigraphical sections using empirical data and theoretical models. *Journal - Geological Society (London)*. https://doi.org/10.1144/gsjgs.147.3.0471

Savi, S., Tofelde, S., Wickert, A. D., Bufe, A., Schildgen, T. F., & Strecker, M. R. (2020). Interactions between main channels and tributary alluvial fans: Channel adjustments and sediment-signal propagation. *Earth Surface Dynamics*, *8*(2). https://doi.org/10.5194/esurf-8-303-2020

Scheingross, J. S., Limaye, A. B., McCoy, S. W., & Whittaker, A. C. (2020). The shaping of erosional landscapes by internal dynamics. *Nature Reviews Earth and Environment*.

https://doi.org/10.1038/s43017-020-0096-0

Scheuring, I., & Zeöld, O. E. (2001). Data estimation and the colour of time series. *Journal of Theoretical Biology*, *213*(3), 427–434. https://doi.org/10.1006/jtbi.2001.2428

Schmidt, K. H. (2009). Hillslopes as evidence of climatic change. In *Geomorphology of Desert Environments*. https://doi.org/10.1007/978-1-4020-5719-9_22

Schneider, H., Schwab, M., & Schlunegger, F. (2008). Channelized and hillslope sediment transport and the geomorphology of mountain belts. *International Journal of Earth Sciences*, *97*(1), 179–192. https://doi.org/10.1007/s00531-006-0164-9

Schumer, R., & Jerolmack, D. J. (2009). Real and apparent changes in sediment deposition rates through time. *Journal of Geophysical Research: Solid Earth*, *114*(3). https://doi.org/10.1029/2009JF001266

Schumm, S. A. (1971). Fluvial geomorphology: the historical perspective. *River Mechanics*, *1*, 4–1.

Schumm, S. A. (1973). Geomorphic Thresholds and Complex Response. *Fluvial Geomorphology*.

Sharman, G. R., Sylvester, Z., & Covault, J. A. (2019). Conversion of tectonic and climatic forcings into records of sediment supply and provenance. *Scientific Reports*. https://doi.org/10.1038/s41598-019-39754-6

Sheets, B. A., Hickson, T. A., & Paola, C. (2002). Assembling the stratigraphic record: Depositional patterns and time-scales in an experimental alluvial basin. *Basin Research*. https://doi.org/10.1046/j.1365-2117.2002.00185.x

Sherriff, S. C., Rowan, J. S., Fenton, O., Jordan, P., & Ó hUallacháin, D. (2019). Influence of land management on soil erosion, connectivity, and sediment delivery in agricultural catchments: Closing the sediment budget. *Land Degradation and Development*, *30*(18), 2257–2271. https://doi.org/10.1002/ldr.3413

Shi, X., Beaulieu, C., Killick, R., & Lund, R. (2022). Changepoint Detection: An Analysis of the Central England Temperature Series. *Journal of Climate*, *35*(19), 2729–2742. https://doi.org/10.1175/JCLI-D-21-0489.1

Shojaeezadeh, S. A., Nikoo, M. R., McNamara, J. P., AghaKouchak, A., & Sadegh, M. (2018). Stochastic modeling of suspended sediment load in alluvial rivers. *Advances in Water Resources*. https://doi.org/10.1016/j.advwatres.2018.06.006

Siegmann, E., Enzinger, S., Toson, P., Doshi, P., Khinast, J., & Jajcevic, D. (2021). Massively speeding up DEM simulations of continuous processes using a DEM extrapolation. *Powder Technology*, *390*, 442–455. https://doi.org/10.1016/j.powtec.2021.05.067

Simons, D. ., & Senturk, F. (1992). *Sediment transport technology: water and sediment dynamics* (Second Edi). Littleton: Water Resources Publication.

Simons, T. A. H., Weiler, R., Strege, S., Bensmann, S., Schilling, M., & Kwade, A. (2015). A ring shear tester as calibration experiment for DEM simulations in agitated mixers - A sensitivity study. *Procedia Engineering*, *102*, 741–748. https://doi.org/10.1016/j.proeng.2015.01.178

Simpson, G., & Castelltort, S. (2012). Model shows that rivers transmit high-frequency climate cycles to the sedimentary record. *Geology*. https://doi.org/10.1130/G33451.1

Singh, A., Porté-Agel, F., & Foufoula-georgiou, E. (2010). On the influence of gravel bed dynamics on velocity power spectra. *Water Resources Research*, *46*(4), 1–10. https://doi.org/10.1029/2009WR008190

Slingerland, R. and Smith, N.D., 2004. River avulsions and their deposits. *Annu. Rev. Earth Planet. Sci.*, *32*, pp.257-285. https://doi.org/10.1146/annurev.earth.32.101802.120201

Smith, D. G. (2020). Misplaced confidence: limits to statistical inference in cyclostratigraphy. *Boletin Geologico y Minero*, *131*(2). https://doi.org/10.21701/BOLGEOMIN.131.2.005

Smith, D. G. (2023). The Orbital Cycle Factory: Sixty cyclostratigraphic spectra in need of re-evaluation. *Palaeogeography, Palaeoclimatology, Palaeoecology*. https://doi.org/10.1016/j.palaeo.2023.111744

Smith, D. G., Bailey, R. J., Burgess, P. M., & Fraser, A. J. (2015). Strata and time: Probing the gaps in our understanding. *Geological Society Special Publication*. https://doi.org/10.1144/SP404.16

Sommerfield, C. K. (2006). On sediment accumulation rates and stratigraphic completeness: Lessons from Holocene ocean margins. *Continental Shelf Research*, *26*(17–18), 2225–2240. https://doi.org/10.1016/j.csr.2006.07.015

Spohn, M., Aburto, F., Ehlers, T. A., Farwig, N., Frings, P. J., Hartmann, H., et al. (2021). Terrestrial ecosystems buffer inputs through storage and recycling of elements. *Biogeochemistry*. https://doi.org/10.1007/s10533-021-00848-x

Stark, C. P., & Hovius, N. (2001). The characterization of landslide size distributions. *Geophysical Research Letters*. https://doi.org/10.1029/2000GL008527

Stølum, H. H. (1996). River meandering as a self-organization process. *Science*, *271*(5256), 1710–1713. https://doi.org/10.1126/science.271.5256.1710

Stouthamer, E., & Berendsen, H. J. A. (2007). Avulsion: The relative roles of autogenic and allogenic processes. *Sedimentary Geology*. https://doi.org/10.1016/j.sedgeo.2007.01.017

Straub, K. M. (2019). Morphodynamics and stratigraphic architecture of shelf-edge deltas subject to constant vs. Dynamic environmental forcings: A laboratory study. *Frontiers in Earth Science*. https://doi.org/10.3389/feart.2019.00121

Straub, K. M., & Esposito, C. R. (2013). Influence of water and sediment supply on the stratigraphic record of alluvial fans and deltas: Process controls on stratigraphic completeness. *Journal of Geophysical Research: Earth Surface*. https://doi.org/10.1002/jgrf.20061

Straub, K. M., & Foreman, B. Z. (2018). Geomorphic stasis and spatiotemporal scales of stratigraphic completeness. *Geology*. https://doi.org/10.1130/G40045.1

Straub, K. M., & Wang, Y. (2013). Influence of water and sediment supply on the long-term evolution of alluvial fans and deltas: Statistical characterization of basin-filling sedimentation patterns. *Journal of Geophysical Research: Earth Surface*. https://doi.org/10.1002/jgrf.20095

Straub, K. M., Li, Q., & Benson, W. M. (2015). Influence of sediment cohesion on deltaic shoreline dynamics and bulk sediment retention: A laboratory study. *Geophysical Research Letters*, *42*(22). https://doi.org/10.1002/2015GL066131

Straub, K. M., Duller, R. A., Foreman, B. Z., & Hajek, E. A. (2020). Buffered, Incomplete, and Shredded: The Challenges of Reading an Imperfect Stratigraphic Record. *Journal of Geophysical Research: Earth Surface*, *125*(3), 1–44. https://doi.org/10.1029/2019JF005079

Strauss, D., & Sadler, P. M. (1989). Stochastic models for the completeness of stratigraphic sections. *Mathematical Geology*. https://doi.org/10.1007/BF00897239

Suehr, Q. J., Marks, B. P., Ryser, E. T., & Jeong, S. (2021). Modeling the Propagation of Salmonella within Bulk Almond Using Discrete Element Method Particle Simulation Technique. *Journal of Food Engineering*, *293*(August 2020), 110363. https://doi.org/10.1016/j.jfoodeng.2020.110363

Swanson, T., Mohrig, D., Kocurek, G., Cardenas, B. T., & Wolinsky, M. A. (2019). Preservation of autogenic processes and allogenic forcings in set-scale aeolian architecture I: Numerical experiments. *Journal of Sedimentary Research*, *89*(8). https://doi.org/10.2110/jsr.2019.42

Syvitski, J., Ángel, J. R., Saito, Y., Overeem, I., Vörösmarty, C. J., Wang, H., & Olago, D. (2022). Earth's sediment cycle during the Anthropocene. *Nature Reviews Earth and Environment*, *3*(3), 179–196. https://doi.org/10.1038/s43017-021-00253-w

Syvitski, J. P. M. (2003). Supply and flux of sediment along hydrological pathways: Research for the 21st century. *Global and Planetary Change*. https://doi.org/10.1016/S0921-8181(03)00008-0

Syvitski, J. P. M., & Kettner, A. (2011). Sediment flux and the anthropocene. *Philosophical Transactions of the Royal Society A: Mathematical, Physical and Engineering Sciences*. https://doi.org/10.1098/rsta.2010.0329

Tang, H., Song, R., Dong, Y., & Song, X. (2019). Measurement of restitution and friction coefficients for granular particles and discrete element simulation for the tests of glass beads. *Materials*, *12*(19). https://doi.org/10.3390/ma12193170

Taylor-Noonan, A. M., Gollin, D., Bowman, E. T., & Take, W. A. (2021). The influence of image analysis methodology on the calculation of granular temperature for granular flows. *Granular Matter*, *23*(4), 1–17. https://doi.org/10.1007/s10035-021-01153-y

Taylor Perron, J., & Huybers, P. (2009). Is there an orbital signal in the polar layered deposits on Mars? *Geology*, *37*(2). https://doi.org/10.1130/G25143A.1

Teng, T. Y., Huang, J. C., Lee, T. Y., Chen, Y. C., Jan, M. Y., & Liu, C. C. (2020). Investigating sediment dynamics in a landslide-dominated catchment by modeling landslide area and fluvial sediment export. *Water (Switzerland)*. https://doi.org/10.3390/w12102907

Thoms, M. C., Piégay, H., & Parsons, M. (2018). What do you mean, 'resilient geomorphic systems'? *Geomorphology*, *305*, 8–19. https://doi.org/10.1016/j.geomorph.2017.09.003

Thomson, D. J. (1982). Spectrum Estimation and Harmonic Analysis. *Proceedings of the IEEE*. https://doi.org/10.1109/PROC.1982.12433

Tilahun, A. K., Verstraeten, G., Chen, M., Gulie, G., Augustijns, F., & Swinnen, W. (2022). Late-Holocene Sediment Storage in Upland Valley Systems in the Gamo Highlands of Southern Ethiopia. *Quaternary*, *5*(4). https://doi.org/10.3390/quat5040046

Ting, J. M., Khwaja, M., Meachum, L. R., & Rowell, J. D. (1993). An ellipse-based discrete element model for granular materials. *International Journal for Numerical and Analytical Methods in Geomechanics*. https://doi.org/10.1002/nag.1610170902

Tipper, J. C. (2015). The importance of doing nothing: Stasis in sedimentation systems and its stratigraphic effects. *Geological Society Special Publication*. https://doi.org/10.1144/SP404.6

Tjiputra, J. F., Negrel, J., & Olsen, A. (2023). Early detection of anthropogenic climate change signals in the ocean interior. *Scientific Reports*. https://doi.org/10.1038/s41598-023-30159-0

Toby, S. C., Duller, R. A., De Angelis, S., & Straub, K. M. (2019). A Stratigraphic Framework for the Preservation and Shredding of Environmental Signals. *Geophysical Research Letters*, *46*(11), 5837–5845. https://doi.org/10.1029/2019GL082555

Toby, S. C., Duller, R. A., De Angelis, S., & Straub, K. M. (2022). Morphodynamic limits to environmental signal propagation across landscapes and into strata. *Nature Communications*, *13*(1). https://doi.org/10.1038/s41467-021-27776-6

Tofelde, S., Bernhardt, A., Guerit, L., & Romans, B. W. (2021). Times Associated With Source-to-Sink Propagation of Environmental Signals During Landscape Transience. *Frontiers in Earth Science*. https://doi.org/10.3389/feart.2021.628315

Trampush, S. M., & Hajek, E. A. (2017). Preserving proxy records in dynamic landscapes: Modeling and examples from the Paleocene-Eocene Thermal Maximum. *Geology*, *45*(11). https://doi.org/10.1130/G39367.1

Trampush, S. M., Hajek, E. A., Straub, K. M., & Chamberlin, E. P. (2017). Identifying autogenic sedimentation in fluvial-deltaic stratigraphy: Evaluating the effect of outcrop-quality data on the compensation statistic. *Journal of Geophysical Research: Earth Surface*. https://doi.org/10.1002/2016JF004067

Tresch, J., & Strasser, A. (2011). Allogenic and autogenic processes combined in the formation of shallow-water carbonate sequences (Middle Berriasian, Swiss and French Jura Mountains). *Swiss Journal of Geosciences*. https://doi.org/10.1007/s00015-011-0064-2

Tu, T., Comte, L., & Ruhi, A. (2023). The color of environmental noise in river networks. *Nature Communications*, *14*(1), 1728. https://doi.org/10.1038/s41467-023-37062-2

Utescher, T., Ivanov, D., Harzhauser, M., Bozukov, V., Ashraf, A. R., Rolf, C., et al. (2009). Cyclic climate and vegetation change in the late Miocene of Western Bulgaria. *Palaeogeography, Palaeoclimatology, Palaeoecology*, *272*(1–2), 99–114. https://doi.org/10.1016/j.palaeo.2008.11.014

VanderPlas, J. T. (2018). Understanding the Lomb–Scargle Periodogram. *The Astrophysical Journal Supplement Series*, *236*(1). https://doi.org/10.3847/1538-4365/aab766

Vaughan, S. (2010). A Bayesian test for periodic signals in red noise. *Monthly Notices of the Royal Astronomical Society*, *402*(1). https://doi.org/10.1111/j.1365-2966.2009.15868.x

Vaughan, S., Bailey, R. J., & Smith, D. G. (2011). Detecting cycles in stratigraphic data: Spectral analysis in the presence of red noise. *Paleoceanography*, *26*(4). https://doi.org/10.1029/2011PA002195

Vendettuoli, D., Clare, M. A., Hughes Clarke, J. E., Vellinga, A., Hizzet, J., Hage, S., et al. (2019). Daily bathymetric surveys document how stratigraphy is built and its extreme incompleteness in submarine channels. *Earth and Planetary Science Letters*, *515*. https://doi.org/10.1016/j.epsl.2019.03.033

Ventra, D., & Nichols, G. J. (2014). Autogenic dynamics of alluvial fans in endorheic basins: Outcrop examples and stratigraphic significance. *Sedimentology*. https://doi.org/10.1111/sed.12077

Vercruysse, K., Grabowski, R. C., & Rickson, R. J. (2017a). Suspended sediment transport dynamics in rivers: Multi-scale drivers of temporal variation. *Earth-Science Reviews*, *166*, 38–52. https://doi.org/10.1016/j.earscirev.2016.12.016

Vercruysse, K., Grabowski, R. C., & Rickson, R. J. (2017b). Suspended sediment transport dynamics in rivers: Multi-scale drivers of temporal variation. *Earth-Science Reviews*. https://doi.org/10.1016/j.earscirev.2016.12.016

Wang, J., Xu, C., Xu, Y., Wang, Z., Qi, X., Wang, J., et al. (2021). Influencing Factors Analysis and Simulation Calibration of Restitution Coefficient of Rice Grain. *Applied Sciences*, *11*(13), 5884. https://doi.org/10.3390/app11135884

Wang, Y., Straub, K. M., & Hajek, E. A. (2011). Scale-dependent compensational stacking: An estimate of autogenic time scales in channelized sedimentary deposits. *Geology*. https://doi.org/10.1130/G32068.1

Waters, C. N., Zalasiewicz, J., Summerhayes, C., Barnosky, A. D., Poirier, C., Gałuszka, A., et al. (2016). The Anthropocene is functionally and stratigraphically distinct from the Holocene. *Science*. https://doi.org/10.1126/science.aad2622

Watkins, S. E., Whittaker, A. C., Bell, R. E., McNeill, L. C., Gawthorpe, R. L., Brooke, S. A. S., & Nixon, C. W. (2018). Are landscapes buffered to high-frequency climate change? A comparison of sediment fluxes and depositional volumes in the Corinth Rift, central Greece, over the past 130 k.y. *Bulletin of the Geological Society of America*. https://doi.org/10.1130/B31953.1

Weedon, G. P. (2003). *Environmental cycles recorded stratigraphically*. *Time-Series Analysis and Cyclostratigraphy*. Cambridge University Press.

https://doi.org/10.1017/cbo9780511535482

Weedon, G. P., Page, K. N., & Jenkyns, H. C. (2019). Cyclostratigraphy, stratigraphic gaps and the duration of the Hettangian Stage (Jurassic): Insights from the Blue Lias Formation of southern Britain. *Geological Magazine*, *156*(9). https://doi.org/10.1017/S0016756818000808

Wellens, T., Shatokhin, V., & Buchleitner, A. (2004). Stochastic resonance. *Reports on Progress in Physics*. https://doi.org/10.1088/0034-4885/67/1/R02

Weltje, G. J., & von Eynatten, H. (2004, October 15). Quantitative provenance analysis of sediments: Review and outlook. *Sedimentary Geology*. Elsevier. https://doi.org/10.1016/j.sedgeo.2004.05.007

Wensrich, C. M., & Katterfeld, A. (2012). Rolling friction as a technique for modelling particle shape in DEM. *Powder Technology*. https://doi.org/10.1016/j.powtec.2011.10.057

Wheaton, J. M., Brasington, J., Darby, S. E., Kasprak, A., Sear, D., & Vericat, D. (2013). Morphodynamic signatures of braiding mechanisms as expressed through change in sediment storage in a gravel-bed river. *Journal of Geophysical Research: Earth Surface*, *118*(2), 759–779. https://doi.org/10.1002/jgrf.20060

Whipple, K. X., & Tucker, G. E. (1999). Dynamics of the stream-power river incision model: Implications for height limits of mountain ranges, landscape response timescales, and research needs. *Journal of Geophysical Research: Solid Earth*. https://doi.org/10.1029/1999jb900120

Whittaker, A. C. (2012). How do landscapes record tectonics and climate? *Lithosphere*. https://doi.org/10.1130/RF.L003.1

Whittaker, A. C., & Boulton, S. J. (2012). Tectonic and climatic controls on knickpoint retreat rates and landscape response times. *Journal of Geophysical Research: Earth Surface*. https://doi.org/10.1029/2011JF002157

Whittaker, A. C., Attal, M., & Allen, P. A. (2010). Characterising the origin, nature and fate of sediment exported from catchments perturbed by active tectonics. *Basin Research*. https://doi.org/10.1111/j.1365-2117.2009.00447.x

Wickert, A. D., Martin, J. M., Tal, M., Kim, W., Sheets, B., & Paola, C. (2013). River channel lateral mobility: Metrics, time scales, and controls. *Journal of Geophysical Research: Earth Surface*. https://doi.org/10.1029/2012JF002386

Van De Wiel, M. J., & Coulthard, T. J. (2010). Self-organized criticality in river basins: Challenging sedimentary records of environmental change. *Geology*. https://doi.org/10.1130/G30490.1

Van De Wiel, M. J., Coulthard, T. J., Macklin, M. G., & Lewin, J. (2011). Modelling the response of river systems to environmental change: Progress, problems and prospects for palaeo-environmental reconstructions. *Earth-Science Reviews*. https://doi.org/10.1016/j.earscirev.2010.10.004

Voller, V.R., Swenson, J.B. and Paola, C., 2020. The thin blue line: A review of shoreline dynamics across time scales and environments. *Earth Surface Processes and Landforms*, *45*(1), https://doi.org/10.1002/esp.4705

Wilkinson, B. H., McElroy, B. J., Kesler, S. E., Peters, S. E., & Rothman, E. D. (2009). Global geologic maps are tectonic speedometers - Rates of rock cycling from area-age frequencies. *Bulletin of the Geological Society of America*. https://doi.org/10.1130/B26457.1

Wobus, C., Whipple, K. X., Kirby, E., Snyder, N., Johnson, J., Spyropolou, K., et al. (2006). Tectonics from topography: Procedures, promise, and pitfalls. *Special Paper of the Geological Society of America*. https://doi.org/10.1130/2006.2398(04)

Wohl, E., Brierley, G., Cadol, D., Coulthard, T. J., Covino, T., Fryirs, K. A., et al. (2019). Connectivity as an emergent property of geomorphic systems. *Earth Surface Processes and Landforms*, *44*(1). https://doi.org/10.1002/esp.4434

Wu, H., Zhang, S., Hinnov, L. A., Jiang, G., Feng, Q., Li, H., & Yang, T. (2013). Time-calibrated Milankovitch cycles for the late Permian. *Nature Communications*, *4*, 1–8. https://doi.org/10.1038/ncomms3452

Xu, Y., Li, T., Musser, J., Liu, X., Xu, G., & Rogers, W. A. (2017). CFD-DEM modeling the effect of column size and bed height on minimum fluidization velocity in micro fluidized beds with Geldart B particles. *Powder Technology*. https://doi.org/10.1016/j.powtec.2017.06.020

Yan, Z., Wilkinson, S. K., Stitt, E. H., & Marigo, M. (2015). Discrete element modelling (DEM) input parameters: understanding their impact on model predictions using statistical analysis. *Computational Particle Mechanics*, *2*(3). https://doi.org/10.1007/s40571-015-0056-5

Yeom, S. Bin, Ha, E., Kim, M., Jeong, S. H., Hwang, S. J., & Choi, D. H. (2019). Application of the discrete element method for manufacturing process simulation in the pharmaceutical industry. *Pharmaceutics*, *11*(8). https://doi.org/10.3390/pharmaceutics11080414

Yiou, P., Baert, E., & Loutre, M. F. (1996). Spectral analysis of climate data. *Surveys in Geophysics*, *17*(6), 619–663. https://doi.org/10.1007/BF01931784

Zabel, M., Schneider, R. R., Wagner, T., Adegbie, A. T., De Vries, U., & Kolonic, S. (2001). Late quaternary climate changes in central Africa as inferred from terrigenous input to the Niger fan. *Quaternary Research*, *56*(2), 207–217. https://doi.org/10.1006/qres.2001.2261

Zalasiewicz, J., Waters, C. N., Williams, M., Barnosky, A. D., Cearreta, A., Crutzen, P., et al. (2015). When did the Anthropocene begin? A mid-twentieth century boundary level is stratigraphically optimal. *Quaternary International*. https://doi.org/10.1016/j.quaint.2014.11.045

Zhang, J., Sylvester, Z., & Covault, J. (2020). How do basin margins record long-term tectonic and climatic changes? *Geology*, *48*(9), 893–897. https://doi.org/10.1130/G47498.1

Zhang, X., & Vu-Quoc, L. (2000). Simulation of chute flow of soybeans using an improved tangential force-displacement model. *Mechanics of Materials*, *32*(2), 115–129.

https://doi.org/10.1016/S0167-6636(99)00043-5

Zhao, H., Huang, Y., Liu, Z., Liu, W., & Zheng, Z. (2021). Applications of discrete element method in the research of agricultural machinery: A review. *Agriculture (Switzerland)*, *11*(5). https://doi.org/10.3390/agriculture11050425

Zhou, C., & Ooi, J. Y. (2009). Numerical investigation of progressive development of granular pile with spherical and non-spherical particles. *Mechanics of Materials*. https://doi.org/10.1016/j.mechmat.2009.01.017

Zhou, Y. C., Xu, B. H., Yu, A. B., & Zulli, P. (2002). An experimental and numerical study of the angle of repose of coarse spheres. *Powder Technology*, *125*(1). https://doi.org/10.1016/S0032-5910(01)00520-4

Zlatanović, S., Fabian, J., Mendoza-Lera, C., Woodward, K. B., Premke, K., & Mutz, M. (2017). Periodic sediment shift in migrating ripples influences benthic microbial activity. *Water Resources Research*, *53*(6). https://doi.org/10.1002/2017WR020656